

# ENERGY EFFICIENT NETWORK FOR RURAL BROADBAND ACCESS

COLIN MCGUIRE

SUBMITTED IN FULFILMENT OF THE REQUIREMENTS FOR THE DEGREE OF  
*Doctor of Philosophy*

CENTRE FOR WHITE SPACE COMMUNICATIONS  
DEPARTMENT OF ELECTRONIC AND ELECTRICAL ENGINEERING  
UNIVERSITY OF STRATHCLYDE

OCTOBER 2014

This thesis is the result of the author's original research. It has been composed by the author and has not been previously submitted for examination which has led to the award of a degree.

The copyright of this thesis belongs to the author under the terms of the United Kingdom Copyright Acts as qualified by University of Strathclyde Regulation 3.50. Due acknowledgement must always be made of the use of any material contained in, or derived from, this thesis.

Signed:

Date:

# Abstract

This thesis proposes and discusses aspects of a low-cost wireless network called “Hopscotch” as a potential solution to the rural broadband problem. Providing broadband internet access to rural locations is challenging due to the long distances between internet backbone and households, the sparse population density and difficult terrain. Hopscotch uses a network of renewable powered base stations, termed “WindFi”, connected by point-to-point links, to deliver internet access to rural communities.

A combination of frequency bands are used within Hopscotch. Standard IEEE 802.11 5 GHz WiFi access technology is used for high capacity links, and an ultra high frequency TV “white space” spectrum overlay in the 600-800 MHz band provides long distance coverage. The advantages of “white space” spectrum are demonstrated for a rural wireless scenario; reducing the number of base stations required to cover a community and decreasing the transmit power required to create long distance links over challenging terrain.

The use of renewable power allows WindFi base stations to be well placed to serve a community, irrespective of available infrastructure. The power system is the biggest cost component of the base station therefore the system must be carefully sized. The design of the WindFi base station is presented and the specification of the renewable power generation system validated with operational data. To reduce the energy required, and therefore the demand on the renewable power system, aspects of energy use within the base station are considered. Models of the power consumption and data rate selection for radios used in Hopscotch are presented.

Hopscotch trials have been running on the Scottish islands of Bute and Tiree. Measurement based models of household distribution, daily network internet traffic and large-scale path loss for a rural community are presented based on trial results, which are useful for simulating rural broadband networks.

To minimise the power consumption of the WindFi base station, an energy optimisation is presented for a Hopscotch scenario. Dynamically altering the assignment of users between two overlay radio access networks, based on the instantaneous capacity required, is shown to reduce power consumption. The optimum assignment between the networks to maximise individual user throughput is also presented.

# Acknowledgements

I would like to thank my advisor, Dr Stephan Weiss, for supporting me over the past four years. His patience and endless enthusiasm have kept me motivated. I appreciate his flexibility and trust. His unmatched willingness to work through the night to help me with papers will never be forgotten.

WindFi and Hopscotch relied on the hard work and determination of a number of people. Therefore I'd like to thank them all for their efforts. Professor Robert Stewart, who was the driving force behind Hopscotch and set me on the path towards my PhD. Malcolm Brew, whose energy, optimism and ambition always motivated me and sparked ideas. Anthony McMahon, who offered all of his experience and let me set my own direction. Dr David Crawford for his professionalism within the project and for the time he spent reviewing my work. Dr Faisal Darbari and Gregour Bolton who accompanied me on numerous trips in good and bad weather to Bute. I would also like to thank Berg Design, BT, BBC and Steepest Ascent for their work and support.

I would like to thank Mark Vale at Tiree Community Broadband Network for taking time to answer my questions and giving me access to the network and data. Weather Underground kindly provided me with free historical weather data for analysis. I would like to acknowledge the Rice Wireless Network Group who were kind enough to host me for a couple of weeks and provide the inspiration required to finish my work. Thank you to everyone at CeSIP who offered kind words, suggestions and support.

I would like to thank all the guys at Steepest Ascent and MathWorks who have been forever patient and have given me time away when I have needed it. A special thank-you to Daniel García-Alís who kept pestering and pushing me to finish, and always offered support.

Finally I would like to thank my friends and family who have suffered a lot of neglect and accepted endless excuses as I locked myself away during evenings and weekends. I hope by completing this thesis I can provide inspiration to some of you to keep working and to not give up; it will be worth it in the end.

# Table of Contents

<b>Abstract</b>	<b>ii</b>
<b>Acknowledgements</b>	<b>iii</b>
<b>List of Figures</b>	<b>v</b>
<b>List of Tables</b>	<b>vi</b>
<b>Abbreviations and Acronyms</b>	<b>vi</b>
<b>1 Introduction</b>	<b>1</b>
1.1 The Rural Broadband Problem . . . . .	1
1.2 Hopscotch: A Rural Broadband Network . . . . .	2
1.3 Contributions . . . . .	2
1.4 Thesis Organisation . . . . .	3
<b>2 Hopscotch Rural Wireless Access Network</b>	<b>5</b>
2.1 Rural Broadband Access Networks . . . . .	5
2.1.1 Asynchronous Digital Subscriber Line . . . . .	6
2.1.2 Fiber Optic Access . . . . .	6
2.1.3 Mobile Broadband . . . . .	6
2.1.4 Satellite Broadband . . . . .	7
2.1.5 Fixed Wireless Links . . . . .	7
2.1.6 Comparison . . . . .	9
2.2 Hopscotch Overview . . . . .	11
2.3 Radio Frequency Bands . . . . .	12

---

2.3.1	WiFi Wireless LAN Spectrum . . . . .	12
2.3.2	TV White Space Spectrum . . . . .	13
2.4	Wireless Links . . . . .	15
2.4.1	Point-to-Point Links . . . . .	16
2.4.2	Point-to-Multipoint Links . . . . .	16
2.5	Frequency Band Selection . . . . .	18
2.5.1	Advantages of TV White Space . . . . .	18
2.5.2	Network Design Considerations . . . . .	20
2.5.3	Link Transmission Power . . . . .	22
2.6	Ring Network Architecture . . . . .	24
2.7	Summary . . . . .	25
<b>3</b>	<b>“WindFi” Base Station</b>	<b>26</b>
3.1	Renewable Powered Wireless Networks . . . . .	26
3.2	The Need for WindFi . . . . .	29
3.3	Radio Equipment . . . . .	31
3.4	WindFi Use-Cases . . . . .	32
3.4.1	Terminating Base Station . . . . .	34
3.4.2	Multi-Hop Repeater . . . . .	34
3.4.3	Multi-Hop Repeater and Base Station . . . . .	35
3.5	Mechanical and Structural Mast Requirements . . . . .	36
3.6	Monitoring and Control . . . . .	37
3.7	Electrical Power System . . . . .	38
3.7.1	Base Load . . . . .	38
3.7.2	Example Base Loads . . . . .	39
3.7.3	Power Generation and Storage . . . . .	40
3.7.4	Power System Dimensioning . . . . .	42
3.8	Crow’s Nest Power System Analysis . . . . .	47
3.8.1	Power System Design . . . . .	47
3.8.2	Expected Energy Production Characteristics . . . . .	48
3.8.3	Day-to-Day Performance Analysis . . . . .	48

---

3.8.4	Wind Power System Failure Analysis . . . . .	54
3.9	Summary . . . . .	56
<b>4</b>	<b>Radio Characterisation</b>	<b>57</b>
4.1	Background . . . . .	57
4.1.1	Radio Hardware Configuration . . . . .	58
4.1.2	Data Rate Selection . . . . .	58
4.1.3	Transmit Power Selection . . . . .	59
4.2	Experimental Setup . . . . .	59
4.2.1	Overview . . . . .	60
4.2.2	Profiling Data Rate Selection . . . . .	61
4.2.3	Profiling Transmit Power . . . . .	62
4.2.4	Profiling Power Consumption . . . . .	63
4.2.5	Programmable Variable Attenuation Calibration . . . . .	64
4.3	Ubiquiti XtremeRange7 Characterisation Results . . . . .	68
4.3.1	Profiling Data Rate Selection . . . . .	68
4.3.2	Profiling Transmit Power . . . . .	71
4.3.3	Profiling Power Consumption . . . . .	72
4.4	Ubiquiti SuperRange71 Characterisation Results . . . . .	74
4.4.1	Profiling Data Rate Selection . . . . .	74
4.4.2	Profiling Power Consumption . . . . .	76
4.5	Radio Characterisation Models . . . . .	79
4.5.1	Relating Path loss and Received Signal Power . . . . .	79
4.5.2	Rate Selection Given Received Signal Power . . . . .	82
4.5.3	Power Consumption Given Transmit Power . . . . .	83
4.6	Summary . . . . .	85
<b>5</b>	<b>Trial Network Analysis</b>	<b>86</b>
5.1	Trials and Deployments . . . . .	86
5.1.1	Isle of Bute Test Bed . . . . .	86
5.1.2	Tiree Broadband . . . . .	87

---

5.1.3	Community or Cooperative Operating Models . . . . .	87
5.2	Household Distribution . . . . .	88
5.3	Rural Large-Scale Path Loss . . . . .	89
5.3.1	Background . . . . .	90
5.3.2	An Empirical Path Loss Model for Tiree . . . . .	90
5.4	Network Bandwidth Utilisation . . . . .	93
5.4.1	Background . . . . .	93
5.4.2	Tiree Network Bandwidth Utilisation . . . . .	93
5.4.3	Bandwidth Utilisation Model . . . . .	93
5.5	Summary . . . . .	97
<b>6</b>	<b>Optimising a Multi-Radio Network for Energy Efficiency</b>	<b>98</b>
6.1	Background . . . . .	99
6.1.1	Selecting Station Assignment by Scaling Transmit Power . . . . .	99
6.1.2	Green Radio Initiatives . . . . .	99
6.1.3	Cell Breathing . . . . .	101
6.2	Problem Formulation . . . . .	101
6.3	Network Model . . . . .	102
6.3.1	Propagation Model . . . . .	103
6.3.2	Transmission Power Selection . . . . .	103
6.3.3	Receiver Model . . . . .	104
6.3.4	Network Throughput Model . . . . .	104
6.3.5	Power Consumption Model . . . . .	105
6.4	Optimum Station Assignment . . . . .	106
6.5	Probabilistic Method . . . . .	106
6.5.1	Probability of Data Rate Selection . . . . .	107
6.5.2	Average Network Performance . . . . .	112
6.6	Monte Carlo Method . . . . .	114
6.7	Bayesian Belief Network Method . . . . .	116
6.7.1	Bayesian Belief Network Formation . . . . .	116
6.7.2	Estimating Network Performance . . . . .	118

---

6.8	Simulation and Results . . . . .	119
6.8.1	Impact of Transmit Power on Station Assignment . . . . .	119
6.8.2	Impact of Transmit Power on Throughput . . . . .	120
6.8.3	Station Assignment, Throughput and Power Consumption . . . . .	124
6.8.4	GHz RAN Breathing to Minimise Power Consumption . . . . .	126
6.8.5	Validation with Monte Carlo Method . . . . .	128
6.9	Approximation with Bayesian Belief Network . . . . .	128
6.9.1	Station Assignment, GHz RAN Transmit Power and Power Consumption . . . . .	128
6.9.2	Station Assignment and Network Throughput . . . . .	130
6.9.3	GHz RAN Breathing to Minimise Power Consumption . . . . .	131
6.10	Summary and Discussion . . . . .	134
<b>7</b>	<b>Conclusions and Further Work</b>	<b>135</b>
7.1	TV “White Space” for Rural Broadband . . . . .	135
7.2	WindFi Base Station . . . . .	136
7.3	Radio Power Consumption and Data Rate Selection Models . . . . .	137
7.4	Models for Rural Fixed Wireless Scenarios . . . . .	138
7.5	Optimised Multi-Radio Network for Energy Efficiency . . . . .	138
7.6	Further Work . . . . .	139

## List of Figures

2.1	Example of an operational Hopscotch network on the the Isle of Tiree off the West Coast of Scotland connecting a remote community to IP-backbone. . . .	12
2.2	TV “white space” availability in the UK. Red: little; green: some; white: much. Diagram taken from [?]. . . . .	14
2.3	470-862 MHz TV “white space” spectrum [?]. . . . .	14
2.4	Elevation and azimuth radiation patterns for a vertically polarized Ubiquiti RD-5G-30 parabolic antenna. The antenna is typically used in point-to-point (PTP) links. The pattern data is supplied by Ubiquiti [?] and visualized using Radio Mobile [?]. . . . .	16
2.5	The elevation and azimuth radiation patterns for a vertically polarized Ubiquiti AM-5G20-90, 90° sector antenna. The antenna is typically used in point-to-multipoint (PTMP) links. The pattern data is supplied by Ubiquiti [?] and visualized using Radio Mobile [?]. . . . .	17
2.6	The elevation and azimuth radiation patterns for a vertically polarized Ubiquiti AMY-9M16 900 MHz yagi antenna. The antenna is used in PTP and PTMP links. The pattern data is supplied by Ubiquiti [?] and visualized using Radio Mobile [?]. . . . .	17
2.7	Knife edge diffraction parameters. . . . .	20
2.8	Example community with areas for a potential base station to provide coverage at 630 MHz at 1 W equivalent isotropically radiated power (EIRP) shaded red. . . . .	21
2.9	Coverage provided by two base stations at 5660 MHz 1 W EIRP, with yellow shading representing coverage provided by base station A (BSA), blue shading representing the coverage provided by base station B (BSB), and the overlapping coverage indicated by green shading. . . . .	22
2.10	Terrain profiles showing elevation between BSA and stations A and D. . . .	23

---

2.11	Example loop network connecting several communities to the internet protocol (IP)-backbone via PTP and PTMP links. PTP links are shown as red dotted lines. PTMP links are shown by a green overlay. . . . .	25
3.1	Prototype “WindFi” base station on the Isle of Bute, Scotland. The base of the unit includes photovoltaic modules and a battery bank (underground). The 10 m mast supports the wind turbine, antennas and radio equipment, housed in an orange weather-proof case just below the wind turbine. . . . .	30
3.2	Use cases for WindFi masts in a Hopscotch rural broadband network: repeater, repeater & base station and terminating base station. . . . .	33
3.3	Estimated coverage of “Site A” terminating base station. . . . .	34
3.4	Estimated coverage of “Crow’s Nest” multi-hop repeater. . . . .	35
3.5	Estimated coverage of “Site B” multi-hop repeater and base station. This relays connectivity between “Crow’s Nest” and “Site F” whilst also serving subscribers. . . . .	36
3.6	Average 10 m wind speed data from Weather Underground [?] and daily solar irradiance data from PVGIS [?] at Tiree Airport (TRE) and Prestwick Airport (PIK) averaged between the years 2000 and 2014. . . . .	41
3.7	Expected power output of a SuperWind SW350 or JetPro JPS200 wind turbine [?, ?]. . . . .	43
3.8	Expected daily power generation at Tiree Airport (TRE) using (a) one 250 W peak power photovoltaic (PV) module and a SuperWind SW350 (SW) 350 W wind turbine to satisfy the small load requirement, (b) two 250 W peak power PV modules and a SuperWind SW350 (SW) 350 W wind turbine to satisfy the small and large load requirements. . . . .	45
3.9	Expected daily power generation at Prestwick Airport (PIK) for a small and large load using (a) one SuperWind SW350 (SW) 350 W wind turbine and one 250 W peak power PV module to satisfy the small load, (b) three JetPro JPS200 (JP) 200 W wind turbines and two 250 W peak power PV modules to satisfy the large load. . . . .	46
3.10	Tristar battery charging states [?]. . . . .	48
3.11	Expected daily power generation at Tiree Airport (TRE) using two 250 W peak power PV modules and a SuperWind SW350 250 W wind turbine. . . .	49
3.12	Impact of surplus energy generation on time to recharge 200 Ah battery bank at Tiree Airport (TRE). . . . .	50

3.13	Crow's Nest power system between 2nd and 4th June 2013; low wind speed days showing (a) target and measured battery voltage, (b) TS-60-MPPT PV charge controller state, and (c) measured PV generation and expected SW generation. . . . .	52
3.14	Crow's Nest power system between 28th and 30th May 2013; high wind speed days, showing (a) target and measured battery voltage, (b) TS-60-MPPT PV charge controller state, and (c) measured PV generation and expected SW generation. . . . .	53
3.15	Crow's nest power system during a failure of the wind power system between 4th and 19th February, showing (a) target and measured battery voltage, (b) TS-60-MPPT PV charge controller state, (c) measured PV generation and expected SW generation, and (d) cumulative daily system energy with broken wind turbine. . . . .	55
4.1	Quoted transmit power for each data rate for the XtremeRange7 (XR7) and SuperRange71 (SR71) [?, ?]. . . . .	59
4.2	radio frequency (RF) characterization test setup showing (a) data rate selection test, and (b) data rate selection test calibration path. . . . .	60
4.3	Programmable variable attenuator. . . . .	61
4.4	ultra high frequency (UHF) radio transmit power profiling setup showing (a) test setup, and (b) calibration paths. . . . .	62
4.5	access point (AP) Power consumption measurement setup. . . . .	64
4.6	Characterising programmable variable attenuator insertion loss at 5.2 GHz showing (a) measured and adjusted attenuation for all programmable values, and (b) offset between measured and expected attenuation. . . . .	66
4.7	Characterising programmable variable attenuator insertion loss at 763 MHz showing (a) measured and adjusted attenuation for all programmable values, and (b) offset between measured and expected attenuation. . . . .	67
4.8	Offset for a given programmed attenuation using measured values and linear least squares extrapolation. . . . .	68
4.9	XR7 automatic rate selection profiling showing (a) reported transmit data rate and (b) Iperf transmission control protocol (TCP) throughput, for different path losses. . . . .	69
4.10	XR7 forced data rate profiling showing (a) mean reported transmit data rate, (b) mode reported transmit data rate, and (c) Iperf TCP throughput, for different path losses. . . . .	70

4.11	Measured burst power and estimated transmit power given path loss. . . . .	71
4.12	Measured burst power and therefore estimated transmit power given path loss. . . . .	72
4.13	Estimated transmit power and measured power consumption for each data rate. . . . .	73
4.14	Power consumption and reported received signal strength indicator (RSSI) when using manual transmit power setting at 1.5 Mbps data rate. . . . .	73
4.15	Power consumption against estimated transmit power at 1.5 Mbps data rate.	74
4.16	SR71 automatic data rate selection profiling showing (a) reported transmit data rate and (b) Iperf TCP throughput for different path losses. . . . .	75
4.17	SR71 forced transmit data rate selection profiling showing (a) mean reported transmit data rate, (b) mode reported transmit data rate, and (c) Iperf TCP throughput, for different path losses. . . . .	77
4.18	Power consumption and reported RSSI when using manual transmit power setting at 6 Mbps data rate. . . . .	78
4.19	Power consumption against estimated transmit power at 6 Mbps data rate. . . . .	78
4.20	Mean and mode reported data rate against reported RSSI. . . . .	80
4.21	Reported RSSI for an estimated receive power when (a) the basic data rate transmit power, and (b) the mode data rate transmit power, is used in (??) . . . . .	81
4.22	Estimated transmit power and measured power consumption for each data rate. . . . .	82
4.23	Model of XR7 5 MHz and SR71 20 MHz data rate selection given a receive signal strength . . . . .	83
4.24	Power consumption model for the (a) XR7 and (b) SR71 for a given transmit power. . . . .	84
5.1	Tiree rural broadband network (source: Google Earth). . . . .	88
5.2	Histogram of household distance from base station on Tiree with fitted Bi-variate approximations. . . . .	89
5.3	Estimated station path losses with fitted path loss exponentials. . . . .	92
5.4	Typical terrain on the isle of Tiree. . . . .	92
5.5	Relative asynchronous digital subscriber line (ADSL) downstream and upstream bandwidth utilisation recorded by Maier [?]. . . . .	94

5.6	Mean daily downstream (a) and upstream (b) bandwidths of Tiree network and fitted models. . . . .	95
5.7	Comparison of (a) upstream and downstream models when Maier's model is scaled to the peak average downstream throughput recorded on Tiree, (b) downstream models as a percentage of maximum utilisation, and (c) upstream models as a percentage of maximum utilisation. . . . .	96
6.1	Controlling the assignment of three stations (STAs) between the GHz and UHF radio access networks (RANs) by scaling the transmit power of the GHz RAN. (a) Initially the GHz RAN transmit power causes the UHF RAN to serve one STA and the GHz RAN to serve two STAs. (b) Reducing the GHz RAN transmit power forces the UHF RAN the serve two STAs and the GHz RAN serves one STA. . . . .	100
6.2	Demonstration of cell breathing: (a) Cell B is overloaded with user equipments (UEs) compared to cells A and C; (b) Cell B contracts to fairly distribute the number of UEs accross all cells. . . . .	101
6.3	Network adjustment model. . . . .	102
6.4	Representations of a joint probability space for two ordered random variables with the same underlying probability density function (PDF). (a) The joint probability space of the receive power of two stations without the constraint $X_1 \geq X_2$ . The probabilities are normalised between 0 and 1. (b) The probability space with bounded intervals of interest. . . . .	109
6.5	Bayesian belief network (BBN) describing dependencies of distance, path loss, receive power and data rate. . . . .	117
6.6	Probabilistic model of the multi-RAN network. . . . .	117
6.7	Mean number of stations connected to GHz RAN with standard deviation, and median number of stations connected to GHz RAN, for a given transmit power. . . . .	121
6.8	Individual (a) zero-renormalised harmonic mean (ZRHM) and (b) median RAN throughputs and number of connected stations on the GHz RAN for a given transmit power. . . . .	122
6.9	Comparison of median and ZRHM throughputs for (a) GHz and (b) UHF RANs. The error bars show the variance of the throughput. . . . .	123
6.10	Mean GHz RAN transmit power required for each station assignment. . . . .	125
6.11	Individual station capacity on each RAN and base station power consumption given possible valid RAN assignments. . . . .	125

- 
- 6.12 Results of solving (??) in 3 min. intervals showing: (a) required and offered capacity, (b) network power consumption, and (c) station assignment . . . . . 127
- 6.13 Comparison of simulation results using BBN and probabilistic methods for, (a) mean GHz RAN transmit power, and (b) corresponding total power consumption. . . . . 129
- 6.14 Beliefs of  $P_u^{rx}$  given  $P^{tx} = 30$  dBm after BBN convergence with data rate boundaries. The 20 ordered PDFs represent the 20 ordered stations. The rightmost PDF is that of the closest station to the base station. . . . . 131
- 6.15 Comparison of throughputs calculated using BBN and probabilistic methods for given RAN assignments: (a) individual station capacity on each RAN, and (b) combined RAN minimum throughput. . . . . 132
- 6.16 Results of solving (??) with the BBN method in 3 min. intervals showing: (a) required and offered capacity, (b) network power consumption, and (c) station assignment . . . . . 133

## List of Tables

2.1	Strengths and weaknesses of competing access technologies for rural broadband. . . . .	10
2.2	5 GHz and 2.4 GHz spectrum and EIRP limitations in the UK for outdoor use [?, ?, ?]. . . . .	13
2.3	Link calculations and transmit and receive powers between the base station and stations A and D, given a transmit power and receive power. . . . .	24
3.1	SolarMESH cost-optimal battery and PV capacities for three locations and a 2 W base load. . . . .	27
3.2	EHAS node power estimates for two hardware combinations. . . . .	28
3.3	Power consumption per sector for AP configuration options. . . . .	32
3.4	PTP and PTMP radio requirements for WindFi use-cases and associated power consumption power system configurations. . . . .	39
3.5	Power consumption used out of maximum using PTP and PTMP radio daughter cards and Mikrotik RouterBOARD 433AH single board computer (SBC) for different use-cases. . . . .	39
3.6	WindFi power system utilisation for given use-cases. . . . .	40
3.7	Power consumption of radio equipment at the “Site A” terminating base station. . . . .	40
3.8	Power consumption of radio equipment at the “Crow’s Nest” repeater. . . . .	40
3.9	Power consumption of radio equipment at the “Site B” repeating base station. . . . .	41
4.1	Radio equipment profiled for links in the 5 GHz and UHF bands. The vendor of the SBCs is Mikrotik and the vendor of the RF daughter cards is Ubiquiti. . . . .	58
4.2	IEEE 802.11a/g modulation and coding scheme (MCS) rates and expected data rates . . . . .	58

---

4.3	Measured fixed attenuation for each frequency band. . . . .	62
4.4	Measured fixed attenuation for each path in Figure ?? at 763 MHz. . . . .	63
4.5	Transmit powers used in (??) to calculate the receive signal power. . . . .	80
4.6	Parameters for XR7 and SR71 power consumption models. . . . .	85
5.1	Parameters used for regression fit to determine $\gamma$ in (??). . . . .	91
6.1	Example of valid permutations of data rates (MCS) for $n$ stations within a network with three MCS $\{0, 1, 2\}$ . MCS 0 signifies the station is not connected. . . . .	113
6.2	Simulation parameters. . . . .	120
6.3	Mean percentage errors between probabilistic and Monte Carlo methods for all GHz RAN transmit powers. . . . .	128
6.4	Comparison between energy savings through dynamic station assignment using results from the BBN and probabilistic methods. . . . .	134

# Abbreviations and Acronyms

<b>3G</b>	3rd generation
<b>4G</b>	4th generation
<b>ADSL</b>	asynchronous digital subscriber line
<b>AP</b>	access point
<b>BBN</b>	Bayesian belief network
<b>BS</b>	base station
<b>BSA</b>	base station A
<b>BSB</b>	base station B
<b>CAN</b>	controller area network
<b>CDF</b>	cumulative density function
<b>COTS</b>	commercial-off-the-shelf
<b>CPE</b>	consumer premises equipment
<b>CPT</b>	conditional probability table
<b>CSMA/CA</b>	carrier sense multiple access with collision avoidance
<b>DAQ</b>	data acquisition system
<b>DC</b>	direct current
<b>DC-HSPA+</b>	dual carrier high speed packet access
<b>DTT</b>	digital terrestrial television
<b>EIRP</b>	equivalent isotropically radiated power
<b>FSPL</b>	free space path loss

---

<b>FTTC</b>	fiber-to-the-cabinet
<b>FTTH</b>	fiber-to-the-home
<b>GIS</b>	geographic information system
<b>GPS</b>	global positioning system
<b>HSPA</b>	high speed packet access
<b>IP</b>	internet protocol
<b>ISP</b>	internet service provider
<b>JP</b>	JetPro JPS200
<b>LEO</b>	low earth orbit
<b>LOS</b>	line of sight
<b>LTE</b>	long term evolution
<b>MAC</b>	medium access controller
<b>MCS</b>	modulation and coding scheme
<b>MIMO</b>	multiple input multiple output
<b>MMSE</b>	minimum mean square error
<b>MPPT</b>	maximum power point tracking
<b>NB-5G22</b>	NanoBridge M5
<b>NSM5</b>	NanoStation NSM5
<b>NLOS</b>	non-line of sight
<b>Ofcom</b>	Office for Communications
<b>PCF</b>	point coordination function
<b>PDF</b>	probability density function
<b>PIK</b>	Prestwick Airport
<b>PMSE</b>	programme making and special events
<b>PTMP</b>	point-to-multipoint

---

<b>PTP</b>	point-to-point
<b>PV</b>	photovoltaic
<b>PVGIS</b>	photovoltaic geographical information system
<b>PWM</b>	pulse width modulation
<b>RAN</b>	radio access network
<b>RF</b>	radio frequency
<b>RSSI</b>	received signal strength indicator
<b>SBC</b>	single board computer
<b>SFBB</b>	superfast broadband
<b>SNR</b>	signal-to-noise ratio
<b>SNMP</b>	simple network management protocol
<b>SR2</b>	SuperRange2
<b>SR71</b>	SuperRange71
<b>SRC</b>	SuperRange Cardbus
<b>STA</b>	station
<b>SW</b>	SuperWind SW350
<b>TCP</b>	transmission control protocol
<b>TDD</b>	time division duplexing
<b>TDMA</b>	time division multiple access
<b>TRE</b>	Tiree Airport
<b>TVWS</b>	TV “white space”
<b>UDP</b>	user datagram protocol
<b>UE</b>	user equipment
<b>UHF</b>	ultra high frequency
<b>VHF</b>	very high frequency

<b>VoIP</b>	voice over internet protocol
<b>WSD</b>	“white space” device
<b>XR2</b>	XtremeRange2
<b>XR5</b>	XtremeRange5
<b>XR7</b>	XtremeRange7
<b>ZRHM</b>	zero-renormalised harmonic mean

# Chapter 1

## Introduction

### 1.1 The Rural Broadband Problem

Broadband internet access is regarded as a key enabling technology in both developed and developing economies. Widespread broadband internet access in developed economies such as the UK and US has led to a move towards online services such as e-government, telemedicine, video conferencing and video streaming. Despite this proliferation, a digital divide has emerged between urban and rural communities [?, ?] as telecommunication providers are unable to roll out broadband internet access to remote, sparsely populated rural communities due to the large infrastructure costs involved and poor return on investment. Currently 73% of UK households have access to an internet connection capable of providing a throughput of more than 24 Mbps, dubbed superfast broadband (SFBB)[?]. Within the Scottish Highlands only 3.6% of households have access to SFBB [?]. This disparity leads to rural communities being excluded from access to online services which could otherwise help ease the distance penalty that accompanies a rural location [?]. Additionally there is evidence of people leaving rural communities to live in urban areas due to a lack of connectivity [?].

In remote areas such as the sparsely populated Highlands and Islands of Scotland, many households are located far from a telephone exchange. This limits the speed of the most common method of broadband delivery, asynchronous digital subscriber line (ADSL), which uses existing copper cabling [?]. Emerging SFBB alternatives such as fiber access and 4th generation (4G) mobile broadband require substantial capital investment, planning permission and access to the electricity grid or the use of diesel generators to ensure uninterrupted power supplies. The large infrastructure costs and the additional operating expense of electrical connection and/or fuel make these solutions, which have been adopted in urban settings, uneconomical for rural deployment without major subsidy.

These reasons have contributed to a number of government schemes to incentivise and sub-

sidise rural broadband. When awarding spectrum for 4G mobile broadband coverage, the German telecommunications regulator included conditions to ensure awardees built-out their networks in areas with no or very low broadband coverage, before deploying in more populated areas [?]. In October 2013 the Scottish government pledged to ensure that 95% of premises in Scotland have access to SFBB by 2018 [?].

## 1.2 Hopscotch: A Rural Broadband Network

This thesis proposes and discusses aspects of a low cost wireless network called “Hopscotch” as a solution the rural broadband problem. Test installations of Hopscotch base stations using IEEE 802.11 5 GHz WiFi and ultra high frequency (UHF) “white space” radios are currently being trialled in Scotland. Communities are illuminated using a point-to-multipoint (PTMP) wireless distribution system connected to internet protocol (IP)-backbone directly or via a series of point-to-point (PTP) relays mounted on Hopscotch renewable energy base stations or elsewhere if electrical power is easily available.

The system presented uses a combination of radio access technologies and frequency bands, served by base stations. Hopscotch base stations, termed “WindFi”, are designed to be low power autonomous units, powered by a combination of renewable sources. One form of the network deployable today, without any licences, uses standard IEEE 802.11 WiFi access technology to create a network. The project also features the use of UHF “white space” radios thus forming a digital dividend “white space” spectrum overlay in the 600-800 MHz band [?]. Hence by setting up an IEEE 802.11 WiFi based network in a community a “white space” test network can be overlaid using the same infrastructure. This aids the study and comparison of access technologies and serves as a test bed for the investigation and development of “white space” links. Operation in “white space” has the potential to provide more comprehensive cover than in existing fixed wireless bands for a rural setting, therefore an overlay network allows the use of cognitive radio techniques, such as dynamically switching between multiple frequency bands, to be explored and evaluated.

## 1.3 Contributions

This work contains a number of contributions towards the Hopscotch wireless rural broadband network. These contributions overcome the limitations of existing rural broadband solutions to allow Hopscotch to provide a realistic cost-effective solution to the rural broadband problem.

The use of UHF “white space” frequency bands is considered in the context of rural broadband and is demonstrated to offer superior performance to existing wireless solutions. This reduces the number of base stations required, and therefore lowers the cost of the network, which is important when there are a limited number of users served [?, ?, ?, ?].

The design of a renewable powered base station for Hopscotch, WindFi, is presented and the performance validated against design decisions using recorded field data. The use of renewable power is key to the success of Hopscotch as base station placement is not constrained to the availability of utilities [?].

Models of household distribution, daily internet traffic patterns, large-scale path loss, radio performance and power consumption are presented for a rural network which can be used when studying a network theoretically or through simulation. These models have been created by analysing data from a Hopscotch rural broadband network on the Scottish island of Tiree and by measuring the performance and power consumption of hardware. Models of daily internet traffic patterns, household distribution and a general path loss model are created and used; providing an alternative to typical urban usage models. Similarly, power consumption models of commonly used radio hardware for fixed wireless links are presented. These allow the impact of wireless link design on power consumption of a base station or network to be considered [?].

Using the network and power consumption models, a heterogeneous network consisting of standard IEEE 802.11 WiFi access technology and UHF access is considered and demonstrated to reduce the power consumption of the network whilst maintaining a level of service for users. The optimisation of users between each networks is presented to minimise the power consumption at a base station. Reducing the power consumption of a base station is key to reduce the cost of a renewable generation system. Therefore, the assignment of users to one of the two networks, driven by the overall aim of minimising power, has been optimised in [?] and developed through the use of belief propagation networks [?].

## 1.4 Thesis Organisation

This thesis presents contributions to the delivery of low-cost, energy-efficient rural broadband using a wireless network powered by renewable energy.

Chapter 1 (this chapter) introduces the rural broadband problem as the motivation for this work and provides an overview of the contributions and organisation of the thesis.

Chapter 2 summarises current rural broadband access technologies and wireless rural broadband networks and describes existing limitations. A potential solution to overcome these limitations, the Hopscotch wireless network, is introduced and compared to existing tech-

nologies. The overall architecture of the network is described including the types of wireless links used. The network can include a UHF “white space” overlay network. The suitability of this band for rural broadband is discussed in this chapter.

Chapter 3 describes the design process and verification of the WindFi base stations used to construct the Hopscotch network. This includes a detailed description of the renewable power generation system design, which is the main cost component of the system. An analysis of the performance of the system when deployed is given for standard and fault conditions to validate the design decisions.

Chapter 4 presents the results of a lab-based characterisation of the performance and power consumption of radio hardware used by Hopscotch under varying conditions. These results are used to create behavioural models of the radios which can be used when analysing and designing rural broadband networks.

Chapter 5 presents analysis of data captured from a trial Hopscotch network on the Scottish island of Tiree. This analysis is used to create two models — an empirical path loss model, and a data usage model — useful for understanding and analysing rural broadband networks. A model of the distribution of households within the community is also presented.

Chapter 6 uses the models created in Chapters 4 and 5 to demonstrate how a combination of frequency bands can serve a community and how varying the assignment of users between the bands can minimise the power consumption of a base station whilst maintaining a desired level of performance for a network. Three methods are used to simulate the optimisation; a probabilistic method, a Monte Carlo method and a Bayesian belief network (BBN). The optimised assignment between the networks is calculated and a dynamic, demand driven assignment is proposed to minimise the power consumption.

Chapter 7 summarises the contributions within this thesis and discusses potential future research directions.

## Chapter 2

# Hopscotch Rural Wireless Access Network

This thesis considers solutions to the rural broadband problem, where the combination of difficult terrain and low population densities makes delivering economical rural broadband a challenge. This chapter reviews relevant technologies and introduces the generic architecture of a potential solution to the rural broadband problem: the Hopscotch rural broadband network. Section 2.1 reviews and compares existing rural broadband access technologies including wireless networks to gain an understanding of their advantages and shortcomings. Section 2.2 introduces the Hopscotch wireless network to overcome the limitations of existing technologies. Sections 2.3 and 2.4 detail the types and properties of the wireless links used within the networks. Section 2.5 compares these links, demonstrates the advantages and disadvantages and discusses how they can be used together in a network. Section 2.6 demonstrates how a network is constructed out of “WindFi” base stations.

### 2.1 Rural Broadband Access Networks

Traditionally wireline technologies are used for the final leg of delivering connectivity from a telecommunication service provider’s infrastructure to a customer’s premises, otherwise known as the “local loop” or “last mile”. The most common technologies used are ADSL and fiber optic access either to the premises or kerb. Wireless last mile access solutions such as cellular mobile broadband, satellite broadband or fixed terrestrial wireless offer an attractive alternative to wireline solutions in rural areas as generally their infrastructure costs are lower.

### 2.1.1 Asynchronous Digital Subscriber Line

Around 75% of UK residential broadband connections are currently delivered by ADSL [?]. ADSL uses existing telephone cabling and therefore requires no new infrastructure for deployment where copper telephone lines exist, provided the line is of sufficient quality. Data rates depend on length and quality of the line between the consumer and local exchange; the closer a consumer lives to the exchange, the better the performance [?]. With ADSL2+ data rates up to 24 Mbps can be achieved within 2 km of the exchange [?]. When the distance between consumer and the exchange exceeds 5.5 km, ADSL typically does not work.

In the Highlands and Islands of Scotland, due to the remoteness of customers and challenging landscape, many household are located far from an exchange limiting ADSL broadband speeds and connectivity. Data collected by the UK regulator, the Office for Communications (Ofcom), shows 14.6% of households in the Scottish Highlands receive less than 2 Mbps [?]. According to Sam Knows [?] as of November 2013 only nine of the Highlands' 176 exchanges had been upgraded from ADSL to ADSL2+, further limiting possible speeds.

### 2.1.2 Fiber Optic Access

Two types of fiber optic access are typically used; fiber-to-the-home (FTTH) and fiber-to-the-cabinet (FTTC).

FTTH uses fiber optic cable as the local loop between exchange and consumer. Of all technologies considered in this section, FTTH offers the highest capacity, reliability and immunity to interference [?]. Fiber optic access is the most common form of fixed access SFBB. Typically speeds up to 100 Mbps are offered and 1 Gbps access is possible. Establishing FTTH in rural areas is expensive as a new infrastructure is required. The civil engineering costs are usually estimated to account for 80%-90% of the total cost of deploying the network [?]. In rural areas the cost per home for installing a new network is significantly higher than in the more densely populated areas, making unsubsidised deployment unprofitable.

FTTC and hybrid fibre-coax networks are less costly than a FTTH network to install as fiber is connected to a cabinet close to the household (typically within 300 m) and a copper twisted pair line serves the remaining distance. Despite the reduction in costs compared to FTTH these solutions are still uneconomical if unsubsidised.

### 2.1.3 Mobile Broadband

Current 3rd generation (3G) mobile broadband services such as high speed packet access (HSPA) typically advertise a peak data rate of 7.2 Mbps but average data rates are generally

around 2 Mbps. As with fiber access, the commercial cost of deployment is high and rate of return low due to the cost of 3G enabled base stations and provisioning the back-haul required for data services. This is why 66% of the geographical area and 18% of households in the Scottish Highlands lack 3G coverage [?]. Moreover, mobile carriers have adopted a pay per megabyte pricing model which makes mobile broadband more expensive for data intensive applications such as video streaming compared to ADSL, especially for low income rural communities. Next generation networks based on dual carrier high speed packet access (DC-HSPA+) and 3GPP long term evolution (LTE) offer greater maximum data rates. For example LTE Release 11 provides a peak data rate of 3 Gbps with 5 aggregated component carriers and 8 spatial streams. These technologies are classed as SFBB, but are unlikely to be deployed in rural areas without major subsidy.

### **2.1.4 Satellite Broadband**

Internet access is provided by satellite broadband via a link between the consumer and a satellite in either geostationary or low earth orbit (LEO). Satellite broadband access suffers from high two-way terminal costs, large latency and limited bandwidth, typically only up to 10 Mbps [?]. Geostationary services such as that provided by Avanti suffer from a high round trip latency of up to 700 ms [?] which can be unacceptable for real-time applications such as voice over internet protocol (VoIP) or online gaming. LEO services such as Iridium provide lower latencies or around 100 ms for a round trip but reduced data rates, typically 64 kbps per channel [?]. Despite these limitations satellite broadband is often the only option for internet access in remote areas and can successfully serve as core back haul for networks in developing countries where communications infrastructures are insufficient. An example of such a use is the Réseau en Afrique Francophone pour la Télémédecine (RAFT) network in Africa for tele-medicine applications [?].

### **2.1.5 Fixed Wireless Links**

Fixed terrestrial wireless links, particularly IEEE 802.16e WiMAX and IEEE 802.11 WiFi are now commonly used for “last mile access”, particularly in developing countries. Wireless internet service providers (ISPs) offer access options worldwide typically using one of these two technologies<sup>1</sup>. Wireless mesh networks have also proven popular for access in developing countries and in research applications.

---

<sup>1</sup>Wireless Internet Service Provides Association: <http://www.wispa.org/member-directory>

### Wireless Link Options

WiMAX provides a theoretical peak data rate of 74 Mbps in a 20 MHz channel [?]. More realistically downlink speeds of 25 Mbps and uplink speeds of 6.7 Mbps are reached using a time division duplexing (TDD) scheme with a 3:1 downlink-to-uplink ratio [?]. A number of WiMAX broadband operators have deployed rural networks in the UK. vFast in Kent offer up to 24 Mbps with at 10:1 contention ratio [?]. Despite its promise WiMAX is under threat from LTE due to enhanced global support from operators and vendors [?], potentially reducing chipset volumes and hence increasing costs.

WiFi achieves theoretical data rates up to 300 Mbps in an IEEE 802.11n network. Typically 25-150 Mbps are possible up to 100 m. The wide-spread adoption has led to large production values and low chipset costs. Commercial modifications to the medium access controller (MAC) have been carried out to make WiFi more suitable for long range fixed wireless links due to the use of carrier sense multiple access with collision avoidance (CSMA/CA) and independent acknowledgements of packets [?]. An example of a commercial modification to the WiFi MAC is AirMax10 from Ubiquiti, based on time division multiple access (TDMA) and smart polling techniques.

The availability of open source drivers has allowed researchers to modify the WiFi MAC to suit rural conditions. One example, WiFiRe [?] is designed for use with a sectorised base station providing PTMP connectivity with multiple consumer premises equipment (CPE). A standard IEEE 802.11 physical layer is used for each sector and a modified MAC allows each sector to share the same channel. A TDD mechanism is used to reduce medium contention. A number of other studies have proposed MAC modifications to reduce power consumption or increase performance over long distances [?, ?, ?, ?].

On July 1st 2011 the IEEE published the 802.22 standard for wireless regional area networks. This incorporates cognitive radio technology such as spectrum sensing to enable broadband wireless access in “white space”. The intention of the standard is to allow broadband access to be provided in rural areas where existing wireless solutions (as those described above) are not sufficient [?]. Despite the promise as of 2014 no commercial-off-the-shelf (COTS) hardware is available.

### Wireless Mesh Networks

Wireless mesh networks are an attractive option to provide connectivity as they self-organise, are flexible, and typically use low-cost hardware [?]. Despite these advantages, performance often suffers from scalability issues [?] and therefore deployments tend to be limited to research networks and deployments in developing countries. The Rice University and “Technology for All” partnership network served 4000 clients with 21 nodes using IEEE 802.11

links in urban Houston, Texas, but suffered from inter-link interference, poor route selection and long outage durations caused by network interface policies and handover techniques [?]. The Tegola testbed connects 15 houses in rural communities on the Glenelg and Knoydart peninsulas to the Sleat peninsula on the Isle of Skye with long distance wireless links between 7.6 km and 19 km [?]. User access is provided by 2.4 GHz WiFi radios, and 802.11a 5 GHz radios create backhaul links. The majority of other mesh networks, such as QuRiNet [?], consisting of 34 mesh nodes, and EHAS [?], use 2.4 GHz WiFi links for connectivity and have proven successful for their intended applications.

### 2.1.6 Comparison

For population densities below 150 inhabitants per square km a techno-economic analysis comparing ADSL and WiMAX for the provision of rural broadband has concluded that ADSL is more cost effective than WiMAX [?]. Yet in even more sparsely populated rural areas not connected to the fiber backbone networks, fixed WiMAX access can be a more cost-effective than ADSL. In [?], Riding compared the capital expenditure required to provide 20 Mbps and 50 Mbps access to rural households using fiber access, ADSL, and fixed WiMAX links. For 20 Mbps access WiMAX was determined to be the most cost efficient for population densities less than one household per square km and ADSL for densities above this. For 50 Mbps fiber access was determined to be the most cost effective. Zhang studied the economic case for using 2.4 GHz IEEE 802.11b as a last mile access technology in rural Montana [?]. Three use cases were evaluated based on high gain antennas, phased array antennas and multi-hop routing. They concluded that WiFi access is economically viable for systems using high gain antennas and phased antenna arrays. With phased antenna arrays maximum data rates of 11 Mbps at 4.2 km and 1 Mbps at 7.2 km were available.

The strengths and weaknesses for each technology discussed in this section are summarised in Table 2.1. For densely populated areas, fiber access provides the highest data rates, but at the highest cost. ADSL2+ provides a lower cost alternative but data rates are limited once the link length grows beyond 2 km from an exchange, making it suitable mainly for urban and suburban areas but by implication not for rural locations. Existing fixed wireless links provides good alternatives to ADSL in rural areas when the distance between IP-access and the consumer is great, but typically are limited by performance (WiFi) or expense (WiMAX). Despite this, fixed wireless links have proved suitable for delivering internet access where circumstances allow, proven by the increase in wireless ISPs, but the use of the 2.4 GHz and 5 GHz bands limits links in challenging terrain as discussed in Section 2.3. 4G Mobile broadband is a good option for occasional users, if coverage allows, but otherwise is prohibitively expensive. Satellite broadband is generally the last option for rural access if no over coverage is available due to its expense and high latency.

<b>Technology</b>	<b>Strengths</b>	<b>Weaknesses</b>
Satellite Broadband	No ground infrastructure required. Can be installed almost anywhere. Data rates up to 10 Mbps	Large latency can limit real-time applications. Large terminal and subscriptions costs.
Digital Subscriber Line	Uses existing copper wiring infrastructure. High data rates up to 24 Mbps over short distances. Low cost for subscribers and operators.	Limited data rates over 2 km from an exchange and no service over 5.5 km.
Fiber Access	Very high data rate of typically 100 Mbps. Very reliable.	Very large infrastructure costs
Mobile Broadband	Low cost user equipment. Large data rates available	Poor coverage in rural areas. High tariffs.
WiMAX Fixed Wireless	Large data rates available. Practical links up to 10 km	High base station and user equipment costs. Technology still maturing
WiFi Fixed Wireless	Low cost equipment, availability of open source drivers, reasonable data rates, mature low power equipment available	Standard WiFi MAC not suited to long distance links

Table 2.1: Strengths and weaknesses of competing access technologies for rural broadband.

## 2.2 Hopscotch Overview

The Hopscotch rural broadband network uses “WindFi” base stations to provide a solution to the rural broadband problem in a cost-effective manner by extending the reach of fixed telecommunication infrastructure using wireless links.

Figure 2.1 shows a simple scenario for a Hopscotch wireless rural broadband network. IP-backbone is provided at a location such as a 21st century network enabled telephone exchange<sup>2</sup>. A number of subscribers are connected to the IP-backbone by a fibre or copper line but some subscribers may be located too far from the exchange, or the quality of the line may be too poor, to receive reliable broadband at speeds of 2 Mbps or more. An unconnected community can be connected to the IP-access, using PTP links to create a network backbone between WindFi base stations, and PTMP links to illuminate the community. In addition to a standard 5 GHz IEEE 802.11 coverage, the “digital dividend”, discussed in Section 2.3.2, creates an opportunity to use a UHF overlay, providing long distance, non-line of sight (NLOS) coverage, in difficult rural terrain. This allows wireless connections not possible in the wireless solutions described in Section 2.1. This improved coverage allows single base stations to serve a greater area, reducing the cost of access per user. Therefore Hopscotch potentially makes broadband access economically viable without the need for satellite broadband and the performance and cost penalties associated with it.

---

<sup>2</sup>An exchange upgraded from a public switched telephone network connection to digital IP

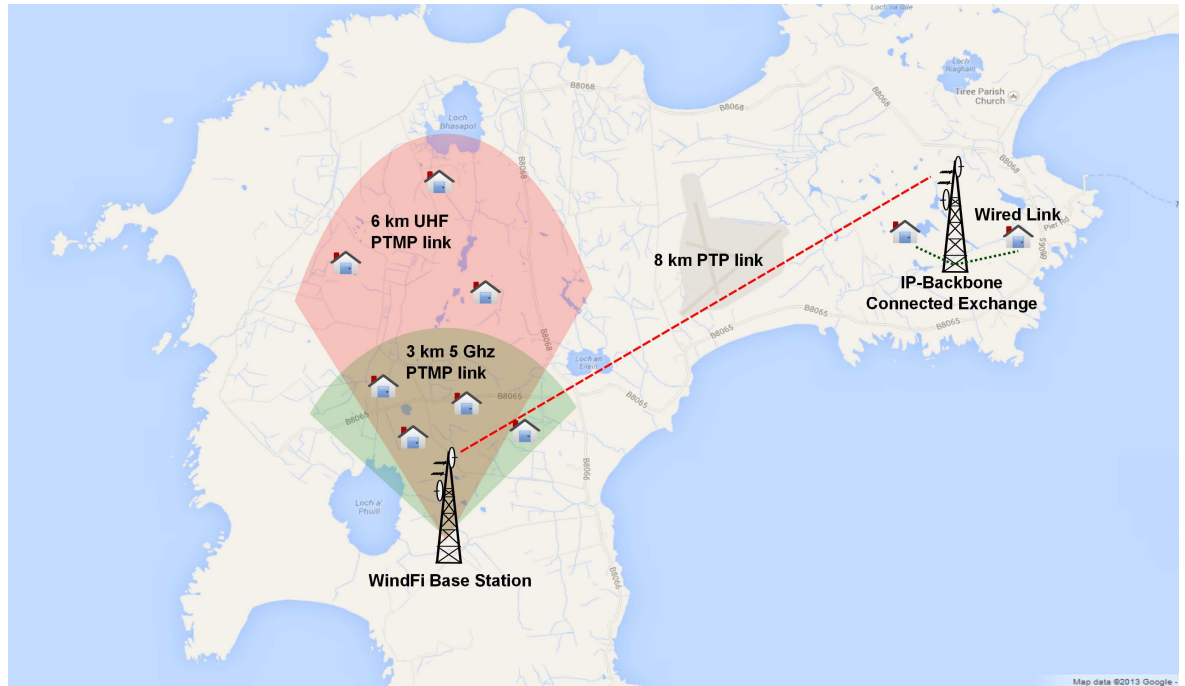


Figure 2.1: Example of an operational Hopscotch network on the the Isle of Tire off the West Coast of Scotland connecting a remote community to IP-backbone.

## 2.3 Radio Frequency Bands

Hopscotch wireless links operate in the 5 GHz band for PTP links and to serve subscribers in close vicinity of the base station. The infrastructure additionally features an overlay TV “white space” (TVWS) network/testbed in a licensed UHF band. A combination of spectral bands allows for an optimum trade-off between channel throughput and coverage for different scenarios. The use of licensed and unlicensed spectrum in the 5 GHz band enables COTS WiFi equipment to operate over a large channel bandwidth with high throughput. TVWS frequencies enable greater coverage from the base station, especially in challenging radio terrain at the expense of a reduced channel bandwidth and throughput. The advantages of TVWS are further discussed in Section 2.5.1.

### 2.3.1 WiFi Wireless LAN Spectrum

Three frequency bands are available for outdoor use with COTS IEEE 802.11a/b/g/n WiFi equipment in the UK, as shown in Table 2.2. The 5 GHz bands B and C are attractive for fixed rural broadband due to the higher equivalent isotropically radiated power (EIRP) limit for transmission compared to 2.4 GHz. Band C is lightly licensed to allow a greater transmit power for fixed wireless links.

Band	2.4 GHz	5 Ghz Band B	5 Ghz Band C
Frequency Range	2400-2483.5 MHz	5470-5725 MHz	5725-5850 MHz
Bandwidth	83.5 MHz	255 MHz	125 MHz
20 MHz Channels	4	11	5
40 MHz Channels	2	6	2
Licence	Licence exempt	Licence exempt	Lightly licensed
Maximum EIRP	100 mW	1 W	4 W

Table 2.2: 5 GHz and 2.4 GHz spectrum and EIRP limitations in the UK for outdoor use [?, ?, ?].

### 2.3.2 TV White Space Spectrum

#### The Digital Dividend

The old analogue television spectrum in Europe is divided into 8 MHz wide channels, ranging from 470 MHz (channel 21) to 862 MHz (channel 69). Spectrum usage in this band varies by geographical location and much of the band is under-utilised, especially in rural areas as shown in Figure 2.2. Globally the switch-over from analogue to digital terrestrial television (DTT) freed a number of channels for alternative uses. This, combined with the ever-increasing demand for connectivity, has caused many national regulators to open up this spectrum for unlicensed secondary use [?, ?]. This has been termed the “digital dividend”.

#### White Space Regulation

In the UK the available TVWS frequencies range between 470 MHz and 790 MHz with 8 MHz wide channels. Secondary reuse of interleaved bandwidths within the DTT range will be allowed by the UK regulator, Ofcom, as long as this will not interfere with a primary, licensed transmission. The interleaved bandwidths available within the DTT range, is referred to as TVWS.

Figure 2.3 shows the current assignment of the old UK analogue TV spectrum by Ofcom. The 600 MHz band (channels 31 to 37) has been cleared but has recently been awarded on an interim basis for DTT multiplexes. The 800 MHz band (channels 61 to 69) has been awarded for licensed 4G services. Channel 38 is reserved for programme making and special events (PMSE). Ofcom has proposed any interleaved spectrum left unused by the new DTT multiplexes should be used for PMSE and “white space” devices (WSDs) [?].

In the UK Ofcom is currently consulting on proposed WSD regulations [?]. A WSD will communicate its device parameters, characteristics and location to a database which will

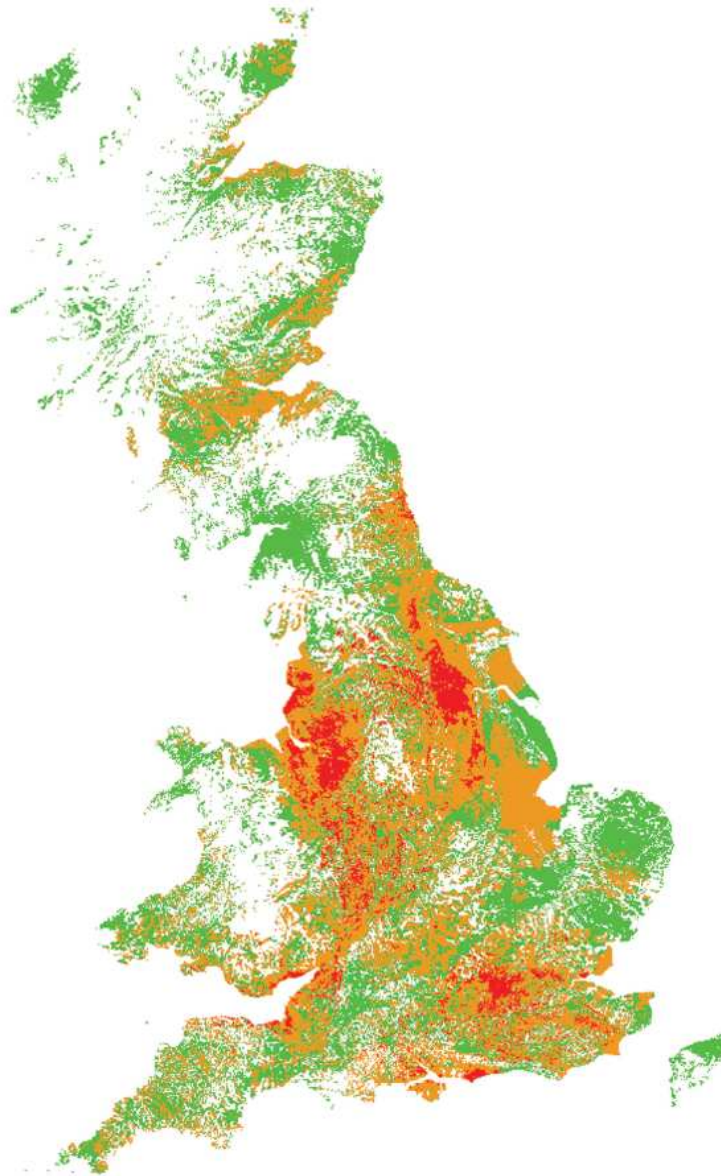


Figure 2.2: TV “white space” availability in the UK. Red: little; green: some; white: much. Diagram taken from [?].

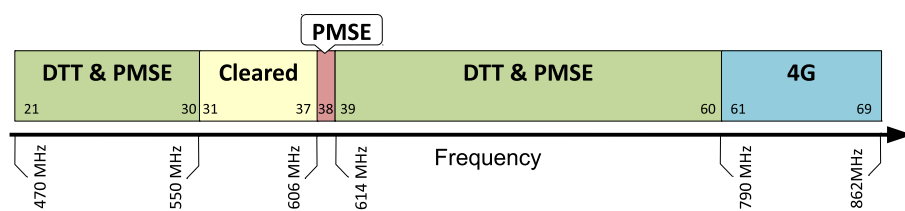


Figure 2.3: 470–862 MHz TV “white space” spectrum [?].

assign the WSD frequency bands and maximum in-band EIRP among other parameters. These parameters will be chosen by the database to assure no interference with a primary user of the band. A WSD will be one of four classes, determined by the spectral mask. This enables the database to allocate WSDs different powers, based on the tightness of their spectral masks, thereby allowing low cost and high performance devices to use TVWS.

In the US, the Federal Communications Commission has already ruled on the use of TVWS frequencies in the US covering 54 MHz to 692 MHz with 6 MHz channels. For fixed devices the maximum allowed EIRP is 4 W in channels 2 to 51 (excluding 3,4 and 37) [?].

### **TV White Space for Rural Broadband**

A number of successful trials using TVWS for wireless broadband access have been carried out all over the world.

In the UK a consortium consisting of the University of Strathclyde, Steepest Ascent, BT, BBC, Berg Design and Net Propagate is testing the use of TVWS for rural broadband access. Eight trialist households are currently served with TVWS on the Isle of Bute [?]. The Cambridge White Spaces Consortium carried out a trial in Cambridge testing TVWS for wireless back haul and as a last mile alternative [?].

There is currently substantial interest in using TVWS for internet access in Africa. Microsoft and Indigo Telecom Ltd. are currently running a pilot in Kenya, providing low-cost wireless broadband access to previously under-served locations with support from the University of Strathclyde's Centre for White Space Communications [?]. Spectrum Bridge and Google trialled TVWS connectivity with ten schools in Cape Town, South Africa [?].

Ofcom has announced a number of projects around the UK to trial TVWS in a working scenario with database lookup [?]. The University of Strathclyde's Centre for White Space Communications together with the Scottish Government, Microsoft, and others, plan to test the provision of wide-area WiFi and broadband access gap-filling in Glasgow using TVWS. Click4internet, KTS and SineCom will trial a rural broadband network on the Isle of White. BT and Neul will use TVWS to monitor traffic congestion along the A14 between Felixstowe and Cambridge. A number of US trials and deployments are currently underway [?, ?].

## **2.4 Wireless Links**

The core of the Hopscotch rural broadband network is based on the IEEE 802.11n standard which exploits techniques such as spatial multiplexing, channel bonding and frame aggregation to maximise throughput [?]. A proprietary TDMA MAC further improves the net throughput of the system over long distances compared to standard IEEE 802.11n.

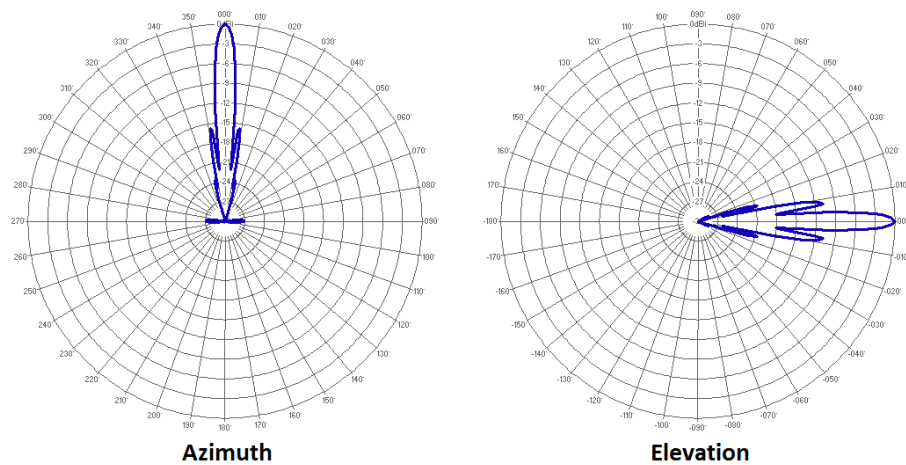


Figure 2.4: Elevation and azimuth radiation patterns for a vertically polarized Ubiquiti RD-5G-30 parabolic antenna. The antenna is typically used in PTP links. The pattern data is supplied by Ubiquiti [?] and visualized using Radio Mobile [?].

Two types of wireless links — PTP and PTMP — are used to create the kind of network described in Section 2.2.

### 2.4.1 Point-to-Point Links

Wireless backhaul between WindFi base stations and IP-backbone is provided by PTP links using very narrow beam widths such as shown in Figure 2.4. In PTP links only two radios are connected to each other, an access point (AP) and a station. PTP links are created using the 5 GHz lightly licensed band-C (5.725-5.850 GHz) with maximum EIRP of 4 W. This 125 MHz spectrum is divided into two non-overlapping 40 MHz wide turbo channels, where each channel supports spatial multiplexing i.e. 2x2 multiple input multiple output (MIMO) streams on vertical and horizontal polarisations. The resulting system with two independent spatial streams supports a theoretical data rate of 300 Mbps.

### 2.4.2 Point-to-Multipoint Links

PTMP links provide access to users over 5 GHz and UHF links. A PTMP link uses one radio, termed the AP to connect to one or more station(s). PTMP links at 5 GHz links provide line of sight (LOS) access up to 3 km, and UHF links provide NLOS coverage up to 6 km.

PTMP links in the 5 GHz band use the unlicensed band-B (5.470-5.725 GHz) with a maximum EIRP of 1 W. The 255 MHz wide spectrum is divided into eleven non-overlapping 20 MHz or six 40 MHz channels. This allows a base station to use a flexible number of sectors to serve a community and provide omni-directional coverage around the base station

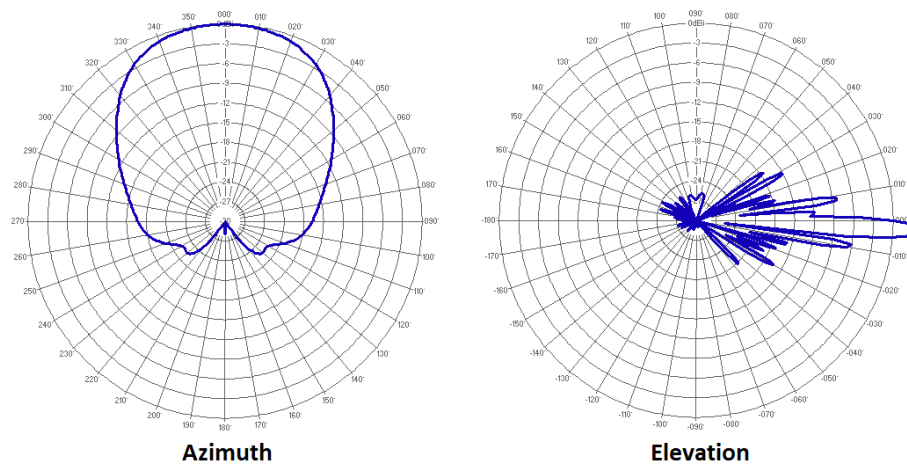


Figure 2.5: The elevation and azimuth radiation patterns for a vertically polarized Ubiquiti AM-5G20-90, 90° sector antenna. The antenna is typically used in PTMP links. The pattern data is supplied by Ubiquiti [?] and visualized using Radio Mobile [?].

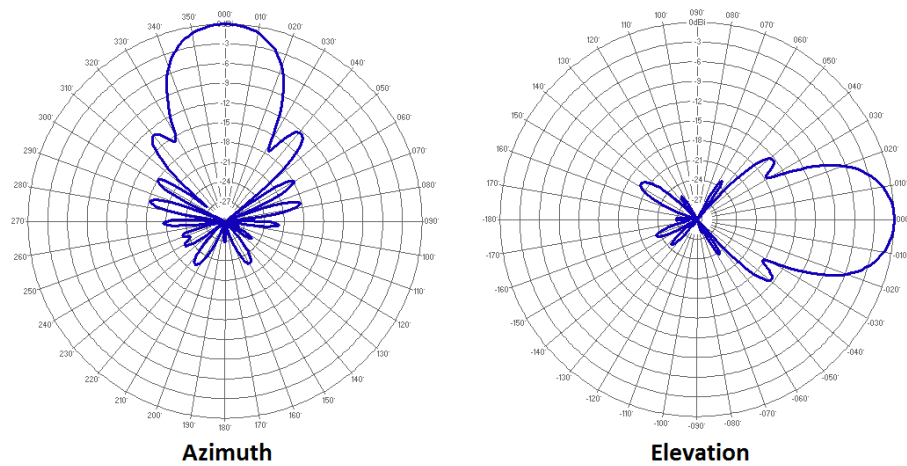


Figure 2.6: The elevation and azimuth radiation patterns for a vertically polarized Ubiquiti AMY-9M16 900 MHz yagi antenna. The antenna is used in PTP and PTMP links. The pattern data is supplied by Ubiquiti [?] and visualized using Radio Mobile [?].

if required. Sector antennas typically cover 60°, 90° or 120° with a radiation pattern similar to Figure 2.5.

UHF links are primarily limited to a 5 MHz bandwidth to fit within an 8 MHz TV channel. It is possible to aggregate adjacent 8 MHz channels depending on their availability within a specific region. This could provide additional channel bandwidth thus resulting in even higher throughput. UHF PTMP links use yagi directional antennas which have a 30%-40% beamwidth as shown in Figure 2.6 and therefore are more selectively positioned to reach households outwith the 5 GHz range.

## 2.5 Frequency Band Selection

The choice of frequency bands used for transmission impacts on the potential coverage and capacity of a wireless network. The use of very high frequency (VHF) or UHF bands is addressed in [?, ?, ?]. Generally it is noted that the propagation characteristics are more benign in the UHF and VHF bands, where NLOS links can be operated, compared to LOS-only transmission in GHz bands. Work in [?] and [?] follows a dual band approach using both UHF and WiMAX / WiFi bands in the 3.5 GHz and 5.2 GHz ranges to provide the best coverage to different population densities. A number of contributions have emerged that suggest the use of cognitive radio techniques within these bands to optimise throughput [?, ?]. The recent use of heterogeneous multiple radio access networks (RANs) is not just regarded as a low cost solution to increase capacity [?], but also offers the opportunity for reducing power consumption by employing complementary technologies whilst maintaining quality of service [?, ?, ?].

While most wireless rural broadband access systems rely on WiFi technologies in the 2.4 GHz and 5 GHz bands, Hopscotch utilises a combination of 5 GHz WiFi and UHF frequency bands for transmission. Therefore, below we analyse how the use of UHF TVWS bands can reduce the burden on base station coverage and transmit power requirements, compared to transmission at 5 GHz.

Section 2.5.1 analyses the differences between UHF and 5 GHz bands, and highlights the advantages of operation within TVWS. Section 2.5.2 analyses how use of UHF frequencies affects the required number of base stations and link transmission power for an example community.

### 2.5.1 Advantages of TV White Space

Wireless networks transmitting in the TVWS band have been estimated to cover four times the area that can be reached via current unlicensed bands in the 2.4 GHz and 5 GHz region, thus reducing the number of base stations required [?]. This can be attributed to the relatively benign propagation characteristics of TVWS frequencies [?]. Conversely, when covering the same area, operation in TVWS frequencies as compared to transmission in the 5 GHz band allows a lower transmit power in the downlink and achieves a better signal-to-noise ratio (SNR) in the uplink. An improved SNR in either link direction increases the capacity of the channel as shown by the Shannon-Hartley theorem [?]. For a communications channel only impaired by additive white Gaussian noise, the channel capacity  $C$  in bits per second is given by:

$$C = BW \cdot \log_2 \left( 1 + \frac{S}{N} \right) \quad (2.1)$$

where  $BW$  is the bandwidth of the channel in Hz,  $S$  is the received signal power in Watts, and  $N$  is the power of the white noise in Watts. Therefore an improved SNR increases the capacity of the channel.

The sections below discuss several factors contributing to the performance of TVWS links which are relevant to rural areas.

### Free Space Path Loss

The transmission loss over a distance  $r$  is frequency dependent as the effective antenna aperture of a fixed gain antenna decreases with increasing frequency. When operating at two different transmission frequencies  $f_1$  and  $f_2$  for isotropic antennas with identical gains, Frii's transmission equation [?] can be rearranged to

$$r_{(f_1)} = \left( \frac{f_2}{f_1} \right) r_{(f_2)} \quad , \quad (2.2)$$

in order to relate the distances  $r_{(f_i)}$ ,  $i = 1, 2$ , over which an equivalent loss is experienced. Thus, given a fixed receive signal level, the propagation range is greater for a lower frequency than a higher frequency [?]. According to (2.2), at 630 MHz, the middle frequency of the TVWS band, range is increased 9 times compared to 5.67 GHz, the middle frequency of 5 GHz bands B and C. Similarly the transmit powers required to receive the same power at the same distance when transmitting at frequencies  $f_i$ ,  $i = \{1, 2\}$  relate by

$$P_{t_{(f_1)}} = \left( \frac{f_2}{f_1} \right)^2 P_{t_{(f_2)}} \quad , \quad (2.3)$$

i.e. to transmit at 630 MHz requires 19.1 dB less power than transmitting at 5.67 GHz under the constraint of identical distances and receive powers.

### Terrain Effects and Diffraction Loss

PTP propagation path loss can be predicted under obstructive, non-LOS conditions between base station and terminal. As the size of the obstruction is much larger than the wavelength of the radio wave, knife-edge diffraction can be used to estimate the shadow loss [?]. The propagation loss  $L_{ke}$  due to knife edge diffraction as sketched in Figure 2.7 can be estimated using the Fresnel diffraction parameter  $v$ . A good approximation is given by

$$v \approx -h_p \sqrt{\frac{2(r_1 + r_2)}{(\lambda r_1 r_2)}} \quad , \quad (2.4)$$

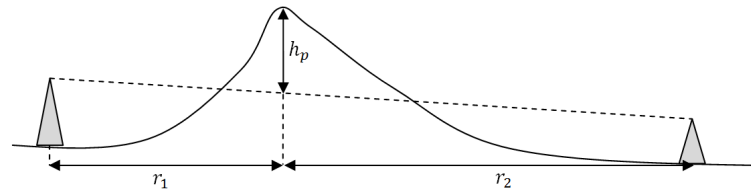


Figure 2.7: Knife edge diffraction parameters.

with  $h_p$  the height difference between the virtual LOS between the transmit and receive antennas and the peak of the obstruction. The quantities  $r_1$  and  $r_2$  are measures of the distances between the edge, and the transmitter and receiver, respectively, as outlined in Figure 2.7. Based on the wavelength  $\lambda$  of the carrier frequency, the propagation loss  $L_{ke}$  can then be calculated using Fresnel integrals [?].

As an example, over a 5 km link with a 30 m knife edge obstruction 900 m from the transmitter, the diffraction loss at 5.67 GHz is 9.4 dB higher than the estimated loss of 20.1 dB at 630 MHz.

## Foliage

Clutter such as vegetation, which can be common in rural environments, affects the propagation of radio waves. Studies have shown the attenuation to depend on both frequency and polarisation of the wave. At vertical polarisation a greater loss is experienced due to the existence of large vertical components in the vegetation medium [?] up to about 1 GHz [?]. Weissberger's mode predicts the propagation loss due to the presence of trees in a point to point link [?], with a path loss  $L_w$

$$L_w = \begin{cases} 0.45 (f)^{0.284} (d) & , \text{ for } 0 \leq d \leq 14 \\ 1.33 (f)^{0.284} (d)^{0.588} & , \text{ for } 14 < d \leq 400 \end{cases} \quad (2.5)$$

for a given frequency  $f$  [GHz] and a depth  $d$  [m] of foliage along the path.

As an example, using Weissberger's model for a foliage depth of 10 m the estimated propagation loss of 7.4 dB due to the foliage obstruction at 5.67 GHz is 3.4 dB higher than the loss experiences at 630 MHz.

## 2.5.2 Network Design Considerations

Using TVWS frequencies provides wider coverage in rural areas compared to the 5 GHz band due to the smaller losses discussed above. This allows households situated further away from the community hub to be reached using fewer base stations or a lower transmit power.

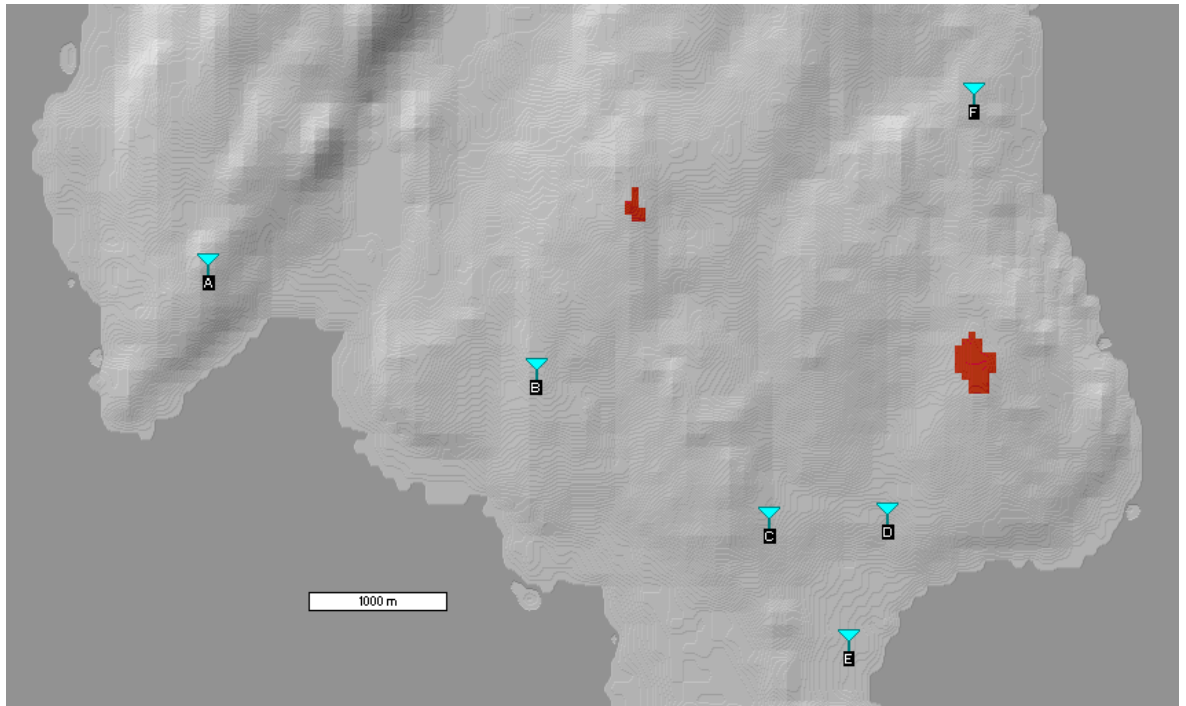


Figure 2.8: Example community with areas for a potential base station to provide coverage at 630 MHz at 1 W EIRP shaded red.

### Base Station Placement

An example community of six households (labelled A to F) for Hopscotch is shown in Figure 2.8. The optimum base station placement to serve this community can be determined using the “Radio Mobile” planning tool [?] for a base station height of 10 m and a maximum permitted transmit power of 1 W EIRP for 5 GHz band-B transmissions. Radio Mobile uses the Longley-Rice propagation model for non-LOS links and the two-ray path model for LOS links [?]. The effects of foliage and other clutter have been ignored for this study but could be the subject of a future study using geographic information system (GIS) data. When using 5 GHz band-B, no single base station can cover all six stations given a minimum received signal strength of  $-85$  dBm, the minimum receive signal strength observed during trial tests to maintain a reasonable connection. At TVWS frequencies (630 MHz for this analysis) two locations allow coverage of all six stations as shown by the red shading in Figure 2.8.

Whilst no single base station using 5 GHz bands can serve the community at 1 W EIRP, coverage for the entire community can be achieved by introducing two communicating base stations as shown in Figure 2.9; base station A (BSA) and base station B (BSB). BSA can serve stations C, D, E and F with omnidirectional coverage and BSB can serve stations A and B.

Using a combination of 5 GHz and UHF frequencies for this scenario allows the available data rate to be maximized for each station using only one base station. BSA can serve stations

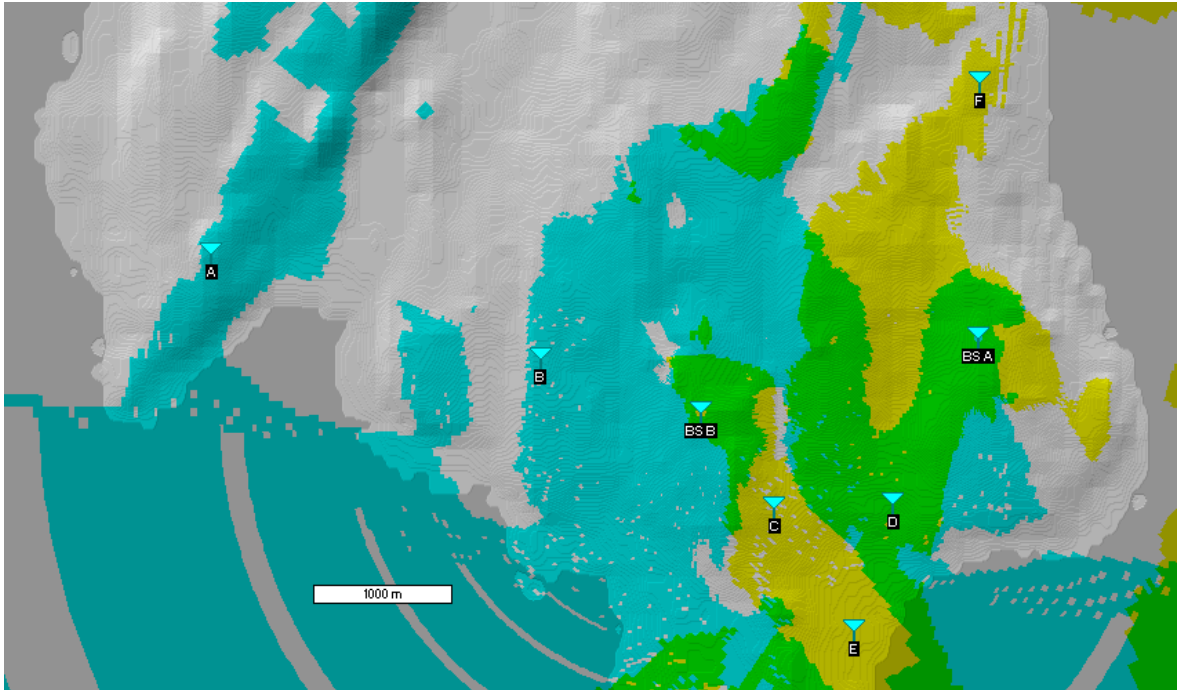


Figure 2.9: Coverage provided by two base stations at 5660 MHz 1 W EIRP, with yellow shading representing coverage provided by base station A (BSA), blue shading representing the coverage provided by base station B (BSB), and the overlapping coverage indicated by green shading.

C, D, E and F at 5 GHz, providing a greater bandwidth and hence data rate for stations. A UHF overlay on BSA also allows it to service stations A and B without the need for an additional base station.

### 2.5.3 Link Transmission Power

An alternative to adding additional base stations at 5 GHz to cover all stations is to increase the transmit power above 1 W EIRP. This may be possible in some regulatory environments. To demonstrate the required transmission power two links are considered between base station BSA and stations A and D. The elevation profiles of two links are shown in Figures 2.10(a) and 2.10(b). The link between BSA and station A is 5.6 km long and is NLOS. The link between BSA and station D is 1.35 km long and contains no obstructions. The expected received signal power  $P^{rx}$  in dBm for a given transmission power  $P^{tx}$ , transmit and receive antenna gains ( $G^{tx}$ ,  $G^{rx}$ ) line losses ( $U^{tx}$ ,  $U^{rx}$ ) and path loss  $L$  is given by:

$$P^{rx} = P^{tx} + G^{tx} - U^{tx} - L + G^{rx} - U^{rx}. \quad (2.6)$$

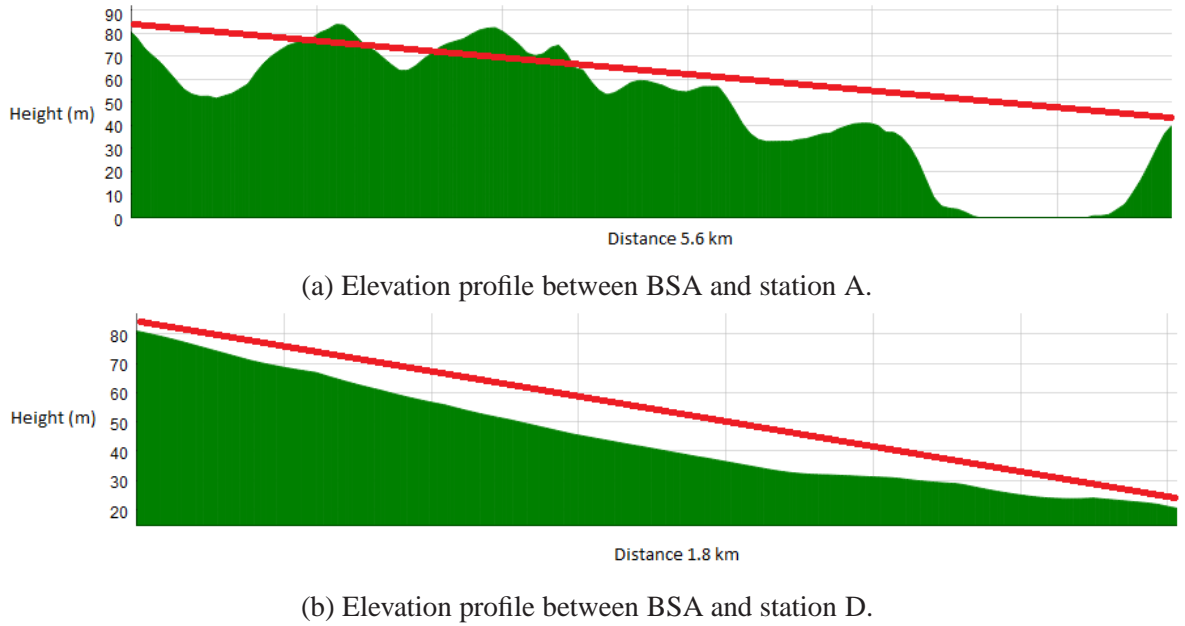


Figure 2.10: Terrain profiles showing elevation between BSA and stations A and D.

Similarly for a given receive power the required transmit power in decibels can be calculated:

$$P^{\text{tx}} = P^{\text{rx}} - G^{\text{tx}} + U^{\text{tx}} + L - G^{\text{rx}} + U^{\text{rx}}. \quad (2.7)$$

Using (2.6) and (2.7), Table 2.3 shows the simulated path loss between BSA and stations A and D and the expected receive power given a transmit and receive antenna gain of 14 dBi, line losses of 0.5 dB and an EIRP of 1 W. The required transmission power to create a link with a received signal strength of  $-85$  dBm is also calculated. To create a link between BSA and station A a substantial EIRP and therefore transmission power would be required in the 5 GHz band which is not permitted in the UK and is detrimental for a renewable powered system due to increased power consumption as demonstrated by the power consumption analysis of radios presented in Chapter 4.

Table 2.3 also contains expected link performance at UHF frequencies using the same system parameters. A substantial reduction in path loss is expected at UHF frequencies compared to 5 GHz, especially in the longer NLOS link. Therefore when using a UHF link, the propagation characteristics allow a reduction in transmit power or an increase in receive power compared to the 5 GHz band, reducing power consumption in the power amplifier or improving station throughputs by allowing higher order modulation and coding scheme (MCS) to be used. Reducing the transmission power is also favourable as interference to neighbouring base stations will be minimised. As each link is fixed the transmission power can be set during installation using channel measurements to achieve the desired receive signal strength.

	Station A, 5.60 km		Station D, 1.53 km	
	630 MHz	5660 MHz	630 MHz	5660 MHz
<b>Path Loss</b>	117.8 dB	144.6 dB	97.2 dB	114.6 dB
$P^{rx}$ given $P^{tx} = 1 \text{ W}$	-74.3 dBm	-101.1 dBm	-53.7 dBm	-71.1 dBm
$P^{tx}$ given $P^{rx} = -85 \text{ dBm}$	5.8 dBm	32.6 dBm	-14.8 dBm	2.6 dBm

Table 2.3: Link calculations and transmit and receive powers between the base station and stations A and D, given a transmit power and receive power.

## 2.6 Ring Network Architecture

An example Hopscotch network serving multiple communities is shown in Figure 2.11. IP-backbone access is available at one location and provides connectivity to a ring network. The network consists of a number of WindFi base stations. These base stations are designed specifically for use in a rural broadband network as discussed in Chapter 3. A number of communities are illuminated using 5 GHz and UHF PTMP links, both mounted on a WindFi base station. WindFi base stations are connected together using 5 GHz PTP links to form a ring between the two access points. This creates redundancy in the network, as in the case of one Hopscotch repeater being shut down, IP access for other nodes is maintained as one path to the backbone will still be available. Spurs from the main loop can connect additional communities as required.

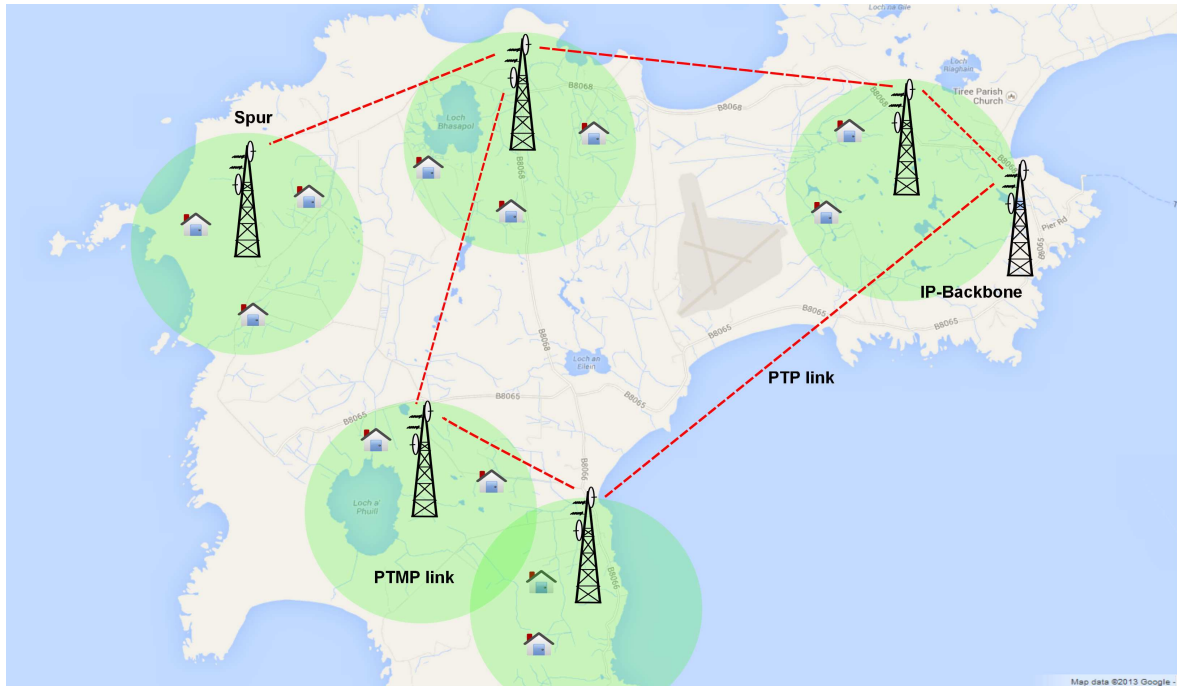


Figure 2.11: Example loop network connecting several communities to the IP-backbone via PTP and PTMP links. PTP links are shown as red dotted lines. PTMP links are shown by a green overlay.

## 2.7 Summary

This chapter presented Hopscotch as a potential solution to the rural broadband problem introduced in Chapter 1. Utilising two radio access networks (RANs) — a 5 GHz network and overlay UHF TVWS network — allows the beneficial properties of UHF TVWS spectrum to overcome the limitations of existing rural access technologies summarised in Section 2.1. The general architecture of a Hopscotch network and the types of links used were introduced. The properties of these links are important when considering the design of base stations to create a network. The design of WindFi base stations used to support these links to create a network is discussed in Chapter 3. The advantages of the TVWS band were presented in a rural broadband access context. These advantages can be traded off against the advantages of using the 5 GHz band. Optimising this trade-off for energy efficiency is discussed in Chapter 6.

## Chapter 3

# “WindFi” Base Station

In order to realise the wireless rural broadband access network of Chapter 2, this chapter reviews the radio equipment currently used in similar networks and reports the design, construction and deployment of equipment used in Hopscotch. Section 3.1 provides review of existing approaches, and establishes the need for a dedicated solution. This system, subsequently termed a “WindFi” base station, is outlined in Section 3.2 and a detailed description of the radio equipment used within the system is given in Section 3.3. This provides an overview of the various radio payloads used on WindFi and the demands they impose on the power system. Section 3.4 provides an overview of the use-cases for the WindFi base station which drives the power requirements of different base station configurations given the radio equipment. Section 3.5 gives an overview of the mechanical structure of the base station and design specification which influences the power system. Section 3.6 discusses the requirements of other supporting electronic systems. In Section 3.7 the power system is sized, and the renewable generation requirement calculated for different WindFi configurations driven by use-cases. Section 3.8 uses recorded data to analyse the performance of a power system for an installation on the Scottish island of Tiree, described in Chapter 5, given design requirements.

### 3.1 Renewable Powered Wireless Networks

Recently a trend has emerged towards using renewable energy to power wireless network infrastructure. Renewable energy sources are appealing for a number of reasons. Remote regions, where grid supplied power is either unavailable or unreliable, often utilise diesel generators to provide power [?]. In addition to emitting CO<sub>2</sub>, diesel generators can be costly to run due to ever increasing fuel costs and the added expense of fuel transportation to remote areas. Renewable energy sources such as wind turbines and photovoltaic (PV) arrays are an attractive alternative for remote telecommunications installations both environmentally and

	Phoenix, AZ	Toronto, ONT	Yellowknife, NWT
Battery Capacity	14.2 Ah	30.5 Ah	92.6 Ah
PV Peak Power	15 W	40 W	67 W

Table 3.1: SolarMESH cost-optimal battery and PV capacities for three locations and a 2 W base load.

economically. An off-grid renewable power system allows a base station to be placed in the optimum location to serve users, as discussed in Chapter 2, requires no infrastructure to connect to an existing power source and, as no fuel is required, has minimal operating costs. A number of projects which use wireless nodes powered by renewable energy sources to create a fixed wireless access network are discussed below.

### Tegola

Tegola is a testbed connecting 15 houses in rural communities on the Glenelg and Knoydart mainland peninsulas to the Sleat peninsula on the Isle of Skye with long distance wireless links between 7.6 km and 19 km [?]. A Rutland Furlmatic FM910-3 wind turbine producing 24 W at 5 m/s and an 130 W Kyocera KC130GH T-2 PV module charge two Elecsol 125 Ah 12 V deep cycle batteries to power networking equipment. An Avila GW2348-4 single board computer (SBC) provides 2.4 GHz access using a Ubiquiti XtremeRange2 (XR2) radio, and three Ubiquiti XtremeRange5 (XR5) radios provide IEEE 802.11a 5 GHz backhaul links. 29 dBi antennas are used for backhaul with dual polarity support. Local access uses a 19 dBi panel antenna. CPEs are Ubiquiti NanoStations. OpenWRT operates on all nodes with a slightly modified MadWiFi driver.

### SolarMESH

SolarMESH is a solar powered IEEE 802.11 mesh and relaying infrastructure solution developed at McMasters University where APs are solar powered and rely on a battery bank [?]. They have studied sizing the PV and battery banks for defined outage probabilities and found a cost-optimal configuration for different locations with different PV power outputs summarised in Table 3.1 for a 2 W load.

### EHAS Group

The Enlace Hispano-Americano de Salud (EHAS) group developed an IEEE 802.11 based mesh network consisting of solar powered nodes for delivering healthcare in remote areas of developing countries [?]. Nodes are based on WRAP and Soekris SBCs and use Ubiquiti

	Daily energy required	PV peak power	Battery capacity
Soekris+ 1 * SR2 + 2 * Proxim	155.75 Wh	62 W	105 Ah
WRAP + 2 * CM9	109.7 Wh	44 W	74 Ah

Table 3.2: EHAS node power estimates for two hardware combinations.

SuperRange2 (SR2), SuperRange Cardbus (SRC) and Wistron CM9 and Proxim Orinoco Gold radios. A power system was dimensioned for each hardware combination used, based on solar irradiation for the worst month of the year. Table 3.2 gives dimensions for two combinations.

### QuRiNet

QuRiNet is situated in the Quail Ridge natural reserve and provides the backbone for transporting ecological and environmental data from the field to the lab [?]. A total of 34 mesh nodes, with multiple radios, are powered with PV modules. Soekris net4826 SBCs are used with Ubiquiti SR2 cards providing 2.4 GHz IEEE 802.11b/g. Three size of PV modules are used: 50 W, 115 W, and 120 W. Morningstar Tristar and SunSaver charge controllers are used with DEKA 12 V 98 Ah gel-cell batteries [?].

### Renewables as a Backup Energy Source

In areas with an unreliable and intermittent power supply, wind and solar have been suggested as suitable technologies to provide backup power to communication infrastructure. In the India Digital Gangetic Plains project, IEEE 802.11a/b/g has been used for long distance links up to 39 km. Nodes use PV and battery banks for backup due to an unreliable power supply [?]. A similar system has been using wind and solar installations to provide backup power to IEEE 802.11 last mile links is used in the Serengeti Broadband Network [?]. Grid power quality data collected over two months from the network is presented and used to calculate the feasibility of using solar and wind energy as alternative energy sources.

### Summary and Comparison

Renewable energy sources are used by wireless networks for two reasons:

*Backup power supply.* Small-dimensioned renewable systems can be used to provide power for a limited time when a standard cheap, but unreliable energy source such as diesel is unavailable [?, ?]. As the power system does not have to be dimensioned to power the

system continuously, this reduces the initial cost of the system, but there is a risk of outages if the normal energy supply is not restored quickly and infrastructure is required.

*Infrastructure Independence.* Networks providing connectivity in remote locations such as EHAS [?], QuRiNet [?] and SolarMESH [?] are solely powered with renewables as this provides the freedom to place radio equipment where connectivity is required and no infrastructure exists. Relay stations such as used in Tegola [?] also benefit by being able to select the most suitable locations for radio propagation. This freedom creates conditions suitable for long distance LOS links required by these networks due to the frequency bands used.

Despite the success of the discussed networks, all of the networks reviewed in this section are mesh networks which suffer from self-interferences which limit performance [?]. Additionally due to the frequency bands used a number of the networks rely on long distances links being LOS. This limits the scope of networks in rural areas where terrain may be challenging.

## 3.2 The Need for WindFi

WindFi offers different capabilities than current renewable-powered wireless network nodes reviewed in Section 3.1. WindFi is designed to operate using PTP and PTMP links and not in a mesh configuration as in [?, ?, ?, ?] introduced above. This removes interference common to mesh networks [?], allowing higher data rates, but leads to reliance on long PTP links in difficult terrain. To overcome this, WindFi uses a mast to gain elevation and motorised antenna mounts to allow accurate antenna bore sighting for long distance links, as discussed in Section 3.6.

The use of both TVWS bands and 5 GHz bands to deliver LOS and NLOS access provides an additional burden on a wireless node, compared to a single band system. The use of multiple overlay networks requires more radios and has a greater power consumption, therefore WindFi offers a larger generation capacity and storage system than the reviewed systems, as discussed in the following sections.

The WindFi wireless base station is a low-power, low-cost autonomous unit, powered by a combination of wind and solar renewable sources. The base station is designed to support multiple radio payloads, allowing it to be used as a flexible research platform and tailored to suit the need of individual communities as a commercial product. The use of renewable energy allows each base station to operate independently of fixed electrical infrastructure, facilitating flexible and optimised placement. Figure 3.1 shows a prototype WindFi mast. The WindFi mast consists of the following components: the mechanical mast structure, the radio payload, the electrical power system and supporting electronics for remote monitoring and control. These are described in detail in the following sections.



Figure 3.1: Prototype “WindFi” base station on the Isle of Bute, Scotland. The base of the unit includes photovoltaic modules and a battery bank (underground). The 10 m mast supports the wind turbine, antennas and radio equipment, housed in an orange weather-proof case just below the wind turbine.

## 3.3 Radio Equipment

The radio equipment requires by far the most energy from the WindFi power system. This section describes the types of radio equipment used and the impact on power consumption. Two categories of radio hardware have been used for Hopscotch networks and are supported on WindFi base stations; integrated radio and antenna units and SBCs with radio daughter cards. Integrated radio and antenna units are low-cost and simple to configure, but consume more power than SBC solutions.

### Integrated Radio and Antenna

The following units have been used with WindFi:

- Ubiquiti NanoStation NSM5 (NSM5) - Integrated radio and sector antenna 60° beam width (16 dBi at 5 GHz), maximum power consumption 8 W [?].
- Ubiquiti NanoBridge M5 (NB-5G22) - Integrated radio and directional antenna (22/25 dBi at 5 GHz), maximum power consumption 5.5 W [?].
- Ubiquiti Rocket M5- High power radio, maximum power consumption 8 W [?].

Ubiquiti NSM5 and NB-5G22 units are typically used within Hopscotch as CPEs in PTMP links due to their low cost. The Rocket M5 can be paired with a sector, dish or omnidirectional antenna for deployment as an AP in PTP or PTMP links. Ubiquiti equipment was used as opposed to alternatives offered by vendors such as EnGenius and Cisco due to lower cost and previous experience within the Hopscotch team [?].

### Single Board Computer with Radio Daughter Cards

The emergence of ultra low voltage yet computationally powerful processors such as the Intel Atom and ARM based embedded processors allow a single processor to manage multiple radio interfaces on a modest power budget. The MAC for each radio runs on the SBC along with routing and control software. The following SBCs have been trialled with WindFi:

- Mikrotik RouterBOARD 411, maximum power consumption 4 W without daughter cards. 1 mini-PCI slot [?];
- Mikrotik RouterBOARD 433AH, maximum power consumption 9 W without daughter cards. 3 mini-PCI slots [?];

Option	$P_{\text{total}}$	$P_{\text{total}}$ per sector	$\tilde{C}_{\text{total}}$ per sector
3 × Ubiquiti Rocket M5	24 W (8 W × 3)	8 W	£80
RSPro + 3 × SR71	19.3 W (7 W + 4.1 W × 3)	6.4 W	£115
433AH + 3 × SR71	21.3 W (9 W + 4.1 W × 3)	7.1 W	£115

Table 3.3: Power consumption per sector for AP configuration options.

- Ubiquiti RouterStation Pro (RSPro), 7 W power consumption when processing 1 Gbps traffic. 3 mini-PCI slots [?].

The following mini-PCI radio cards have been used with the SBCs:

- Ubiquiti SuperRange71 (SR71) - 2.4/5 GHz radio with 10/20 MHz bandwidth, maximum power consumption 4.1 W [?].
- Ubiquiti XtremeRange7 (XR7) - 700 MHz radio with 5/10/20 MHz bandwidth support, maximum power consumption 3.6 W [?].

These SBCs and radio cards have been selected over alternatives such as Avila and Soekris used in [?, ?, ?] due to availability and the quality of supplied software [?, ?].

### Comparison

When multiple sectors are required at one location to serve a community, a combination of SBC and radio daughter cards consumes less power than multiple discrete Ubiquiti Rocket M5s. This is the scenario for WindFi base stations. Table 3.3 gives three options for providing access to three sectors and the associated total power consumption of each configuration,  $P_{\text{total}}$ , and approximate cost,  $\tilde{C}_{\text{total}}$ . The total power consumption is the reported maximum according to the supplied data sheet. The SBC with daughter cards has a combined lower maximum power consumption per sector than individual Ubiquiti Rocket M5s, but costs more.

## 3.4 WindFi Use-Cases

The Hopscotch network relies on the use of WindFi masts and base stations. The WindFi mast is designed to support different types of radio hardware as payload described in Section 3.3. All equipment is attached to the main mast via standard jaw clamps, and powered

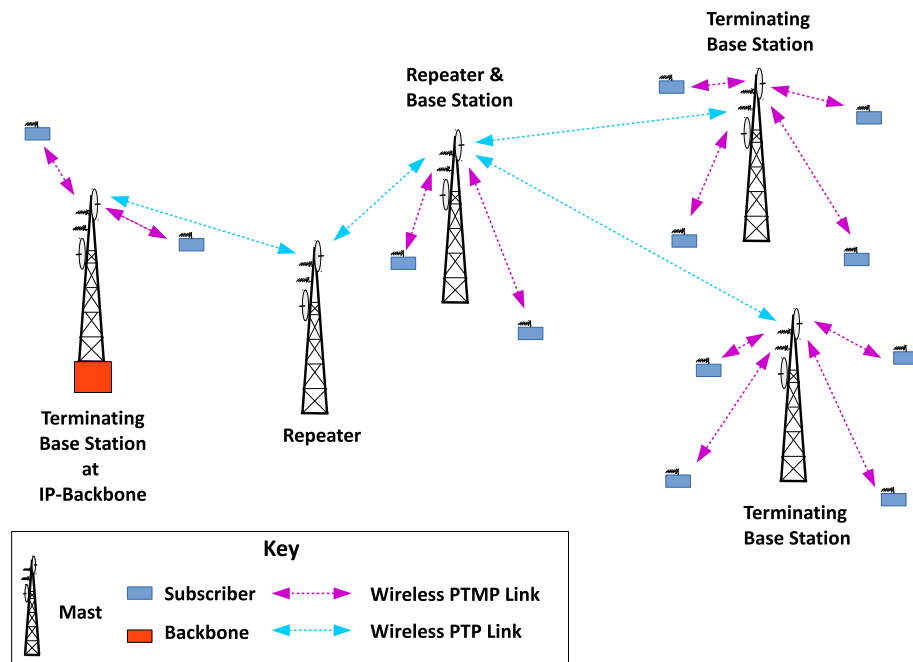


Figure 3.2: Use cases for WindFi masts in a Hopscotch rural broadband network: repeater, repeater & base station and terminating base station.

by the mast's power system via cables which run through the centre of the mast. The masts provide elevation which is desirable for wireless links to remove objects from the Fresnel zone [?]. Figure 3.2 shows three different use-cases for a mast:

- Terminating base station
- Multi-hop repeater
- Multi-hop repeater and base station

The following subsections describe each of these use-cases exemplified by base stations on Tiree with the aid of coverage maps in Figures 3.3, 3.4 and 3.5. In the maps, markers plot the locations of users covered by the base stations on Tiree. Overlaid is an estimate of the use-case radio coverage area calculated using the Radio Mobile planning tool [?]. Radio Mobile uses the Longley-Rice propagation model for NLOS links and the two-ray path model for LOS links [?]. The tool was used with the radiation patterns of the specific antennas (as shown in Section 2.4), a frequency range of 5.2 to 5.8 GHz, transmit powers of 30 dBm, and antenna heights of 6 m. The coloured areas represent coverage exceeding a minimum receive signal power of  $-95$  dBm. All parameters are consistent with equipment operating within the network.

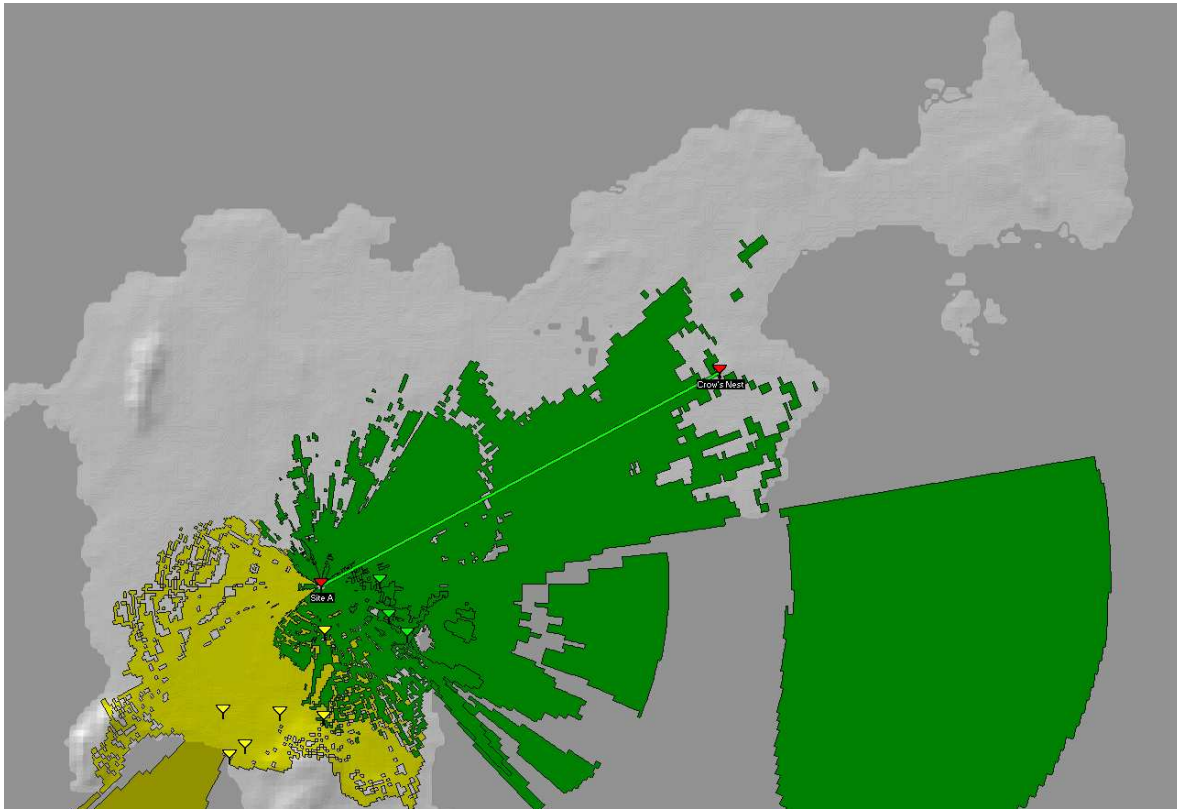


Figure 3.3: Estimated coverage of “Site A” terminating base station.

### 3.4.1 Terminating Base Station

In this scenario the WindFi base station is connected to IP-backbone by a wireless backhaul link and serves a number of subscribers using one or more radio frequency (RF) channel. The WindFi mast therefore requires a single PTP radio and one or more PTMP radio(s).

Figure 3.3 shows the estimated coverage of the terminating base station “Site A” and associated stations. This base station provides coverage to two 90° sectors, shown in yellow and green in Figure 3.3. The yellow sector provides coverage for six subscribers and the green sector provides coverage for three subscribers. IP access is provided by a PTP link with the relay “Crow’s Nest”. The two PTMP sectors are provided by Ubiquiti Rocket M5 radios and the PTP backhaul is provided by a Ubiquiti NB-5G22.

### 3.4.2 Multi-Hop Repeater

In the multi-hop repeater scenario the WindFi mast serves as a repeater between the backbone and subscribers but does not serve subscribers directly. The WindFi mast therefore requires two or more PTP radios. Repeaters are also likely to be located in remote and exposed areas to suit radio propagation characteristics, therefore on-grid power may not be available.

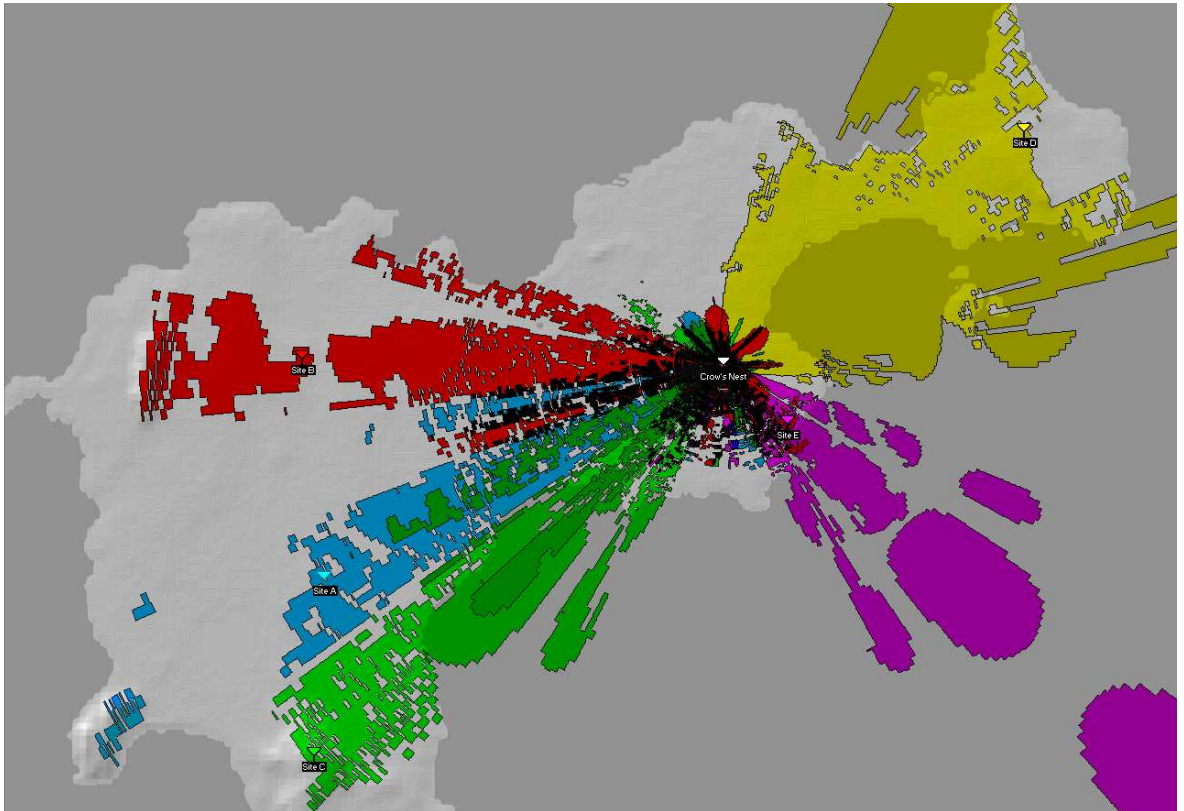


Figure 3.4: Estimated coverage of “Crow’s Nest” multi-hop repeater.

Figure 3.4 shows the estimated coverage provided by a repeater WindFi base station to a number of other base stations and users<sup>1</sup>. This repeater base station is the white marker labelled as “Crow’s Nest”. This base station is key to the Tiree rural broadband network as it repeats IP-backbone from “Site E” (the purple marker) to other base stations on the island. It is located on an exposed elevation with no mains power. The red, blue, green and yellow coverage areas in Figure 3.4 are PTP links to provide connectivity to base stations “Site A”, “Site B”, “Site C” and “Site D”. The IP-backbone is provided by “Site E” and the purple coverage area denotes the PTP link between the repeater base station and this IP-backbone. The red, blue and green coverage areas are using directional Ubiquiti NB-5G22s and the yellow and purple areas are using Ubiquiti NSM5s.

### 3.4.3 Multi-Hop Repeater and Base Station

This is the most complex scenario where a WindFi base station will serve subscribers and also act as a repeater to other base stations. In this scenario multiple PTP radios and one or more PTMP radios are required.

Figure 3.5 shows the estimated coverage of a multi-hop base station “Site B” on the isle of

<sup>1</sup>The fading in-and-out of signal strength over water, visible by disconnected blocks of colour, is likely due to the model of propagation over water as the effect is not visible on land.

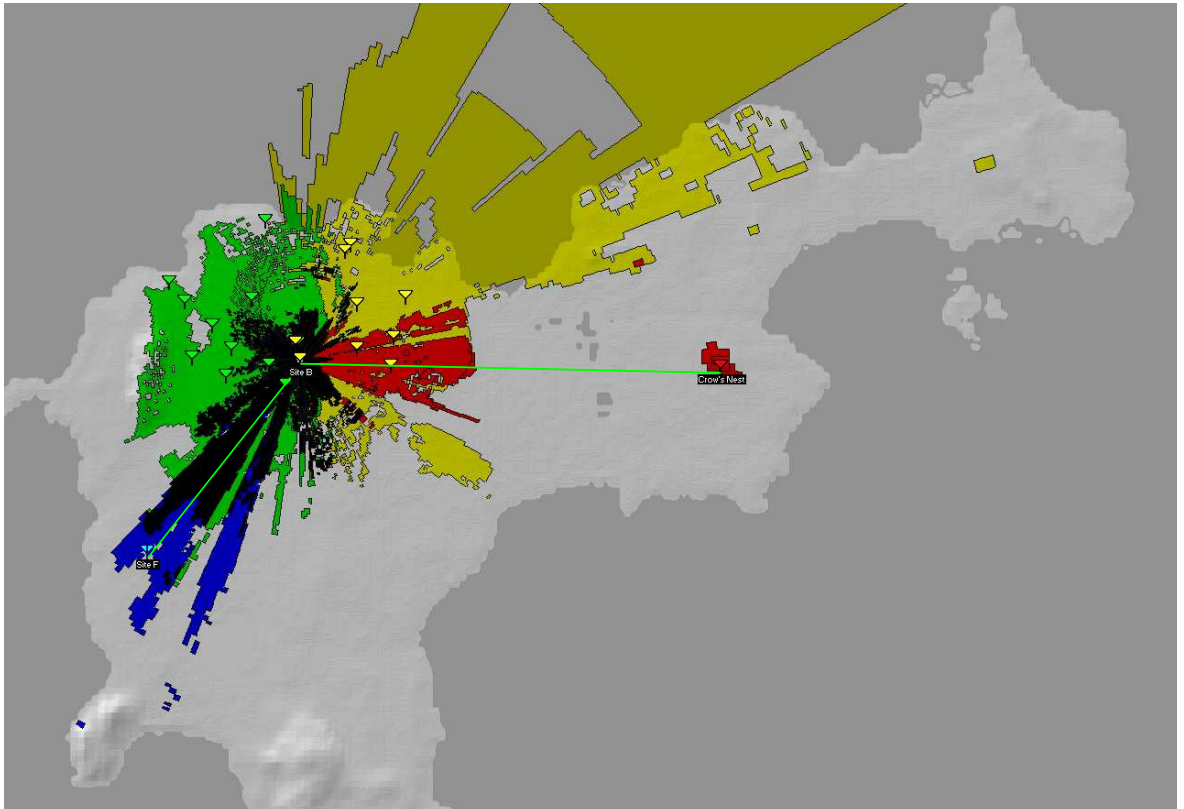


Figure 3.5: Estimated coverage of “Site B” multi-hop repeater and base station. This relays connectivity between “Crow’s Nest” and “Site F” whilst also serving subscribers.

Tiree. Two sectors provide coverage in the green and yellow areas. The green PTMP sector is created with a  $120^\circ$  sector antenna and serves eleven subscribers (the green markers). The yellow PTMP sector is created with a  $90^\circ$  sector antenna and serves eight subscribers (the yellow markers). This terminating base station is provided with IP connectivity via a PTP link from “Crow’s Nest” and repeats this access to a terminating base station “Site F”. The red and blue areas are PTP coverage to repeat IP access. The two PTMP sectors are provided by Ubiquiti Rocket M5 radios and the PTP backhaul is provided by and extended using Ubiquiti NB-5G22s.

### 3.5 Mechanical and Structural Mast Requirements

The WindFi mast is a single-pole design, anchored to the ground without the use of permanent foundations. Guy wires are used to add stability and reduce flexing. The pole’s outside diameter is sized to allow standard jaw clamps to be attached and serve as a platform for radio equipment.

The mechanical structure was designed by a Scottish mechanical design firm, Berg Design. A tripod base structure with a circumference diameter of up to 3 m provides structural stability

as a base for the pole. The feet of the tripod are capable of being anchored to the ground in one of three possible ways:

1. bolted to wooden posts that have been sunk into the ground to a depth of at least 1 m;
2. bolted to a non-penetrating, surface-mount frame that has suitable weights to keep it stationary and stable; or
3. bolted directly to a pre-existing concrete base at the installation site.

A hinged bracket is mounted to the top of the tripod, and the main mast pole is supported by the hinge bracket for raising and lowering the mast from horizontal to vertical.

The mast is designed so installers do not have to climb the mast when it is in the vertical position. This reduces the required strength and size of the mast. Therefore, all payload is attached while the mast is horizontal, and the mast is then raised and secured in the vertical position. All assembly and manual adjustment of components takes place at a height no greater than 2.5 m from ground level.

The WindFi mast is designed to be packaged within a volume of 3 m x 1 m x 1 m and weigh no more than 300 kg (including all electronic equipment and radio antennas, but not including batteries). This requires that the mast structure, battery housing, solar panel framework, and dish antenna tracking modules all have a combined weight of no more than 200 kg. All parts and tools are transportable by Land Rover-style vehicles and/or aircraft. Individual parts weigh no more than 25 kg to allow single-person lifting.

## 3.6 Monitoring and Control

In addition to the radio hardware the WindFi mast includes supporting hardware for remote monitoring and control.

A Modtronix SBC68EC SBC [?] has been selected as the mast controller which enables devices with a controller area network (CAN) or RS-232 interface to be controlled or monitored remotely. The mast controller was developed to control an antenna motorisation system using CAN bus, and monitor a charge controller over RS-232. An Ethernet connection allows remote monitoring and control via simple network management protocol (SNMP). The mast controller has a nominal power consumption of 0.7 W.

PTP links using highly directional and narrow beam-width parabolic antennas need to be precisely positioned in elevation and azimuth to ensure the strongest possible link is created. As the WindFi mast is designed not to be scaled when vertical, a remote motorised antenna positioning system is required for accurate antenna positioning and, if required, remote network

reconfiguration. A brushed direct current (DC) motor is used to drive the azimuth rotator and a linear actuator used to drive the elevation control. Motors run at a nominal 12 V or 24 V and therefore can be selected according to the size of battery bank (12 V or 24 V). The motorisation of each antenna is controlled by a motor control unit which consists of a CAN bus enabled AVR microcontroller and power electronics to control the elevation and azimuth motors. The motor control units are only powered when in use and the motorisation system is only infrequently activated, therefore motor control energy consumption is not considered when dimensioning the WindFi power system.

## 3.7 Electrical Power System

The electrical power system for the WindFi base station is designed to support the radio hardware required for the use-cases discussed in Section 3.4 and the supporting monitoring and control hardware discussed in Section 3.6. WindFi base stations can be powered by mains electricity when available but the use of low-power equipment allows renewable energy sources to be used with a battery bank to power the base station.

### 3.7.1 Base Load

Two generalised WindFi power system configurations are proposed to meet the three use-cases; “large” and “small”. Two configurations allow the mechanics of the base station, such as wind generator mountings, PV dimensions and battery bank housing volume to be standardised for production:

- the “large” configuration allows for a maximum base load of 50 W; and
- the “small” configuration allows for a maximum base load of 25 W.

These base loads are designed to allow the combination of the most power hungry radio equipment required to satisfy the use cases introduced in Section 3.4.

Table 3.4 shows how a large or small power generation configuration,  $P_{\text{config}} = \{50 \text{ W}, 25 \text{ W}\}$ , can be used to satisfy each generic base station (BS) use-case described in Section 3.4. The total power consumption,  $P_{\text{total}}$ , is calculated by summing the maximum power required for each item of radio equipment. It is assumed that 8 W integrated radio and antennas such as the Ubiquiti NSM5 and Ubiquiti Rocket M5 are used, with four PTMP sectors providing community access. As discussed in Sections 3.4.1 and 3.4.3, two 5 GHz PTMP sectors provide suitable coverage for a small number of users in flat terrain. The provision for four PTMP sectors allows a UHF overlay to be used with a third 5 GHz PTMP sector to provide

Use-case	Configuration	PTP	PTMP	Radios Used	$P_{\text{total}}/P_{\text{config}}$
Terminating BS	Large	1 × 8 W	4 × 8 W	5/6	40/50 W
Repeater	Small	2 × 8 W	0 × 8 W	2/3	16/25 W
Repeater and BS	Large	2 × 8 W	4 × 8 W	6/6	48/50 W

Table 3.4: PTP and PTMP radio requirements for WindFi use-cases and associated power consumption power system configurations.

Use-case	PTP	PTMP 5 GHz	PTMP UHF	SBCs	$P_{\text{total}}/P_{\text{config}}$
Terminating BS	1 × 4.1 W	2 × 4.1 W	2 × 3.6 W	2 × 9 W	37.5/50 W
Repeater	2 × 4.1 W	0	0	1 × 9 W	17.2/25 W
Repeater and BS	2 × 4.1 W	2 × 4.1 W	2 × 3.6 W	2 × 9 W	41.6/50 W

Table 3.5: Power consumption used out of maximum using PTP and PTMP radio daughter cards and Mikrotik RouterBOARD 433AH SBC for different use-cases.

additional capacity as required. Two PTP links are required when repeating IP, while only one PTP link is needed for a terminating base station. If the combined power consumption of the radio hardware and monitoring and control equipment on a base station is less than the power offered by a configuration, this creates power headroom which provides an extra buffer to ensure uninterrupted operation.

The most power-hungry radio configurations are given in Table 3.4. A lower power consumption is expected using SBCs with radio daughter cards, at the expense of added development and radio cost. Table 3.5 shows the total power consumption,  $P_{\text{total}}$ , when using radio daughter cards for different use-cases when using two UHF and two 5 GHz PTMP sectors with a Mikrotik RouterBOARD 433AH SBCs. Note when using only two radio daughter cards, such as for a repeater mast with two PTP links, the power consumption is higher than when using the integrated radio-antenna solution due to the inefficiency of the unused third mini-PCI interface.

### 3.7.2 Example Base Loads

Table 3.6 shows how the three examples of WindFi use-cases introduced in Section 3.4 can be met with the large and small configurations. The total power consumption,  $P_{\text{total}}$ , and resultant power headroom,  $P_{\text{headroom}}$ , is calculated for each use-case, given the configuration. The  $P_{\text{total}}$  calculations for each example are given in Tables 3.7, 3.8 and 3.9.

*Terminating Base Station.* The “Site A” base station is one of several on Tiree which have one link for IP access and additional PTMP links for serving subscribers. This setup creates

Use-case	Configuration	Radios Used	$P_{\text{total}}/P_{\text{config}}$	$P_{\text{headroom}}$	Example
Terminating BS	Small	3/3	21.5/25 W	3.5 W	Figure 3.3
Repeater	Large	5/6	32.5/50 W	17.5 W	Figure 3.4
Repeating BS	Large	4/6	27/50 W	23 W	Figure 3.5

Table 3.6: WindFi power system utilisation for given use-cases.

Radio Equipment	Number	$P_{\text{radio}}$	$P_{\text{total}}$
PTMP Ubiquiti Rocket M5	2	8 W	16 W
PTP Ubiquiti NB-5G22	1	5.5 W	5.5 W
			21.5 W

Table 3.7: Power consumption of radio equipment at the “Site A” terminating base station.

a maximum base load of 21.5 W as shown in Table 3.7.

*Repeater.* The repeating mast “Crow’s Nest” on Tiree serves as a hub, providing IP access to all parts of the island, hence a large number of PTP links and therefore radios are required. In this configuration the mast has a maximum base load,  $P_{\text{total}}$ , of 32.5 W as shown in Table 3.8 given an individual radio equipment item power consumption,  $P_{\text{radio}}$ .

*Repeating Base Station.* The repeating base station “Site B” uses two sectors to serve users and relays AP to another part of the island, creating two PTP and two PTMP links. This creates a maximum base load of 27 W as shown in Table 3.9.

### 3.7.3 Power Generation and Storage

For deployment in Scotland, WindFi uses both wind turbines and PV modules to harvest a combination of wind and solar energy. A battery bank is used to buffer energy generation and a charge controller regulates battery charging. As discussed in [?], wind and solar energy sources are complementary in Scotland; in the summer months solar energy peaks whilst in the winter months winds prevail. Figure 3.6 shows this trend for two locations, Tiree Airport (TRE) and Prestwick Airport (PIK), by plotting the average wind speed and daily

Radio Equipment	Number	$P_{\text{radio}}$	$P_{\text{total}}$
PTMP Ubiquiti NanoStation NSM5	2	8 W	16 W
PTP Ubiquiti NB-5G22	3	5.5 W	16.5 W
			32.5 W

Table 3.8: Power consumption of radio equipment at the “Crow’s Nest” repeater.

Radio Equipment	Number	$P_{\text{radio}}$	$P_{\text{total}}$
PTMP Ubiquiti Rocket M5	2	8 W	16 W
PTP Ubiquiti NB-5G22	3	5.5 W	11 W
			27 W

Table 3.9: Power consumption of radio equipment at the “Site B” repeating base station.

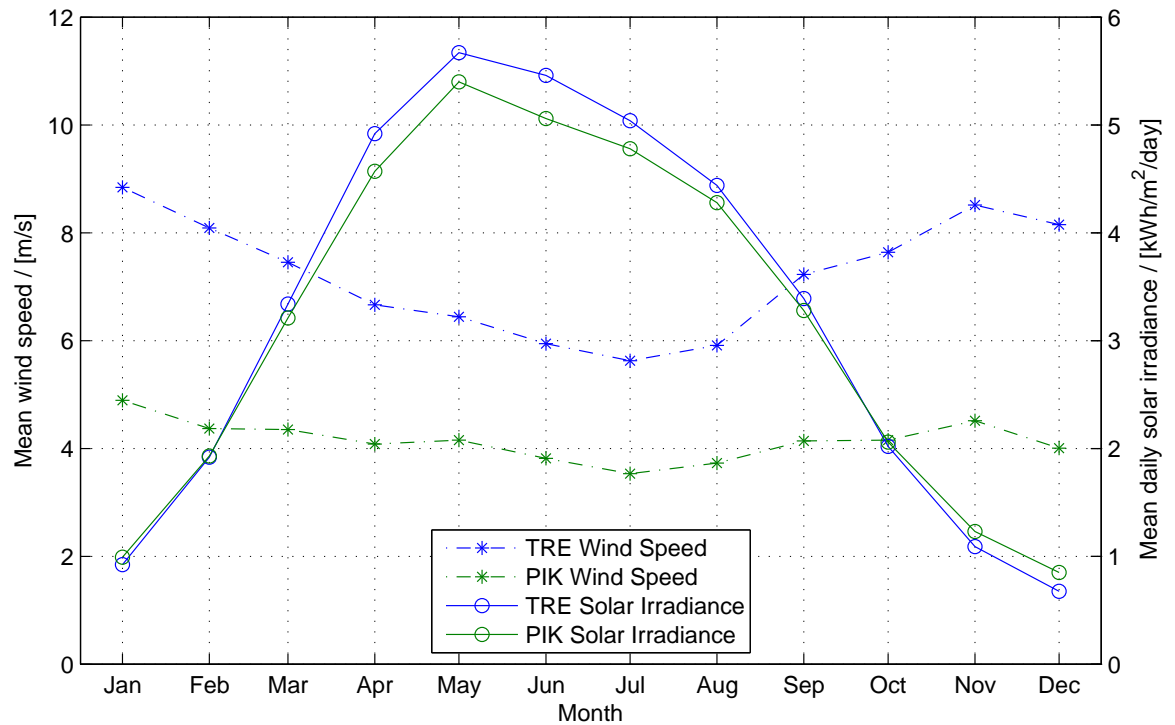


Figure 3.6: Average 10 m wind speed data from Weather Underground [?] and daily solar irradiance data from PVGIS [?] at Tiree Airport (TRE) and Prestwick Airport (PIK) averaged between the years 2000 and 2014.

solar irradiation. These two locations are used as examples as they are situated close to WindFi test locations on the islands of Tiree and Bute as discussed in Chapter 5 and detailed historical weather data is available. The variation in wind speed between locations is an important factor when designing the power generation requirements and these two locations highlight these differences. The types of battery bank, wind turbine and PV modules used are discussed in the following sections.

### Battery Bank

Antares 66050 12 V 40 Ah cyclic gel batteries are used in WindFi [?]. Cyclic gel batteries are designed for applications where the batteries are repeatedly charged and part discharged day-to-day. The depth of discharge affects the number of cycles before the battery performance

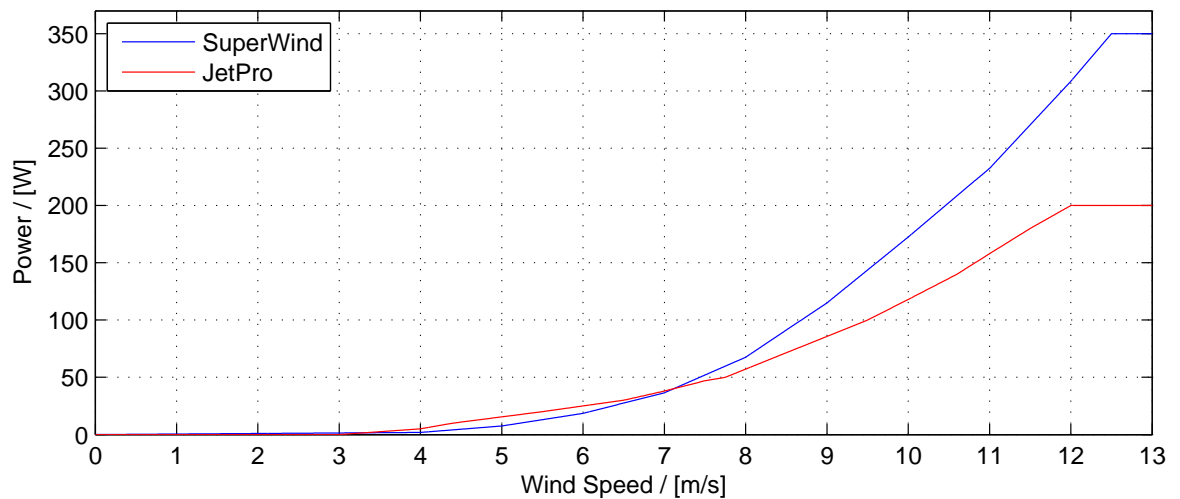


Figure 3.7: Expected power output of a SuperWind SW350 or JetPro JPS200 wind turbine [?, ?].

is affected, with a lower depth of discharge prolonging the battery lifespan. Generally a maximum depth of discharge of 50% is recommended [?]. A charge controller is required to regulate the charging of the batteries to prevent overcharging. Strings of two 12 V batteries wired in series to create a 24 V bank can in turn be arranged in parallel to accumulate the total bank size. A 24 V battery bank is preferred to a 12 V bank as the majority of radio equipment operated requires a nominal voltage of 24 V.

### Wind Turbine

Two types of wind turbine have been used in WindFi:

- SuperWind SW350 (SW) - A 350 W peak output mechanically feathering wind turbine suited for high wind speeds [?].
- JetPro JPS200 (JP) - A 200 W peak output modular shrouded wind turbine suited for lower wind speeds [?].

The expected power generated by each turbine for a given wind speed is shown in Figure 3.7. The JP produces marginally more power than the SW at lower wind speeds up to 7 m/s. Above this the SW produces much more power, allowing it to take greater advantage of gusts and the higher wind speeds in the winter months. The SW also has a greater tolerance to higher wind speeds due to the mechanical feathering, making it more suitable for environments high wind speeds. Due to the mechanical design of the shrouded JP wind turbines, two or three units can be mechanically connected to act as one unit. This provides a great deal of flexibility in sizing wind generation for a particular application.

### Photovoltaic Array

Panasonic HIP-H250 250 W peak power, 34.9 V nominal voltage PV modules are used with WindFi. These modules can be wired in parallel to accumulate the generated power [?].

#### 3.7.4 Power System Dimensioning

Due to the high cost of PV arrays, wind turbines and batteries, research has focused on sizing solar and wind sources and battery banks for given loads and conditions [?, ?, ?, ?]. The battery bank in a WindFi system is sized to allow for continuous operation without any additional energy input for  $N_d$  days and without the capacity dropping below the maximum discharge depth  $D$  to prolong the battery lifespan.  $D$  is a fraction within the range  $0 \leq D \leq 1$ . The required battery bank capacity  $C_b$  in kWh for a daily energy demand  $E_d$  in kWh is given by

$$C_b = \frac{N_d E_d}{D} \quad . \quad (3.1)$$

A base load creates a maximum daily energy demand. As discussed in Section 3.7.1, two base loads are possible,  $P_{load} = \{25 \text{ W}, 50 \text{ W}\}$  creating a maximum daily energy demand of  $E_d = \{0.6 \text{ kWh}, 1.2 \text{ kWh}\}$  assuming 24 hour operation under full load.

The system must remain operational for  $N_d = 3$  days without any energy input and without the stored energy dropping below  $D = 0.5$  (50%) of the total capacity. This mitigates against overcast, wind free days and protects the batteries from over-discharge. Therefore the battery bank must be able to store  $C_b = \{3.6 \text{ kWh}, 7.2 \text{ kWh}\}$ , leading to a required battery bank capacity of  $\{150 \text{ Ah}, 300 \text{ Ah}\}$  when using 24 V batteries.

The energy production of the mast must be capable of recharging the batteries from the lowest allowed charge depth in  $N_r$  days in addition to maintaining the base load. The required energy production per day  $E_p$  required to recharge the battery bank over  $N_r$  days is

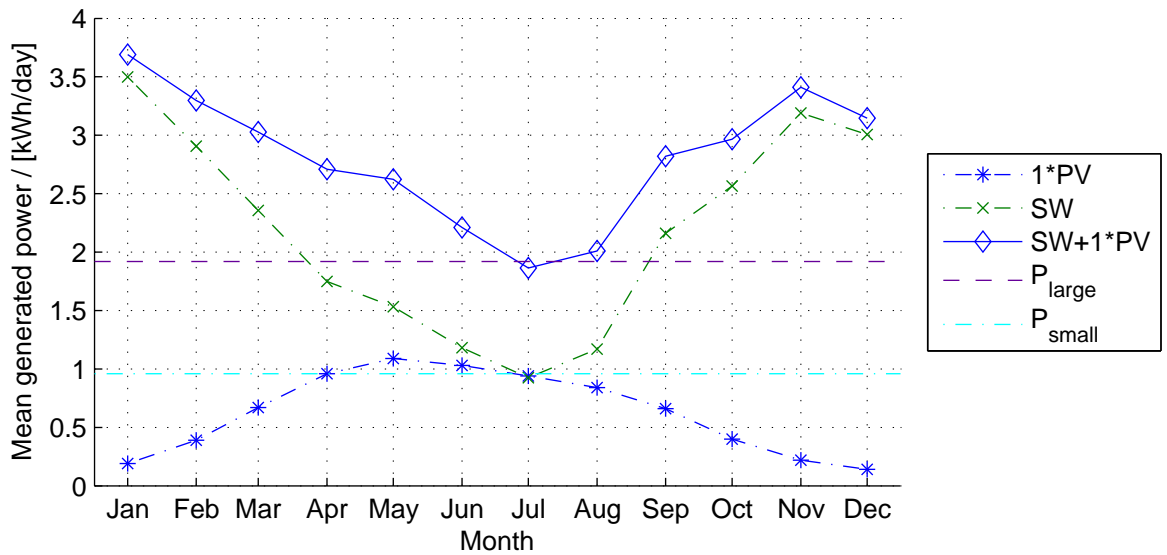
$$E_p = E_d + E_r = E_d + \frac{DC_b}{N_r} \quad . \quad (3.2)$$

Therefore the total energy production required per day,  $E_p$ , is the base load energy demand  $E_d$  plus the recharge energy demand  $E_r$ . When allowing  $N_r = 5$  days to recover from a maximum lost charge, an extra energy demand of  $E_r = \{360 \text{ Wh}, 720 \text{ Wh}\}$  is required, creating a total daily demand to be satisfied by the generation system of  $E_p = \{0.96 \text{ kWh}, 1.92 \text{ kWh}\}$ .

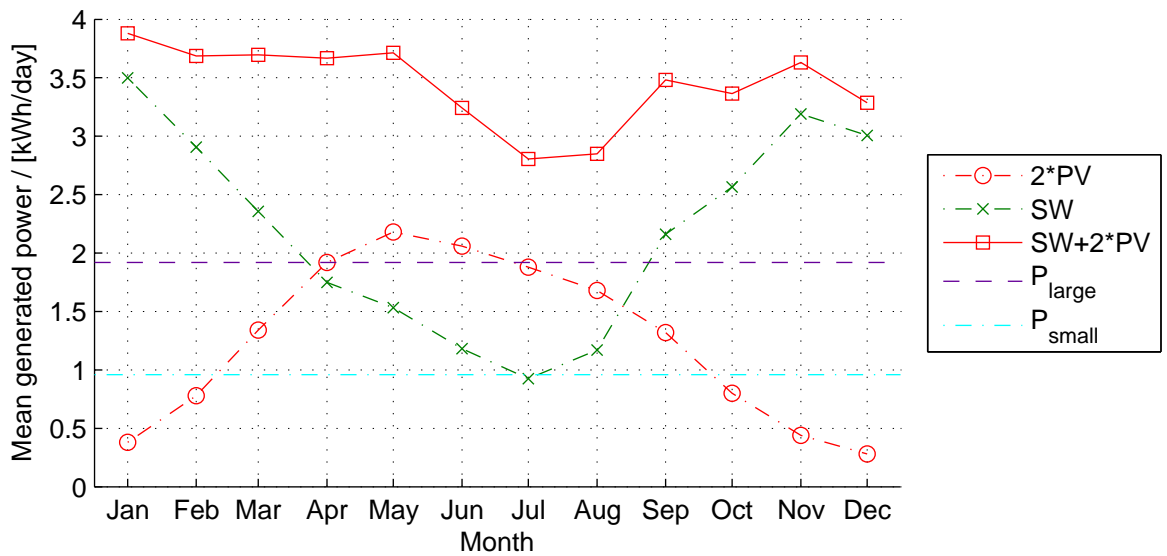
Figures 3.8(a) and 3.8(b) show the expected power generated per day using an SW wind turbine and one or two PV modules on the island of Tiree. Only the SW wind turbine can be used due to the excessive wind speeds. In the Highlands and Islands of Scotland the potential of wind energy is greater than that of PV. In the winter months the mean wind turbine

output of around 3 kWh per day is more than sufficient to meet the small and large base load power requirements,  $P_{\text{small}}$  and  $P_{\text{large}}$ , while in the summer months the output drops to around 1 kWh per day. To meet the system's energy demand of  $E_p = \{0.96 \text{ kWh}, 1.92 \text{ kWh}\}$ , the PV must be capable of making up the shortfall shown in Figure 3.8. One or two PV modules at an optimal orientation given by photovoltaic geographical information system (PVGIS) create a combined energy generation capable of sustaining the small or large load. Note in Figure 3.8(a), one PV module cannot guarantee enough power for the large base load in July, therefore two modules are required, as shown in Figure 3.8(b).

As the mean winter wind speed at Prestwick Airport is 4 m/s less than Tiree Airport the SW wind turbine cannot support both a small and large base load. Figure 3.9 shows how a small and large load can be supported using different options. The generation requirements for a small base load of  $E_p = 0.96 \text{ kWh}$  consisting of a single SW wind turbine and one PV module is shown in Figure 3.9(a). To support a large base load of  $E_p = 1.92 \text{ kWh}$  throughout the winter months, a more powerful wind turbine than the SW is required. This large base load can be satisfied using three JP wind turbines combined with two PV modules as shown in Figure 3.9(b).

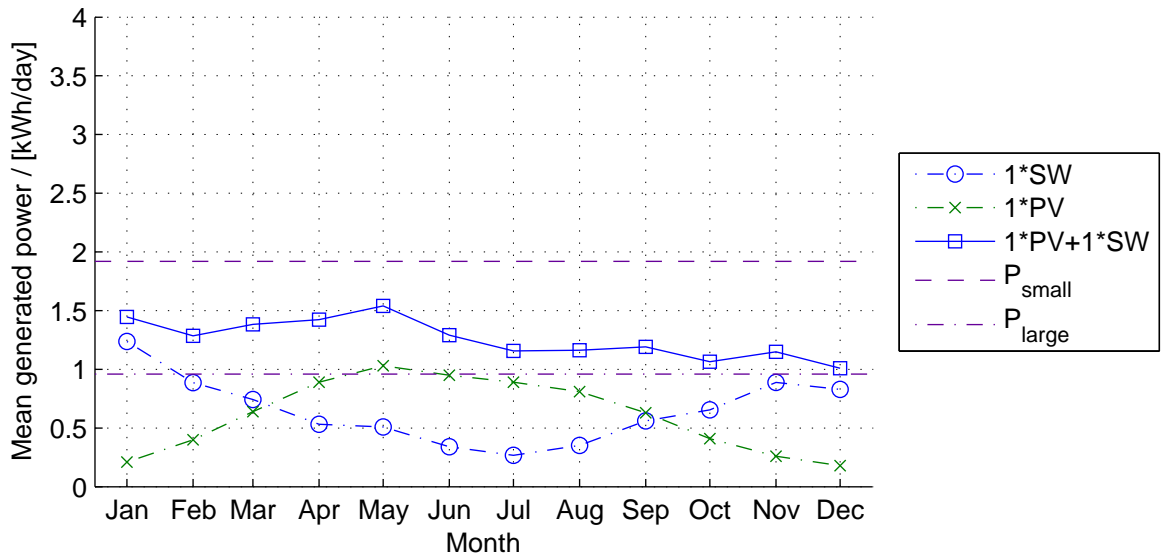


(a)

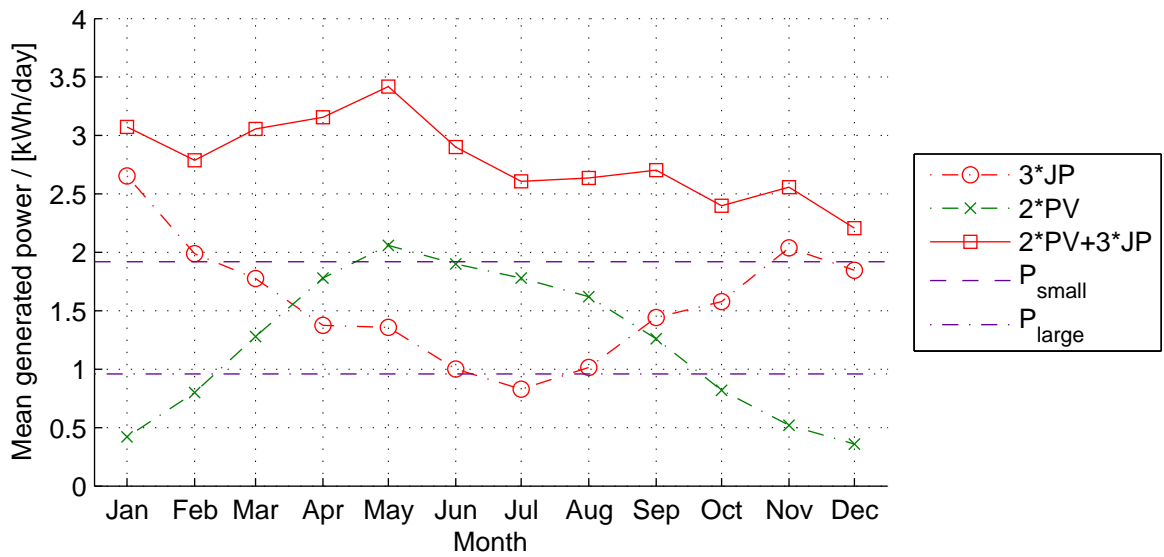


(b)

Figure 3.8: Expected daily power generation at Tiree Airport (TRE) using (a) one 250 W peak power PV module and a SuperWind SW350 (SW) 350 W wind turbine to satisfy the small load requirement, (b) two 250 W peak power PV modules and a SuperWind SW350 (SW) 350 W wind turbine to satisfy the small and large load requirements.



(a)



(b)

Figure 3.9: Expected daily power generation at Prestwick Airport (PIK) for a small and large load using (a) one SuperWind SW350 (SW) 350 W wind turbine and one 250 W peak power PV module to satisfy the small load, (b) three JetPro JPS200 (JP) 200 W wind turbines and two 250 W peak power PV modules to satisfy the large load.

## 3.8 Crow's Nest Power System Analysis

Section 3.4.2 introduced a test deployment of a WindFi base station named the “Crow's Nest”, shown in Figure 3.4. The Crow's Nest relays IP-access to other base stations across the island and lies on an exposed hill with no mains power. For this reason a renewable power system was sized using the equations in Section 3.7.4, capable of supporting a base load of 32.5 W as calculated in Table 3.8. This section analyses the performance of the base station power system based on the sizing decisions made in Section 3.7.4, specifically the number of days a load can be sustained when the power generation system is not producing enough energy to sustain a load, and the recovery after such a deficit.

### 3.8.1 Power System Design

Ten Antares 66050 40 Ah 12 V batteries provide a capacity  $C_b = 4.8$  kWh at 24 V. Using (3.1) for a base load of 32.5 W,  $E_d = 780$  Wh, the required battery bank capacity is 4.68 kWh at 24 V with  $N_d = 3$  days and  $D = 0.5$ . Using (3.2) a daily energy production  $E_d = 1.248$  kWh is required to replenish the battery over  $N_r = 5$  days.

A Morningstar Tristar TS-60-MPPT charge controller is used to provide maximum power point tracking (MPPT) control of the PV array voltage and regulate solar battery charging. This charge controller allows for remote monitoring and logging of variables used in this analysis. The SW wind turbine is regulated by a SCR-24 charge controller which splits power between a dump load and the battery bank using pulse width modulation (PWM) to regulate charging. This is wired in parallel with the TS-60-MPPT but provides no logging capability. The Tristar TS-60-MPPT PV charge controller can be in one of four states shown in the battery charging cycle in Figure 3.10:

- *Night.* The charge controller has detected it is night therefore no solar energy is present.
- *MPPT.* Maximum power point tracking bulk charging delivers all of the available solar power to provide around 80% of battery charging.
- *Absorption.* The charge controller maintains a constant voltage once a voltage set-point is reached but reduces the charging current to allow the battery to absorb remaining 20% of charge without overheating the battery.
- *Float.* The charge voltage is reduced from absorption and the charge is maintained.

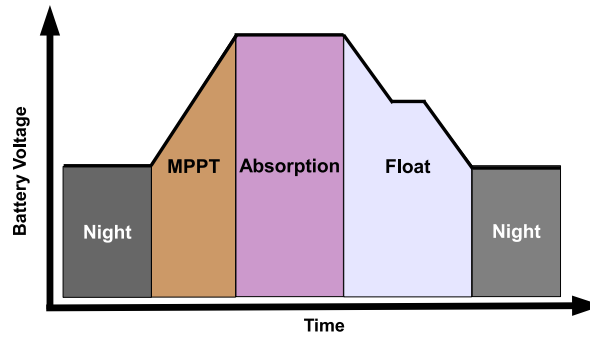


Figure 3.10: Tristar battery charging states [?].

### 3.8.2 Expected Energy Production Characteristics

An SW wind turbine and two HIP-H250 PV modules provide power generation for the base station. The expected generation potential of this configuration is shown in Figure 3.11. This was calculated using historical average wind speed data and the expected solar irradiance as described in Section 3.7.3. The generation system is overproducing for the maximum load,  $P_{load}$ , and desired discharge and recharge characteristics.

As summarised in Section 3.7.4, the high wind speeds create a substantial amount of excess energy. This excess energy causes the battery bank to be recharged quickly. Figure 3.12 shows the expected impact of generation over-production on the time to recharge. The minimum, maximum and mean expected daily over-production for the Crow's Nest are indicated to highlight the impact on recharging a 50% discharged 4.8 kWh battery bank. The  $N_r = 5$  days allocated to recharging given a 50% discharge is reduced to around one day given the expected over production at the site.

### 3.8.3 Day-to-Day Performance Analysis

The TS-60-MPPT PV charge controller provides remote monitoring capabilities. This allows the recording of the battery bank voltage, charging state information, instantaneous power, and cumulative energy produced, by the PV system. As the wind turbine charge controller has no logging capability the behaviour of the wind power generation system is estimated using wind speed measurements and a model of the power generation shown in Figure 3.7.

Figures 3.13 and 3.14 plot the state of the Crow's Nest power system over a number of days, highlighting periods of low and high wind speeds. Both Figures consist of three parts:

1. *Target and measured battery voltage.* Figures 3.13(a)/3.14(a) plot the measured and target PV battery charging voltages. The nominal battery voltage is 24 V but batteries are kept at a higher voltage during charge and float. During nights the target voltage of the charge controller drops to 0 V.

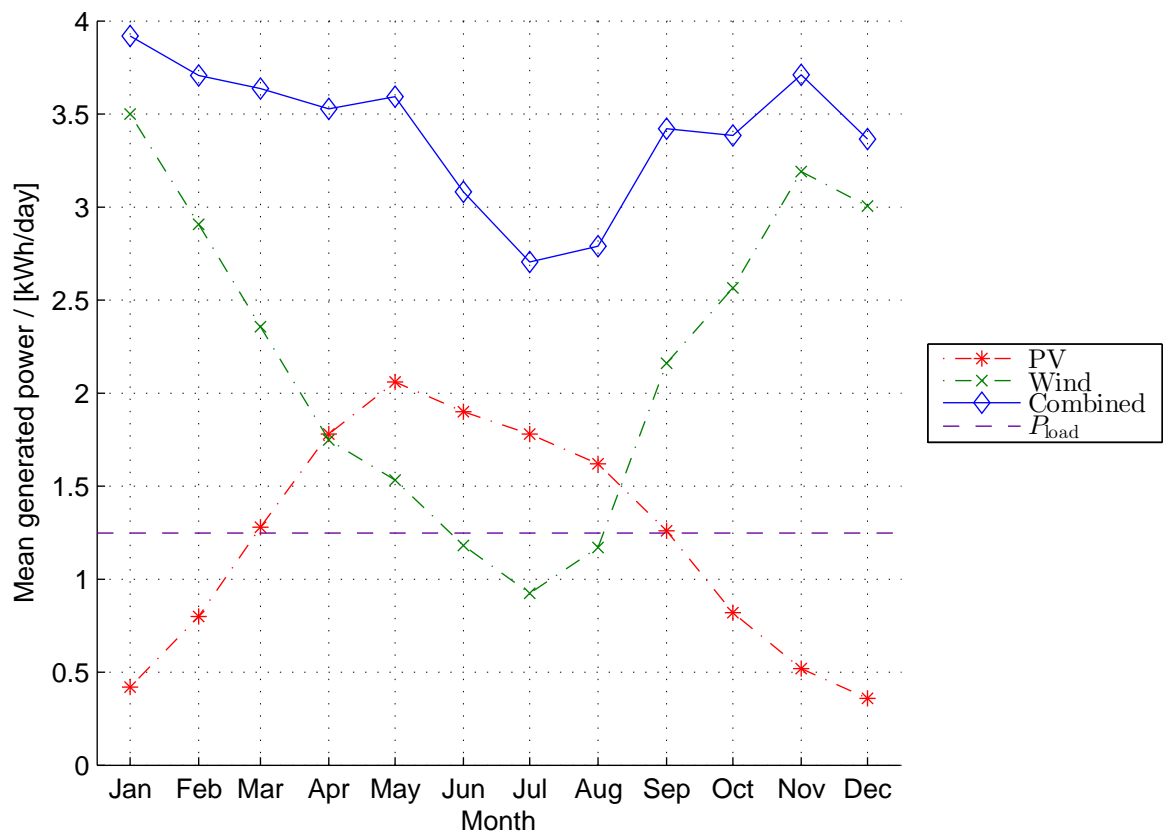


Figure 3.11: Expected daily power generation at Tiree Airport (TRE) using two 250 W peak power PV modules and a SuperWind SW350 250 W wind turbine.

2. *Charging state.* Figures 3.13(b)/3.14(b) plot the charging state of the TS-60-MPPT.
3. *Instantaneous wind and PV power generated.* Figure 3.13(c)/3.14(c) plot the measured instantaneous power provided by the PV array and the estimated power provided by the wind turbine given the measured wind speed. The PV power is taken from the charge controller log and the wind power is estimated using measured wind speeds at TRE provided by [?] and the model of the SW wind turbine.

### Low Wind Speed Day

Figure 3.13 plots power system behaviour on low wind speed days between the 2nd and 4th June 2013. The information shown by the graph on the 3rd and 4th of June is indicative of a PV only system.

Wind power was generated in only two periods (11:00-14:00 on the 2nd June and 19:00-02:00 on 2nd/3rd June) and is visible in Figure 3.13(c) by the estimated power generation. This is mirrored in Figure 3.13(a) as the measured battery voltage becomes fast changing due to the nature of the charging voltage of a wind turbine. During these periods the PV charge

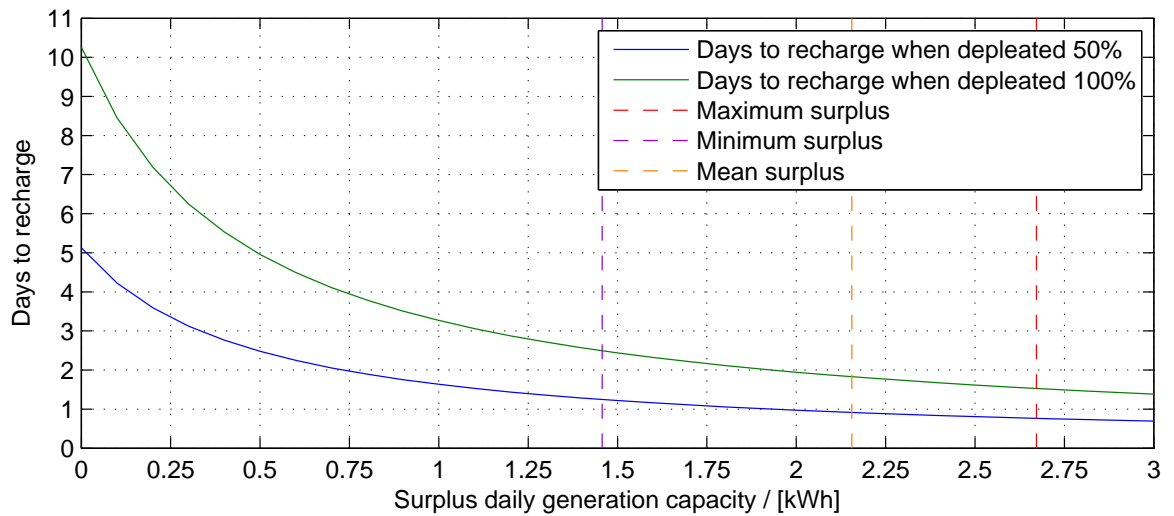


Figure 3.12: Impact of surplus energy generation on time to recharge 200 Ah battery bank at Tiree Airport (TRE).

controller detects an increased voltage and reduced the PV power provided to the battery, as visible between 12:00-15:00 in Figure 3.13(c), to prevent overcharging.

When little to no wind power is present the measured battery voltage change is smooth as visible on the 3rd and 4th June. The stages of charging shown in Figure 3.13(b) are matched by the target and measured battery voltage. The target and measured voltage match during daylight hours after the absorption state as the battery is charged. During the MPPT phase the maximum power is extracted from the PV array as shown by the measured voltage peaks at 09:00 on the three days. The target and measured voltage reduce during the float stage as the battery voltage is maintained and the PV power point is reduced to maintain the voltage of the batteries.

### High Wind Speed Day

Figure 3.14 plots power system behaviour on high wind speed days between the 28th and 30th May 2013. In comparison with the low wind-speed days, the measured battery voltage is generally higher than the PV charge controller target voltage in Figure 3.14(a). The charge controller state in Figure 3.14(b) is also less frequently in the MPPT state than in the low wind-speed Figure 3.13(b). This is due to the wind charge controller feeding power to the batteries constantly via PWM. During these periods the PV charge controller detects an increased voltage and reduces or stops the PV power generation to prevent overcharging. During two periods, 16:00-20:00 on 28th May and 05:00-09:00 on 29th May the wind speed has dropped, visible by the drop in expected power in Figure 3.14(c). This corresponds to a drop in measure voltage level in Figure 3.14(a). On these occasions the MPPT PV charge controller provides power to charge the batteries from the PV system.

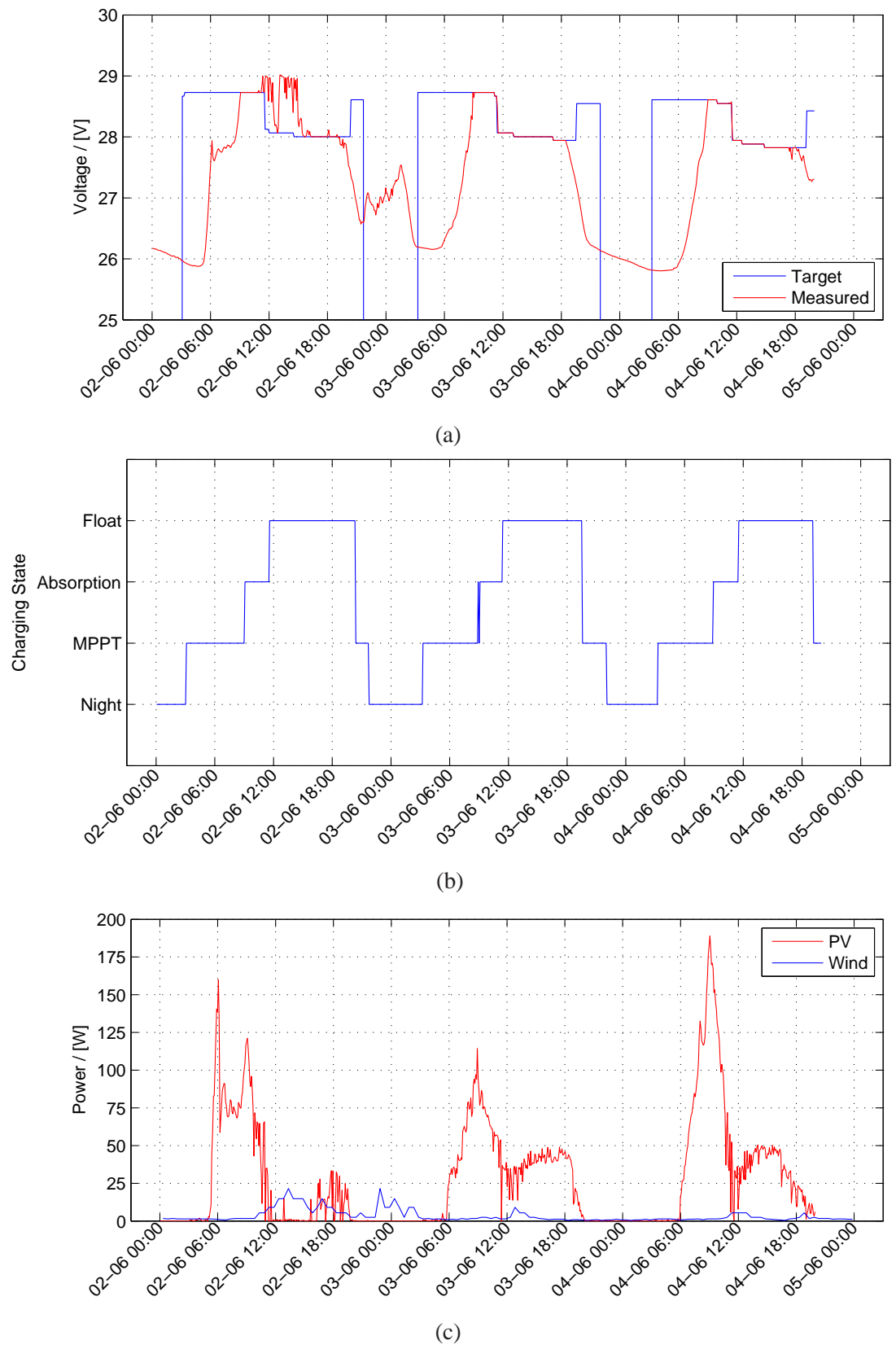


Figure 3.13: Crow's Nest power system between 2nd and 4th June 2013; low wind speed days showing (a) target and measured battery voltage, (b) TS-60-MPPT PV charge controller state, and (c) measured PV generation and expected SW generation.

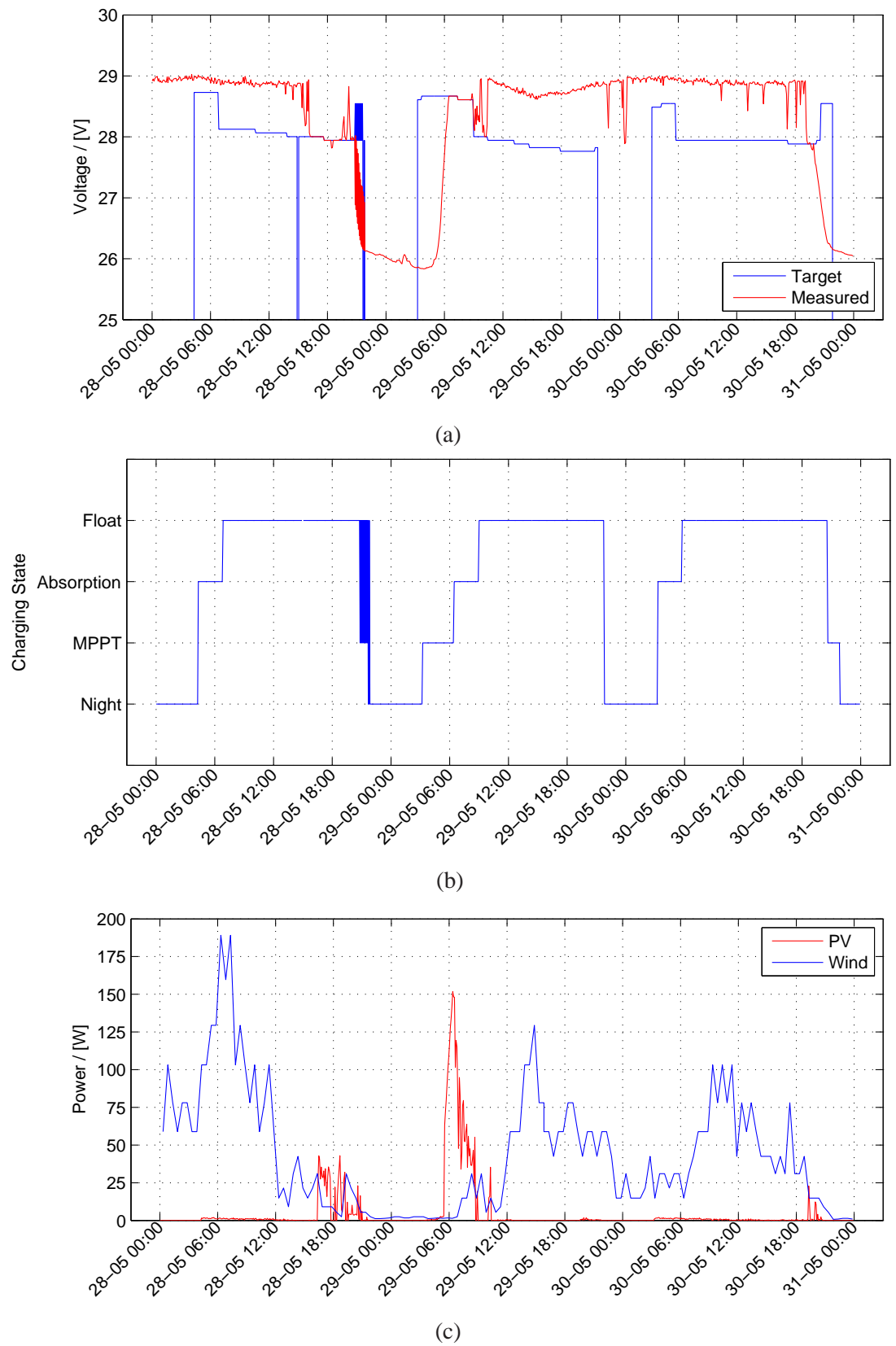


Figure 3.14: Crow's Nest power system between 28th and 30th May 2013; high wind speed days, showing (a) target and measured battery voltage, (b) TS-60-MPPT PV charge controller state, and (c) measured PV generation and expected SW generation.

### 3.8.4 Wind Power System Failure Analysis

Figure 3.15 shows the state of the MPPT PV charge controller and WindFi power system over a 17 day period between 4th and 20th of February 2013. During this period the wind turbine charge controller failed, providing no power to the batteries between the evening of the 5th, and the 15th of February.

Figure 3.15(a) plots the MPPT charge controller target battery voltage and measured battery voltage. Between the 5th and 14th of February the lack of wind input is visible in this graph as the actual battery voltage slowly drops, not meeting the target voltage even with PV energy. On the 14th February the battery bank can no longer sustain the electrical load and the voltage drops suddenly which causes the radio equipment to become un-powered due to the low voltage. This causes the logging of data to stop. On the 15th February the wind power system was repaired and the measured battery voltage increases as the battery bank is recharged and logging restarts.

Figure 3.15(b) shows the charge controller state. When no wind power is available the charge controller is constantly in either the MPPT or Night state, trying to produce as much power as possible to charge the batteries given that the measured battery voltage in Figure 3.15(a) is consistently less than the target voltage.

Figure 3.15(c) shows the recorded power generation of the PV system and expected wind generation using wind speed records over this period. Note that the expected power output saturates at 350 W due to very high wind speeds. Despite substantial wind speeds visible by the expected power on the 10th, 12th and 13th of February, the battery voltage shown in Figure 3.15(a) still decreases indicating no charging. The PV power produced over this period is low, as expected during this time of year.

Figure 3.15(d) plots the estimated individual daily energy contributions from the wind and PV system and the total energy of the system, combining the wind, PV and load during the period of the wind power system failure. As the days preceding and including the 4th February had a very high average wind speed, it is assumed that the battery bank is fully charged. Given the daily  $E_d = 0.78$  kWh load, when no energy from the wind system is provided, the battery bank is expected to be depleted on the 13th or 14th of February, as the cumulative sum of the daily energy deficit approaches the size of the battery banks,  $C_b = 4.8$  kWh. This prediction based on the design of the system matches the observed outage on the 14th February. When the wind power system is repaired on the 15th February, a surplus of energy is created by the PV and wind turbine, causing the cumulative difference between load and production to become positive within 3 days, recovering the battery bank. Given the sum of the surplus of 6 kWh, due to the overproduction of the wind turbine as shown in Figure 3.12 after 2.5 days the battery bank is recharged.

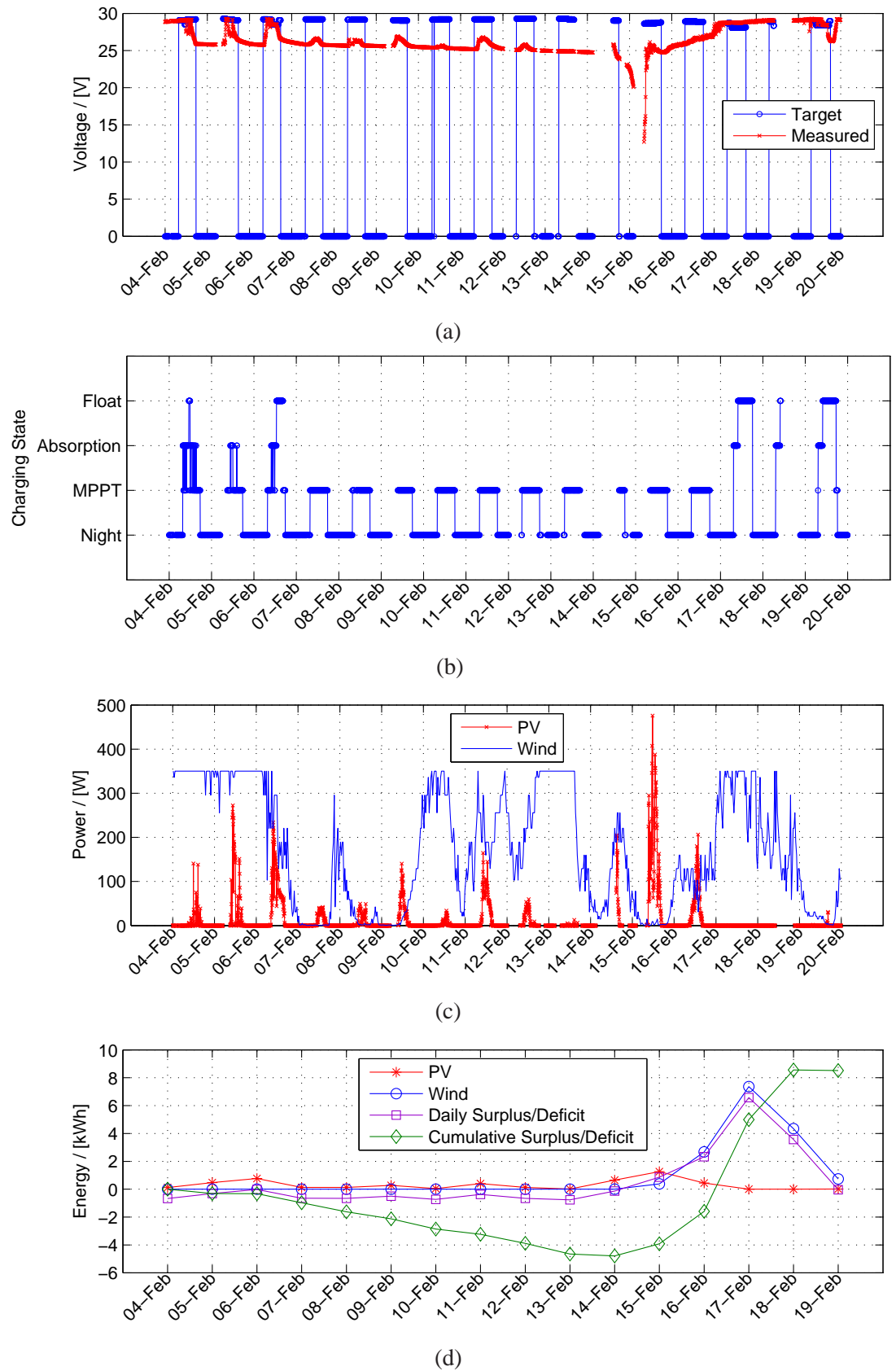


Figure 3.15: Crow's nest power system during a failure of the wind power system between 4th and 19th February, showing (a) target and measured battery voltage, (b) TS-60-MPPT PV charge controller state, (c) measured PV generation and expected SW generation, and (d) cumulative daily system energy with broken wind turbine.

## 3.9 Summary

This chapter presented the design and analysis of the “WindFi” base station as a component to realise the rural broadband network discussed in Chapters 2 and 5.

WindFi can rely solely on a combination of wind and solar power to support wireless network equipment. The use of both TVWS bands and 5 GHz bands to deliver access provides an additional burden on the power consumption of a wireless node, compared to a single band system as reviewed. Therefore the dimensioning of a larger generation capacity and storage system was presented. A retrospective analysis of the power system performance under three different scenarios in an actual deployment was presented; low wind speeds, high wind speeds, and a faulty wind turbine causing the battery to deplete. The behaviour of the system under these scenarios met the design conditions, thereby validating the design.

Common use-cases for the base station were presented and the impact on system design discussed. This included how specific radio equipment could be utilised. As the main cost component of a WindFi base station is the renewable power system, understanding and minimising the power consumption of radio equipment is key to minimise costs, and make the system economically viable. Therefore Chapter 4 profiles utilised radio hardware to understand the power consumption impact for a WindFi base station. Chapter 6 then explores how power savings can be achieved in a common use-case for a WindFi base station.

# Chapter 4

## Radio Characterisation

Chapter 3 showed that the radio payload for WindFi is the largest consumer of energy within the base station, and therefore is the main contributor to the size and cost of the renewable energy generation system. Reducing the power consumption of the radio payload is an option to reduce the cost of Hopscotch, and make it an economically viable solution in more rural broadband scenarios. To facilitate the development of energy saving methods such as the method presented in Chapter 6, the performance and power consumption of the radio equipment used to create the networks discussed in Chapters 2 and 5 must be well understood. This chapter describes the lab-based characterisation of radios used in Hopscotch, with the goal of creating two useful models:

- the data rate selection for a given receive signal power; and
- the relationship between power consumption and transmit power

Secondary to producing these models, the tests provided an opportunity to characterise the actual transmission control protocol (TCP) throughput of both radios when configured to use a specific data rate.

Section 6.1 introduces the radio hardware configuration profiled and the concepts of data rate and transmit power selection by the radios. Section 4.2 describes the experimental methodology to obtain data to create the models. Sections 4.3 and 4.4 give experimental results for the two radios profiled, the Ubiquiti XR7 and SR71. Section 4.5 presents the radio characterisation models using the results.

### 4.1 Background

This section introduces the radio hardware profiled and concepts of transmit power and data rate selection used by the radios profiled.

Band	Bandwidth	Access Point SBC	Station SBC	RF Card
5 GHz	20 MHz	RouterBOARD 433AH	RouterBOARD 411	SR71
UHF	5 MHz	RouterBOARD 433AH	RouterBOARD 411	XR7

Table 4.1: Radio equipment profiled for links in the 5 GHz and UHF bands. The vendor of the SBCs is Mikrotik and the vendor of the RF daughter cards is Ubiquiti.

MCS Index	Modulation Type	Code Rate	Data Rate (Mbps)	
			5 MHz	20 MHz
0	BPSK	1/2	1.5	6
1	QPSK	1/2	2.2	9
2	QPSK	3/4	3	12
3	16-QAM	1/2	4.5	18
4	16-QAM	3/4	6	24
5	64-QAM	2/3	9	36
6	64-QAM	3/4	12	48
7	64-QAM	5/6	13.5	54

Table 4.2: IEEE 802.11a/g MCS rates and expected data rates

### 4.1.1 Radio Hardware Configuration

The radio hardware required to create the dual-band 5 GHz and UHF network discussed in Chapter 2 is profiled to create models for analysis. The category of radio hardware profiled is SBC with RF daughter card, introduced in Section 3.3. Only this category is considered as it was shown in Section 3.7 to consume less power than integrated COTS radios and antennas. Table 4.1 highlights the equipment profiled. A Mikrotik RouterBOARD 433AH is configured as an AP with one RF daughter card providing connectivity. A Mikrotik RouterBOARD 411 is configured as a station with one RF daughter card. The Ubiquiti SR71 and XR7 daughter cards are interchanged to provide 5 GHz and UHF radios. The SR71 occupies the standard 20 MHz bandwidth and the XR7 occupies 5 MHz bandwidth.

### 4.1.2 Data Rate Selection

Table 4.2 shows the available standard IEEE 802.11g data rates (MCS), including the quoted data rate for 5 MHz and 20 MHz bandwidths. The XR7 and SR71 radio cards are based on the IEEE 802.11 physical layer, providing the rates quoted in Table 4.2. Note the radios use the proprietary Ubiquiti MAC, *Nstream*. As the XR7 is used within TVWS, a 5 MHz bandwidth is configured. To obtain the 5 MHz data rate the standard 20 MHz data rates are scaled by the bandwidth ratio 1/4. The Mikrotik software used to configure the radios quotes the 20 MHz data rates when referencing the MCS for both 5 MHz and 20 MHz bandwidths.

A higher MCS index provides a greater theoretical bandwidth but requires a greater SNR

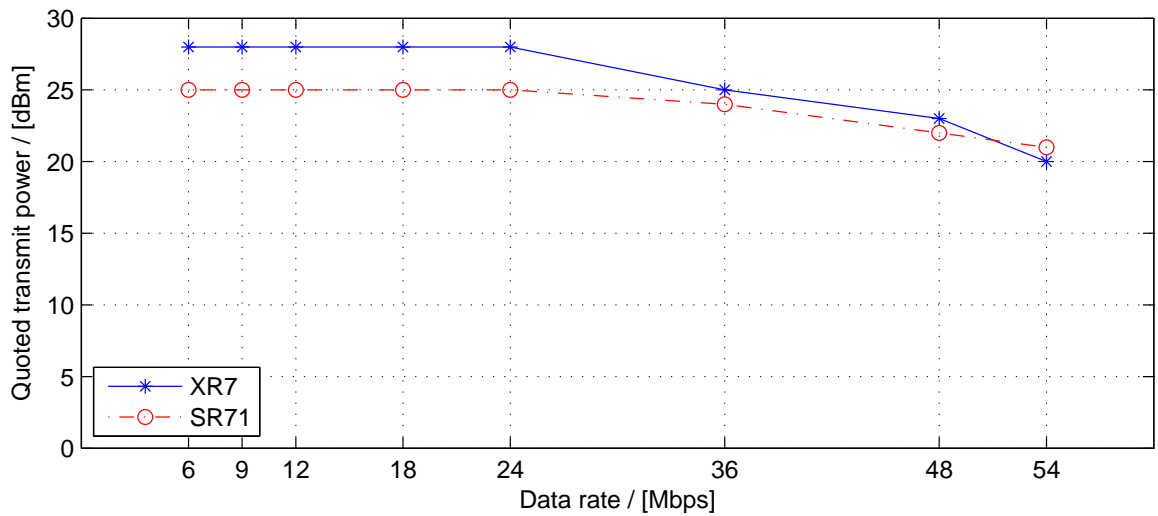


Figure 4.1: Quoted transmit power for each data rate for the XR7 and SR71 [?, ?].

to successfully demodulate and decode symbols encoded at a higher MCS. Generally a transmitter selects a data rate to use based on the measured signal strength at the receiver for all data rates. If different transmit powers are used for each data rate then the received signal strength for each data rate will differ. The Ubiquiti radios can be forced to use a single data rate or automatically select between an allowed set of data rates. A change in data rate does not require the receiver to resynchronise as the physical layer convergence procedure preamble used for synchronisation, and to inform the station (STA) of the data rate used, is transmitted with a fixed data rate.

### 4.1.3 Transmit Power Selection

The transmit power of the SR71 and XR7 can be fixed or dynamically scaled based on the data rate. The data sheets for both the SR71 and XR7 state the transmit power for each data rate [?, ?]. Figure 4.1 plots the quoted transmit power for both radios for each 20 MHz data rate. This scaling reduces the transmit power when high order modulation schemes are used to reduce the impact of distortion caused by the power amplifier.

## 4.2 Experimental Setup

The data rate selection of the radios for a given receive power, the transmit power selected for a given data rate, and the power consumption for a given transmit power were profiled in the laboratory. The setup and calibrations required for each test and are described in Sections 4.2.1, 4.2.2, 4.2.3, and 4.2.4 below. A programmable attenuator provided the capability to control the radio powers. The required calibration is described in Section 4.2.5.

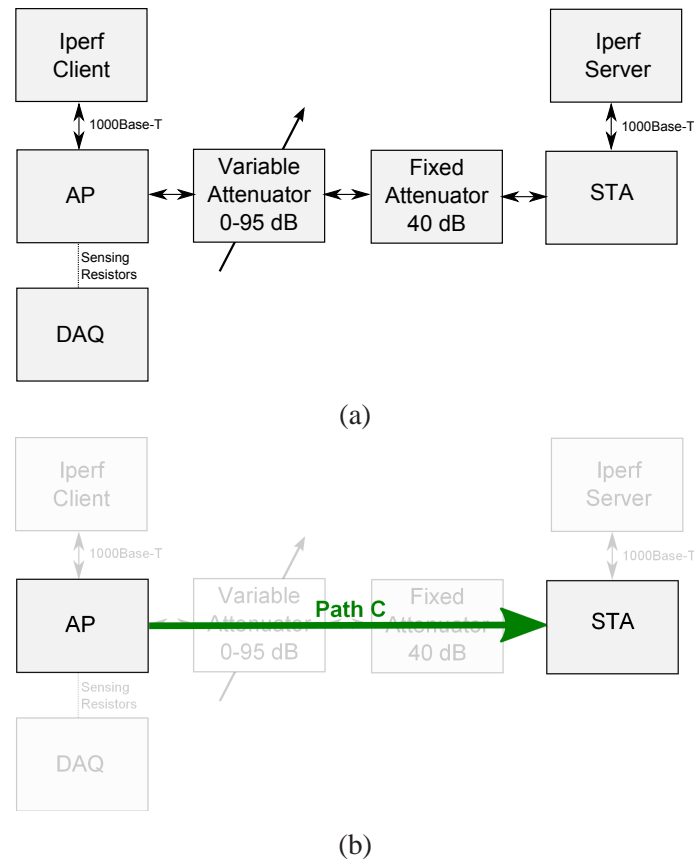


Figure 4.2: RF characterization test setup showing (a) data rate selection test, and (b) data rate selection test calibration path.

### 4.2.1 Overview

In order to characterise the radio performance and power consumption a laboratory setup was created, shown in Figure 4.2(a). A link was created between the two radios, one configured as an AP and the other configured as a STA. A Gaussian channel between the two radios was created using a wire link and fixed and variable attenuators. This allowed the path loss between the AP and STA to be scaled. A Tilithic 0–95 dB programmable variable attenuator allowed the path loss between AP and STA to be accurately scaled in 1 dB steps, shown in Figure 4.3. A fixed 40 dB attenuator increased the path loss further to meet realistic levels. The received power and signal quality experienced by the STA is used by the AP to select the data rate for transmission. Therefore scaling the path loss forces the AP to select a different data rate.

Two computers, one running an Iperf<sup>1</sup> server and the other an Iperf client, generate TCP data and measure throughput. These were connected by 1000Base-T Ethernet to the AP and STA as shown in Figure 4.2(a). Data was sent from the client to server through the

<sup>1</sup>A networking test tool to create and measure TCP and user datagram protocol (UDP) data streams, <http://iperf.fr/>

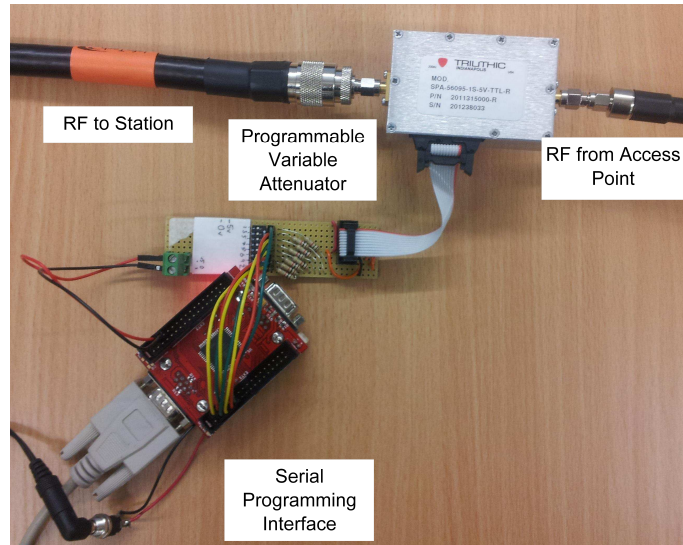


Figure 4.3: Programmable variable attenuator.

AP and STA during an Iperf session. The AP radio statistics, including the received signal strength indicator (RSSI) and data rate, were polled using the available Mikrotik application programming interface<sup>2</sup>. The XR7 was configured to use a center frequency of 763 MHz, within channel 57. The SR71 was configured to use channel 40 at 5.2 GHz. A National Instruments USB-6210 data acquisition system (DAQ) measured the instantaneous power consumption of the radios as discussed in Section 4.2.4.

### 4.2.2 Profiling Data Rate Selection

The data rate selection of XR7 and SR71 when configured as an AP was characterised with the setup in Figure 4.2(a). This allowed the path loss between AP and STA to be scaled to reduce the signal strength at the receiver. For each path loss the AP radio statistics were polled every 250 ms during a 40 s downlink TCP transmission, between the AP and STA. This allowed the data rate selected for each path loss to be recorded. For a forced data rate the radio can only select either the forced rate, for example 54 Mbps (which is equivalent to 13.5 Mbps for 5 MHz operation as per Table 4.2), or the basic data rate (6/1.5 Mbps at 20/5 MHz).

The received signal power,  $P^{\text{rx}}$ , can be estimated from the transmit power,  $P^{\text{tx}}$ , the variable attenuation applied (modelled in Section 4.2.5),  $L_{\text{var}}$ , and fixed losses produced by the cables and attenuation,  $L_{\text{fixed}}$

$$P^{\text{rx}} = P^{\text{tx}} - L_{\text{fixed}} - L_{\text{var}} \quad . \quad (4.1)$$

<sup>2</sup><http://wiki.mikrotik.com/wiki/Manual:API>

Frequency	$L_{\text{fixed}}$
763 MHz	50.9 dB
5.2 GHz	59.5 dB

Table 4.3: Measured fixed attenuation for each frequency band.

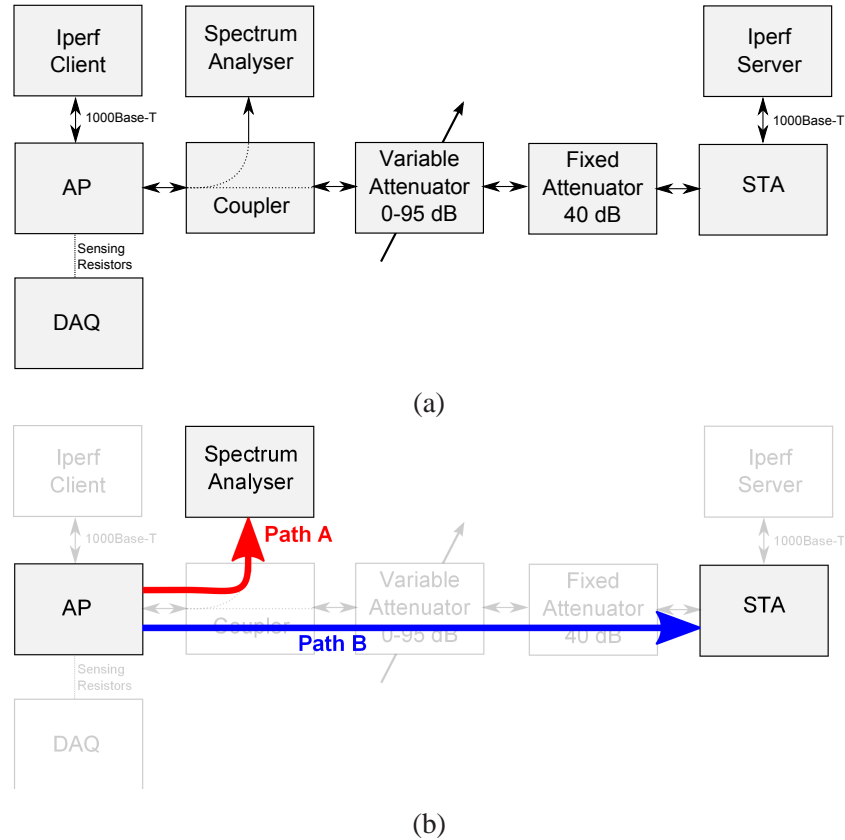


Figure 4.4: UHF radio transmit power profiling setup showing (a) test setup, and (b) calibration paths.

To determine  $L_{\text{fixed}}$ , a 0 dBm tone at the appropriate center of each band of interest was produced by a signal generator and the power measured using a signal analyser with  $L_{\text{var}} = 0$  dB. The path measured between the AP and STA is labelled as *Path C* in Figure 4.2(b). Table 4.3 gives the measured fixed attenuation at each frequency.

### 4.2.3 Profiling Transmit Power

The availability of a UHF directional coupler provided the opportunity to measure the transmit power used by the XR7 radio. A modified version of the lab experiment discussed in Section 4.2.1 was constructed as shown in Figure 4.4. This setup differs from the data rate selection characterisation setup as it features a spectrum analyser which is used with a directional RF coupler to view the transmitted signal from AP to STA and measure the signal power.

Path	$L_{\text{fixed}}$
Path A	23.0 dB
Path B	49.9 dB

Table 4.4: Measured fixed attenuation for each path in Figure 4.4(b) at 763 MHz.

The spectrum analyser was configured to measure the zero-span burst power,  $P^{\text{burst}}$ . From this the transmit power,  $P^{\text{tx}}$ , can be estimated given the fixed attenuation,  $L_{\text{fixed}}$ ,

$$P^{\text{tx}} = P^{\text{burst}} + L_{\text{fixed}} \quad . \quad (4.2)$$

The parameter  $L_{\text{fixed}}$  was measured by generating a 736 MHz 0 dBm tone and measuring the received power at the spectrum analyser as the XR7 operates in TVWS. The path measured between the AP and spectrum analyser is labelled as *Path A* in Figure 4.4(b). The path between the AP and STA, labelled *Path B* in Figure 4.4(b), was also measured with  $L_{\text{var}} = 0$  dB to determine the receive power using (4.1). The measurements are summarised in Table 4.4.

To determine the transmit power used for each data rate, the AP and STA were configured to use only one data rate at a time. The burst power of data packets was measured using the spectrum analyser during a TCP transfer with the variable attenuator set to 20 dB creating a path loss of  $L_{\text{fixed}} + L_{\text{var}} = 71.6$  dB between the AP and STA. To determine the actual transmit power used with a manually fixed transmit power the data rate was set to 1.5 Mbps and the burst power was measured for each fixed transmit power setting. The results of this experiment will be discussed in Section 4.3.2.

#### 4.2.4 Profiling Power Consumption

A National Instruments USB-6210 DAQ was used to measure the power consumption of the AP. The supply voltage to the AP is measured and a sensing resistor network measures the current draw. Using Ohm's law the power consumption can be calculated. Figure 4.5 shows the setup for the power consumption measurements. The DAQ records the appropriate voltages at a sampling rate of 1 kHz over the duration of the experimental data transfer. The setup in Figure 4.2(a) was used to measure the power consumption. The data rate was manually fixed to 1.5/6 Mbps for the XR7/SR71 radios and the variable attenuator set to 20 dB. The transmit power was fixed to one value within the range 0 dB to 30 dB. For each transmit power TCP data was sent from the AP to STA for twenty seconds and the power consumption recorded at a sampling rate of 1 kHz.

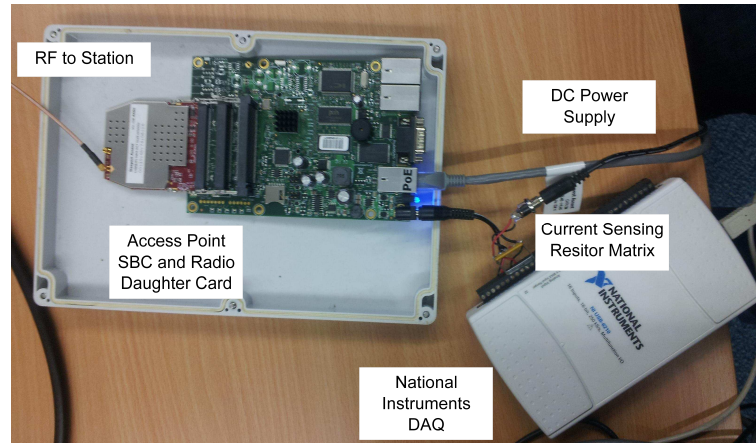


Figure 4.5: AP Power consumption measurement setup.

### 4.2.5 Programmable Variable Attenuation Calibration

All RF equipment has insertion losses<sup>3</sup> which are dependent on the operating frequency. The expected loss produced by the variable attenuator should equal the sum of the programmed attenuation and insertion loss. To determine the accuracy of the variable attenuation, the loss at the two frequency bands of interest, 763 MHz and 5.2 GHz, was measured for different programmed attenuations. Tones at 763 MHz and 5.2 GHz with 0 dBm power were created using a signal generator and passed through the attenuator. A spectrum analyser was used to measure the received signal power. Twenty measurements were made at each attenuation setting and the mean taken to provide an average measured attenuation. The measured attenuation for a programmed 0 dB attenuation was taken as the insertion loss of the programmable variable attenuation and was subtracted from the measured received power to give the actual attenuation applied by a given programmed attenuation. This measured variable attenuation was compared to the expected attenuation to give an offset between the requested attenuation and actual attenuation.

Figures 4.6 and 4.7 show the measured and expected attenuation for each programmed attenuation at 5.2 GHz and 763 MHz and the corresponding offset. The error bars show the standard deviation. The measured attenuation drops below the expected attenuation as the programmed attenuation increases at both 763 MHz and 5.2 GHz in Figures 4.6(a) and 4.7(a). This creates the negative offsets in Figures 4.6(b) and 4.7(b). As the signal generator used to produce the tones had a limited transmit power, for programmed attenuation greater than 63/71 dB at 5.2 GHz/763 MHz, the received power dropped below the noise threshold of the spectrum analyser as shown by the noise thresholds in Figures 4.6 and 4.7. As visible in Figures 4.6(a) and 4.7(a), below the noise threshold the measured attenuation saturates and the standard deviation of the measurements increase (shown by the error bars). The

<sup>3</sup>Reflection losses, dielectric losses and copper losses when inserting a device into a transmission line

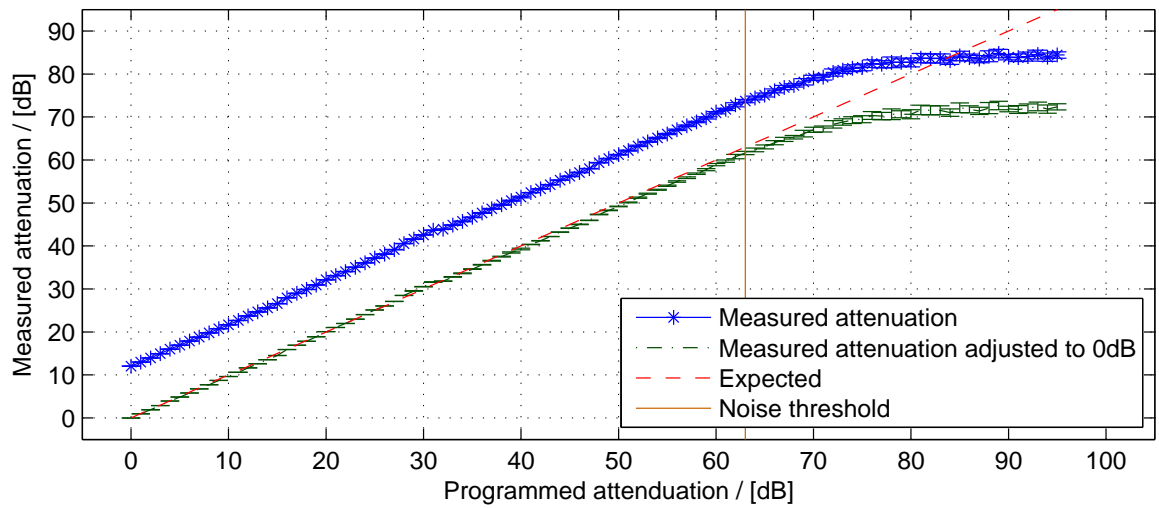
offset between the programmed and measured attenuation above the noise threshold was extrapolated by a linear least squares approximation from the offset between a programmed attenuation of 0 dB and the noise threshold. The linear least squares approximation is shown in Figures 4.6(b) and 4.7(b).

From these measurements a model is constructed which provides the actual attenuation applied by the variable attenuator,  $L_{\text{var}}$ , for a given attenuation setting,  $\text{prog\_atten}$ ,

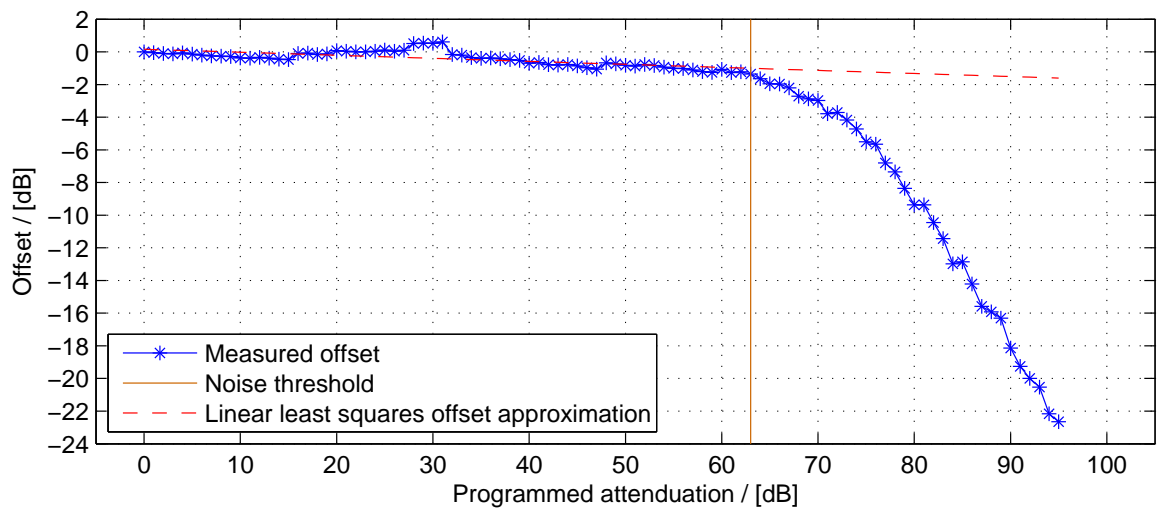
$$L_{\text{var}} = L_{\text{prog\_atten}} - L_{\text{offset}}, \quad L_{\text{offset}} = f(\text{prog\_atten}) \quad . \quad (4.3)$$

The offset between the programmed attenuation and actual attenuation,  $L_{\text{offset}}$ , is shown in Figure 4.8. This figure clearly shows an offset between the programmed and measured attenuation in 8 dB steps. This is most likely due to the attenuator being programmed in a binary pattern (inclusive combinations of 1 dB, 2 dB, 4 dB, 8 dB, 16 dB, 32 dB and a second 32 dB). Therefore to obtain  $L_{\text{var}}$ , when the programmed attenuation is greater than the noise floor,  $L_{\text{offset}}$  is used as the measured offset. When the programmed attenuation is below the noise floor, a measured value of  $L_{\text{offset}}$  is not available, therefore the linear least squares approximation is used, as shown in Figure 4.8. Note  $L_{\text{var}}$  does not include the insertion loss of the variable attenuator, i.e.  $L_{\text{var}} = 0$  dB when the attenuator is set to 0 dB.

Calibrating the fixed and variable attenuations,  $L_{\text{fixed}}$  and  $L_{\text{var}}$ , by measuring the fixed and variable attenuation offsets allows accurate receive, transmit and burst powers to be calculated with (4.1) and (4.2). With an accurate understanding of these figures, models of power consumption and performance for a given transmit power and station receive power can be created.

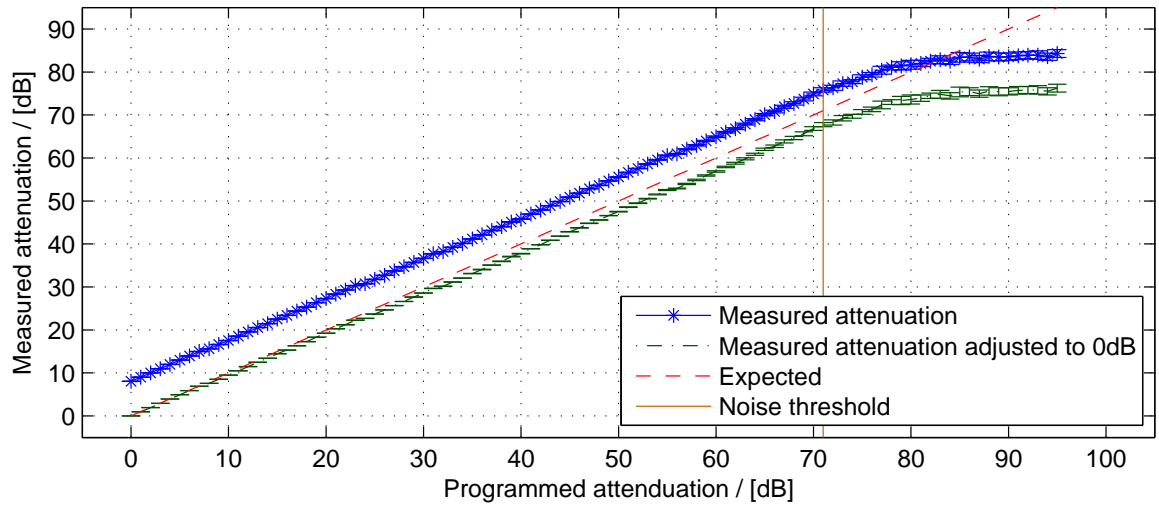


(a)

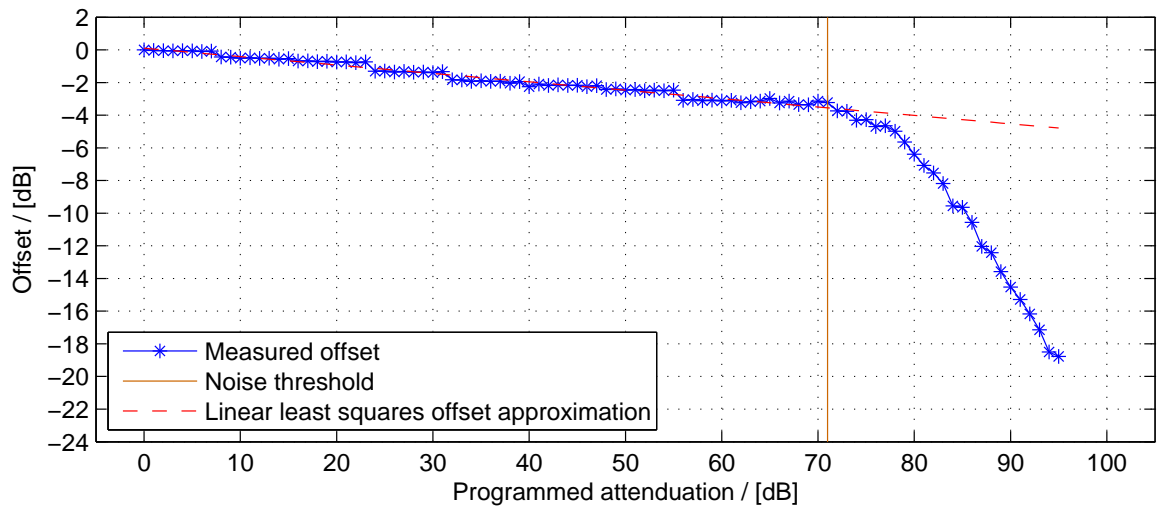


(b)

Figure 4.6: Characterising programmable variable attenuator insertion loss at 5.2 GHz showing (a) measured and adjusted attenuation for all programmable values, and (b) offset between measured and expected attenuation.



(a)



(b)

Figure 4.7: Characterising programmable variable attenuator insertion loss at 763 MHz showing (a) measured and adjusted attenuation for all programmable values, and (b) offset between measured and expected attenuation.

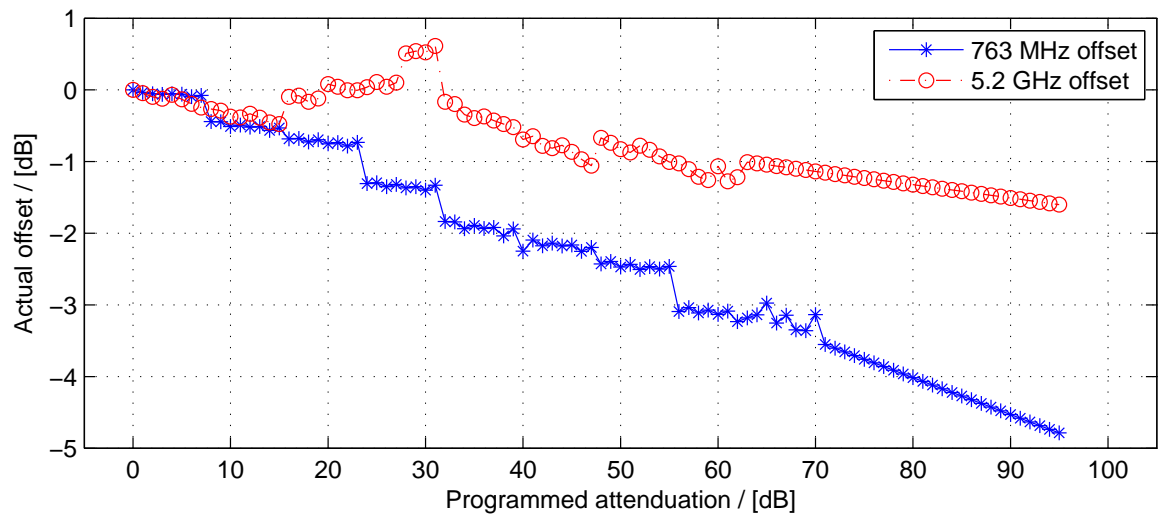


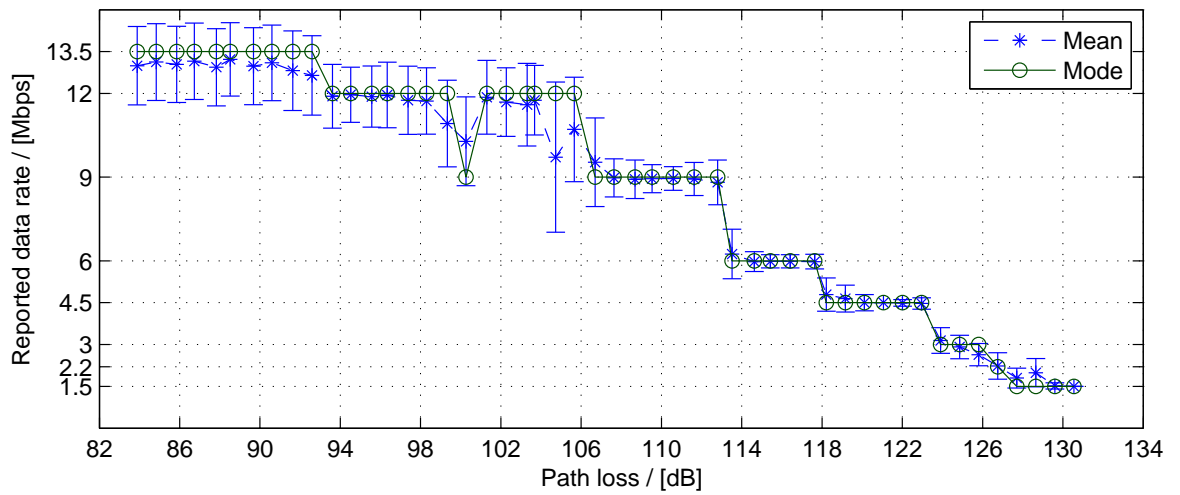
Figure 4.8: Offset for a given programmed attenuation using measured values and linear least squares extrapolation.

## 4.3 Ubiquiti XtremeRange7 Characterisation Results

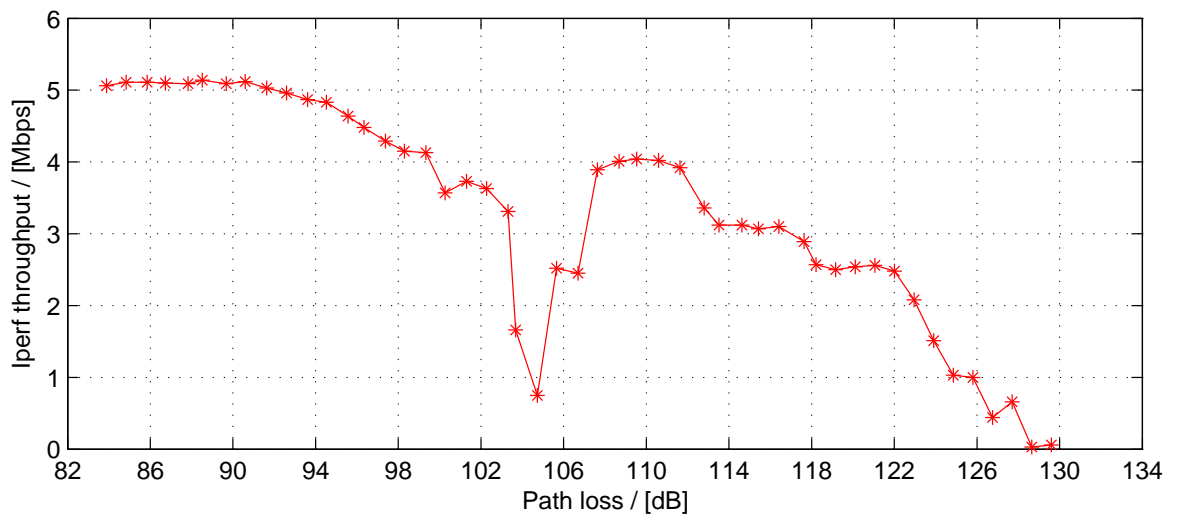
### 4.3.1 Profiling Data Rate Selection

Figure 4.9 plots the mean and mode reported data rates and the recorded TCP Iperf throughput when the radio data rate selection is set to automatic. Intuitively the data rate selection should decrease in steps as the path loss increases. As expected, Figure 4.9(a) shows the selected data rate decreases as the path loss increases until after 131 dB the connection is dropped. The throughput recorded by Iperf in Figure 4.9(b) also degrades but shows unexpected behaviour between a path loss of 98 dB and 108 dB. The Iperf throughput drops drastically before recovering. This is matched by a drop in the mean data rate in Figure 4.9(a) and a large standard deviation, shown by the error bars.

To explore this unexpected behaviour further, Figure 4.10 plots the mean and mode reported data rates and the recorded TCP Iperf throughput when the radio data rate selection is forced to a single rate. For a forced data rate the radio can only select either the forced rate, for example 54 Mbps (which is equivalent to 13.5 Mbps for 5 MHz operation as per Table 4.2), or the basic data rate (6/1.5 Mbps at 20/5 MHz). As the path loss increases there comes a point where the forced data rate can no longer be sustained and the data rate drops to the basic data rate. The higher the forced data rate, the earlier this threshold appears. The thresholds are clearly visible in the mode data rate selection plot in Figure 4.10(b). When comparing this to the mean data rate selection in Figure 4.10(a), the large error bars visible before a drop to the basic data indicate the data rate is switching frequently. This is why the automatic rate selection shown in Figure 4.9(a) occurs at a lower path loss than the individual data rates can sustain.

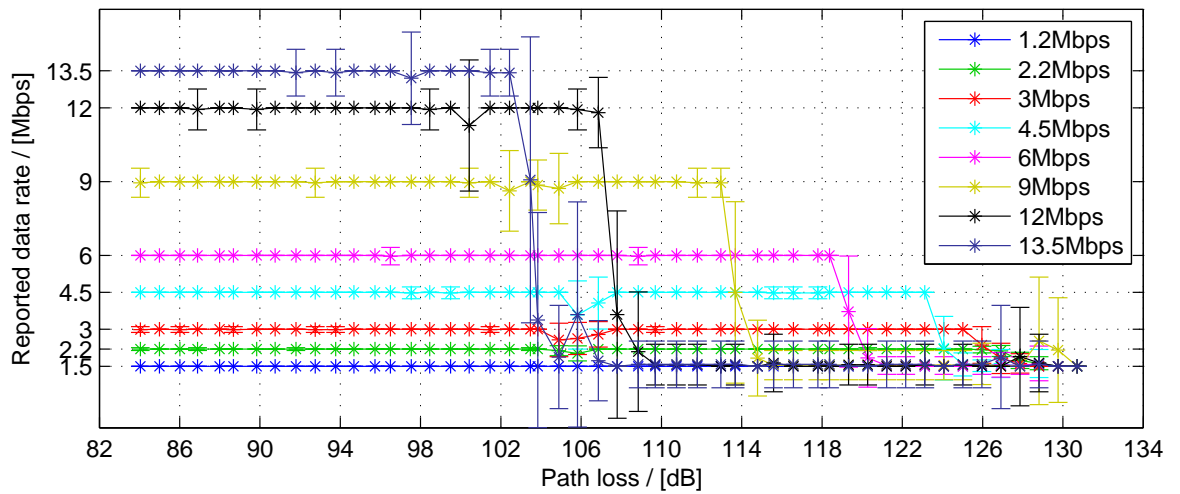


(a)

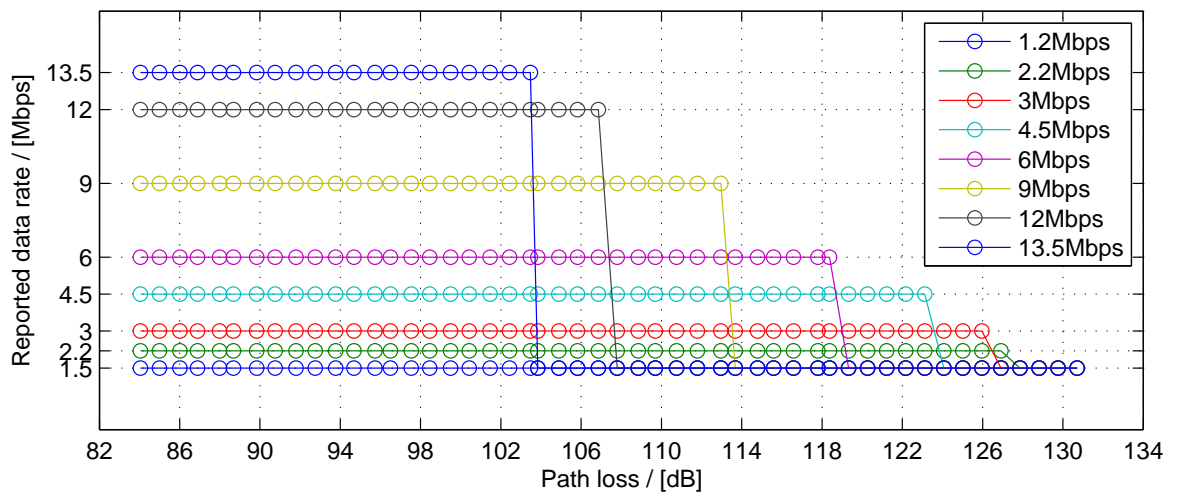


(b)

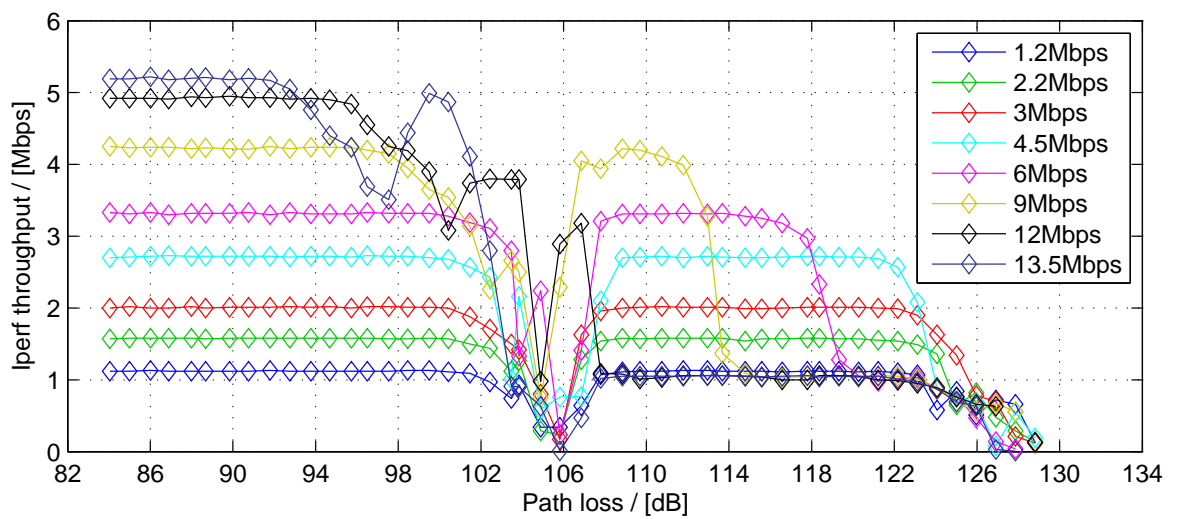
Figure 4.9: XR7 automatic rate selection profiling showing (a) reported transmit data rate and (b) Iperf TCP throughput, for different path losses.



(a)



(b)



(c)

Figure 4.10: XR7 forced data rate profiling showing (a) mean reported transmit data rate, (b) mode reported transmit data rate, and (c) Iperf TCP throughput, for different path losses.

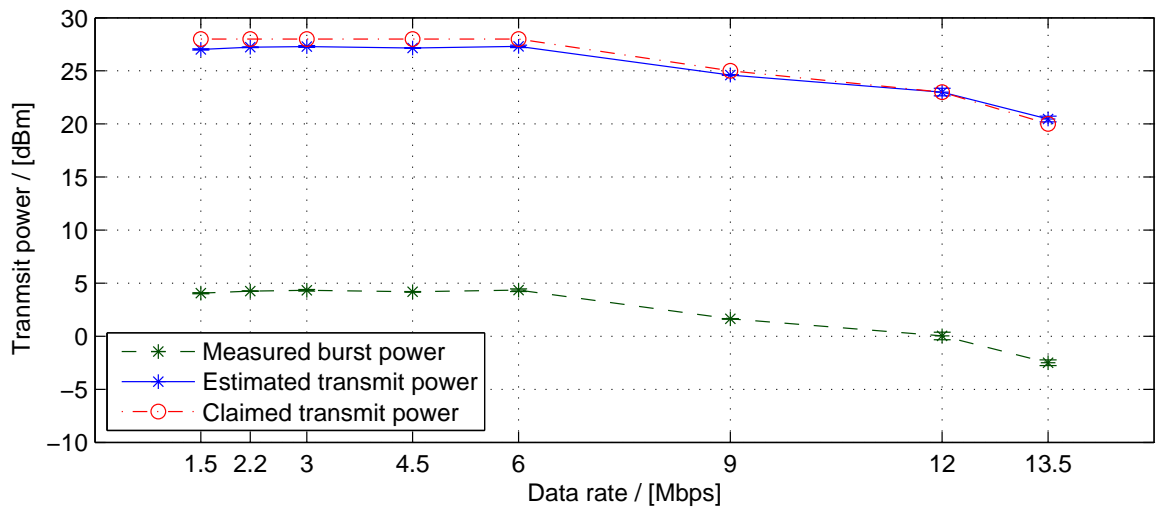


Figure 4.11: Measured burst power and estimated transmit power given path loss.

The large standard deviation visible between 98 dB and 110 dB in the mean reported data rate in Figure 4.10(a) matches the behaviour when automatic selection is used. This is likely causing the poor Iperf performance between these path losses which is visible for individual data rates between these path losses in Figure 4.9(b). This drop is likely due to the radio design.

### 4.3.2 Profiling Transmit Power

The transmit power of the XR7 was estimated using the burst power and measured losses as described in Section 4.2.3. The transmit power was estimated for two scenarios: automatic transmit power selection and manually configured, fixed transmit power.

#### Automatic Transmit Power Selection

Figure 4.11 shows the claimed transmit power according to the datasheet [?], measured burst power,  $P^{\text{burst}}$  and estimated transmit power using (4.2),  $P^{\text{tx}}$ , for each data rate. A small offset, averaging 0.5 dB, exists between the estimated transmit power and quoted transmit power. This is within the 1 dB tolerance quoted by the data sheet.

#### Fixed Transmit Power Selection

Figure 4.12 plots the measured burst power against the estimated transmit power, calculated given the measured fixed losses using (4.2). A large offset averaging 9.2 dB (the square root of the mean squared error) exists between the manually set power and estimated transmit power between a setting of 1 dBm and 20 dBm. This offset appears constant across this

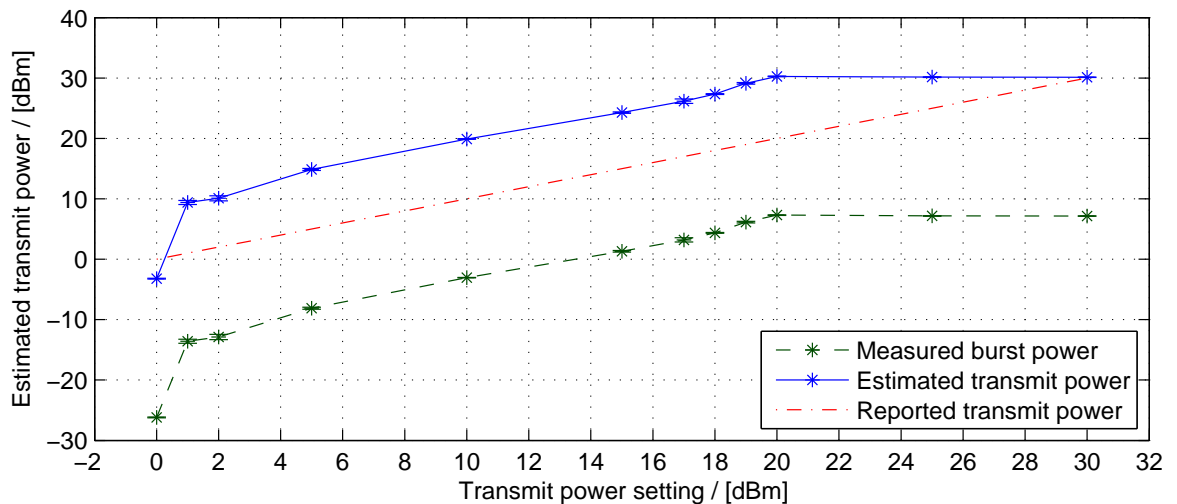


Figure 4.12: Measured burst power and therefore estimated transmit power given path loss.

range. The transmit power also saturates at an estimated 30 dBm indicating the transmit power of the radio is limited to this value.

## Discussion

For automatic transmit power selection the measured transmit power follows the quoted transmit power by reducing as the data rate increases. For a manually configured transmit power an offset of 9.2 dBm exists between the configured power and measured power. This is consistent with a reported 10 dB configuration offset [?]. As this offset is constant we can assume this is a configuration offset and must be accounted for when configuring the radios. With this offset, the quoted transmit power of the radio is accurate but saturates at 30 dBm.

### 4.3.3 Profiling Power Consumption

Figure 4.13 plots the mean recorded power consumption of the AP with the XR7 during TCP data transmission for different forced data rates. The error bars show the standard deviation around the mean rate. The measured transmit power is overlaid for each data rate. As expected, the power consumption decreases with the transmission power. This is due to the power amplifier consuming less energy when a smaller amplification is required.

To determine the power consumption of the XR7 when the transmit power is manually set, the set-up described in Section 4.2.2 was used. The transmit power was increased in 1 dB steps between and including 0 dBm and 30 dBm. The variable attenuator was set to 20 dB and the data rate was fixed to 1.5 Mbps.

The RSSI reported by the receiving radio can be used to infer the output power of the transmitting radio as given the loss between transmitter and receiver is constant, changing the

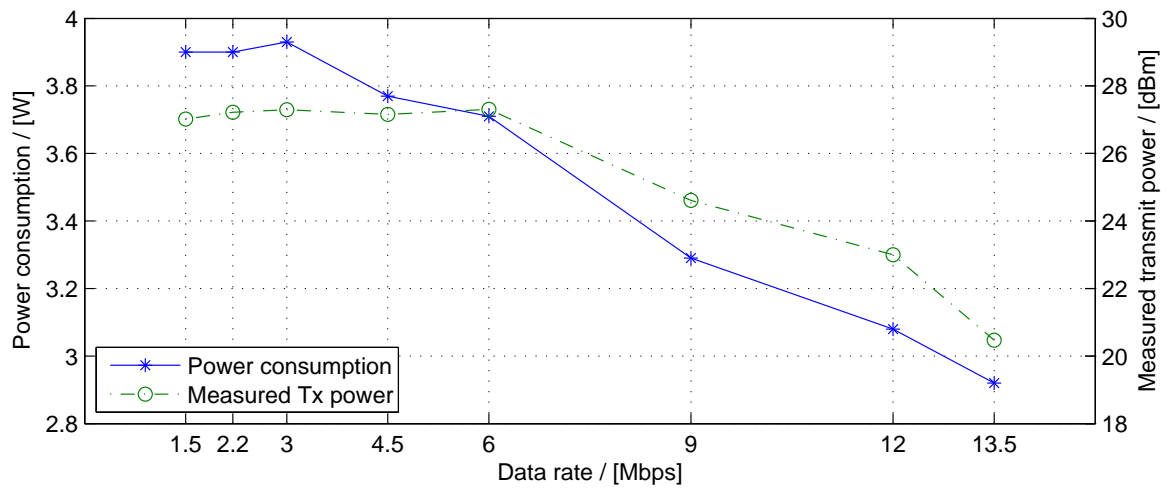


Figure 4.13: Estimated transmit power and measured power consumption for each data rate.

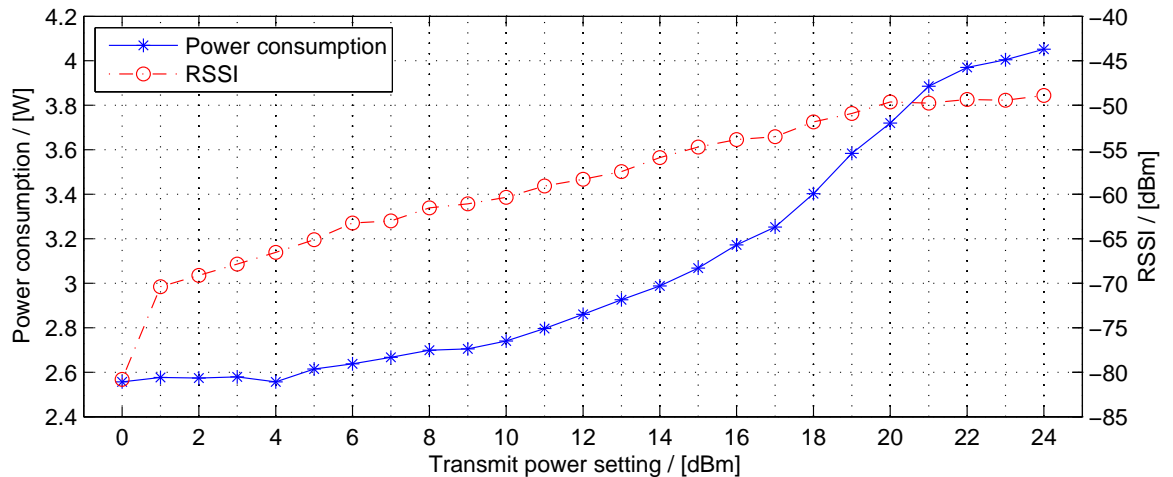


Figure 4.14: Power consumption and reported RSSI when using manual transmit power setting at 1.5 Mbps data rate.

transmit power will cause the RSSI to change. Figure 4.14 plots the measured power consumption and reported RSSI against the configured transmit power. The RSSI and power consumption increase with transmit power until 20 dBm. This mirroring indicates the actual power output by the radio is increasing with the set transmit power as the RSSI would not increase otherwise. Over the 20 dBm setting the RSSI is constant, indicating the actual output power of the radio is constant. This shows the radio limits the output power and therefore transmit power settings above 20 dBm are invalid. Above 20 dBm the power consumption still increases despite the measured output power being constant. This is likely due to the design of hardware power limitation controls within the radio.

Using the measured power consumptions for a given transmit power setting, Figure 4.15 plots the power consumption against estimated transmit power. Only valid transmit powers

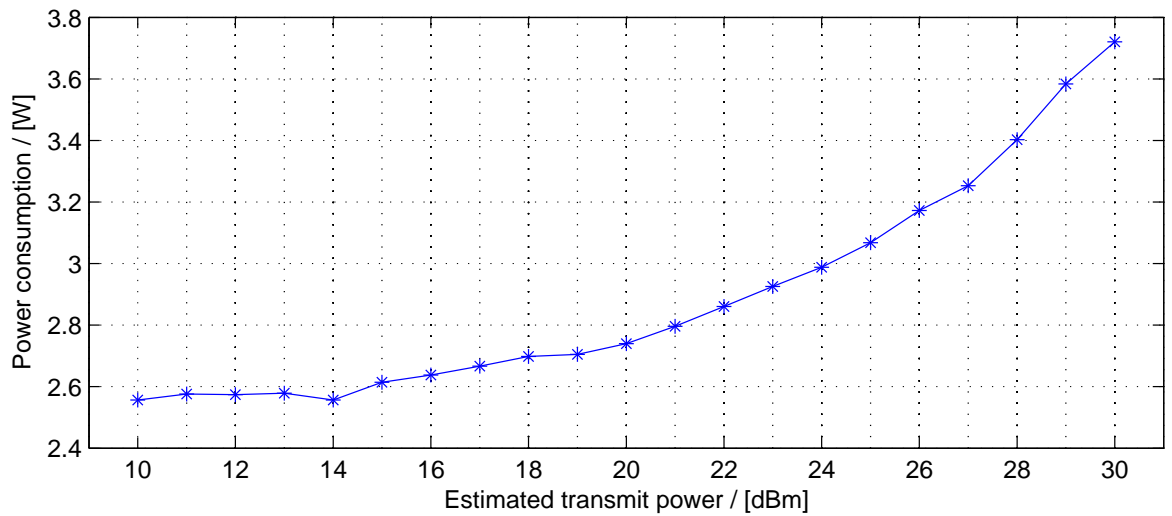


Figure 4.15: Power consumption against estimated transmit power at 1.5 Mbps data rate.

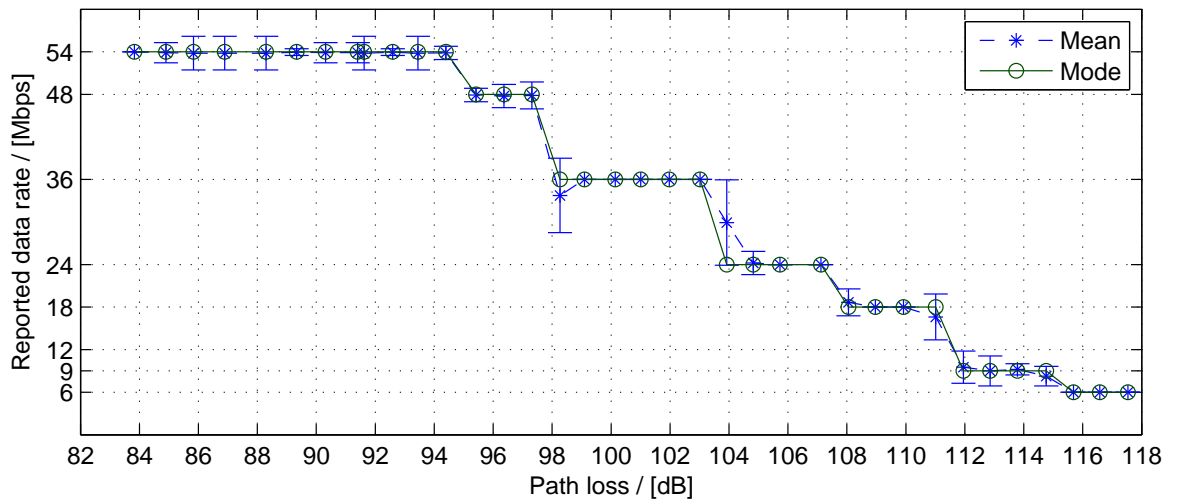
settings from Figure 4.14 are plotted. These settings are adjusted by an expected 10 dB configuration offset to obtain the estimated transmit power. This plot is used as the basis of modelling the relationship between transmit power and power consumption discussed in Section 4.5.3.

## 4.4 Ubiquiti SuperRange71 Characterisation Results

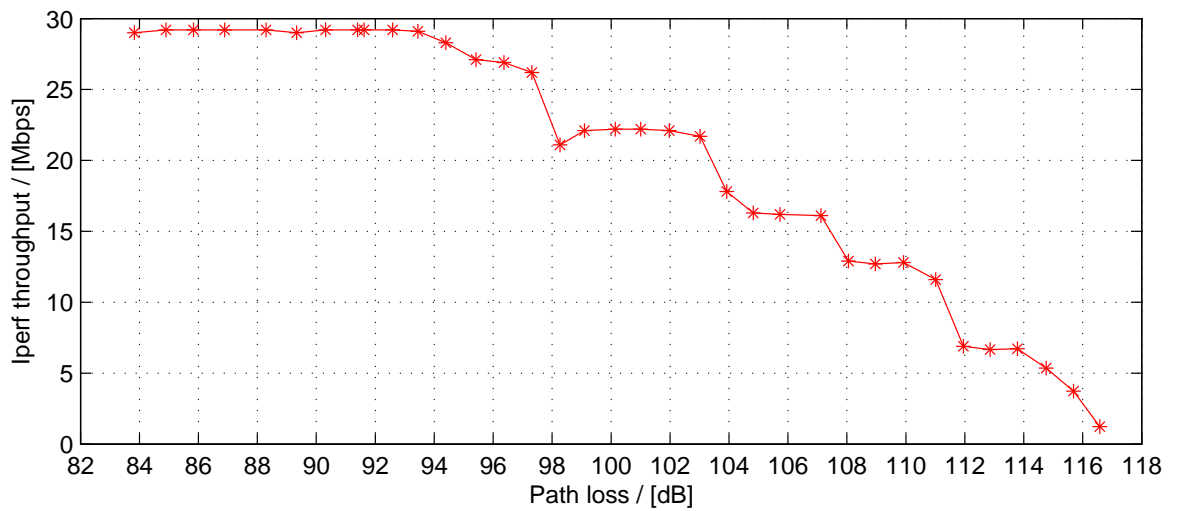
### 4.4.1 Profiling Data Rate Selection

Figure 4.16 plots the mean and mode reported data rates when the radio data rate selection was set to automatic, and the recorded TCP Iperf throughput. The error bars show the standard deviation around the mean data rate. Figure 4.16(a) shows the selected data rate decreases as the path loss increases until after 118 dB the connection is dropped. The throughput recorded by Iperf in Figure 4.16(b) also degrades with data rate. This behaviour is similar to that of the XR7 radio profiled in Section 4.3.1. Unlike the XR7 performance, no unusual behaviour or large deviation is apparent at specific path losses but the 12 Mbps data rate is never selected.

To explore why the 12 Mbps data rate is never selected, Figure 4.17 plots the mean and mode reported data rates and the recorded TCP Iperf throughput when the radio data rate selection is forced to a single rate. The reported mode data rate for each forced transmit data rate is shown in Figure 4.17(b). As observed when profiling the XR7, as the path loss increases there comes a point where the forced data rate can no longer be sustained and the data rate drops to the basic data rate. The higher the forced data rate, the earlier this threshold occurs. The reported mean data rate is a lot less variable for the SR71, as visible in



(a)



(b)

Figure 4.16: SR71 automatic data rate selection profiling showing (a) reported transmit data rate and (b) Iperf TCP throughput for different path losses.

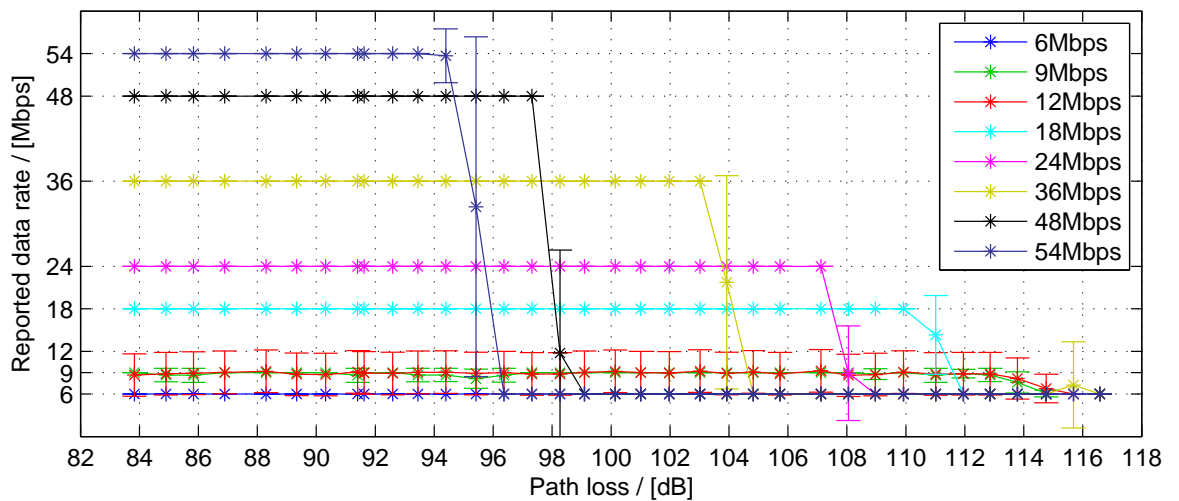
to Figure 4.17(a), than observed when profiling the XR7. The exception is the performance for a forced 12 Mbps rate. The variance of this rate is high and the mean is around 9 Mbps, indicating the radio is switching between 12 Mbps and the 6 Mbps basic rate frequently. The mode reported data rate for a forced 12 Mbps also switches between 12 Mbps and 6 Mbps. This variability is likely the reason why the 12 Mbps rate is never used in the automatic selection.

#### 4.4.2 Profiling Power Consumption

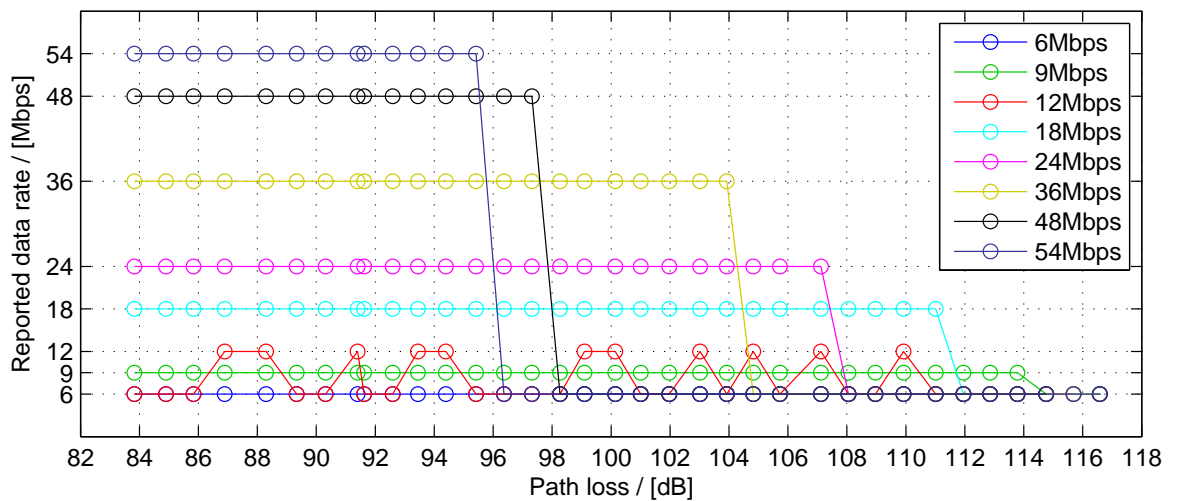
To determine the power consumption of the SR71 for manual transmit power settings, the set-up described in Section 4.2.2 was used. Power measurements were made using the equipment described in Section 4.2.4. The transmit power was increased in 1 dB steps between and including 0 dBm and 30 dBm. The variable attenuator was set to 20 dB and the data rate was fixed to 6 Mbps.

Figure 4.18 plots the measured power consumption and reported RSSI against transmit power. The RSSI and power consumption increase with transmit power until a plateau at 24 dBm before a sharp drop at 27 dBm. This mirroring indicates the actual transmit power is being increased with the setting as the RSSI would not increase otherwise. When the 26 dBm setting is exceeded the measured power consumption and RSSI drop drastically indicating the limit of the card has been reached and this is an invalid setting. The behaviour above the threshold differs significantly from the XR7 shown in Figure 4.14 showing the variability caused by different implementations.

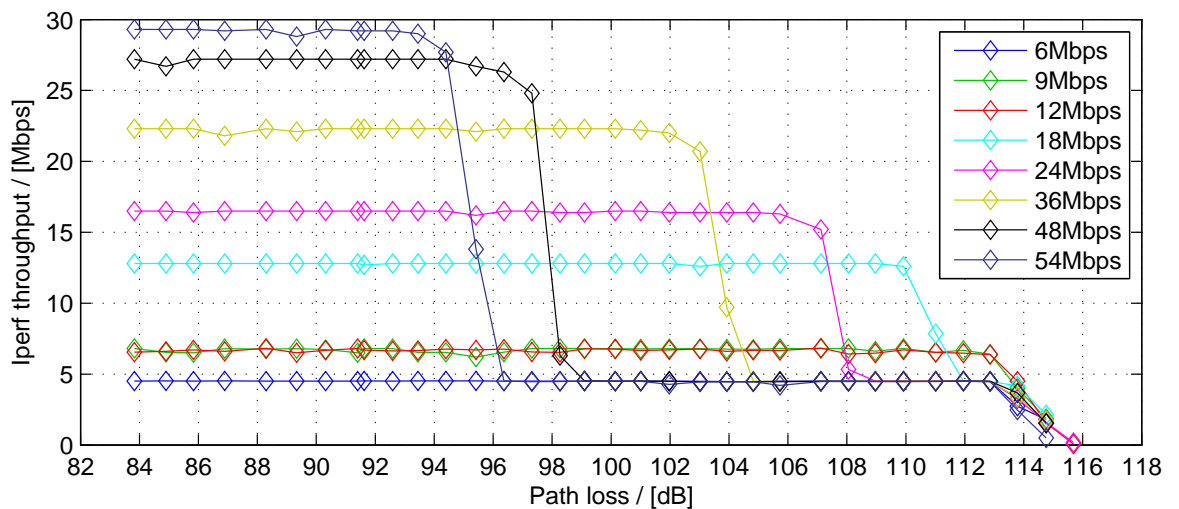
Figure 4.19 plots the measured power consumptions against estimated transmit power. Only valid transmit powers settings from Figure 4.19 are plotted. These settings are adjusted by an expected 7 dB configuration offset [?] to obtain the estimated transmit power. This plot is used as the basis of modelling the relationship between transmit power and power consumption described in Section 4.5.3.



(a)



(b)



(c)

Figure 4.17: SR71 forced transmit data rate selection profiling showing (a) mean reported transmit data rate, (b) mode reported transmit data rate, and (c) Iperf TCP throughput, for different path losses.

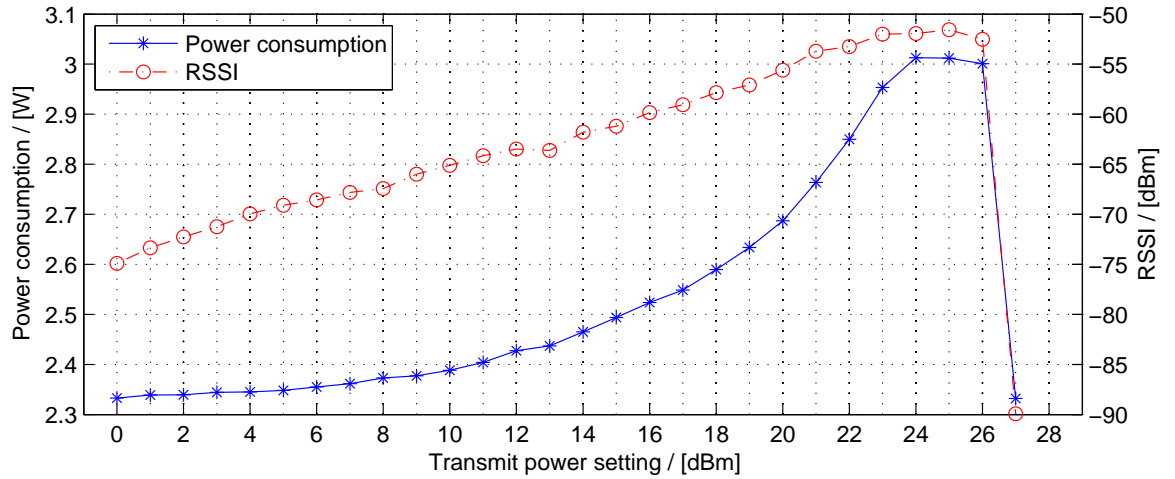


Figure 4.18: Power consumption and reported RSSI when using manual transmit power setting at 6 Mbps data rate.

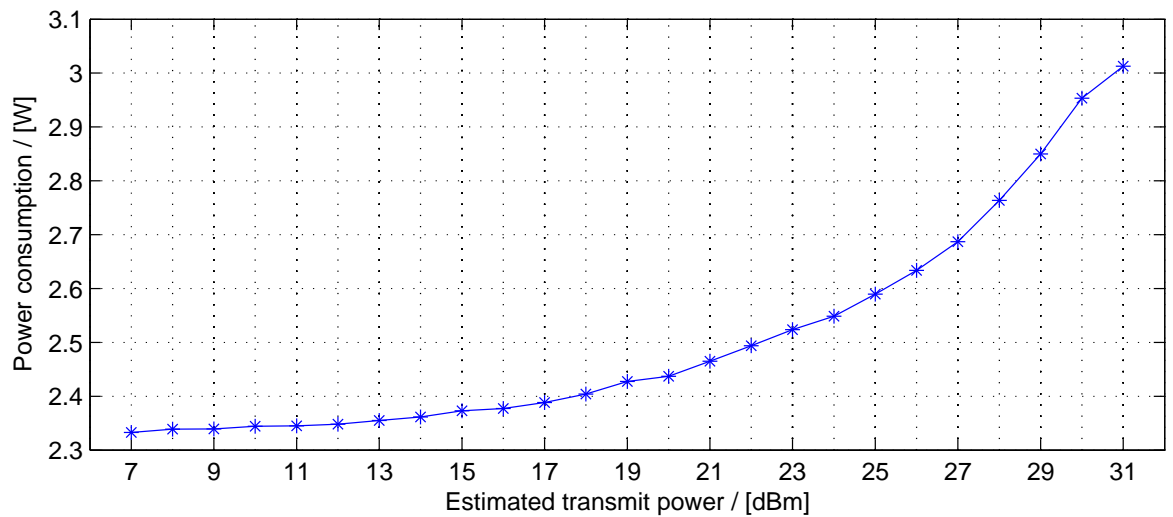


Figure 4.19: Power consumption against estimated transmit power at 6 Mbps data rate.

## 4.5 Radio Characterisation Models

The results in Sections 4.3 and 4.4 provide the data rate selection for a given path loss. To create a model of the data rate selection for a given receive signal power the relationship between path loss and received signal power must be known. This is determined in Section 4.5.1. Using this relationship Section 4.5.2 presents a model of data rate selection given receive power for both radios. Section 4.5.3 presents a model for power consumption given transmit power selection for both radios.

### 4.5.1 Relating Path loss and Received Signal Power

The Ubiquiti XR7 and SR71 radios report the received signal power in the form of RSSI. There is no standardised format for RSSI in IEEE 802.11 nor do Ubiquiti publish this information. The RSSI is likely part of the algorithm used to select the transmit rate. To understand this relationship the reported RSSI and selected data rates are investigated for estimated receive signal powers.

#### Rate Selection vs RSSI

Figure 4.20 plots the mean and mode reported data rate against the reported RSSI for each radio. As expected the selected rate decreases as RSSI decreases as the SNR will be poorer. The rate selection for both radios is very similar when the RSSI is less than 73 dBm. Above this the SR71 outperforms the XR7 by selecting and maintaining the maximum data rate at a lower RSSI. This may be due to the design of the cards. The similarity in rate selection give a strong indication that RSSI is part of the algorithm used for rate selection and is comparable for both radios.

#### RSSI vs Estimated Receive Signal Power

The receive signal power  $P^{rx}$  is estimated according to (4.1), as:

$$P^{rx} = P^{tx} - L_{\text{fixed}} - L_{\text{var}} \quad .$$

As the receive signal power is dependent on the transmit power, understanding the relationship between the received signal power and RSSI is important. Two values of transmit power  $P^{tx}$  were tested to determine the receive power and compare this to the reported RSSI:

- “Basic” data rate. The transmit power used is that associated with the “basic” data rate of the radio; 1.5 Mbps for the XR7 and 6 Mbps for the SR71. The “basic” data

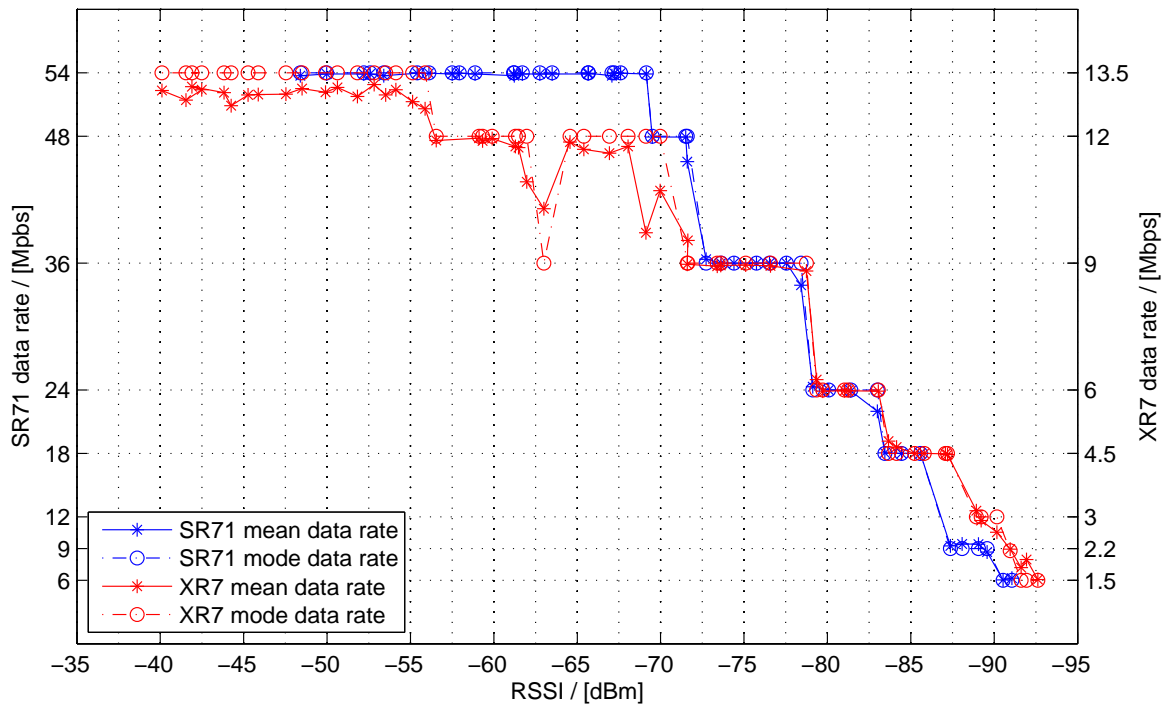


Figure 4.20: Mean and mode reported data rate against reported RSSI.

Radio	$P^{tx}$
XR7	28 dBm
SR71	25 dBm

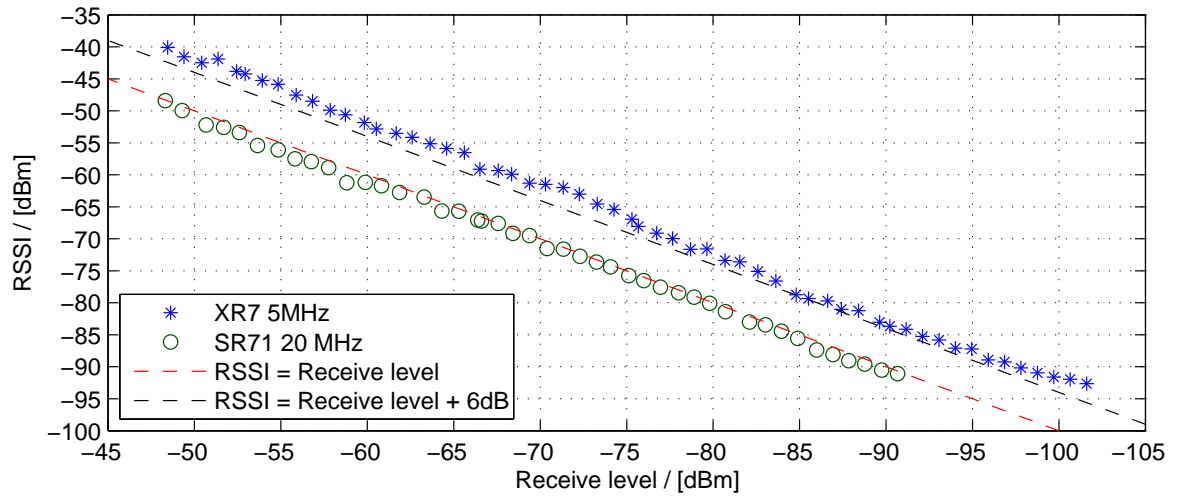
Table 4.5: Transmit powers used in (4.1) to calculate the receive signal power.

rate is used to transmit control frames in IEEE 802.11 [?].

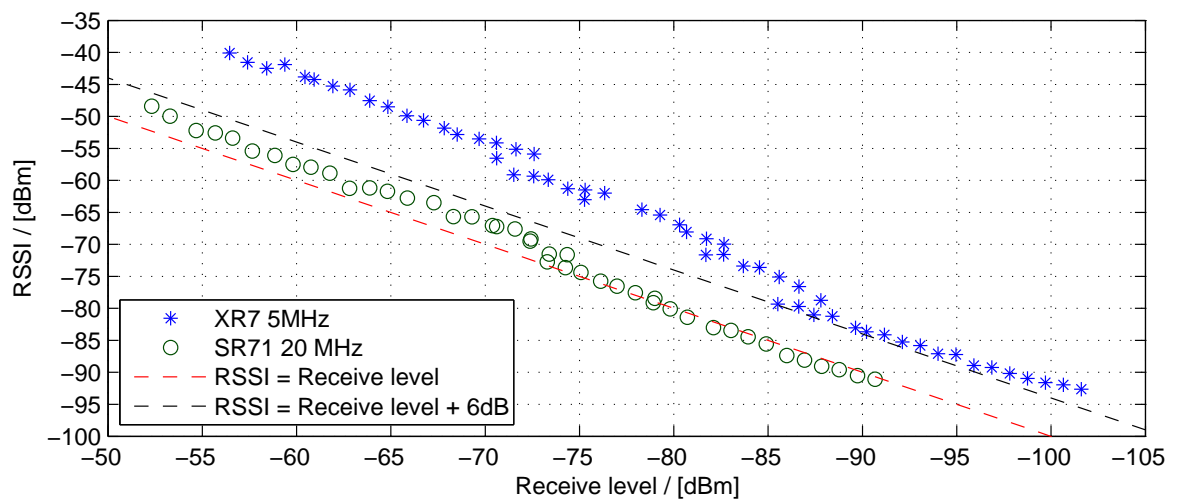
- *Selected data rate.* The transmit power used is that associated with the actual data rate mode reported data rate.

The “basic” data rate transmit powers used for the XR7 and SR71 are shown in Table 4.5. For the XR7 the transmit power was measured as discussed in in Section 4.3.2 and for the SR71 the transmit power was obtained from the data sheet [?].

Figure 4.21(a) plots the reported RSSI against estimated receive signal power when using the transmit power associated with the basic data rate. For the SR71 the RSSI follows the estimated receive signal power. For the XR7 the RSSI is greater than the receive signal power by a fixed constant. A 6 dB offset is plotted as reference as this would be the expected gain of a 5 MHz bandwidth signal over a 20 MHz bandwidth signal if the transmitted energy is the same for both. This is due to the power spectral density of the 5 MHz bandwidth transmitted signal being four times (6 dB) that of the 20 MHz signal; the energy is concentrated within the narrower bandwidth. This creates a greater SNR at the receiver. The offset of the XR7 is greater than 6 dB but given the transmit power tolerance of 1 dB [?], this meets expectations.



(a)



(b)

Figure 4.21: Reported RSSI for an estimated receive power when (a) the basic data rate transmit power, and (b) the mode data rate transmit power, is used in (4.1)

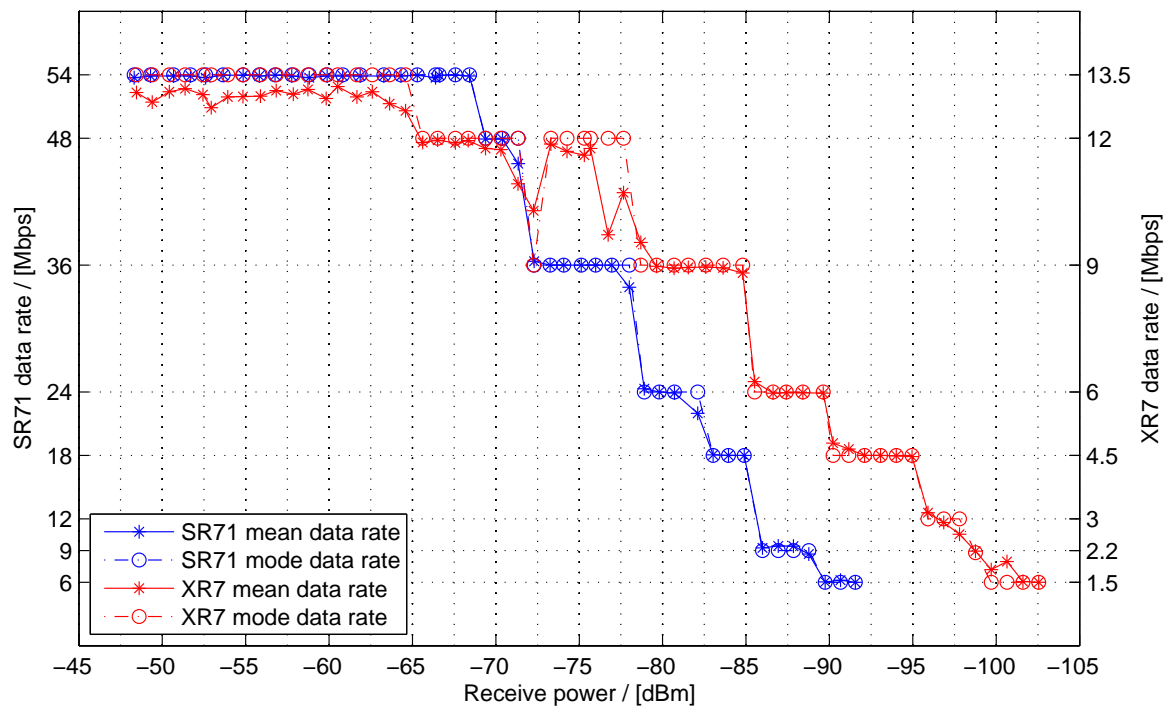


Figure 4.22: Estimated transmit power and measured power consumption for each data rate.

The constant relationship between RSSI and estimated receive power for both radios imply the measured RSSI is not based on the data rate used for transmission. This is because different data rates use different transmit powers. This would create visible steps in the RSSI as different rates are selected. Figure 4.21(b) plots the reported RSSI against the estimated receive power when the transmit power for each radio is selected which corresponds to the mode data rate (as introduced in Section 4.1.3 and measured for the XR7 in Section 4.3.2). Note the steps visible in the RSSI-receive power relationship formed when a higher transmit power is used when a lower data rate is selected (as discuss in Section 4.1.3). The fact that these steps are not visible in Figure 4.21(a), and the assumption that RSSI is based on the received power at the basic rate, imply the radios use the basic rate (and hence than transmit power) to calculate the RSSI and select the data rate.

### Rate Selection vs Estimated Receive Signal Power

With the received signal power estimated using the basic data rate transmit power, Figure 4.22 plots the mean and mode transmit rates against receive power for the XR7 and SR71 radios with data taken from Section 4.3.1 and 4.4.1. The 5 MHz bandwidth XR7 has a lower threshold for each of the rates than the 20 MHz SR71 except for the highest rate. This is expected due to the increased SNR of the 5 MHz XR7 signal compared to the 20 MHz SR71 signal, with the difference visible in Figure 4.20.

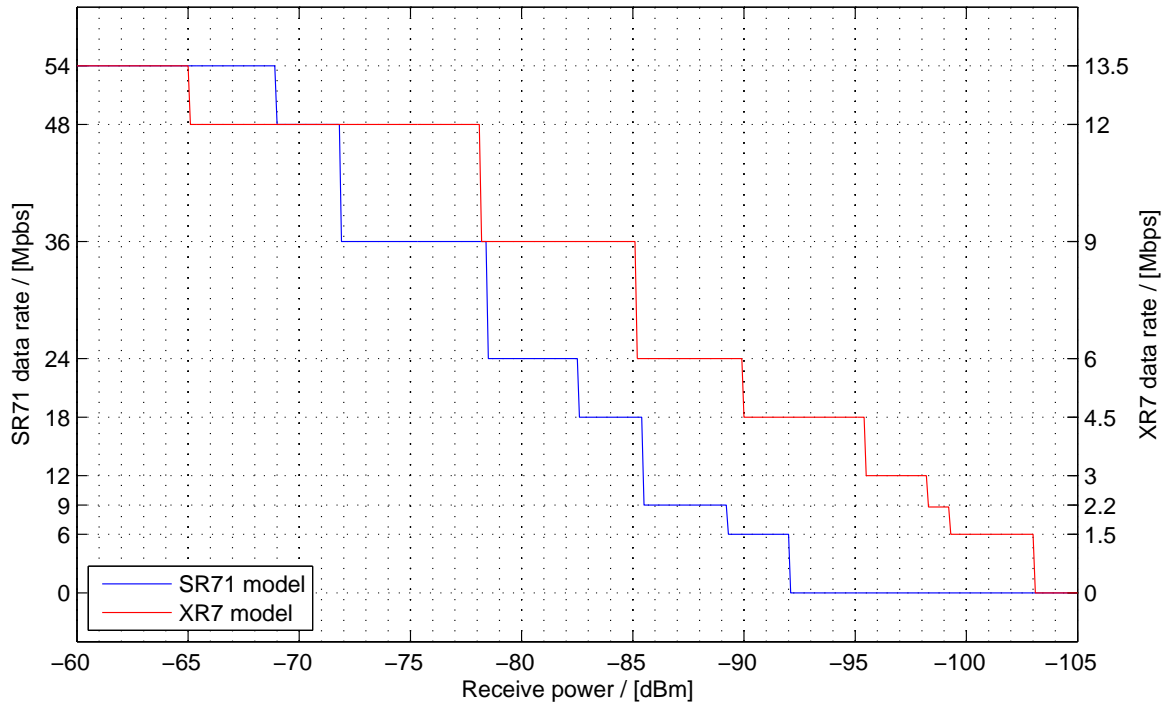


Figure 4.23: Model of XR7 5 MHz and SR71 20 MHz data rate selection given a receive signal strength .

### 4.5.2 Rate Selection Given Received Signal Power

The relationship in Figure 4.22 is used to create a model of rate selection given a received signal power. The function  $\tilde{m} = f_m(P^{\text{rx}})$  provides a transmit data rate,  $\tilde{m}$ , for a given receive power,  $P^{\text{rx}}$ . For each estimated receive signal power,  $P^{\text{rx}}$ , there is a corresponding mode transmit data rate,  $m$ , obtained through experimentation (Section 4.3.1 and Section 4.4.1). If all values of  $P^{\text{rx}}$  are ordered high to low in a set,  $P^{\text{rx}} \in \mathcal{P}^{\text{rx}}$ , then the corresponding mode transmit data rates are contained a set,  $m \in \mathcal{M}$ . The mode data rates,  $\mathcal{M}$ , are filtered to remove the unexpected behaviour of the rate increasing when the received power has decreased.

$$\begin{aligned} \Delta m_n &= m_{n+1} - m_n, \quad n \in \{0 \dots |\mathcal{M}| - 1\} \quad , \\ m_{n+1} &= m_n, \quad \forall \{\Delta m_n > 0\} \quad . \end{aligned} \quad (4.4)$$

Nearest-neighbour interpolation is used by the model to provide an expected data rate selection for a given receive signal power.

	$\alpha$	$\beta$	$\gamma$
XR7	3.395e-07	4.424	2.555
SR71	1.135e-07	4.545	2.342

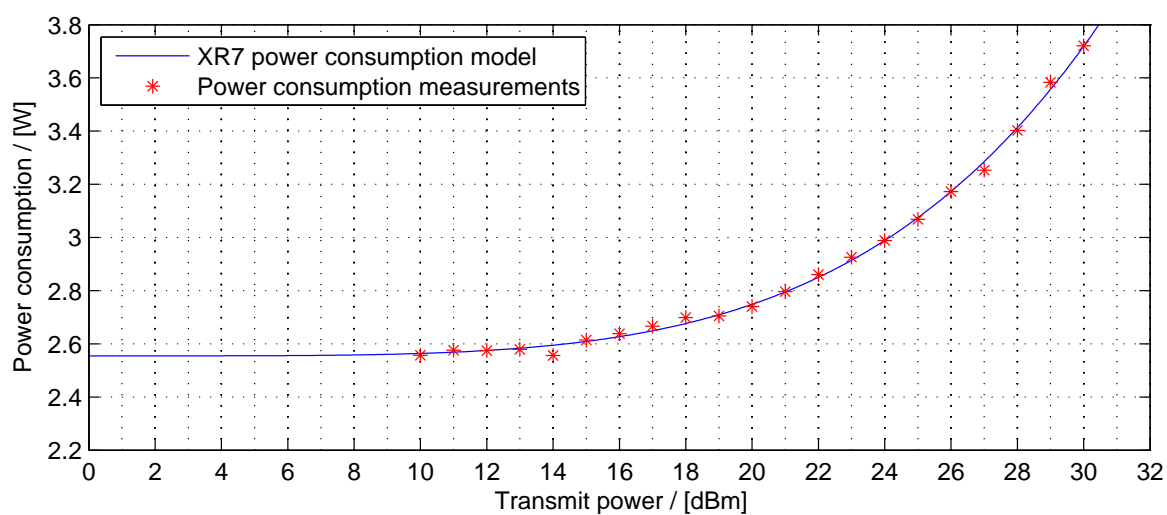
Table 4.6: Parameters for XR7 and SR71 power consumption models.

### 4.5.3 Power Consumption Given Transmit Power

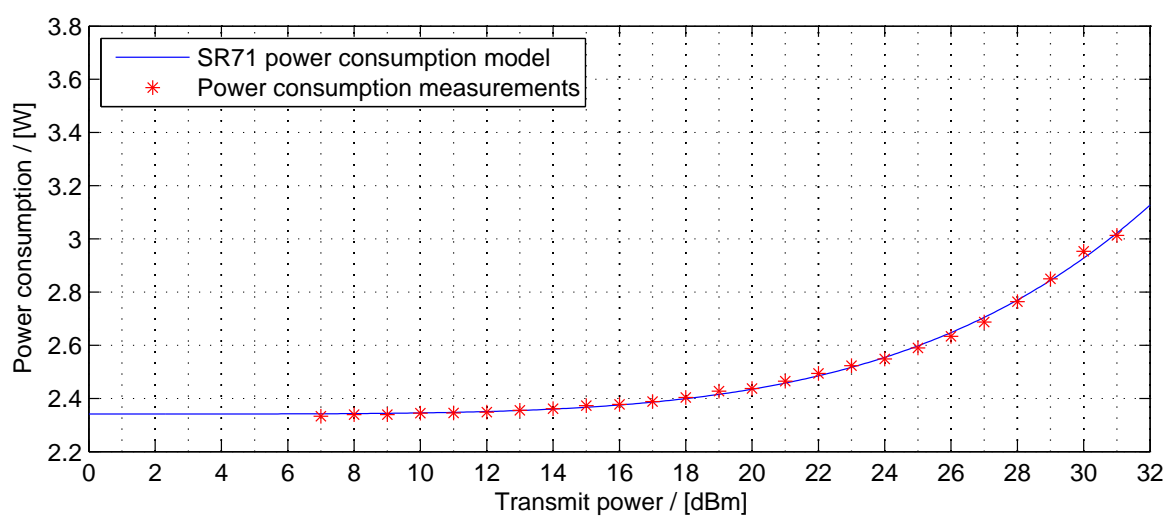
To model the power consumption of the SR71 and XR7 for a given transmit power a function,  $P_{\text{radio}} = f_p(P^{\text{tx}})$ , provides a power consumption,  $P_{\text{radio}}$ , for a given transmit power,  $P^{\text{tx}}$ . A power curve provides a good fit for the measured power consumption for valid transmit powers discussed in Sections 4.3.3 and 4.4.2. Three coefficients  $\alpha$ ,  $\beta$  and  $\gamma$  are used to describe the curve, which differ for the XR7 and SR71. The power curve is only valid when  $P^{\text{tx}} > 0$ . When this condition is not met  $\gamma$  is used as the approximation:

$$P_{\text{radio}} = \begin{cases} \alpha P^{\text{tx}\beta} + \gamma & P^{\text{tx}} > 0; \\ \gamma & P^{\text{tx}} \leq 0. \end{cases} \quad (4.5)$$

Figure 4.24 plots the modelled power consumption and measured power consumption for the XR7 and SR71 using the parameters in Table 4.6. These parameters were determined using the MATLAB *fit* tool with default parameters for a “two parameter” power fit [?].



(a)



(b)

Figure 4.24: Power consumption model for the (a) XR7 and (b) SR71 for a given transmit power.

## 4.6 Summary

This chapter presented two models obtained from lab-based measurements for Ubiquiti XR7 and SR71 radios used within Hopscotch networks discussed in Chapters 2 and 5. These models are used to provide realistic simulation results for the energy saving scheme proposed in Chapter 6.

*Data rate selection.* The data rate selected by the AP for a given receive power was characterised by using a variable attenuator to simulate a Gaussian channel. The transmit power of the radios was measured to provide an accurate estimate of the receive power required for a given data rate. A model of supported data rates for a given receive power allows estimation of link throughput for a given path loss. Interestingly both radios demonstrated unexpected behaviour. The throughput using the XR7 dropped considerably for a path loss between 98 dB and 110 dB for all data rates. The SR71 struggled to maintain the 12 Mbps data rate for all path losses and therefore was never automatically selected. The profiling also showed the 5 MHz bandwidth XR7 has a greater sensitivity than the 20 MHz SR71.

*Power consumption.* The power consumption of both radio daughter cards with a Mikrotik RouterBOARD 411 SBC was measured for configured transmission powers. The results of these measurements show the power consumption increases with transmit power and can be approximated with a power curve. The resulting model allows the power consumption of radio payload to be estimated for a configured transmit power. The knowledge that reducing the transmit power reduces power consumption allows the possibility of using this as a parameter to reduce the power consumption of a base station.

# Chapter 5

## Trial Network Analysis

This chapter presents analysis of data collected from a trial Hopscotch network on the island of Tiree. Useful models for household distribution, propagation loss and traffic patterns for a rural scenario are derived from this data.

Hopscotch trials have been running in Scotland, on the islands of Bute and Tiree. An overview of these two trials is given in Section 5.1. The trials provide an opportunity to analyse how the networks and base stations are utilised by rural communities. This analysis allows models to be constructed, and therefore network behaviour to be studied for a realistic rural scenario. Sections 5.2, 5.3 and 5.4 use data from the Tiree trial network to create models for household distribution within a rural community, the path loss experienced in open rural terrain and the bandwidth utilisation within the network. As discussed in Chapter 2, there are advantages to using a dual-band TVWS and GHz network, therefore the models derived here are important in enabling the exploration of energy saving opportunities in a rural broadband network in Chapter 6. Data collected from this network also provides an excellent opportunity to validate the design of the renewable-powered base station, WindFi, as discussed in Chapter 3.

### 5.1 Trials and Deployments

#### 5.1.1 Isle of Bute Test Bed

An 18-month collaborative research and development project was set up in 2010 to install a trial network to assess the viability of delivering broadband using TVWS spectrum to a small rural community on the south part of the Isle of Bute in Scotland. Performance was measured on a number of levels, ranging from data rates and latencies through to user experience for applications such as video-conferencing and video streaming.

As part of the trial, a renewable and mains powered WindFi base station has been operating with different IEEE 802.11 WiFi and IEEE 802.16 WiMAX radio payloads. Outdoor tests on Bute using TVWS test-kit based on a modified WiFi radio with a 5 MHz bandwidth (operating in an 8 MHz channel) have demonstrated TCP throughput up to 4 Mbps for a 4.8 km non-LOS link in a UHF channel at 4 W EIRP, and higher than 10 Mbps for 2 km connections. Results from the trial are presented in [?].

### 5.1.2 Tiree Broadband

In 2011 a Hopscotch trial was established on Tiree, using a renewable powered base station and 5 GHz wireless links to replace legacy equipment maintained by Tiree Broadband. Tiree Broadband is a not for profit company established to provide broadband access to the people of Tiree. A commercial quality wireless network linked to a multi-feed ADSL backhaul allows Tiree Broadband to reach areas of the island outwith the reach of conventional broadband. Tiree Broadband has been operating successfully since 2005; a base of 100 subscribers makes it one of the largest and most successful community broadband networks in Scotland. Results have demonstrated longest link TCP throughputs of up to 80 Mbps over a 9 km 5 GHz Band-C PTP link and up to 20 Mbps over a 3 km LOS, 5 GHz Band-B PTMP link. Further expansion of the Tiree trial network is planned with three more renewable base station deployments, five mains powered base stations, and redundancy planning to create a ring of eight base stations serving all subscribers and providing visitor access.

### 5.1.3 Community or Cooperative Operating Models

In addition to the technology issues and the challenge of finding good backhaul connectivity, it is also worth noting that an effective operating and business model is required. One potential operating and business model is that of a community or cooperatively owned network [?]. It may be possible with managed community cooperatives to operate in locations and environments that are uneconomical and have no return on investment for larger companies. For example infrastructure and ISP services could be owned by the community and operated by a network manager who will set the tariffs and access charges in consultation with a cooperative or community type trust (as already operates on Tiree). Besides network coverage, the network can serve as a framework to test and develop network support for important evolving applications such as smart grid communications [?] and real time services such as BBC iPlayer for video streaming. The network on Tiree can operate to provide connectivity to homes connected on the Hopscotch network, and also provide a platform to further test and develop, in particular for TVWS radio given the potential of the beachfront UHF spectrum available in many rural areas.

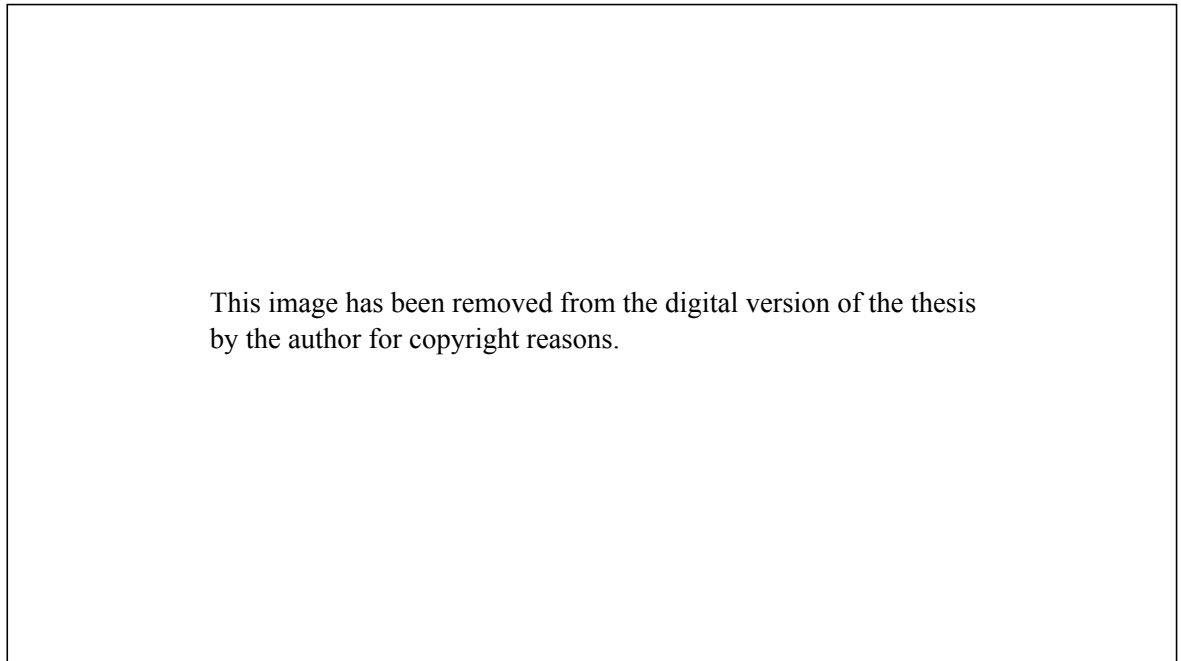


Figure 5.1: Tiree rural broadband network (source: Google Earth).

## 5.2 Household Distribution

The Tiree rural broadband network serves over 100 households and businesses on the island of Tiree. Fourteen sectors based at six base station sites provide access for the island community. Figure 5.1 shows base stations and connecting stations, which are households and businesses. White lines denote wireless links between an AP and station. Clusters are visible in different parts of the island where individual communities exist in the form of small villages or hamlets.

The majority of households are located close to the “hub” of a community, where a base station is typically situated. Figure 5.2 shows the distribution of households from community base stations on the island of Tiree, formed by measuring the distance of 118 stations in the network from all base station sites using global positioning system (GPS) coordinates.

A circularly symmetric normal distribution depending on  $x$  (North) and  $y$  (West) coordinates with the base station at the origin has been fitted with good approximation to the relative distribution of households in Figure 5.2. This provides an alternative from the uniform distribution typically used when simulating mobile station locations [?].

The distance of a household from a base station  $r$  can be described using Cartesian coordinates  $x$  (North) and  $y$  (West) if the base station is located at  $(x, y) = (0, 0)$ . The distance is given by

$$r = \sqrt{(x^2 + y^2)} \quad . \quad (5.1)$$

$x$  and  $y$  are modelled using independent standard normal distributions  $N(\mu, \sigma^2)$ . The circle

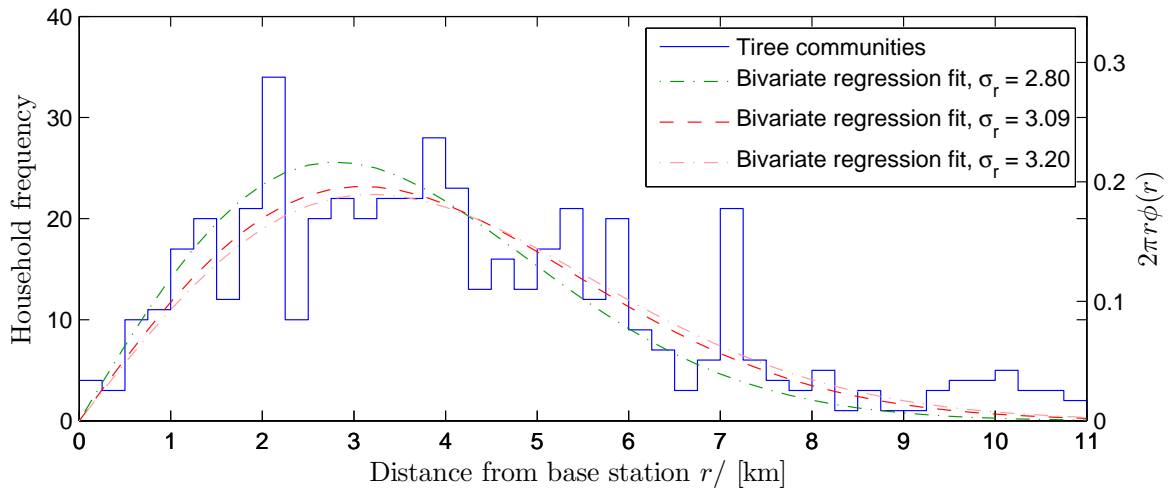


Figure 5.2: Histogram of household distance from base station on Tiree with fitted Bivariate approximations.

normal distribution is a special case of a normal bivariate distribution with no correlation between the two distributions. The joint probability density function (PDF) is given by

$$\phi(x, y) = \frac{1}{2\pi\sigma^2} \exp \left\{ -\frac{1}{2} \left[ \left( \frac{x - \mu}{\sigma} \right)^2 + \left( \frac{y - \mu}{\sigma} \right)^2 \right] \right\}, \quad (5.2)$$

where the standard deviation and mean of both individual distributions are the same and given by  $\sigma$  and  $\mu$  respectively. When the mean of both distributions is zero,  $\mu = 0$ , the PDF in a polar form for  $r = \sqrt{x^2 + y^2}$ , when  $\sigma_r = \sigma$ , is given by

$$\phi(r) = \frac{1}{2\pi\sigma_r^2} \exp \left\{ -\frac{1}{2} \left( \frac{r}{\sigma_r} \right)^2 \right\}. \quad (5.3)$$

Figure 5.2 shows the probability of finding a household between radii  $r$  and  $r + dr$  with  $\sigma_r = \{2.80, 3.09, 3.20\}$  km. The standard deviation  $\sigma_r = 3.09$  was determined to be the best fit by performing non-linear least squares fit.

### 5.3 Rural Large-Scale Path Loss

The radio equipment used within the Tiree network enables various statistics to be recorded for all radios. Access to the signal statistics of radios used within the network allowed a simple rural-large scale path loss model to be created by fitting a model to the measured data. The receive signal power, and locations of all stations was recorded every 20 minutes between November 2013 and February 2014 and used for the analysis.

### 5.3.1 Background

Propagation models allow link designers to characterise path loss based on parameters such as frequency, distance and terrain. Propagation models have been developed using either empirical measurements or modelling [?].

It is widely known through both theoretical and measurement-based propagation models that the received signal power decreases logarithmically with distance [?]. The average large-scale path loss,  $L$ , between a transmitter and receiver in dB for a distance in meters,  $d$ , is given by the simplified path-loss formula [?]

$$L = K + 10\gamma \log\left(\frac{d}{d_0}\right) + \Psi \quad , \quad (5.4)$$

where  $\gamma$  is the path loss exponent and  $\Psi$  a log-normal distributed random variable to model shadow fading. The constant  $K$  is the reference path loss at a close-in distance,  $d_0$ . This depends on antenna characteristics and the average channel attenuation, and can be obtained through field measurements or can be set to the free-space path gain at a reference distance,  $d_0$ , in the antenna's far field. Assuming omni-directional antennas for an operating wavelength,  $\lambda$  the reference path loss is

$$K = 20 \log\left(\frac{\lambda}{4\pi d_0}\right) \quad . \quad (5.5)$$

In addition to popular models based on empirical measurements such as Longley-Rice [?] and Okumara-Hata [?], other work has focused on determining the suitability of models for specific scenarios, such as fixed wireless access in the 3.5 GHz band [?], or creating a model based on measurements for an urban network [?]. This section differs by presenting a model based on 5 GHz links for a rural environment.

### 5.3.2 An Empirical Path Loss Model for Tiree

Similar to [?, ?] , the suitability of a simple path loss model based on (5.4) using a fitted path loss exponent,  $\gamma$ , is determined for the Tiree network using received signal strength measurements and known parameters and distances.

Knowledge of the link distance  $d$ , estimated link path loss  $L$  and reference path loss  $K$ , allows  $\gamma$  to be estimated for each link using (5.4). Therefore, given an estimated path loss for all links, the model in (5.4) is fitted to the data using a least squares linear regression fit by determining a value for  $\gamma$  to minimise the minimum mean square error (MMSE). The calculation and justification of each of the parameter required from the regression fit is given in Table 5.1. Figure 5.3 shows a scatter chart with error bars representing standard deviation,

Symbol	Parameter	Description
$d$	Link distances	The distance of each link is known as the precise location of each AP and station is known.
$K$	Reference path loss	Calculated using (5.5) with an operating frequency of 5.6 GHz, giving $K = 47.4$ dB.
$L$	Individual link path losses	The receive power, $P^{rx}$ , in dBm is reported by the radio and can be related to path loss, $L$ , by rearranging (5.6) as discussed in Sections 2.5.3 and 4.5.1. The transmit power $P^{tx} = 30$ dBm is the maximum permissible EIRP for the band of interest as introduced in Section 2.3. The receive antenna gain $G^{rx} = 22$ dBi is given by the Ubiquiti NB-5G22 5 GHz data sheet [?], which is the radio and antenna used by the vast majority of stations within the network.

Table 5.1: Parameters used for regression fit to determine  $\gamma$  in (5.4).

of estimated path losses for each station,  $L$ , using

$$L = P^{tx} - P^{rx} + G^{rx} \quad . \quad (5.6)$$

Two path loss approximations are plotted; free space path loss (FSPL)  $\gamma = 2.0$  and  $\gamma = 2.39$ . The path-loss exponent with the MMSE after least square linear regression was calculated as  $\gamma = 2.39$  with a root mean error of 9.3 dB.

Tiree is an interesting radio environment as there are no trees due to the high wind-speeds, therefore foliage is unlikely to affect the measurements. Figure 5.4 gives an impression of the terrain on Tiree. The weather is very changeable, leading to varied atmospheric conditions which will affect GHz radio propagation [?]. Rain fading in addition to uncertainties in the antenna gain (due to the bore-sight of the antennas not being aligned with the maximum antenna gain), clutter and interference all add to the variance in recorded receive powers.

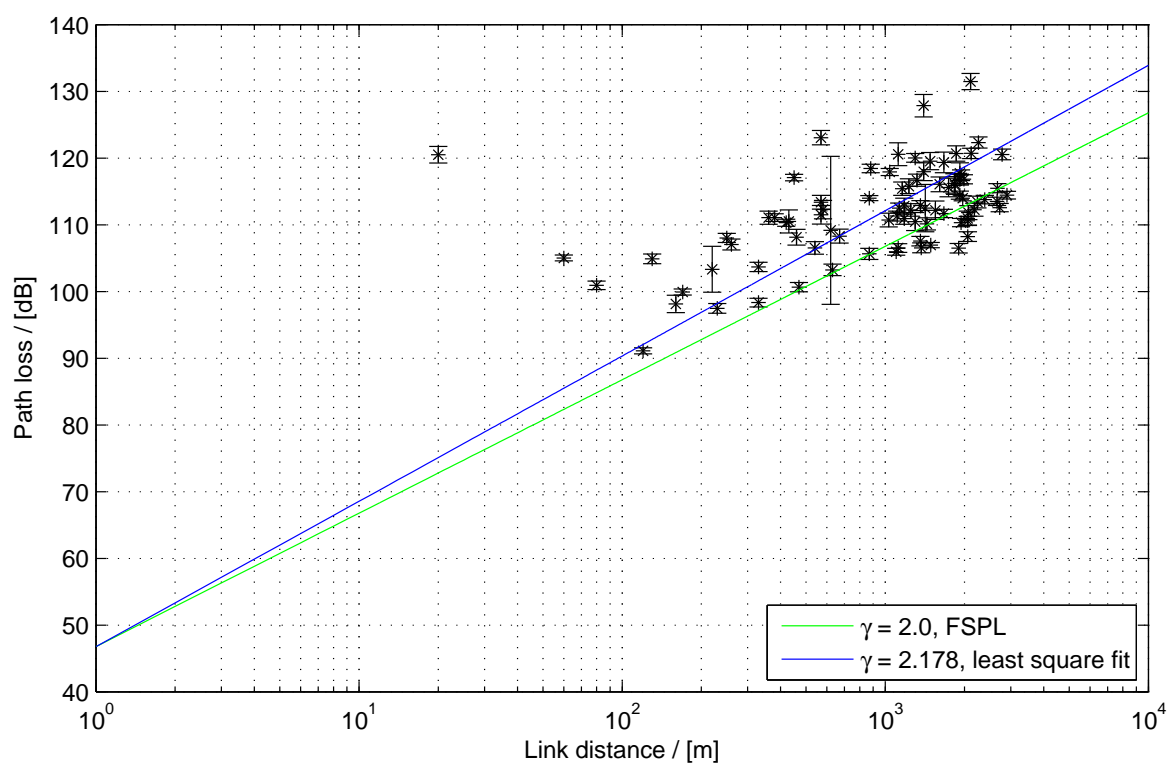


Figure 5.3: Estimated station path losses with fitted path loss exponentials.



Figure 5.4: Typical terrain on the isle of Tiree.

## 5.4 Network Bandwidth Utilisation

The Tiree Broadband network allowed the instantaneous bandwidth used on each link within the network to be monitored. This allowed a profile of the bandwidth requirements of the network to be constructed to investigate potential energy saving methods.

### 5.4.1 Background

A model for residential ADSL downstream and upstream traffic has been presented by Maier in [?]. Maier's model is based on measurements of urban communities in Europe and presents the relative volume of bandwidth for downstream and upstream traffic. Figure 5.5 plots the relative downstream and upstream throughput as a percentage of the maximum downstream throughput.

### 5.4.2 Tiree Network Bandwidth Utilisation

Within the network individual stations are normally limited to a peak throughput of 2 Mbps to protect against congestion. Figures 5.6(a) and 5.6(b) show the mean daily downstream and upstream bandwidth of traffic on the link between the Crow's Nest relay and the network IP backhaul; this link carries almost all of the traffic on the network.

The downstream bandwidth is the volume of traffic sent from the backhaul to stations within the network. The upstream bandwidth is the volume of traffic sent from stations within the network to the backhaul. To create the graphs the downstream and upstream bandwidth were polled every 20 minutes between November 2013 and February 2014. The mean bandwidth used per hour was averaged over the recording period to create hourly means for the entire period. The error bars represent the standard deviation from the mean. The error bars indicate a large variance which is expected as the network only consists of around 100 users, therefore large usage swings are expected day-to-day.

### 5.4.3 Bandwidth Utilisation Model

A model of the hourly downstream and upstream bandwidth utilisation was created from the averaged bandwidth measurements by using a smoothing spline fit<sup>1</sup> to give the upstream and downstream bandwidth utilisation as a percentage of the peak mean given the time of day. These models are overlaid onto the averaged measurements in Figure 5.6.

---

<sup>1</sup>The MATLAB *fit* tool [?] was used with a default recommended smoothing parameter  $\rho = 0.999991962513161$ .

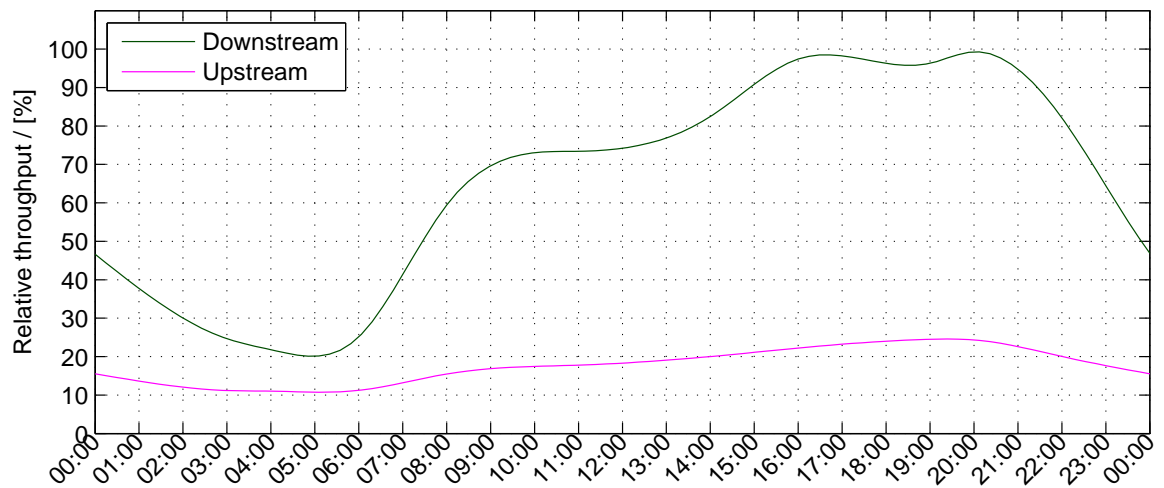
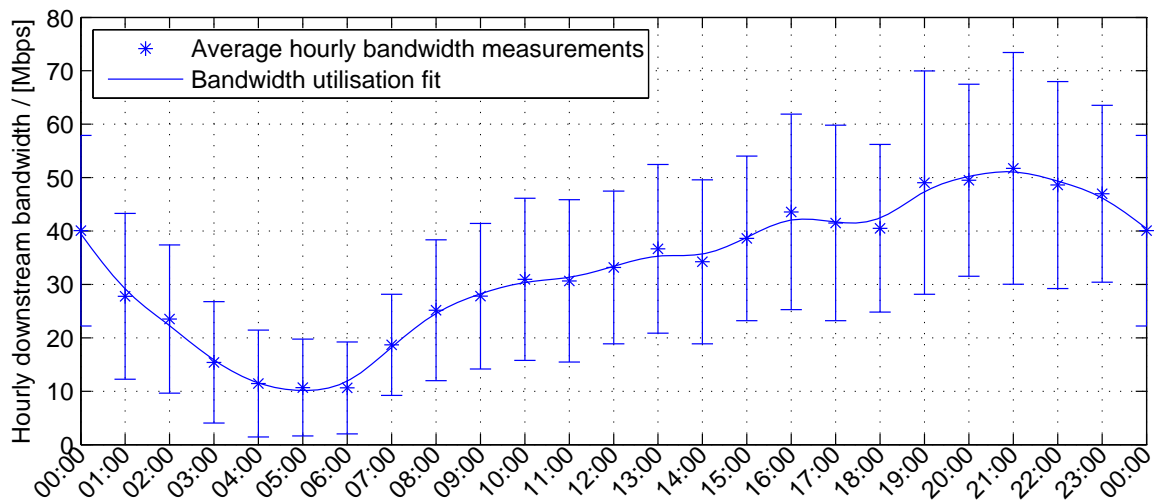


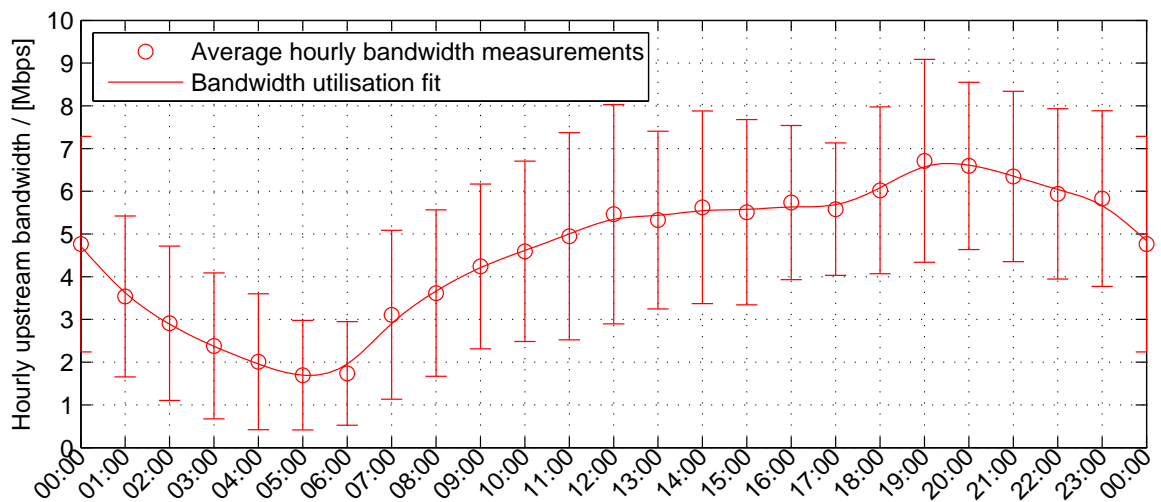
Figure 5.5: Relative ADSL downstream and upstream bandwidth utilisation recorded by Maier [?].

A diurnal pattern is visible, where substantially less bandwidth is used during the night than the day. For both the upstream and downstream the peak bandwidth used is roughly five times that of the minimum at 05:00. The ratio between the bandwidth used for the downstream and upstream varies around a mean of 7 Mbps, peaking at 8.5 Mbps at midnight and decreasing to a low of 6 Mbps at 04:00.

When Maier's model is compared to the fitted Tiree data similarities and differences are visible. Figure 5.7 compares the downstream and upstream utilisation for the two models. Figure 5.7(a) plots the two models when scaled to the peak mean Tiree downstream bandwidth. The upstream utilisation is much lower for the Tiree model than using Maier's model, with a mean difference around 5 Mbps. Figure 5.7(b) compares the downstream utilisation as a percentage of peak bandwidth. The general shape of the measured bandwidth usage matched Maier with the notable difference of the peak Tiree utilisation being delayed by an hour compared to Maier. After peaking the Tiree utilisation decreases with a more gradual gradient from 21:00 until 05:00 than the sharp decrease of Maier. Figure 5.7(c) compares the upstream utilisation as a percentage of peak bandwidth. The trends shown by the models are similar apart from the bandwidth utilisation being substantially lower between 02:00 and 07:00 using the Tiree model.

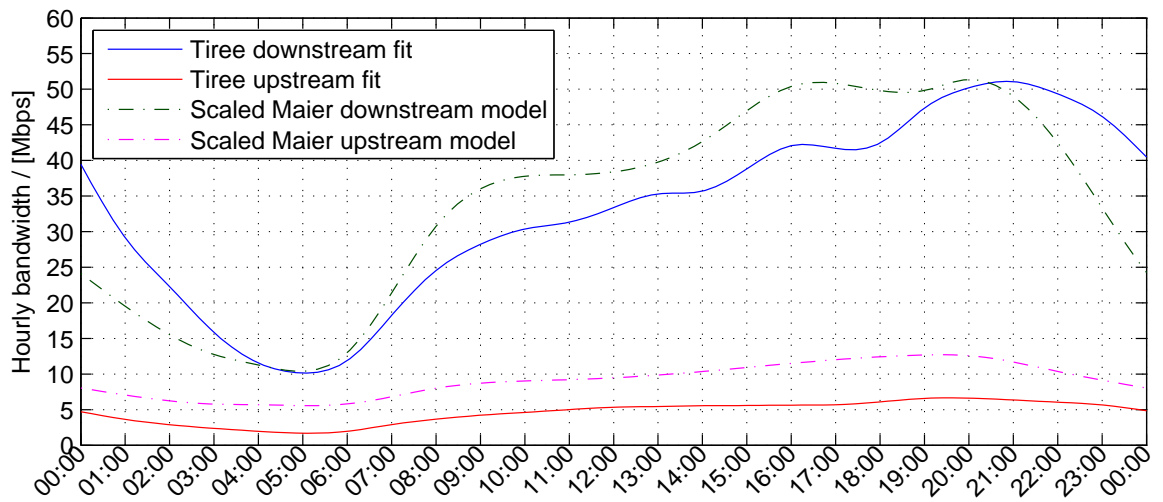


(a)

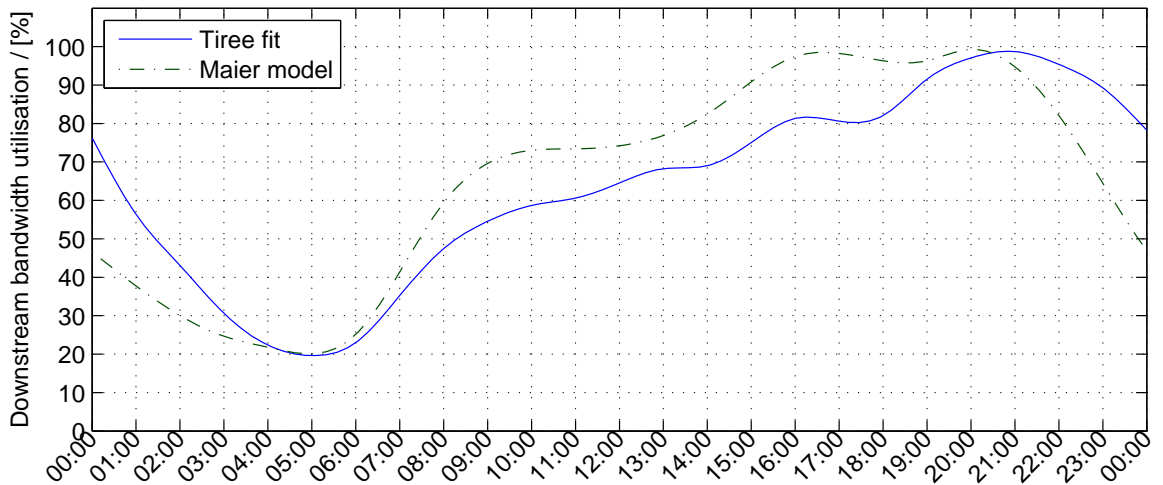


(b)

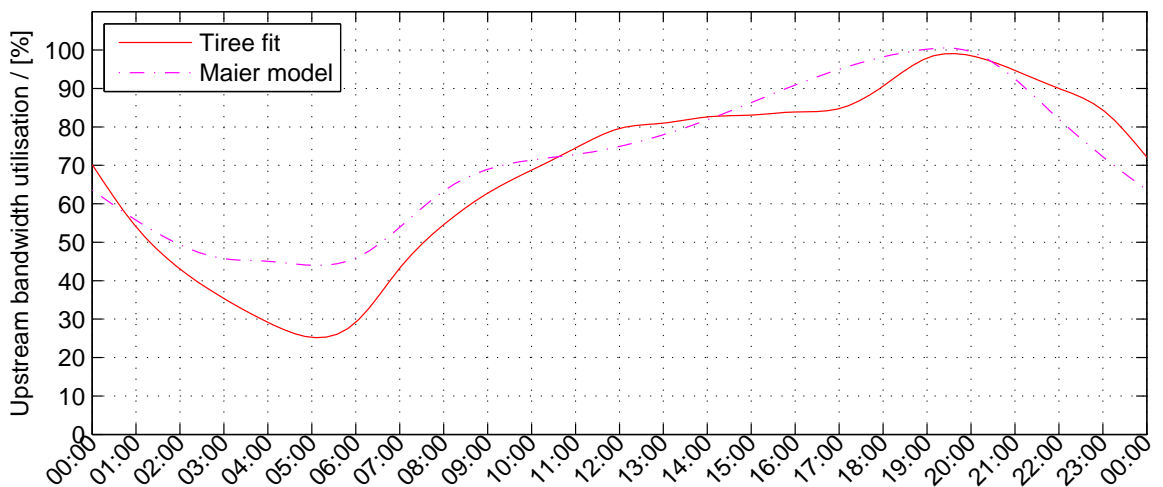
Figure 5.6: Mean daily downstream (a) and upstream (b) bandwidths of Tiree network and fitted models.



(a)



(b)



(c)

Figure 5.7: Comparison of (a) upstream and downstream models when Maier’s model is scaled to the peak average downstream throughput recorded on Tiree, (b) downstream models as a percentage of maximum utilisation, and (c) upstream models as a percentage of maximum utilisation.

## 5.5 Summary

This chapter presented analysis on a trial network on the island of Tiree. The data captured was used to create three models relevant to studying rural broadband networks:

*Household distribution.* A circularly symmetric normal distribution was shown as a good fit to the known location of households on the island of Tiree, relative to the location of base stations. This probabilistic model will be used in Chapter 6 as a basis for optimising multi-RAN network assignment for energy efficiency. This distribution is more suitable than the uniform distribution typically used, as it better reflects a rural community.

*Large-scale path loss.* Recorded signal strength values were used to estimate a path loss coefficient for a simple large-scale path loss model. This model will be used within Chapter 6 to estimate receive powers when varying a transmit power to trade-off power consumption and network performance. This model differs from existing models as measurements are made in the 5 GHz band, commonly used for rural broadband, and the area of interest is rural.

*Traffic usage.* A daily traffic model was created using recorded traffic loads at base station locations. This model, and in particular the variance in traffic throughput the day it implies, will be used in Chapter 6 to demonstrate how energy consumption can be minimised when scaling the network performance to satisfy temporal traffic demand fluctuations. As this model was created using data from a rural community, it provides a good alternative to the existing model which was created using data from urban communities.

## Chapter 6

# Optimising a Multi-Radio Network for Energy Efficiency

Hopscotch serves a rural community by using two RANs; an IEEE 802.11 RAN in the 5 GHz band and an overlay UHF RAN in TVWS. The 5 GHz RAN provides high capacity over a short range whilst the UHF RAN handles the “hard to reach” households. The assignment of individual stations which can be served by either RAN to a single RAN can be considered as a parameter when designing a network. The ability to dynamically allocate stations between RANs through cell breathing is an example of a cognitive radio application, where situational awareness can lead to energy savings which is hugely important for a renewables-powered system, as discussed in Chapter 3.

This chapter presents two contributions; the optimisation of the assignment to provide the maximum throughput for stations within the network, and a scheme to minimise base station power consumption by dynamically changing the assignment. As shown in Chapter 4, the power consumption of a radio is proportional to the transmit power. Therefore by changing the assignment dynamically, through scaling the network transmit power, the power consumption of the base station at any given point in time is minimised, while heeding constraints on the transmit power due to regulatory restrictions and on the data rate due to a required minimal fulfilment of a target data rate.

A probabilistic method is used to calculate the impact of scaling the transmission power on the average throughput and station assignment within the network. Using this information, the station assignment is optimised for throughput and power consumption. The probabilistic method calculates continuous PDFs of the network throughput which are marginalised to determine expected performance under specified conditions. A Monte Carlo method is used to validate the results of the probabilistic method by aggregating the performance of an ensemble of network configurations under specified conditions to calculate an expected performance. The problem is additionally modelled using a BBN, where stations are modelled

as discrete independent random variables. This allows the relationships between different aspects and properties of the network to be conveniently explored. To provide as realistic a scenario as possible for simulating all methods, the Hopscotch radio performance and power consumption models, characterised in Chapter 4, are used along with the household distribution, large-scale path loss, and traffic usage models presented in Chapter 5.

This chapter is structured as follows. Section 6.1 introduces the concept of selecting assignment by scaling the transmit power of a RAN and discusses relevant prior work in green radio initiatives and cell breathing. Section 6.2 presents the problem formulation. Section 6.3 introduces a general model of the network used to determine the impact of an assignment on network throughput and power consumption. Section 6.4 describes optimising the assignment to maximise station data rates. To solve this optimisation, Section 6.5 utilises the probabilistic method. Section 6.6 validates the probabilistic model with a Monte Carlo method. Section 6.7 proposes the alternative BBN method. Section 6.8 shows through simulation with the probabilistic model how the assignment of stations within a community can be optimised and the base station power consumption minimised as the station assignment dynamically changes with traffic requirements. The results of validating with the Monte Carlo method are also discussed. Section 6.9 presents analysis using the BBN method and describes the differences to the probabilistic method. Section 6.10 provides a discussion of the methods and summarises the chapter.

## 6.1 Background

### 6.1.1 Selecting Station Assignment by Scaling Transmit Power

Figure 6.1 shows the premise of changing the assignment of stations by scaling the reach of the GHz RAN using the transmit power. In Figure 6.1(a) a large transmit power causes stations within range to associate with the GHz RAN. In Figure 6.1(b) the transmit power has been decreased, therefore the range of the GHz RAN has decreased causing fewer stations to associate. All stations out-with the range of the GHz RAN associate with the far-reaching UHF RAN. This scheme is similar to the concept of cell breathing introduced in Section 6.1.3.

### 6.1.2 Green Radio Initiatives

The collective goal of green radio research is to reduce energy requirements in radio systems. This reduced energy consumption further facilitates the use of renewable energy for

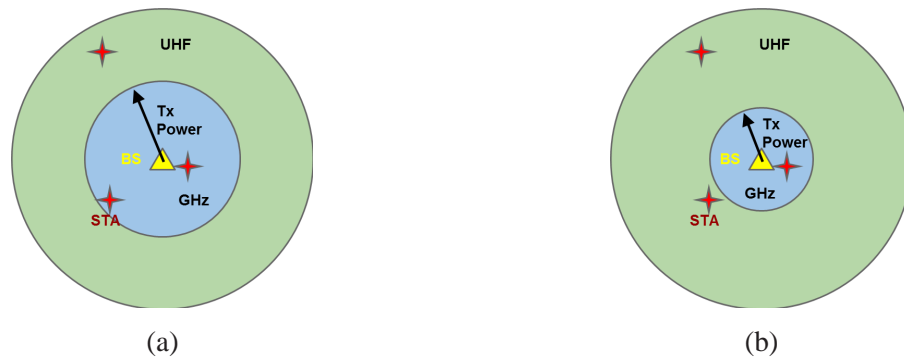


Figure 6.1: Controlling the assignment of three STAs between the GHz and UHF RANs by scaling the transmit power of the GHz RAN. (a) Initially the GHz RAN transmit power causes the UHF RAN to serve one STA and the GHz RAN to serve two STAs. (b) Reducing the GHz RAN transmit power forces the UHF RAN to serve two STAs and the GHz RAN serves one STA.

rural broadband solutions, as discussed in Sections 3.1 and 3.2. Studies into front end efficiency [?], savings in the network layer [?, ?, ?], transmission protocols [?] and radio resource management [?] all contribute to energy efficiency.

Adapting a device or network to varying conditions to fulfil a specific criterion is an example of cognitive radio [?]. Optimising power and spectrum efficiency based on an awareness of surroundings is actively being researched. Dynamic spectrum access allows transmission power to be minimised by selecting the optimum frequency and bandwidth to minimise propagation losses [?]. Energy consumption can also be scaled in relation to throughput requirements and available bandwidth by modifying the MCS [?]. Similar techniques have also been applied to mobile devices, such as using the desired user data rate as a driver for access technology selection for reduced power consumption [?].

Within a radio, the power amplifier is generally considered the most power-hungry component in the transmitter [?], and reducing the transmit power is therefore the first target when aiming to reduce power consumption. Other components, such as the processing, have also been addressed, and savings can be achieved by e.g. scaling the processor clock according to throughput [?].

Heterogeneous networks combine different radio access technologies, RANs and cell sizes. Heterogeneous networks are not just regarded as a low cost solution to increase capacity [?], but also offers the opportunity for reducing power consumption using complementary technologies whilst maintaining quality of service [?, ?, ?]. The benefits of heterogeneous networks are widely appreciated, therefore wireless standards such as LTE-Advanced have evolved to support heterogeneous scenarios [?].

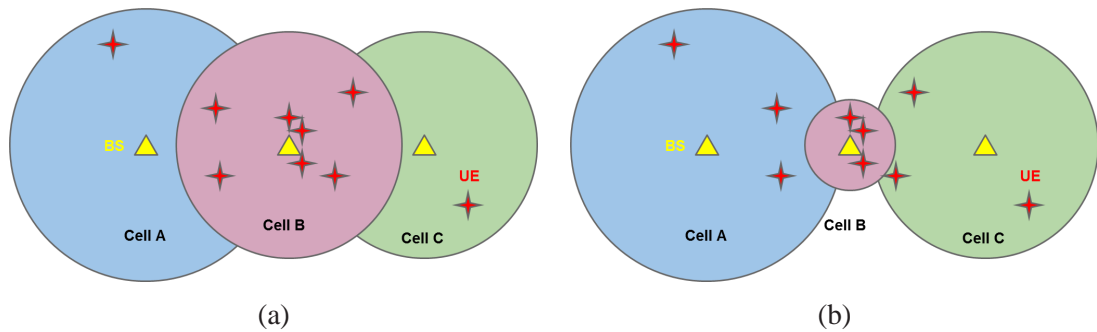


Figure 6.2: Demonstration of cell breathing: (a) Cell B is overloaded with UEs compared to cells A and C; (b) Cell B contracts to fairly distribute the number of UEs across all cells.

### 6.1.3 Cell Breathing

Cell breathing is a well known method for load balancing in cellular networks [?, ?]. Cells can expand or contract to control the number of users associated with a base station, thus controlling capacity of the network as shown in Figure 6.2.

Cell breathing is also an energy saving feature, allowing cells to be turned off when capacity is not required [?], thus enabling such networks to be powered by renewable energy [?]. The diurnal fluctuation in network traffic patterns discussed in Section 5.4 has been proposed as trigger for scaling network capacity through breathing [?], increasing capacity at the expense of power consumption during peak demand times.

## 6.2 Problem Formulation

A community of households is represented by a set  $\mathcal{S}$ , with individual households denoted as stations  $s \in \mathcal{S}$ . The stations in  $\mathcal{S}$  are ordered in ascending radial distance — and therefore in ascending path loss according to the propagation models defined later — from a single base station serving the community via a set  $\mathcal{A} = \{a_u, a_g\}$  of RANs. A UHF network  $a_u$  and a GHz network  $a_g$  are available, and stations associated with each RAN are contained in the sets  $\mathcal{S}_u$  and  $\mathcal{S}_g$ . All stations must be assigned to only one RAN such that  $\mathcal{S}_g \cup \mathcal{S}_u = \mathcal{S}$  and  $\mathcal{S}_g \cap \mathcal{S}_u = \emptyset$ . The assignment of stations in the network is therefore described as  $\mathcal{N} = \{\mathcal{S}_g, \mathcal{S}_u\}$ .

The problem addressed in this chapter is to determine the optimum assignment  $\mathcal{N}$ , which will depend on parameters of the network and the environment, and will be driven by time-varying throughput requirements placed on  $\mathcal{A}$  by the stations in  $\mathcal{S}$ . Below, Section 6.3 describes the network model, where the impact of  $\mathcal{N}$  on the individual data rates and the power consumption at the base station is derived. The cost function for optimising  $\mathcal{N}$  is then defined in Section 6.4.

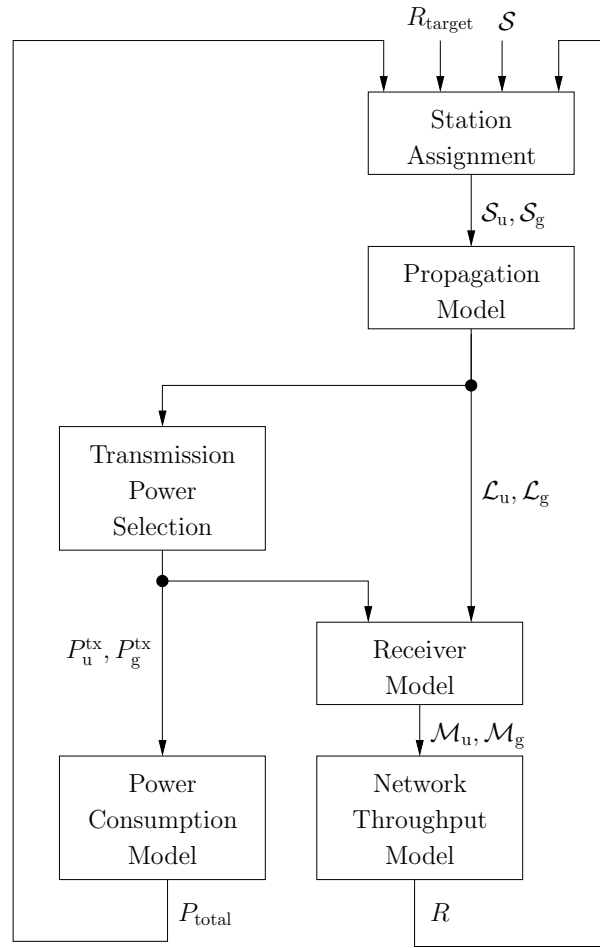


Figure 6.3: Network adjustment model.

## 6.3 Network Model

A model of the network, as outlined in Figure 6.3, relating the station assignment  $\mathcal{N}$  to an expected minimum station throughput  $R$  and power consumption  $P_{\text{total}}$  is used to study the impact of station assignments. Each station in  $\mathcal{S}_a$ ,  $a \in \{u, g\}$ , has a corresponding path loss calculated using a path loss model,  $f_l : \mathcal{S}_a \rightarrow \mathcal{L}_a, \forall a \in \mathcal{A}$ . The path losses for the stations and for each RAN form  $\mathcal{L}_a$ , which, for a given assignment  $\mathcal{N}$ , determines the transmission power  $P_a^{\text{tx}}$  for RAN  $a$ . Note that  $P_g^{\text{tx}}$  determines which stations can be reached by the GHz RAN, with the remaining stations assigned to  $\mathcal{S}_u$ . If transmit power permits, the preference of any station  $s$  is to associate with  $a_g$ .

Data is delivered to stations at one data rate from a feasible set,  $\mathcal{M}^{\text{avail}}$ . The data rate used for each station on each RAN,  $f_m : \mathcal{L}_a \rightarrow \mathcal{M}_a, \forall a \in \mathcal{A}$ , depends on the path loss of the station and transmission power of the RAN. Given a set of station data rates for each RAN,  $\mathcal{M}_a$ , the minimum throughput for an individual station within the network,  $R$ , is calculated using a network throughput model. The base station power consumption  $P_{\text{total}}$  is a function of the transmit powers, which, together with the individual station data rate  $R$ , can be used

to select a station assignment  $\mathcal{N}$  given a target data rate  $R_{\text{target}}$ . Below, the various models and components contained in the network model are analysed in order to operate the overall approach outlined in Figure 6.3.

### 6.3.1 Propagation Model

The propagation model for Figure 6.3 uses the simplified formula introduced in Section 5.3. For station  $s$  at a distance  $d$  from the base station, the path loss measured in dB is

$$L_{s,a} = K_a + 10\gamma \log(d) \quad . \quad (6.1)$$

Here,  $K_a$  is the reference path loss for RAN  $a$  operating at wavelength of  $\lambda_a$ , as discussed in Section 5.3. The constant  $\gamma = 2.39$  is the path loss exponent determined through analysis of the Ttree network presented in Section 5.3.2. Given (6.1), the parameters  $\mathcal{L}_a$  in Figure 6.3 can be calculated.

### 6.3.2 Transmission Power Selection

The transmit powers of  $\mathcal{A}$ ,  $P_a^{\text{tx}}$ , depend on the assignment  $\mathcal{N}$  and the path losses for stations in  $\mathcal{S}$  and their association with either of the RANs. The crucial component is the GHz network  $a_g$ , which must provide the transmission power  $P_g^{\text{tx}}$  to support the  $|\mathcal{S}_g|$  associated stations.

To determine  $P_g^{\text{tx}}$ , the minimum required transmit power  $P_{s,m}^{\text{tx,min}}$  is considered to establish a connection with station  $s$  on the GHz RAN at a data rate  $m$ ,

$$P_{s,m}^{\text{tx,min}} = L_{s,g} + P_m^{\text{rx}} - G^{\text{rx}} \quad , \quad (6.2)$$

where the receive antenna gain  $G^{\text{rx}}$  and the minimum receive signal level  $P_m^{\text{rx}}$  are measured in dB. The combination of all possible minimum transmission powers for each station and modulation scheme are members of the set  $\mathcal{P}^{\text{tx,min}}$ .

When  $i$  represents the index of  $s$  in  $\mathcal{S}_g$ :  $i \in \{1 \dots |\mathcal{S}_g|\}$ , then the mean transmission power required to associate station  $i$  and not  $i + 1$  is given by

$$P_i^{\text{tx,mean}} = \text{mean}\{P^{\text{tx,min}} \in \mathcal{P}^{\text{tx,min}} | P^{\text{tx,min}} < P_{i+1,0}^{\text{tx,min}}\} \quad , \quad (6.3)$$

where  $m = 0$  is the minimum data rate required for a reliable connection. Extrapolation is used for the case  $i = |\mathcal{S}_g|$ . Therefore, for a desired number of stations on the GHz RAN,  $|\mathcal{S}_g|$ ,

the required transmission power is

$$P_g^{\text{tx}} = P_{|\mathcal{S}_g|}^{\text{tx,mean}} \quad . \quad (6.4)$$

The transmission power for the UHF RAN  $a_u$ ,  $P_u^{\text{tx}}$ , is 30 dBm, which is a possible limit for TVWS transmissions recommended in the Cambridge TVWS Trial [?]. This is assumed to create a reliable connection for all stations.

### 6.3.3 Receiver Model

For a given transmission power and path loss, the receive power for station  $s$  on RAN  $a$  is given by

$$P_{s,a}^{\text{rx}} = P_a^{\text{tx}} - L_{s,a} + G^{\text{rx}} \quad , \quad (6.5)$$

assuming all quantities are measured in dB. The data rates for a set of stations in a RAN is denoted as  $\mathcal{M}_a$ . Each data rate has a corresponding minimum receive power which is obtained through a lookup table. The set of minimum receive powers for all possible data rates is denoted as  $\mathcal{P}^{\text{mcs,rx}}$ . For this analysis, these values were taken from the radio profiling models discussed in Section 4.5.2. For each station receive power, the data rate used by station  $s$ ,  $M_{s,a}$ , is determined by the range within which  $P_{s,a}^{\text{rx}}$  falls. The data rate receive power  $P_{s,a}^{\text{mcs,rx}} \in \mathcal{P}^{\text{mcs,rx}}$  best suited for station  $s$  is

$$P_{s,a}^{\text{mcs,rx}} = \max \{ P^{\text{mcs,rx}} \in \mathcal{P}^{\text{mcs,rx}} | P^{\text{mcs,rx}} \leq P_{s,a}^{\text{rx}} \} \quad . \quad (6.6)$$

Therefore, the data rate for the set of stations in each RAN is  $f_m : \mathcal{P}_a^{\text{mcs,rx}} \rightarrow \mathcal{M}_a$ , which according to Figure 6.3 provides the input to the network throughput model.

### 6.3.4 Network Throughput Model

Given a set of data rates for each station on a RAN, the network throughput model calculates the expected UDP downlink data rate for each station using a model of the IEEE 802.11 MAC layer in point coordination function (PCF) mode [?]. This model is used for both networks.

With the expected data rate  $R_a$  in bits/s (bps) for each of the  $N = |\mathcal{S}_a|$  stations in  $\mathcal{S}_a$ ,

$$R_a = \frac{L_{\text{DATA}}}{T_{\text{PCF},a}} \quad , \quad (6.7)$$

the minimum data rate for an individual station in the network,  $R$ , is given by

$$R = \min (R_a), \forall a \in \mathcal{A} \quad . \quad (6.8)$$

In (6.7),  $L_{\text{DATA}}$  is the length of the data packet in bits, which for simplicity is assumed to be uniform across all stations to simulate a congested network. Further, the total time required for a PCF exchange between the point coordinator and all associated stations is

$$\begin{aligned} T_{\text{PCF}} &= T_{\text{PIFS}} + T_{\text{BEACON}} \\ &+ \sum_{n=0}^{N-1} (T_{\text{DATA\_CF\_POLL}}[n] + T_{\text{CF\_ACK}}[n]) \\ &+ (2N + 1) T_{\text{SIFS}} + \max (T_{\text{CF\_END}}) \quad , \end{aligned} \quad (6.9)$$

where for each station

$$\begin{aligned} T_{\text{DATA\_CF\_POLL}} &= T_{\text{PRE}} + T_{\text{PHY}} + \left\lceil \frac{22 + L_{\text{MAC}} + L_{\text{DATA}}}{N_{\text{DBPS}}} \right\rceil \\ T_{\text{CF\_ACK}} &= T_{\text{PRE}} + T_{\text{PHY}} + \left\lceil \frac{22 + L_{\text{MAC}}}{N_{\text{CBPS}}} \right\rceil \\ T_{\text{CF\_END}} &= T_{\text{PRE}} + T_{\text{PHY}} + \left\lceil \frac{22 + L_{\text{CF\_END}}}{N_{\text{CBPS}}} \right\rceil \end{aligned} \quad (6.10)$$

are derived from standard IEEE 802.11a parameters and values. The number of data bits per symbols  $N_{\text{DBPS}}$  and number of control bits per symbols  $N_{\text{CBPS}}$  depend on the MCS index of the data rate used (Table 4.2). The length of the beacon is denoted by  $T_{\text{BEACON}}$ ,  $T_{\text{PIFS}}$  is the PCF interframe space,  $T_{\text{SIFS}}$  the short interframe space,  $T_{\text{PRE}}$  the preamble length,  $T_{\text{PHY}}$  the signal symbol overhead in the physical protocol unit,  $L_{\text{MAC}}$  is the number of bits of MAC data within the physical layer convergence protocol service data unit, and  $L_{\text{CF\_END}}$  is the length of the contention free period end frame contents in bits. For a channel bandwidth  $B$ ,  $T_{\text{SIFS}}$ ,  $T_{\text{PIFS}}$ ,  $T_{\text{PRE}}$  and  $T_{\text{PHY}}$  are scaled by  $\frac{20\text{MHz}}{B}$  [?].

### 6.3.5 Power Consumption Model

The power consumption of the radio is approximated as a function of the power consumption as obtained through measurements discussed in Section 4.5.3. As the EIRP is considered as the transmit power in this analysis, to obtain the configured radio transmit power the model described by (4.5) must be modified. Given the EIRP  $P_a^{\text{tx}}$  and transmit antenna gain  $G_a^{\text{tx}}$ ,

$$P_{\text{radio},a} = \alpha_a (P_a^{\text{tx}} - G_a^{\text{tx}})^{\beta_a} + \gamma_a \quad . \quad (6.11)$$

The coefficients  $\alpha$ ,  $\beta$  and  $\gamma$  in (6.11) differ for each RAN, as summarised in Table 4.6. Therefore the total power consumption of the base station is

$$P_{\text{total}} = \sum_{\mathcal{A}} P_{\text{radio},a} \quad . \quad (6.12)$$

## 6.4 Optimum Station Assignment

The optimum station assignment minimises the difference between the time-varying target downstream data bandwidth,  $R_{\text{target}}$ , and the bandwidth  $R(\mathcal{N}_i)$  provided by a specific station assignment  $\mathcal{N}_i = \{\mathcal{S}_{u,i}, \mathcal{S}_{g,i}\} \in \mathcal{N}^{\text{All}}$  where  $\mathcal{N}^{\text{All}}$  is a set of all possible station assignments, with  $|\mathcal{N}^{\text{All}}| = |S| + 1$ . Achieving only a lower rate will penalise station users, while a higher rate utilises more transmit power than necessary. Therefore the optimum assignment  $\mathcal{N}_{\text{opt}}$  can be obtained by solving the constrained optimisation problem

$$\begin{aligned} \mathcal{N}_{\text{opt}} &= \arg \min_{\mathcal{N}_i \in \mathcal{N}^{\text{All}}} |R_{\text{target}} - R(\mathcal{N}_i)| \quad , \\ \text{s.t.} \quad &R(\mathcal{N}_i) \geq R_{\text{target}} \\ &P_a^{\text{tx}} \leq P_{a,\text{max}}^{\text{tx}}, \forall a \in \mathcal{A} \quad , \end{aligned} \quad (6.13)$$

where  $P_{a,\text{max}}^{\text{tx}}$  is the maximum permissible transmission power. By seeking to keep the data rate to a permissible minimum, (6.13) will also directly minimise transmission power.

The optimisation problem in (6.13) is not guaranteed to be convex, and a closed form solution can be challenging. Therefore, using the three methods described in the following sections, a feasible set of assignments is first identified that satisfies the constraints, and thereafter a graphical, but unconstrained optimisation is performed over this feasible set.

## 6.5 Probabilistic Method

A probabilistic method is used to determine the average station assignment and throughput, given the transmit power of the GHz RAN based on the network model described in Section 6.3. These results are used to perform the optimisation described in Section 6.4. For a given transmission power the probability of the stations being received at a particular data rate is calculated in Section 6.5.1. The average throughput and assignment are then calculated by assessing the probability of all possible permutations of data rates, discussed in Section 6.5.2.

Both the assignment and network throughput are a function of the receive power of each station, therefore the distribution of the receive power of stations is required for analysis. For

$n$  stations within a network with a fixed transmit power, the receive power of each station can be modelled as a random variable  $X_r$  where  $r \in \{1, 2, \dots, n\}$ . The stations are ordered by receive power, from strongest to weakest, to create a set of independent and identically distributed random variables  $\{X_1, X_2, \dots, X_n\}$  such that  $X_1 \geq X_2 \geq \dots \geq X_n$ . This set represents the receive power of all stations within the network. The random variables have a PDF  $f_X(x)$  and cumulative density function (CDF)  $F_X(x)$ .

### 6.5.1 Probability of Data Rate Selection

Each station can be served at one rate out of a set of possible data rates, denoted by an MCS index  $m \in \mathcal{M}^{\text{avail}}$ . As discussed in Section 6.3.3 the data rate selected is based on the measured receive power at the station. Therefore each data rate requires a corresponding minimum receive power. The set of minimum receive powers for all possible data rates is denoted as  $\mathcal{P}^{\text{mcs,rx}}$ . Therefore, for a station with receive power  $x_r$  to be served with data rate  $m$ , the receive power must be within the range  $x_m^M \leq x_r < x_{m+1}^M$ , where  $x_m^M \in \mathcal{P}^{\text{mcs,rx}}$  is the minimum receive power required for the  $m$ th data rate. The stations are ordered from strongest receive power to weakest, therefore the data rates selected for each station are also ordered such that  $m_r \geq m_{r+1}$ , where  $m_r$  is the data rate adopted for use with station  $r$ . More generally, for each station represented by  $X_r$ , a data rate is selected when the receive power is within the interval  $x_r^l \leq x_r < x_r^u$ , where  $x_r^l$  and  $x_r^u$  are the lower and upper limits of a data rate receive power range and  $x_r^l, x_r^u \in \mathcal{P}^{\text{mcs,rx}}$ .

When considering all stations within the network, each station is served with a data rate which has a corresponding pair of bounds forming a receive power interval. As the potential data rates are the same for all stations, the receive power bounds for all data rates and stations are members of the set  $\mathcal{P}^{\text{mcs,rx}}$ . The probability of  $n$  stations, each being served at a specified data rate is described as

$$P[x_1^l \leq X_1 \leq x_1^u, x_2^l \leq X_2 \leq x_2^u, \dots, x_n^l \leq X_n \leq x_n^u] \quad , \quad (6.14)$$

given that  $x_1^l \geq x_2^l \geq x_3^l, \dots, \geq x_n^l$  and  $x_1^u \geq x_2^u \geq x_3^u, \dots, \geq x_n^u$  and  $x_r^u \geq x_r^l$ .

The joint density function of  $n$  ordered statistics  $X_1, X_2, \dots, X_n$ , given the constraint  $X_1 \geq X_2 \geq \dots \geq X_n$ , and a common continuous PDF  $f(x_r)$ , is given by [?]

$$f_{1,2,\dots,n;n}(x_1, x_2, \dots, x_n) = n! \prod_{r=1}^n f(x_r), \quad x_1 > x_2 > \dots > x_n \quad . \quad (6.15)$$

The probability that the receive power of each station is within a particular range is required to determine the data rate used. This probability is obtained by jointly integrating over the

receive power ranges for each station which provide the data rate of interest

$$P[x_1^l \leq X_1 \leq x_1^u, \dots, x_n^l \leq X_n \leq x_n^u] = \int_{x_n^l}^{x_n^u} \dots \int_{x_1^l}^{x_1^u} f_{1,\dots,n;n}(x_1, \dots, x_n) \partial x_1 \dots \partial x_n \quad (6.16)$$

Figure 6.4 illustrates the probability space of the receive power of two stations, which are represented using random variables  $X_1$  and  $X_2$ . Figure 6.4(a) shows the joint density,  $f_{1,2;2}$ , calculated using (6.15), for all values of  $X_1$  and  $X_2$ , without the constraint  $X_1 \geq X_2$ . If the constraint  $X_1 \geq X_2$  was imposed, joint density in the upper left triangle of Figure 6.4(a) would consist of zeros. The constraints imposed on the probability space are illustrated in Figure 6.4(b). The shaded region represents the valid region where  $f_{1,2;2} \neq 0$ . Outside of this region  $f_{1,2;2} = 0$  as  $X_1 < X_2$ .

The horizontal and vertical dashed lines, at  $a, b, c$  and  $d$  in Figure 6.4(b), represent potential bounds to areas of interest for both random variables. As the bounds are the same for both variables, the probability space is divided into a number of squares and rectangles in this two-dimensional case. The probability space within the areas formed by differing bounds of the two variables is valid as long as the constraint  $X_1 \geq X_2$  is met. The area labelled “3” in Figure 6.4(b) does not meet this condition and therefore is invalid. The area labelled “1” in Figure 6.4(b) is an example where  $c \geq X_1 \geq b > a \geq X_2$ . As the individual distributions do not overlap and the base PDF is the same for both variables, the joint probability of the variables occurring within both intervals can be calculated using the individual probability of each variable occurring within its interval. For  $n$  ordered variables, the joint probability of the variables occurring within both intervals is

$$P[x_1^l \leq X_1 \leq x_1^u, x_2^l \leq X_2 \leq x_2^u, \dots, x_n^l \leq X_n \leq x_n^u] = n! \prod_{r=1}^n [F(x_r^u) - F(x_r^l)] \quad , \quad (6.17)$$

$$x_r^u, x_r^l \in \mathcal{P}^{\text{mcs,rx}} \quad ,$$

if the limit constraints  $x_1^u > x_2^l, x_2^u > x_3^l, \dots, x_{n-1}^u > x_n^l$  are met.

To calculate the joint probability of variables bounded by the same interval, a different approach must be used. In Figure 6.4(b) the bounds used for evaluating the joint density for  $X_1$  and  $X_2$  are the same in region “2”;  $c > X_1 \geq X_2 \geq b$ . Not the entire region within these bounds is admissible, since the half of this region where  $X_1 < X_2$  is invalid. Within this region the density is symmetric across the diagonal where  $X_1 \simeq X_2$  (the diagonal  $[b, b] \rightarrow [c, c]$  in area “2”). This symmetry is visible in the joint density in Figure 6.4(a). This symmetry is exploited by calculating the density for the entire region and then scaling with a value  $\zeta$  to account for only the contribution from the valid portions of probability within the shared

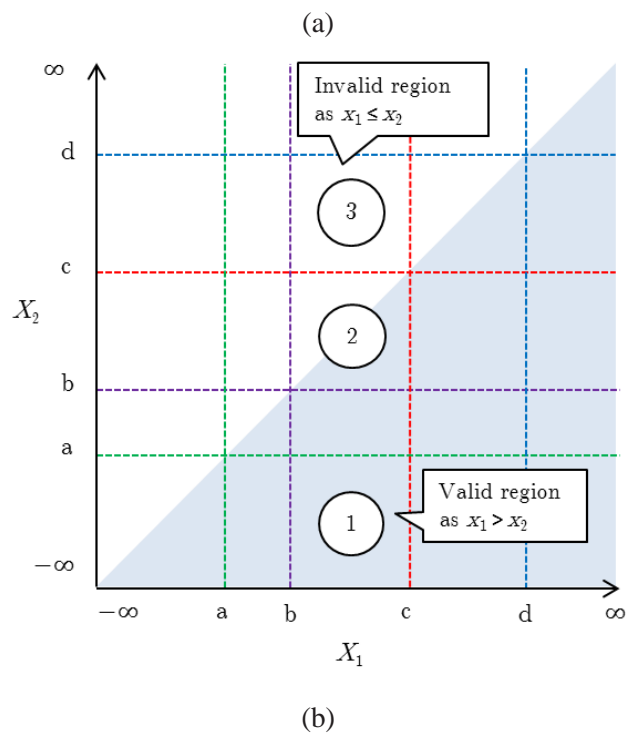
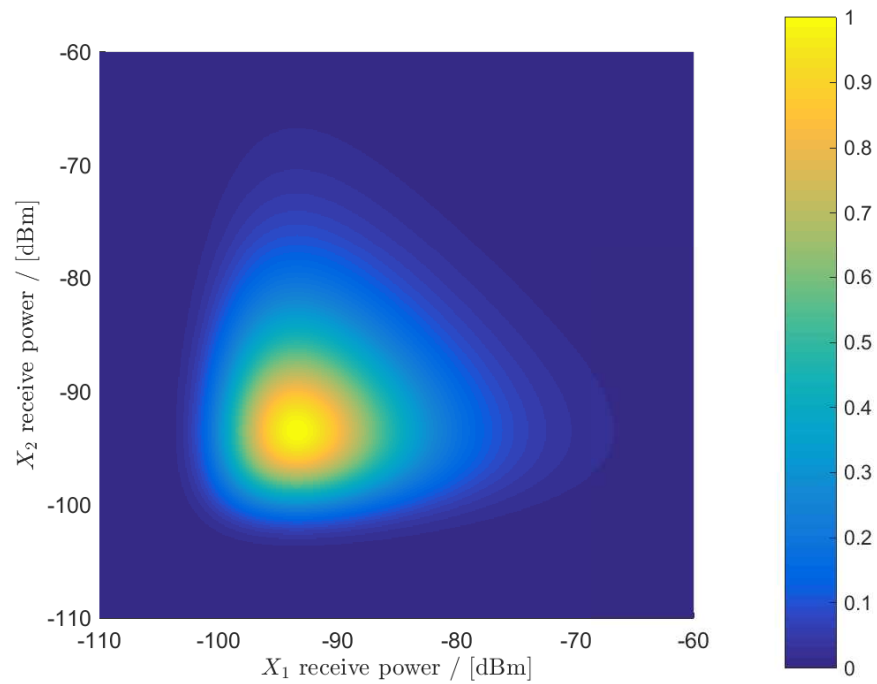


Figure 6.4: Representations of a joint probability space for two ordered random variables with the same underlying PDF. (a) The joint probability space of the receive power of two stations without the constraint  $X_1 \geq X_2$ . The probabilities are normalised between 0 and 1. (b) The probability space with bounded intervals of interest.

intervals:

$$P \left[ x_1^l \leq X_1 \leq x_1^u, x_2^l \leq X_2 \leq x_2^u, \dots, x_n^l \leq X_n \leq x_n^u \right] = \frac{n!}{\zeta} \prod_{r=1}^n \left[ F(x_r^u) - F(x_r^l) \right] \quad , \quad (6.18)$$

$$x_1^l = x_2^l = x_3^l \cdots = x_n^l \leq x_1^u = x_2^u = x_3^u \cdots = x_n^u \quad ,$$

$$x_r^u, x_r^l \in \mathcal{P}^{\text{mcs,rx}} \quad .$$

To determine  $\zeta$ ,  $\mathcal{W}$  is defined as the set of lower limits:  $\{x_1^l, x_2^l, \dots, x_n^l\}$ , and  $\mathcal{V}$  as a set containing distinct lower limits such that  $\mathcal{V} \subset \mathcal{W}$ . The value of  $\zeta$  is based on the number of times a distinct bound  $v_i$  is used in the evaluation in any of the variables, i.e. the number of random variables to be evaluated within the same interval

$$\zeta = \prod_{v \in \mathcal{V}} \left[ \sum_{w \in \mathcal{W}} \mathbb{1}(w, v) \right]! \quad , \quad w \in \mathcal{W}, v \in \mathcal{V} \quad , \quad (6.19)$$

where  $\mathbb{1}$  is an indicator function used to indicate a match between a variable bound  $w$  and the distinct bound  $v$ :

$$\mathbb{1}(w, v) = \begin{cases} 1 & \text{if } w = v \\ 0 & \text{if } w \neq v \end{cases} \quad . \quad (6.20)$$

When a bound  $v$  is not shared between variables

$$\sum_{w \in \mathcal{W}} \mathbb{1}(w, v) = 1 \quad , \quad (6.21)$$

therefore the calculation of  $\zeta$  in (6.19) remains valid as the contribution of other shared bounds between variables is unaffected. This allows (6.19) to be used for calculating the joint probability of the variables occurring within intervals:

$$P \left[ x_1^l \leq X_1 \leq x_1^u, x_2^l \leq X_2 \leq x_2^u, \dots, x_n^l \leq X_n \leq x_n^u \right] = \frac{n!}{\zeta} \prod_{r=1}^n \left[ F(x_r^u) - F(x_r^l) \right] \quad , \quad (6.22)$$

$$x_r^u, x_r^l \in \mathcal{P}^{\text{mcs,rx}} \quad ,$$

with relaxed constraints for the bounds  $x_1^l \geq x_2^l \geq x_3^l, \dots, \geq x_n^l$  and  $x_1^u \geq x_2^u \geq x_3^u, \dots, \geq x_n^u$  and  $x_r^u \geq x_r^l$ .

### Station Receive Power PDF

The receive power of a station  $x$  in dBm is a function of the distance  $y$  in meters, the path loss exponent  $\gamma$ , transmit power  $P^{\text{tx}}$  in dBm, receive antenna gain  $G^{\text{rx}}$  in dB, and the reference

path loss  $K$  as discussed in Section 6.3.3

$$x = g(y) = P^{tx} - 10\gamma \log(y) + K + G^{rx} \quad . \quad (6.23)$$

The distance between the station and the base station can be described with a random variable  $Y$ . As  $g(y)$  is differentiable, and strictly monotonically decreasing for all values within the range of  $Y$  for which  $f_Y(y) \neq 0$ , then for each value of  $y$ , the equation  $x = g(y)$  can be uniquely solved for  $y$  to give  $y = g^{-1}(x)$ . Given (6.23),  $g^{-1}(x) = 10^{\frac{P^{tx} + K + G^{rx} - x}{10\gamma}}$  and its derivative  $\frac{\partial}{\partial x} g^{-1}(x) = -\frac{\ln 10}{10\gamma} 10^{\frac{P^{tx} + K + G^{rx} - x}{10\gamma}}$  can be calculated. This allows the PDF of the random variable  $Y$  to be transformed to give the PDF of  $X$  using the method of transformations for a single variable:

$$f_X(x) = f_Y[g^{-1}(x)] \cdot \left| \frac{\partial}{\partial x} g^{-1}(x) \right| \quad . \quad (6.24)$$

Section 5.2 described how the distance between a base station at the center of a community and the served households could be modelled as a circle normal distribution. Therefore, a random variable  $Y$  can be used to represent the distance between a station and the base station in meters, with a PDF, evaluated at  $y$ , given by

$$f_Y(y) = \frac{10^{-3}y}{\sigma^2} \exp \left\{ -\frac{1}{2} \left( \frac{10^{-3}y}{\sigma} \right)^2 \right\} \quad , \quad (6.25)$$

where  $\sigma$  is the variance that parametrises the distribution of the community. The  $10^3$  scaling of  $y$  converts m to km.

Therefore using (6.24), this PDF can be transformed to create the receive power PDF

$$f_X(x) = \frac{10^{\left(\frac{P^{tx} + K + G^{rx} - x}{10\gamma} - 3\right)}}{\sigma^2} \exp \left\{ -\frac{1}{2} \left( \frac{10^{\left(\frac{P^{tx} + K + G^{rx} - x}{10\gamma} - 3\right)}}{\sigma} \right)^2 \right\} \left| -\frac{\ln 10}{10\gamma} 10^{\frac{P^{tx} + K + G^{rx} - x}{10\gamma}} \right| \quad . \quad (6.26)$$

As  $\frac{\partial}{\partial x} g^{-1}(x) \leq 0 \forall x$ , (6.26) can be simplified to

$$f_X(x) = \frac{\ln 10}{\gamma \sigma^2} 10^{\left(\frac{P^{tx} + K + G^{rx} - x}{5\gamma} - 4\right)} \exp \left\{ -\frac{1}{2} \left( \frac{10^{\left(\frac{P^{tx} + K + G^{rx} - x}{10\gamma} - 3\right)}}{\sigma} \right)^2 \right\} \quad . \quad (6.27)$$

### Station Receive Power CDF

The CDF, can be obtained by integrating the PDF in (6.27)

$$F_X(x) = \int_{-\infty}^{\infty} f_X(x) dx \quad ,$$

$$F_X(x) = 10^{-\frac{10 \left( \frac{P^{\text{tx}} + K + G^{\text{rx}} - x}{5\gamma} - 6 \right)}{2\sigma^2 \ln 10}} \quad . \quad (6.28)$$

The CDF of the receive power is used to calculate the joint density in (6.22).

### 6.5.2 Average Network Performance

To assess the network performance for differing station assignment between the RANs, the average throughput of each RAN is considered. As the GHz RAN transmit power is the driver for station assignment, the impact of changing the transmit power on the assignment and throughput is calculated. Through these calculations, the optimal station assignment to maximise the throughput of the network can be determined as presented in Section 6.8.

#### Station Data Rate Permutations

To calculate average performance, the probability of all permutations of station data rate selections within the network are considered. The probability of one such permutation is calculated using (6.22). As the stations are ordered according to receive power strength, not all combinations of data rates are valid. The valid permutations of data rates for all stations in each RAN  $a \in \mathcal{A}$  are contained in a set  $\mathcal{Q}_a$ , where each element has associated upper and lower receive limits,  $x_r^u, x_r^l$ , for all stations within the network. Table 6.1 is an example of valid permutations when three data rates are possible.

As stations associated with the GHz RAN cannot simultaneously connect to the UHF RAN, the sets of station data rate permutations  $\mathcal{Q}_a$  for each RAN are dependent. The set of valid data rates and the associated receive power levels for the UHF RAN,  $\mathcal{Q}_u$ , only include rates which require a receive power out-with the possible receive power range of the GHz RAN, when there is a path loss difference between the two RANs. Given the reference path loss  $K_a$  for each RAN, a data rate receive power limit for the UHF RAN must be  $\Delta_L$  less than any GHz RAN minimum receive power,

$$\Delta_L = K_g - K_u + P_g^{\text{tx}} - P_g^{\text{rx}} \quad . \quad (6.29)$$

As the transmit power of the GHz RAN increases, the lower data rates of the UHF RAN are no longer possible. Unsupported data rates are removed from the valid set of permutations

Permutation #	Station MCS				# Connected Stations ( $ \mathcal{S}_g $ )
	$X_1$	$X_2$	$\dots$	$X_n$	
1	0	0	$\dots$	0	0
2	1	0	$\dots$	0	1
3	2	0	$\dots$	0	1
4	1	1	$\dots$	0	2
5	2	1	$\dots$	0	2
6	2	2	$\dots$	0	2
$\vdots$	$\vdots$	$\vdots$	$\vdots$	$\vdots$	$\vdots$
$ Q $	2	2	$\dots$	2	n

Table 6.1: Example of valid permutations of data rates (MCS) for  $n$  stations within a network with three MCS  $\{0, 1, 2\}$ . MCS 0 signifies the station is not connected.

$\mathcal{Q}_u$ . For example if the path loss of a station served by the UHF RAN is 30 dB less than when served by the GHz RAN, the minimum receive power of the station on the GHz RAN must be at least 30 dB less than the minimum receive power of the UHF RAN for the station to connect to the GHz RAN, if the transmit powers are the same.

### Average Station Assignment Calculation

If the GHz RAN receive power of a station exceeds the minimum required for a connection, the station is associated with the GHz RAN. Therefore the mean number of stations assigned to the GHz RAN for a given transmit power,  $|\bar{\mathcal{S}}_g|$ , can be calculated using the probability,  $P$ , of each possible permutation of station data rate within the network,  $q \in \mathcal{Q}_g$ , and the number of stations connected in each permutation  $|\mathcal{S}_{g,q}|$ ,

$$|\bar{\mathcal{S}}_g| = \sum_{\mathcal{Q}_g} [P_q \cdot |\mathcal{S}_{g,q}|] \quad . \quad (6.30)$$

The variance is given by

$$\text{Var} (|\bar{\mathcal{S}}_g|) = \sum_{\mathcal{Q}_g} \left[ P_q \cdot (|\mathcal{S}_{g,q}| - |\bar{\mathcal{S}}_g|)^2 \right] \quad . \quad (6.31)$$

The median number of connected stations  $|\tilde{\mathcal{S}}_g|$  provides a robust assignment which minimizes the impact of outliers. This median number of stations associated with the GHz RAN is

$$|\tilde{\mathcal{S}}_g| = \arg \min_{|\mathcal{S}_{g,k}|} k, \quad \text{s.t.} \quad \sum_{m=1}^k \check{P}_m \geq 0.5 \quad , \quad (6.32)$$

where  $\check{P}_m$ ,  $m = 0 \dots n$  is the probabilities of the ordered possible assignments. The value  $k$  is the index of the median assignment and corresponds to one permutation within  $Q$ .

### Average RAN Throughput Calculation

The throughput estimation of the network and each RAN within the network is based on the data rate selected by each station, and therefore the receive power of each station. As data rates are being averaged, the zero-renormalised harmonic mean (ZRHM) [?] is used to calculate the expected overall throughput of a RAN,  $\bar{R}_a$ , for a given transmit power. An expected throughput  $R_q$  for each permutation  $q \in \mathcal{Q}_a$  is calculated using the throughput model described in Section 6.3.4. For each throughput permutation, the non-zero throughput permutations are indexed by  $k = \{1, 2, \dots, N_z\}$ , where  $N_z$  is the number of non-zero throughput permutations. The probability of the  $k$ th non-zero throughput is  $w_k$ , therefore the ZRHM throughput,  $\bar{R}_a$ , is

$$\bar{R}_a = \sum_{k=1}^{N_z} w_k \cdot \left( \sum_{k=1}^{N_z} \frac{\hat{w}_k}{R_k} \right)^{-1}, \quad (6.33)$$

where  $\hat{w}_k$  are the normalised non-zero throughput probabilities for each permutation such that  $\sum_{k=1}^{N_z} \hat{w}_k = 1$ . The variance of the throughput given the probability,  $P_q$ , of each permutation  $q \in \mathcal{Q}_a$  is

$$\text{Var}(R_a) = \sum_{\mathcal{Q}_a} \left[ P_q \cdot (R_q - \bar{R}_a)^2 \right]. \quad (6.34)$$

The median throughput,  $\tilde{R}_a$ , provides an average which is suited to skewed distributions and the presence of large outliers. As potential throughputs vary substantially, for example for a 20 MHz bandwidth ranges from 0 Mbps to 32 Mbps, the median

$$\tilde{R}_a = \arg \min_{R_k} k, \quad \text{s.t.} \quad \sum_{m=1}^k \hat{P}_m \geq 0.5, \quad (6.35)$$

is a suitable metric to use where  $\hat{P}_m$  is the  $m$ th probability when the throughputs are ordered from low to high.

## 6.6 Monte Carlo Method

To confirm the calculations based on probabilistic method described in Section 6.5, a Monte Carlo method is used to calculate the performance metrics for the network for a given GHz RAN transmission power.

An ensemble,  $\mathcal{Z}$ , of  $10^6$  random sets of stations are created. For a given transmit power the throughput of each RAN and power consumption for each network set are aggregated to form the averaged metrics. These calculations are described in this section. Each of the random

samples in  $\mathcal{Z}$  is a set of distances between stations and a base station, denoted by  $\mathcal{S}$ . This set is the distances of each station from a base station, taken from the household distribution discussed in Section 5.2. The distances are created from  $2|\mathcal{S}|$  random numbers, taken from a normal distribution  $\mathcal{N}(\mu = 0, \sigma^2)$ . Half of the  $2|\mathcal{S}|$  numbers represent an  $x$  coordinate and half represent a  $y$  coordinate of a station. The radial distances for each station are calculated using (5.1). The network model described in Section 6.3 is applied to each set of distances to determine a network throughput and power consumption.

To assess the performance of the network, the same metrics described in Section 6.5.2 are used but the calculations are different. These calculations are outlined below.

### Average Station Assignment Calculation

The mean,  $|\bar{\mathcal{S}}_g|$ , and median,  $|\tilde{\mathcal{S}}_g|$ , number of stations connected to the GHz RAN are used to average the ensemble. The mean with a corresponding variance provides insight into the variability of station assignment for a given transmit power, whilst the median provides an average assignment which minimises the impact of outliers.

The mean number of stations associated with the GHz RAN is

$$|\bar{\mathcal{S}}_g| = \frac{1}{|\mathcal{Z}|} \sum_{\mathcal{Z}} |\mathcal{S}_{g,z}| \quad . \quad (6.36)$$

The variance is given by

$$\text{Var}(|\bar{\mathcal{S}}_g|) = \frac{1}{|\mathcal{Z}|} \sum_{\mathcal{Z}} (|\mathcal{S}_{g,z}| - |\bar{\mathcal{S}}_g|)^2 \quad . \quad (6.37)$$

When  $\mathcal{Z}_{|\mathcal{S}_g|}$  is the set of GHz station assignments for all samples in  $\mathcal{Z}$ , the median GHz assignment is

$$|\tilde{\mathcal{S}}_g| = \text{Median}(\mathcal{Z}_{|\mathcal{S}_g|}) \quad . \quad (6.38)$$

### Average RAN Throughput Calculation

The ZRHM [?] and median are used as average throughput metrics for the samples  $\mathcal{Z}$ . For each sample  $z \in \mathcal{Z}$ , the non-zero throughput are indexed by  $k = \{1, 2, \dots, N_z\}$ , where  $N_z$  is the number of non-zero throughput elements in  $\mathcal{Z}$ . Therefore

$$\bar{R}_a = \frac{|\mathcal{Z}| - N_z}{|\mathcal{Z}|} \left( \frac{1}{N_z} \sum_{k=1}^{N_z} \frac{1}{R_k} \right)^{-1} \quad . \quad (6.39)$$

The variance is

$$\text{Var}(R_a) = \sum_{\mathcal{Z}} (R_z - \bar{R}_a)^2 \quad . \quad (6.40)$$

When  $\mathcal{Z}_{R_a}$  is the set of RAN  $a$  throughputs for all samples in  $\mathcal{Z}$ , the median throughput is

$$\tilde{R}_a = \text{Median}(\mathcal{Z}_{R_a}) \quad . \quad (6.41)$$

## 6.7 Bayesian Belief Network Method

A BBN is used to display the relationships between variables in a graph [?]. Dependent random variables, or nodes, are connected by directed edges. The missing edges between nodes indicate independences [?]. BBNs are based on the premise that only nodes connected by an edge to the node of interest can influence it. Forcing the network to be constructed with a clear mapping of conditional dependences allows the posterior marginal probability distribution of nodes to be calculated given observed information. Therefore the network model in Section 6.3 is described using a BBN. The ability to insert observed information allows the effect of a fixed transmission power on the receive power PDFs of nodes to be simulated. Conversely, given a fixed node receive power, the BBN allows the PDF of the transmit power to be determined. Section 6.7.1 presents the BBN used to model the network and the relationships between the nodes. Section 6.7.2 describes how the BBN is used to model network performance by inserting observed information into the network.

### 6.7.1 Bayesian Belief Network Formation

The relationship between  $\mathcal{S}_a$ ,  $\mathcal{L}_a$ ,  $\mathcal{P}_a^{\text{tx}}$ ,  $\mathcal{P}_a^{\text{rx}}$  and  $\mathcal{M}_a$  introduced in Section 6.3 is modelled as the BBN shown in Figure 6.5. For nodes connected by conditional dependencies, conditional probability tables (CPTs) are used at each node to describe the relationship a node and its parent node(s) in the directed graph. The CPTs are constructed by modelling the relationships between nodes, as described in Section 6.3: distance between base station and consecutive nodes, distance and path loss, receive power given path loss and transmit power and data rate given receive power. Using Pearl's algorithm [?], information across the graph is exchanged through nodes, by passing messages. As the graph is acyclic, the PDFs of all nodes, also called the beliefs, will converge to a solution. The resultant beliefs of the data rates for each station can then be averaged to create  $\mathcal{M}_a$  and estimate the throughput of the network.

The individual station distances,  $\mathcal{S}$ , are described using an ordered set of  $n$  discrete random

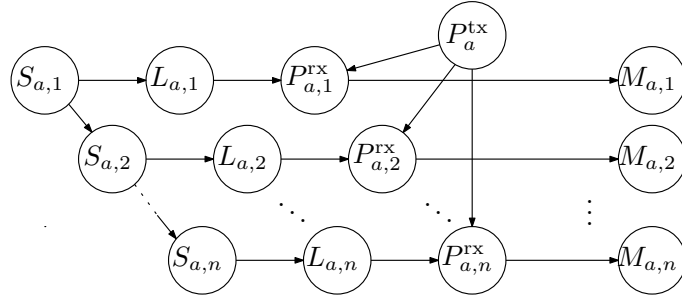


Figure 6.5: BBN describing dependencies of distance, path loss, receive power and data rate.

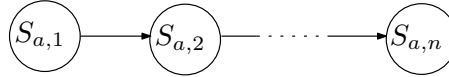


Figure 6.6: Probabilistic model of the multi-RAN network.

variables  $\{S_1, S_2, \dots, S_n\}$  such that  $S_1 \leq S_2 \leq \dots \leq S_n$ . The underlying PDF and CDF of the ordered set is  $f_S(r)$  and  $F_S(r)$ . The PDF of the distance of the households is given in (6.25). The CDF is obtain by integrating (6.25) over the range 0 to  $y$ .  $S$  is ordered from closest station to farthest station, therefore the random variables representing each distance are conditionally dependent as shown in the graph in Figure 6.6. The distances evaluated correspond to transformed path losses using (6.1) between 80 dB and 140 dB in 0.25 dB steps.

The node  $S_{a,1}$  is the root of the network shown in Figure 6.5 as it has no parents. Therefore subjective evidence is used to seed the belief of  $S_{a,1}$  using the PDF of the station closest to the base station,  $f_{1:n}(r)$ . For a set of ordered statistics, the PDF of station  $k$  in the set of  $n$  is given by [?]

$$f_{k:n}(r) = n f_S(r) \binom{n-1}{k-1} F_S(r)^{k-1} (1 - F_S(r))^{n-k} \quad (6.42)$$

Messages propagate from node  $S_{a,1}$  to  $S_{a,2}$ , where  $S_{a,2}$  is the node representing the distance of the second closest stations in the network. The conditional dependency, and hence the CPT, linking any two stations  $S_{a,i}$  to  $S_{a,j}$ , where  $0 \leq i < j < n$ , at distances  $u$  and  $v$ , where  $u < v$ , is given by

$$f_{i|j:n}(u, v) = \frac{f_{i,j:n}(u, v)}{f_{j:n}(v)} \quad (6.43)$$

The joint PDF  $f_{i,j}(u, v)$  of station  $i$  at a distance  $u$  and station  $j$  at a distance  $v$ , where  $0 \leq i < j < n$  and  $u < v$  is

$$f_{i,j:n}(u, v) = \frac{n!}{(i-1)!(j-1-i)!(n-j)!} f_S(u) f_S(v) F_S(u)^{i-1} \cdot (F_S(v) - F_S(u))^{j-1-i} (1 - F_S(v))^{n-j} \quad (6.44)$$

The CPTs used to relate nodes which are functions of distance, e.g. path loss and receive

power, are identity matrices which map each possible input to the relevant equation to the calculated result with a probability of 1 for all possible values of the input.

### 6.7.2 Estimating Network Performance

The BBN shown in Figure 6.5 is used in two ways to determine the impact of station assignment. First, the mean GHz transmit power,  $P_g^{\text{tx}}$ , required for each possible assignment is estimated which in turn is used to determine the throughput for each assignment.

To determine  $P_g^{\text{tx}}$  the minimum required transmit power  $P_s^{\text{tx},\text{min}}$  to establish a connection with the farthest station  $s$  on the GHz RAN with the lowest data rate  $m_{\text{CS}} = 0$  is considered. The BBN in Figure 6.5 is solved with node  $P_s^{\text{rx}}$  set as evidence,  $P_{g,s}^{\text{rx}} = P_{g,s}^{\text{mcs}=0,\text{rx}}$ , and the belief of node  $P_g^{\text{tx}}$  uninitialised. When the BBN converges, the mean of the belief of  $P_g^{\text{tx}}$  is taken as the transmit power  $P_{g,s}^{\text{tx}}$  required to associate station  $s$  with the GHz RAN. This is repeated to give the mean required transmit power for allocations  $s = \{1, \dots, n\}$ .

The BBN is rerun with no evidence for station receive powers but with the GHz RAN transmit power,  $P_{g,s}^{\text{tx}}$ , used as evidence for the transmit power for all required non-zero assignments. Once converged, this provides the PDF of individual station receive powers for the GHz RAN. The belief of the GHz RAN receive powers can be directly evaluated to determine the expected data rate of each station on the RAN. The beliefs of individual station receive powers for the UHF RAN are calculated from the beliefs of GHz RAN station receive powers. The GHz RAN receive powers are offset by the path loss and transmit power differences such that

$$\text{belief}(P_{u,s}^{\text{rx}}) = \text{belief}(P_{g,s}^{\text{rx}}) \quad , \quad (6.45)$$

where

$$P_{u,s}^{\text{rx}} = P_{g,s}^{\text{rx}} - (K_g - K_u + P_{g,s}^{\text{tx}} - P_u^{\text{tx}}) \quad , \quad (6.46)$$

and  $K_a$  is the reference path loss for RAN  $a$ . To determine the beliefs of the station receive powers when all stations are served by the UHF RAN ( $s = 0$ ), the BBN is configured for use with the UHF RAN with the transmit power,  $P_u^{\text{tx}}$ , set as described in Section 6.3.2.

The median data rate selection for each station is used to estimate the throughput of the network using the beliefs of station receive powers. For station  $k$  of RAN  $a$ , the median data rate  $\tilde{M}_{a,k}$ , is

$$\tilde{M}_{a,k} = \arg \min_{M_l} l, \quad \text{s.t.} \quad \sum_{m=1}^l \hat{P}_{m,a} \geq 0.5 \quad , \quad (6.47)$$

where  $\hat{P}_{m,a}$  is the probability of the  $m$ th receive power. The value  $l$  is the index of the median receive power within all possible receive powers and  $M_l$  is the data rate selected for the  $l$ th receive power. Given the median data rates of all stations in each RAN for a given transmit power, the throughput of the RANs are estimated using the network throughput model introduced in Section 6.3.4.

## 6.8 Simulation and Results

This section demonstrates how a station assignment problem formulated in (6.13) can be optimised for individual station throughput. Furthermore the assignment is dynamically optimised based on instantaneous network capacity requirements to minimise the total power consumption. A scenario of a base station serving 20 stations is used. Based the WindFi parameters two networks are used to provide connectivity,

- a UHF RAN at  $f_u = 630$  MHz with 5 MHz bandwidth; and
- a GHz RAN at  $f_g = 5.66$  GHz with 20 MHz bandwidth.

To provide a realistic simulation the parameters in Table 6.2 are used in the model. These parameters are based on radio and network measurements and observations.

For a given transmission power the average station assignment is presented in Section 6.8.1 and the average throughput for each RAN is outlined in Section 6.8.2. Considering the station assignment, Section 6.8.3 describes the impact of station assignment on station throughput and base station power consumption, and presents the optimum assignment. Section 6.8.4 describes how the power consumption of the base station can be minimised by dynamically changing the station assignment to meet throughput requirements.

The results presented in this section were calculated using the probabilistic method described in Section 6.5. These results were also validated using the Monte Carlo method described in Section 6.6. The differences between the calculations using these two methods are presented in Section 6.8.5.

### 6.8.1 Impact of Transmit Power on Station Assignment

Figure 6.7 plots the mean and median number of stations associated with the GHz RAN calculated using (6.30) and (6.32), and the standard deviation calculated using (6.31), for a given GHz RAN transmit power. The mean and median station assignment agree closely due to the low variance in the assignment. The number of stations associated with the GHz RAN increases with the transmit power, as expected. If a transmit power limit of  $P_g^{\text{tx,max}} = 30$  dBm

Parameter	Value
$n$	20
$\gamma$	2.39
$d_0$	1 m
$\sigma_x$	3.09 km
$f_g, f_u$	5660 MHz, 630 MHz
$K_g, K_u$	-47.50 dB, -28.43 dB
$\mathcal{P}_g^{\text{mcs,rx}}$	$\{-92, -89, -85, -85, -82, -78, -71, -68\}$ dB
$\mathcal{P}_u^{\text{mcs,rx}}$	$\{-103, -99, -98, -95, -89, -85, -78, -65\}$ dB
$L_{\text{DATA}}$	2312 bits
$\alpha_g, \beta_g, \gamma_g$	1.135e-07, 4.545, 2.342
$\alpha_u, \beta_u, \gamma_u$	3.395e-07, 4.424, 2.555
$G^{\text{tx}}, G^{\text{rx}}$	10 dB
$P_g^{\text{tx,max}}$	30 dBm
$P_u^{\text{tx}}$	30 dBm

Table 6.2: Simulation parameters.

is imposed, only a maximum of 9 stations can be served by the GHz RAN, based on the median number of connected stations.

### 6.8.2 Impact of Transmit Power on Throughput

Figure 6.8 shows the expected throughput of each RAN for a given GHz RAN transmit power, using two different metrics, the ZRHM and the median. Two metrics are presented to provide a complete overview of the impact of transmit power on throughput.

The GHz RAN ZRHM throughput in Figure 6.8(a) increases to a peak at 18 dBm before decreasing as the transmit power increases. The increase in transmit power provides a higher receive power to connected stations and therefore a high MCS and throughput. When the transmit power exceeds 18 dBm, the number of stations associating with the GHz RAN increases and therefore the capacity of the RAN is now shared amongst more stations, lowering the individual GHz RAN throughput. When the transmit power exceeds 37 dBm the GHz RAN throughput increases again as now the majority of stations are associated with the GHz RAN and therefore an increase in transmit power will cause all stations to connect with higher MCS, improving the throughput. At low transmit powers all stations are associated with the UHF RAN therefore the UHF RAN throughput is at a saturated level. As the transmit power increases the UHF RAN throughput increases as more stations associate with the GHz RAN and the UHF RAN capacity is shared between fewer stations, peaking at 38 dBm. When the transmit power exceeds 38 dBm the throughput drops as the ZRHM accounts for both the 0 Mbps throughput when no stations are associated with the UHF RAN and the high throughput associated with few stations connected.

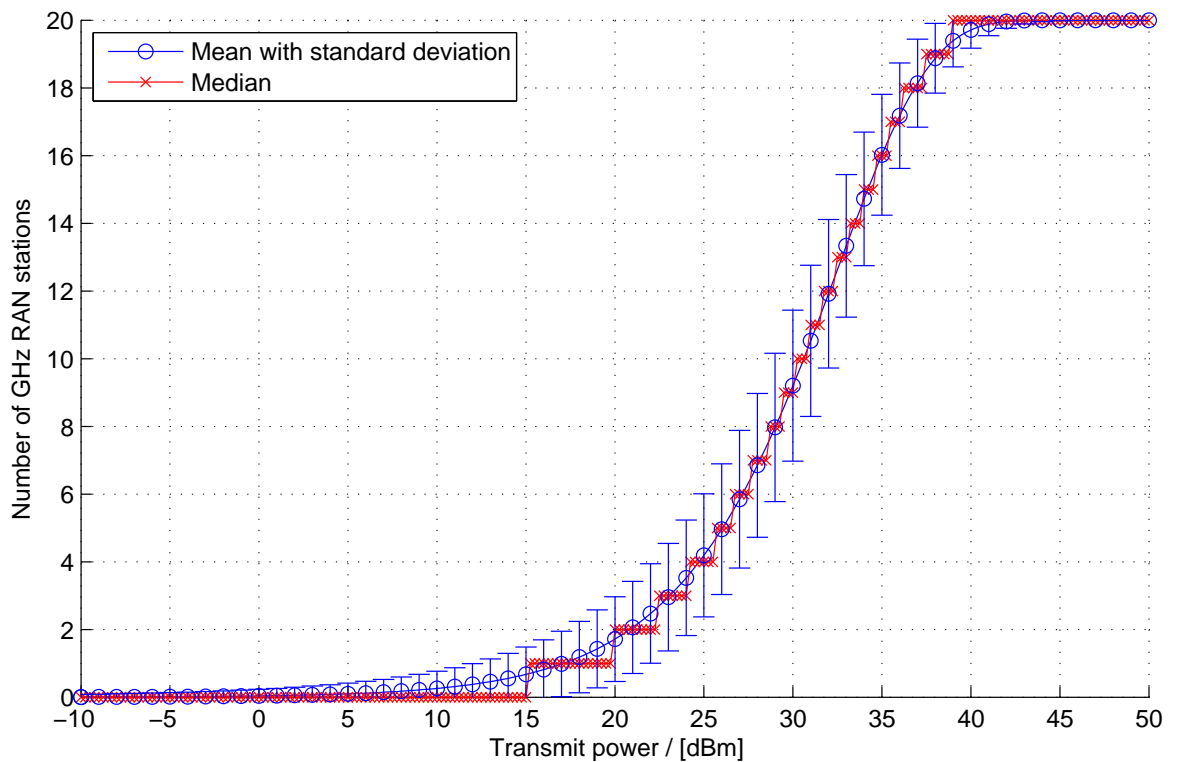
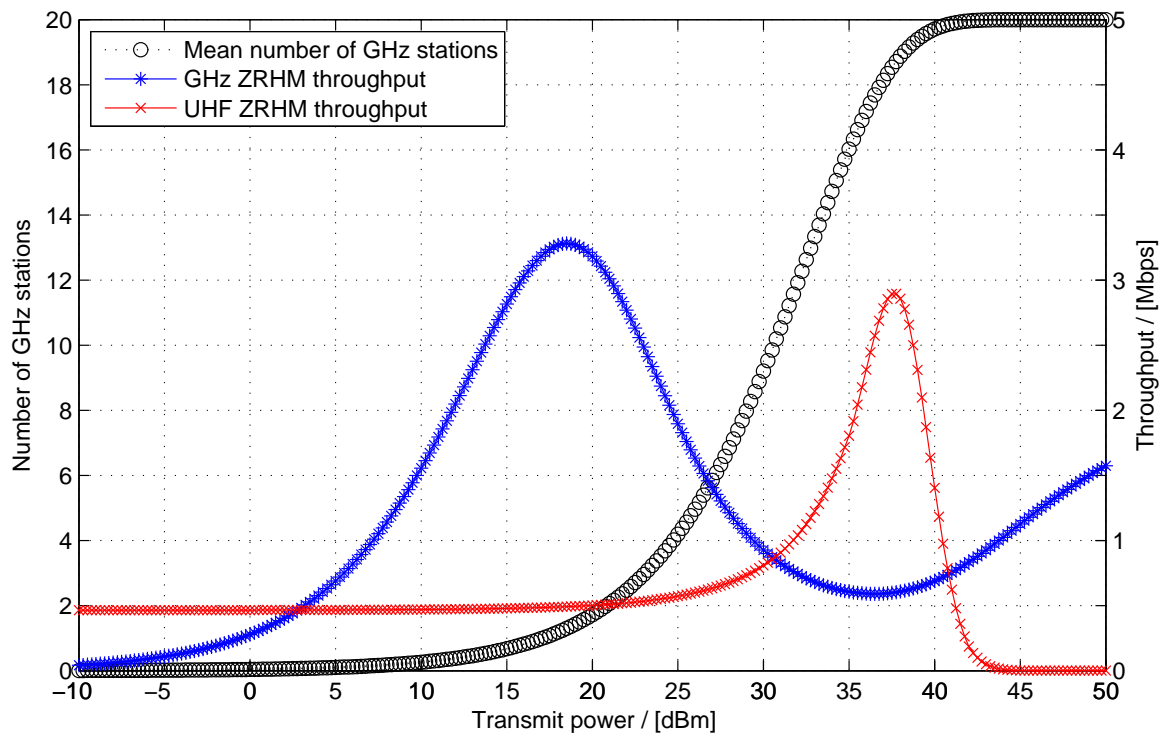
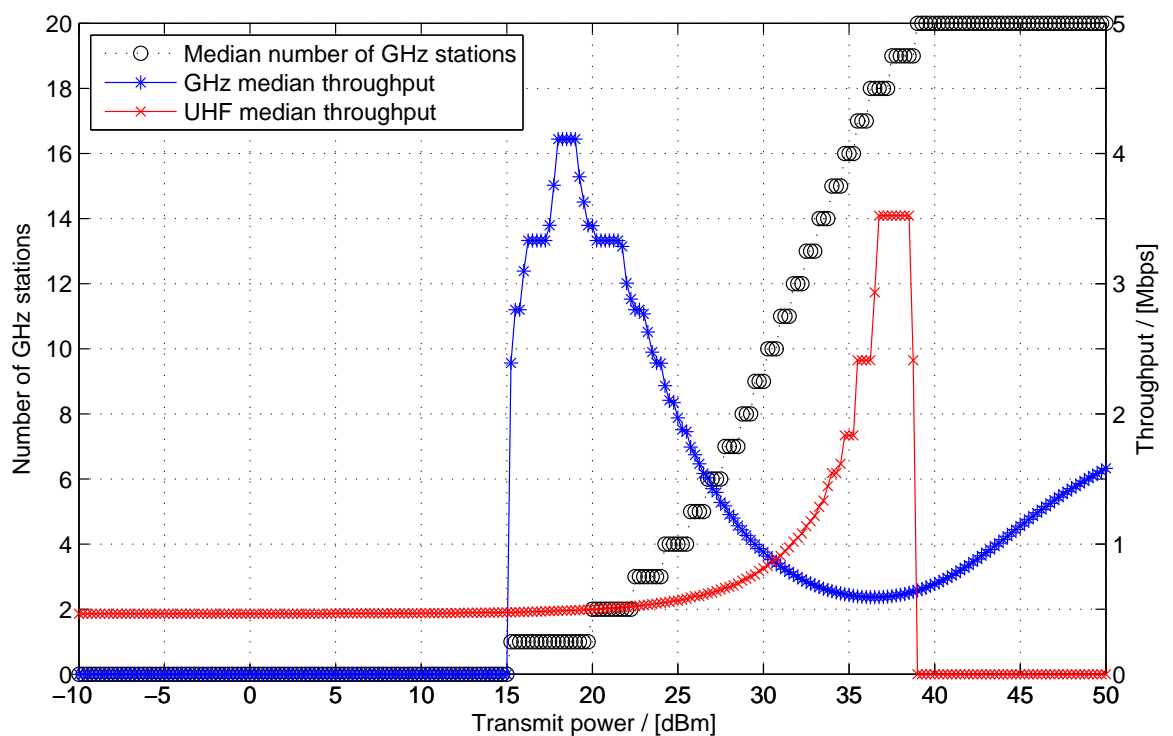


Figure 6.7: Mean number of stations connected to GHz RAN with standard deviation, and median number of stations connected to GHz RAN, for a given transmit power.

The median, shown in Figure 6.8(b), provides a better estimate of station throughput in this scenario than the ZRHM as large outliers do not influence the result. For each individual RAN, Figure 6.9 overlays the ZRHM with variance and median throughputs for given GHz RAN transmit powers. The variance of the throughput is very large as the possible throughput range is very large. For example, in Figure 6.9(a), when the transmit power is 12 dBm the median GHz throughput is 0 Mbps whilst the ZRHM is 2 Mbps. At this transmit power, the receive power is generally too low for stations to connect to the GHz RAN, therefore this is why the median throughput is 0 Mbps. But when stations do connect, the throughput is very high as only a few stations share the capacity. Therefore the ZRHM at this transmit power accounts for two scenarios; a throughput of 0 Mbps when no stations are connected, and a high throughput when few stations are connected. Similarly when the transmit power exceeds 38 dBm the median number of stations associated with the UHF RAN is zero and therefore the median throughput is 0 Mbps but the ZRHM throughput is skewed by the throughput of a few connected stations.

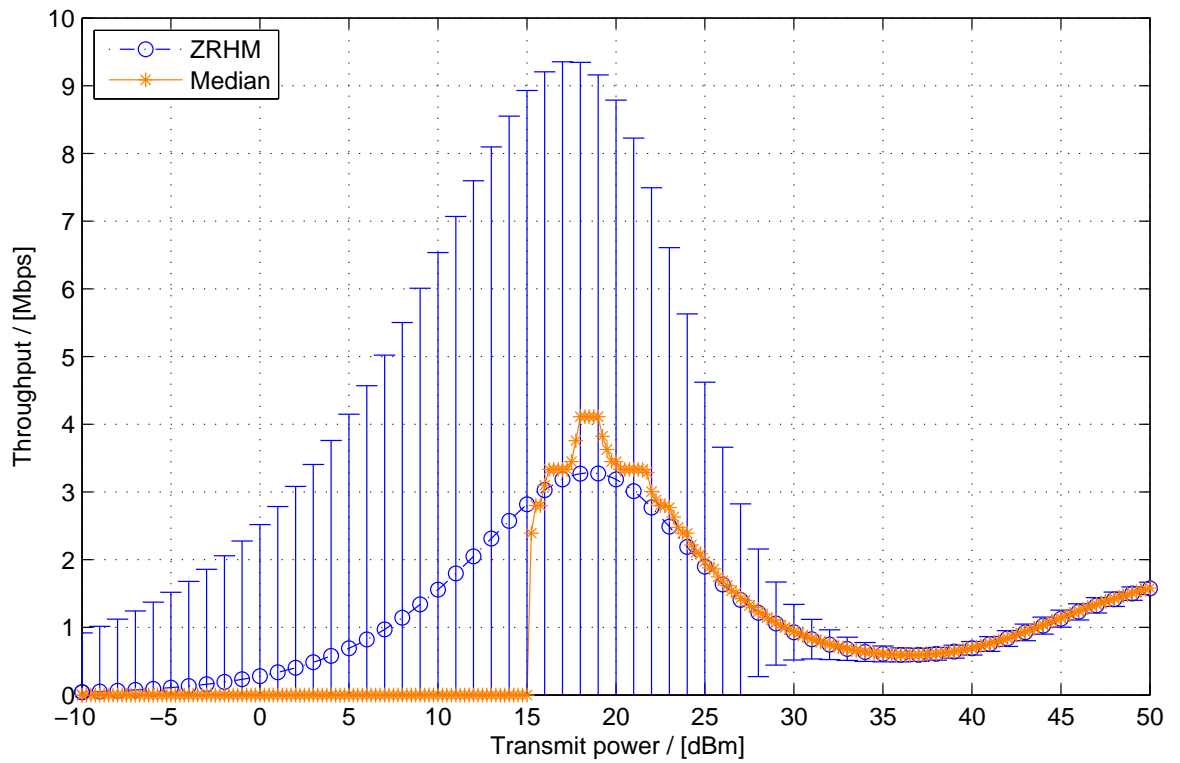


(a)

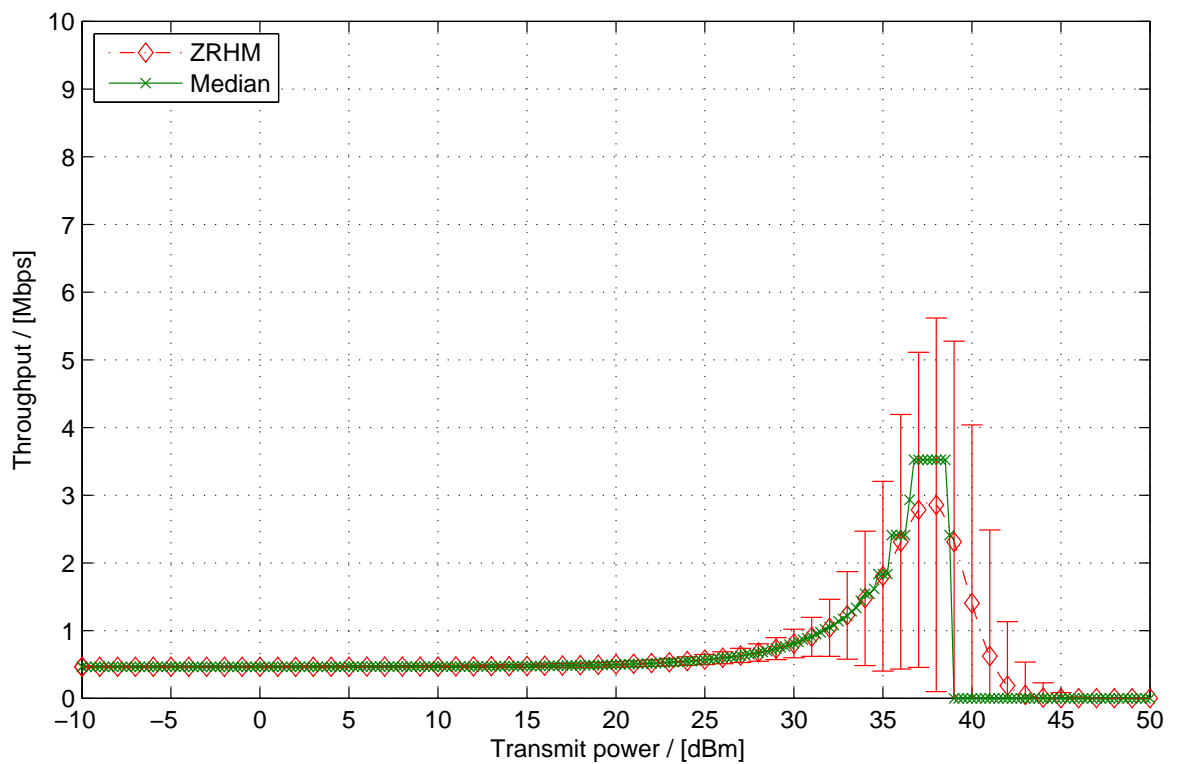


(b)

Figure 6.8: Individual (a) ZRHM and (b) median RAN throughputs and number of connected stations on the GHz RAN for a given transmit power.



(a)



(b)

Figure 6.9: Comparison of median and ZRHM throughputs for (a) GHz and (b) UHF RANs. The error bars show the variance of the throughput.

### 6.8.3 Station Assignment, Throughput and Power Consumption

To simplify the interpretation of the network performance, the station allocation is used as the tunable variable when designing the network. The number of stations connected to the GHz RAN is altered by scaling the GHz RAN transmit power. For the mean number of stations connected on the GHz RAN  $\bar{s}$ , the associated transmit power is used to calculate the relevant metrics. Figure 6.10 plots the transmit power for a given number of stations on the GHz RAN. The GHz RAN radio is un-powered when no stations are connected, hence no transmit power is plotted on the graph in the case of no connect stations.

Using the above transmit power, Figure 6.11 shows the station data throughput for each RAN for potential station assignments. The flat peaks on the individual GHz and UHF RAN throughputs at  $s = \{1, 2, 18, 19\}$  are due to the median throughputs being used. For the transmission powers of interest the median throughputs are the same, as evident in Figure 6.8(b). The minimum combined station capacity increases by 75%, from 0.48 Mbps when all stations are served by the UHF RAN to 0.84 Mbps in case stations are optimally assigned between RANs. Note that if the constraint of the GHz RAN transmission power to not exceed the maximum permissible power,  $P_{\max}^{\text{tx}} = 30$  dBm, is enforced, then only 9 stations can be connected to the GHz RAN, and the maximum combined throughput would be 0.76 Mbps, providing an increase of 58% compared to when all stations are served by the UHF RAN.

As discussed in Section 6.4 the optimum station assignment can be viewed graphically from Figure 6.11. The optimum assignment is  $|S_{\text{opt},g}| = 10$  which is visible in Figure 6.11 where the combined minimum throughput peaks. This optimum assignment exceeds the transmit power limit, therefore the maximum legal assignment is when  $|S_{\text{opt},g}| = 9$ . Intuitively given that the GHz RAN has four times the bandwidth of the UHF RAN, the GHz RAN should serve more users than the UHF RAN to balance the throughput between the RANs. These results disagree with this statement as the optimum number of stations to serve with GHz is only 50% of the stations. This is due to the better propagation characteristics of the UHF RAN leading to stations being served at a higher data rate rate than those by the GHz RAN at the same distance. The transmit power of the UHF RAN serves the farthest station at a reasonable data rate, therefore additional stations closer to the base station are served with a higher data rate. The GHz RAN serves additional stations further from the base station at a comparably lower data rate, leading to the difference.

Figure 6.11 also plots the base station power consumption for given stations assignments, calculated from the mean transmission power required for the assignment using the power consumption model in Section 6.3.5. As the GHz RAN transmit power increases to associate more stations, the power consumption of the base station increases as shown in Chapter 4. When no stations are associated with the GHz RAN the GHz radio can be un-powered.

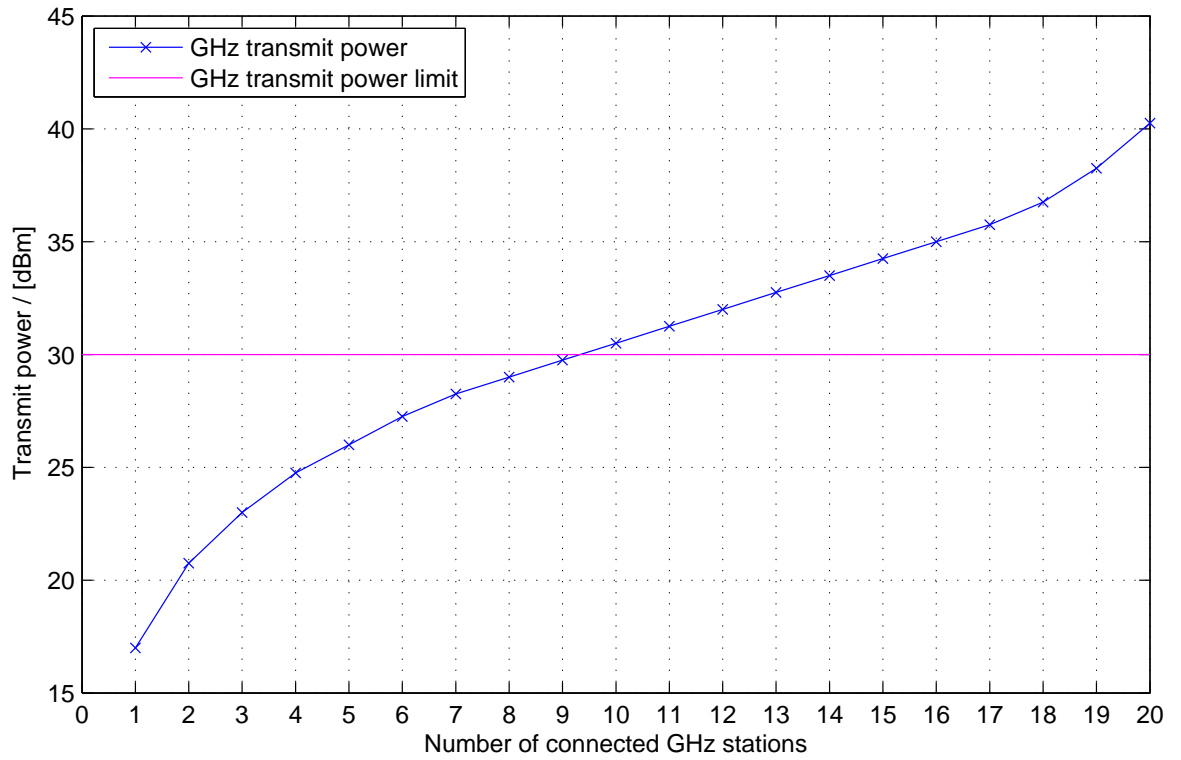


Figure 6.10: Mean GHz RAN transmit power required for each station assignment.

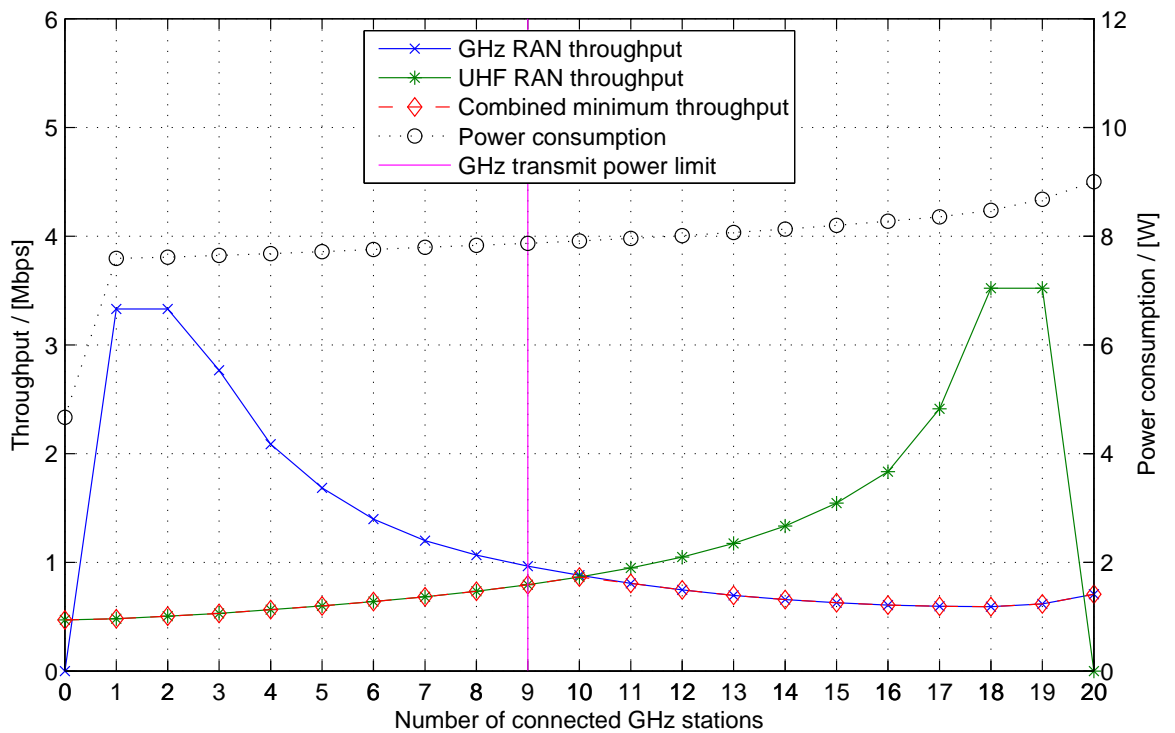


Figure 6.11: Individual station capacity on each RAN and base station power consumption given possible valid RAN assignments.

Therefore the base station power consumption only consists of the UHF RAN radio, leading to the minimum power consumption of 4.67 W.

#### 6.8.4 GHz RAN Breathing to Minimise Power Consumption

To obtain realistic figures for the time-varying target rate  $R_{\text{target}}$  that drives (6.13), we have used the downstream traffic model for the Tiree rural broadband network presented in Section 5.4 as a network utilisation  $u \in [0, 1]$  over a day. The target data rate for optimisation as discussed in Section 6.4 can be derived from this utilisation by normalising the optimum data rate for an assignment set  $\mathcal{N}$ , such that

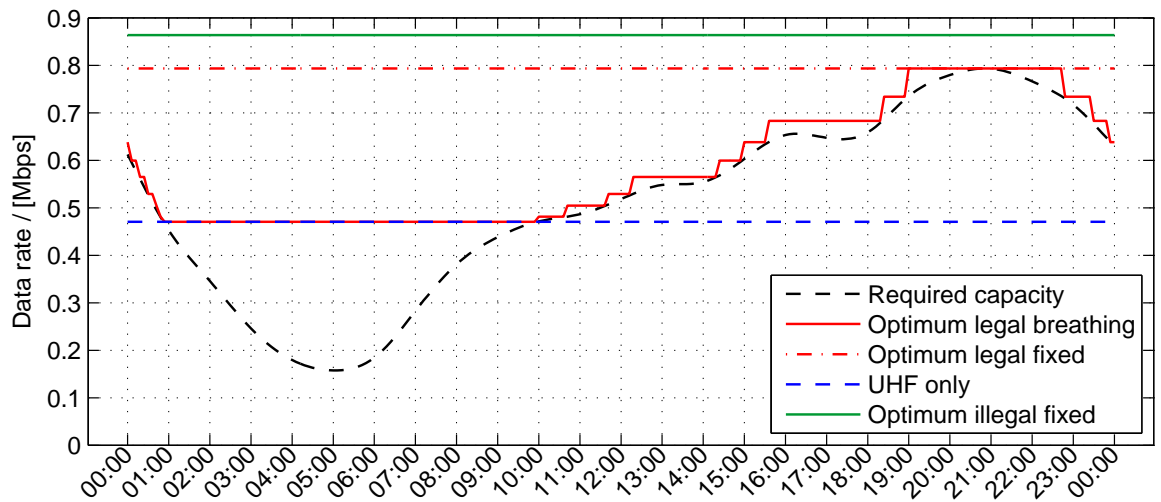
$$R_{\text{target}} = u \cdot R(\mathcal{N}_{\text{opt}}) \quad . \quad (6.48)$$

Figure 6.11 is used to perform the unconstrained optimisation alluded to in Section 6.4 to decrease the number of stations on the GHz RAN as much as possible, as long as  $R_{\text{target}}$  is met, thus minimising the power consumption.

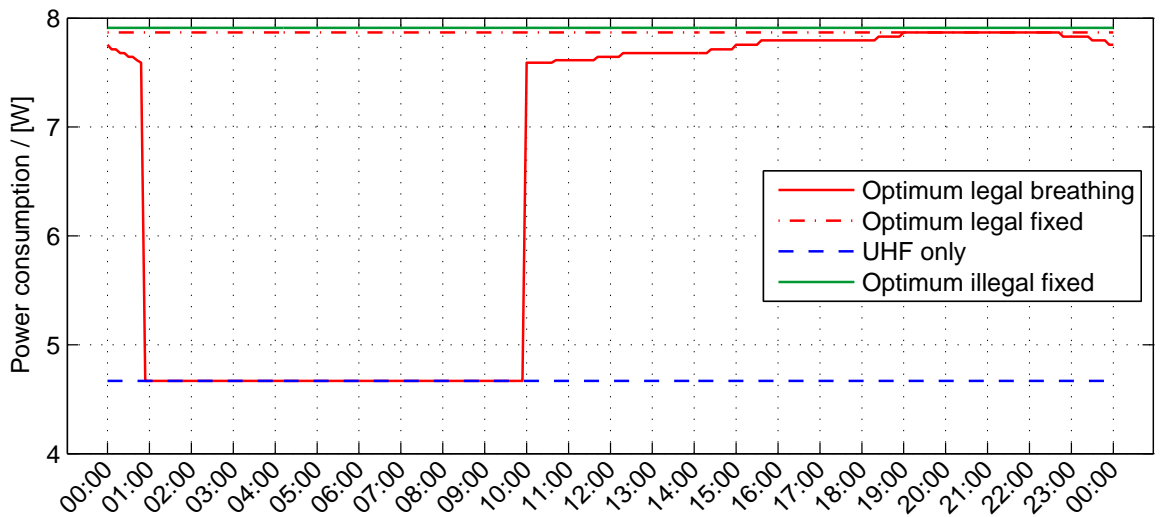
Figure 6.12 presents the analysis when using a dynamic target data rate. Figure 6.12(a) shows the required capacity and capacity offered when using different dynamic and static assignment schemes. In general, the data rate provided by the optimised scheme closely follows the target data rate from above, thus satisfying the constraint and minimising transmission power. Figure 6.12(b) compares the power consumption, where the optimised scheme exhibits a step up in power when the GHz RAN is required to satisfy the throughput demand during the peak time of the day. The fluctuating optimum station assignment is depicted in Figure 6.12(c).

Looking at extreme assignments, when only the UHF RAN is used, the power consumption of the network is minimised but it cannot meet the capacity requirement during peak times from 09:00h to 01:00h. Maximising the size of the GHz RAN using the highest legal transmit power provides a substantially higher data rate than using only the UHF RAN. Due to the transmit power limitations the maximum data rate is not achieved. This is the legal optimum obtained from Figure 6.11. The power consumption is also substantially greater. The illegal optimum offers the greatest data rate with the highest power consumption.

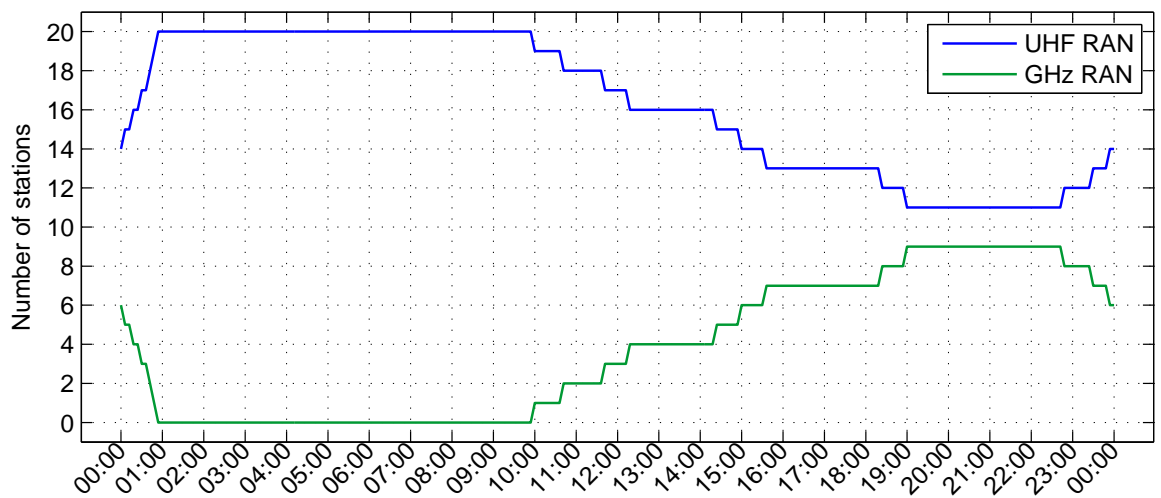
When the assignment is fixed to give the maximum throughput obtained from Figure 6.11 the power consumption is constantly high even though the data rate is not required at all times, but the data rate is the highest possible for all stations. Dynamically changing the assignment, as proposed with the solution to (6.13), optimises the system at each moment with respect to power consumption, providing reduction of 16.2% compared to using the fixed legal optimum assignment and 16.6% compared to using the illegal optimum GHz transmit power.



(a)



(b)



(c)

Figure 6.12: Results of solving (6.13) in 3 min. intervals showing: (a) required and offered capacity, (b) network power consumption, and (c) station assignment

Performance Metric	Mean % Error
Mean number of connected stations to GHz RAN	-27.2 dB
Standard deviation	-12.6 dB
Median number of connected stations to GHz RAN	$-\infty$ dB
GHz RAN ZRHM throughput	-27.0 dB
Standard deviation	-25.5 dB
GHz RAN median throughput	-33.6 dB
UHF RAN ZRHM throughput	-12.3 dB
Standard deviation	-12.6 dB
UHF Median throughput	-40.8 dB

Table 6.3: Mean percentage errors between probabilistic and Monte Carlo methods for all GHz RAN transmit powers.

### 6.8.5 Validation with Monte Carlo Method

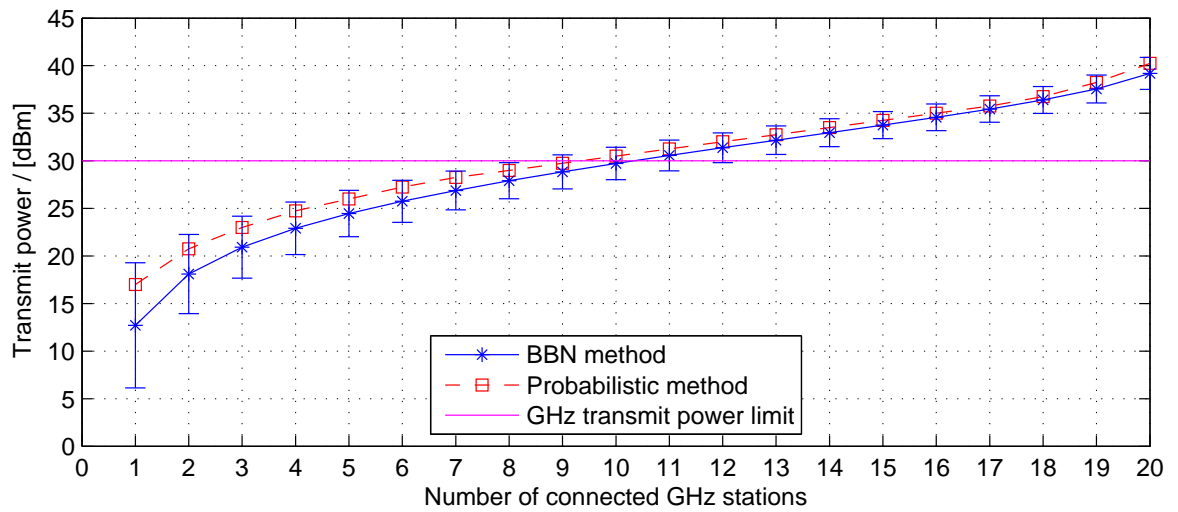
When comparing the calculated metrics of interest using the probabilistic method described in Section 6.5 and Monte Carlo method described in Section 6.6 the resulting errors are within reasonable bounds, given the number of Monte Carlo samples, demonstrating both methods provide the same result. Table 6.3 reports the mean percentage errors of the calculated performance metrics reported in Section 6.8 between the probabilistic and Monte Carlo methods.

## 6.9 Approximation with Bayesian Belief Network

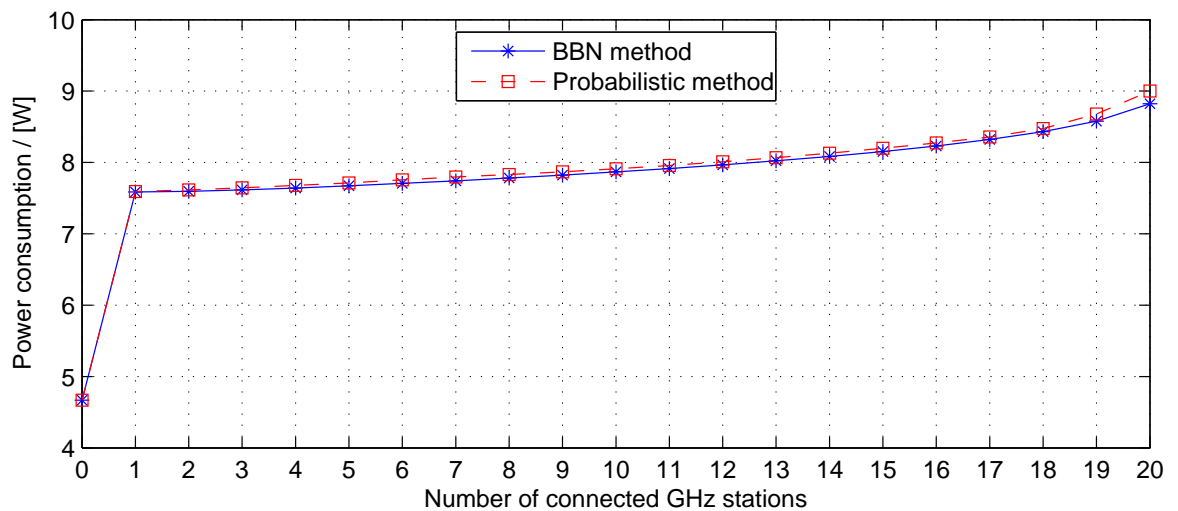
To solve the optimum station assignment problem in (6.13), we calculate the BBN described in Section 6.7 using Pearl's algorithm and benchmark it against the results obtained by the probabilistic method of Section 6.8. For simulations, the parameters in Table 6.2 are used to configure the BBN and allow comparison with the probabilistic method.

### 6.9.1 Station Assignment, GHz RAN Transmit Power and Power Consumption

To determine the impact of station assignments, the BBN in Figure 6.5 is used to estimate the transmit power required for each possible assignment. Figure 6.13(a) plots the resulting mean transmit power with standard deviation after convergence for each assignment. The results using the probabilistic method are plotted for comparison. The transmit power required to associate stations on the GHz RAN increases as stations are located further from the base



(a)



(b)

Figure 6.13: Comparison of simulation results using BBN and probabilistic methods for, (a) mean GHz RAN transmit power, and (b) corresponding total power consumption.

station, matching the trend calculated with the probabilistic method. The difference between the two methods is due to two factors:

*GHz RAN transmit power calculation.* When determining the mean GHz RAN transmit power required to create each assignment, the BBN method calculates the transmit power needed to serve the farthest station at the lowest data rate. This approach simplifies adding evidence to the BBN as the receive power of the node of interest is set to a single value. The probabilistic method determines the mean transmit power for an allocation by averaging across all farthest station data rates. Therefore the GHz RAN transmit power required for each assignment is higher using the probabilistic method.

*Node independence.* Pearl's algorithm assumes the parents of a node are mutually indepen-

dent. When calculating the mean transmit power required for each assignment, a dependence exists between the path loss of the station of interest and transmit power. This dependency will lead to a convergence error. For example in Figure 6.5 the node  $P_{a,2}^{\text{rx}}$  representing receive power for station 2 has two parents; the path loss  $L_{a,2}$  and transmit power  $P_a^{\text{tx}}$ . These nodes are not mutually independent as required by the algorithm, they are dependent through the path  $P_a^{\text{tx}} \rightarrow P_{a,1}^{\text{rx}} \rightarrow L_{a,1} \rightarrow D_{a,1} \rightarrow D_{a,2} \rightarrow P_{a,2}^{\text{rx}}$ . A convergence error thus arises from combining the information of the dependent parents of a convergence node as if these parents were independent [?].

The calculated total power consumption for each assignment is shown for both the BBN and probabilistic methods in Figure 6.13(b). The power consumption is a function of the GHz RAN transmit power but the difference in total power consumption between the two methods is minimal. At low transmit powers, where the difference in transmit power between the two methods is greatest, the power is dominated by the fixed cost of the radio, not the variable portion associate with the scaling of transmission power.

## 6.9.2 Station Assignment and Network Throughput

Re-running the BBN with the calculated mean GHz RAN transmit powers as evidence of  $P_{g,s}^{\text{tx}}$  provides individual station receive power beliefs within each RAN once converged. As an example of the convergence result, Figure 6.14 plots the resultant beliefs of UHF RAN station receive powers when all stations are associated with the UHF RAN. The BBN models the stations as independent random variables, therefore the PDFs of station receive powers overlap, given a fixed transmit power. The vertical dashed lines mark the lower boundary of the receive power required for each data rate. The data rate thresholds are used to determine the median data rate used by each station in both RANs. The median data rates for all stations are used to calculate the expected average throughput of both RANs.

Figure 6.15(a) shows the station data throughput for each RAN for all assignments using both the BBN and probabilistic methods. The median GHz RAN transmit power for each assignment differs between the two methods for small assignments. The UHF RAN throughput matches for both methods apart from the assignment where a single station is served on the UHF RAN. Figure 6.15(b) shows the minimum combined throughput calculated using both methods. The minimum combined throughput is very similar for both methods within the region of interest up to the GHz transmit power limit, as the individual UHF RAN throughput matches for the two methods. The differences between the two methods are due to two reasons:

*Network throughput estimation.* The BBN method calculates the expected throughput for each RAN using the median data rate selected for each station, i.e the averaging is performed

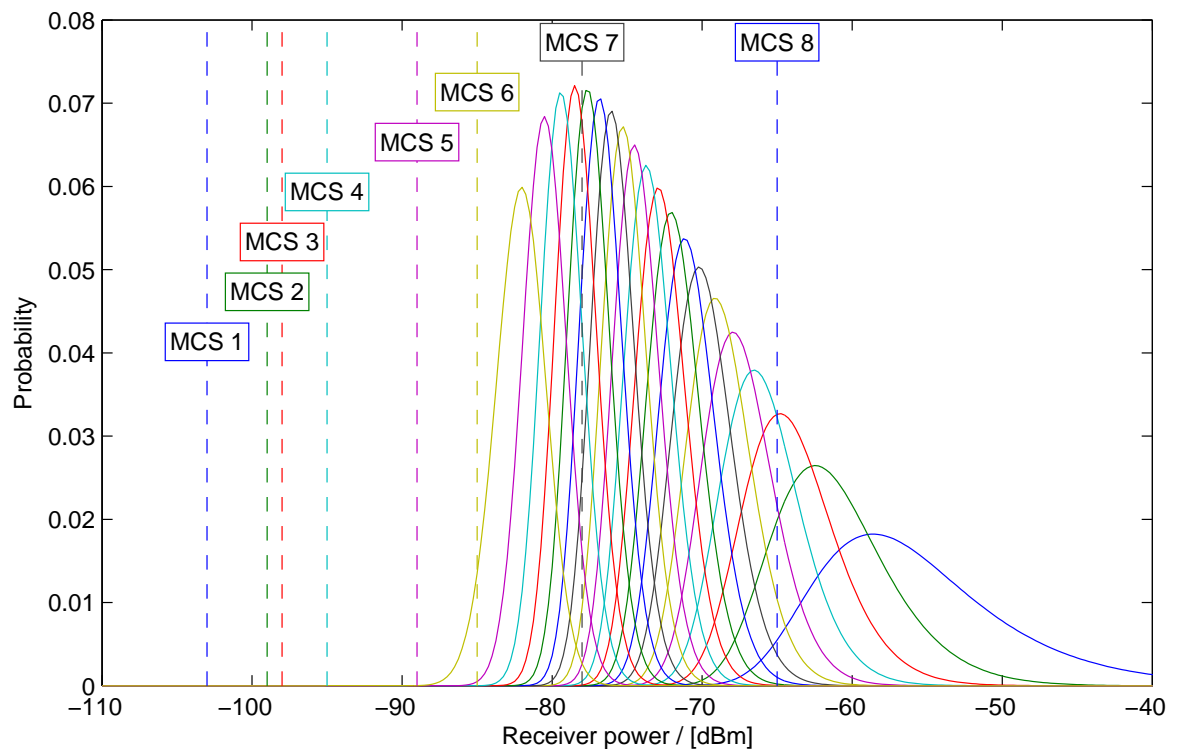


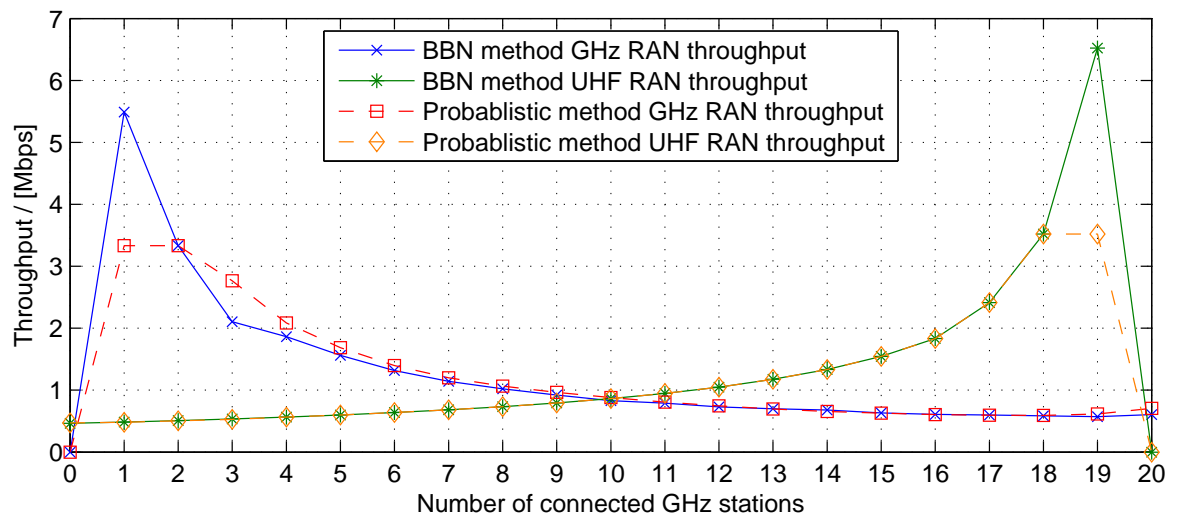
Figure 6.14: Beliefs of  $P_u^{rx}$  given  $P^{tx} = 30$  dBm after BBN convergence with data rate boundaries. The 20 ordered PDFs represent the 20 ordered stations. The rightmost PDF is that of the closest station to the base station.

on the individual station data rates and the average data rates are used to determine the throughput. The probabilistic method differs as the network throughput for all combinations of station data rates is calculated then averaged based on the probability of each combination.

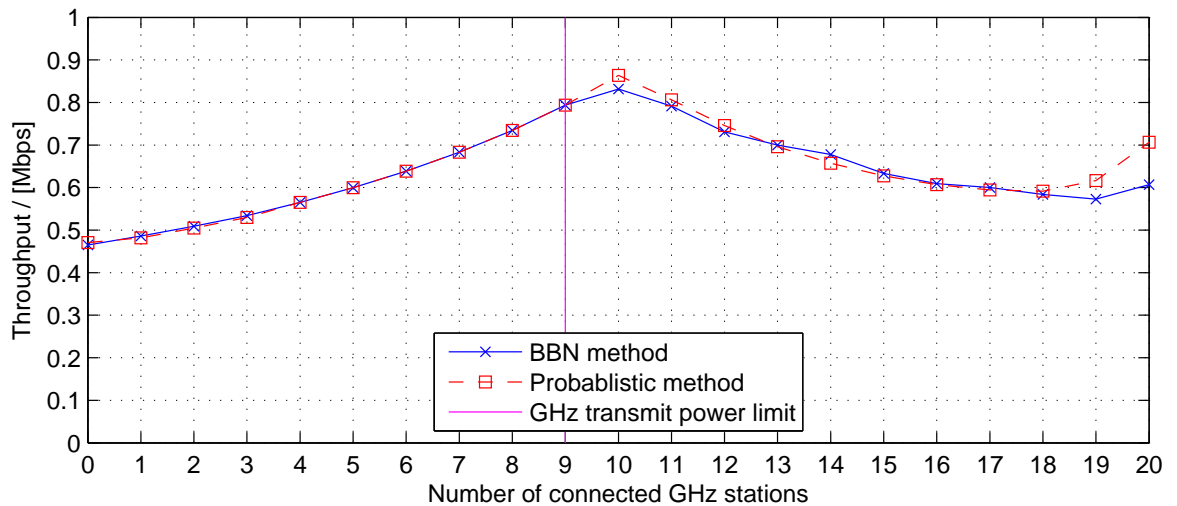
*GHz RAN transmit power.* As shown in Figure 6.13(a) for small assignments the mean GHz RAN transmit power is lower using the BBN method when compared to the probabilistic method. Therefore the resultant station receive powers and data rates and hence RAN throughput will be lower.

### 6.9.3 GHz RAN Breathing to Minimise Power Consumption

As described in Section 6.8.4, the throughput estimation in Figure 6.15(a) can be used to evaluate the power consumption when dynamically scaling the number of associated stations given a required capacity. Figure 6.16 presents the analysis of using a dynamic target data rate with the calculated assignment throughputs from the BBN method. Figure 6.16(a) shows both the required and offered capacities for different dynamic and static assignment schemes. Figure 6.16(b) compares the power consumption of the schemes. The fluctuating optimum station assignment is depicted in Figure 6.16(c). This analysis using the BBN method produces very similar results to that of the probabilistic method.



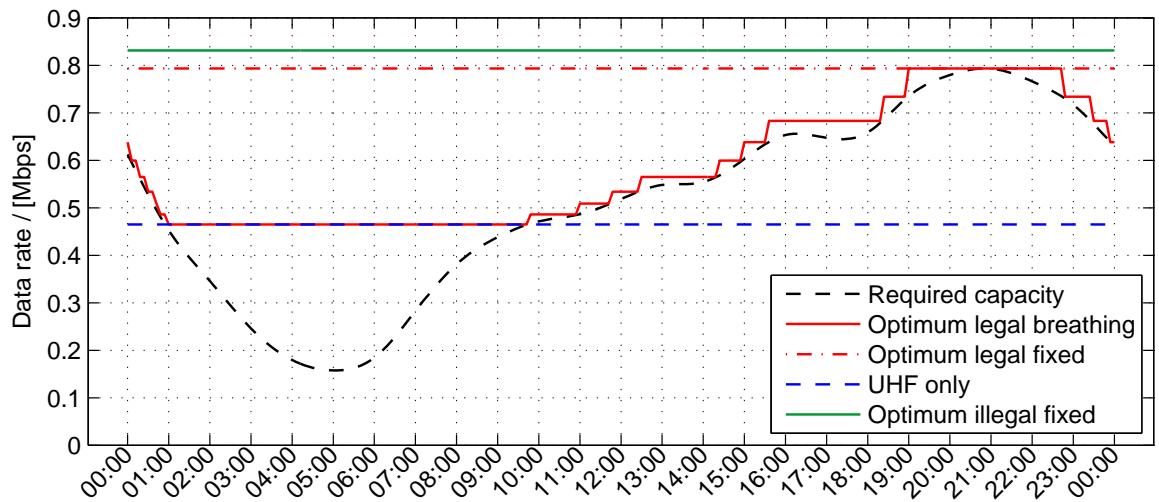
(a)



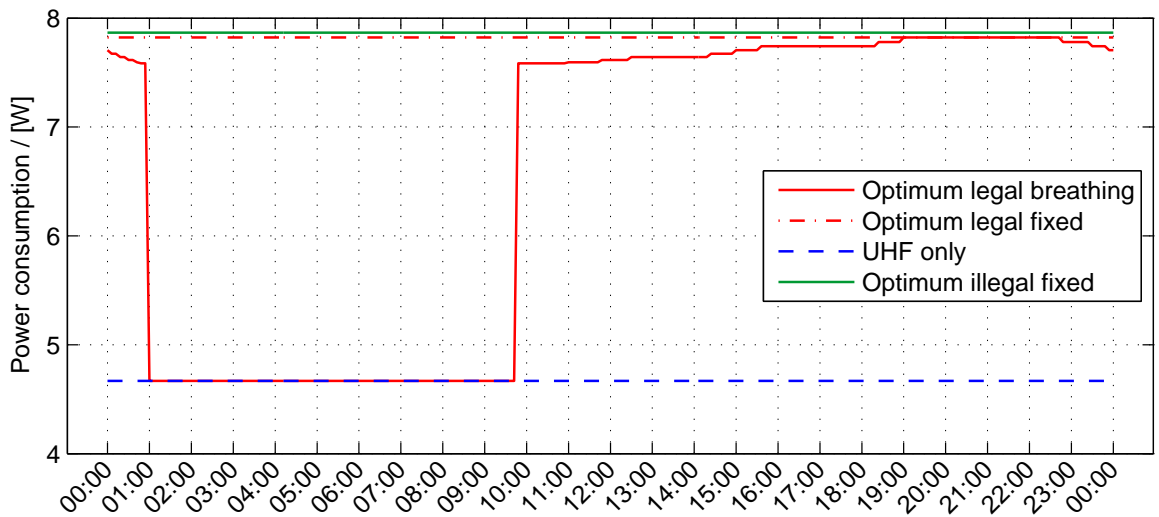
(b)

Figure 6.15: Comparison of throughputs calculated using BBN and probabilistic methods for given RAN assignments: (a) individual station capacity on each RAN, and (b) combined RAN minimum throughput.

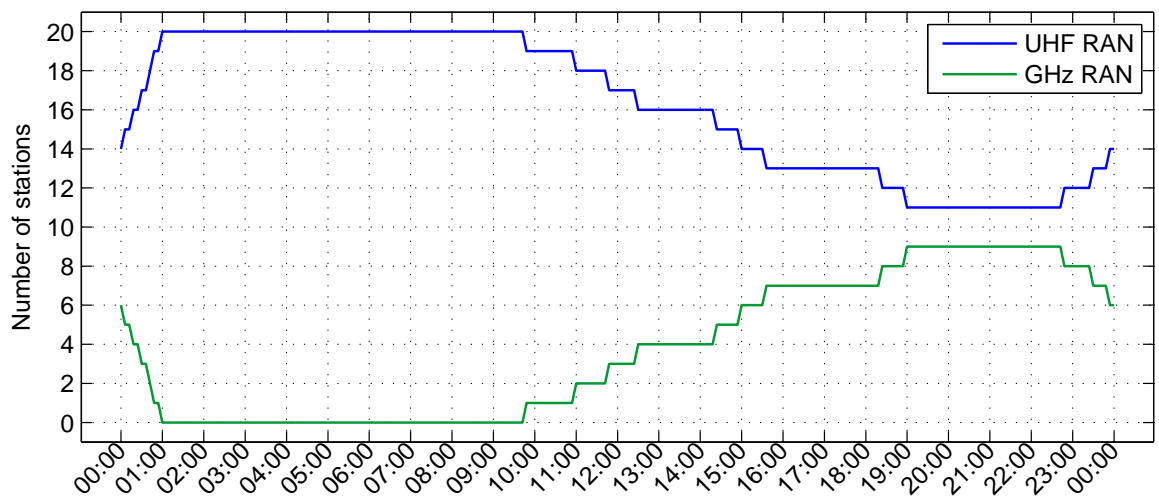
Table 6.4 compares the resultant power consumption savings using the results from the BBN and probabilistic methods. The savings are comparable due to the similar minimum combined data rate and power consumption for each assignment. The difference between the methods for the calculation of energy saved when comparing the breathing to the legal fixed optimum is due to the transmit power requirements for each assignment differing between the methods. For a given assignment the probabilistic method selects a higher transmit power, and therefore consumes more power, than the BBN. This reason also contributes to the difference between the methods when calculating the energy saved by breathing compared to a fixed transmission at the illegal optimum power. Additionally the peak minimum combined throughput differs between the methods, visible in Figure 6.15(b).



(a)



(b)



(c)

Figure 6.16: Results of solving (6.13) with the BBN method in 3 min. intervals showing: (a) required and offered capacity, (b) network power consumption, and (c) station assignment

Metric	BBN	Probabilistic
Saving over fixed legal optimum transmit power	15.6%	16.2%
Saving over fixed illegal optimum transmit power	16.1%	16.6%

Table 6.4: Comparison between energy savings through dynamic station assignment using results from the BBN and probabilistic methods.

## 6.10 Summary and Discussion

This chapter presented three methods to optimise the station assignment in a dual RAN situation, comprising of a 5 GHz and UHF TVWS network, with respect to minimum power consumption while fulfilling transmit power constraints and the minimal achievement of a target data rate prescribed by a utilisation pattern. Using a probabilistic method, the assignment of stations to each RAN was optimised to maximise individual station data rates. The probabilistic model created of the network, and the resultant optimisation, was validated using on a Monte Carlo simulation. A BBN was presented as an alternative method to optimize the network with Pearl's algorithm.

The optimisation was simulated by applying the three methods, with parameters obtained from the analysis and measurement of the Hopscotch network and radio equipment presented in Chapters 4 and 5. These parameters were used to ensure as realistic results as possible. Interestingly, the optimum assignment of stations between the RANs differs from intuitively assigning as many stations as possible to the higher bandwidth GHz RAN, as the UHF RAN can serve stations at the edge between both network assignments with higher data rates. Power consumption was shown to be reduced by dynamically changing the assignment based on traffic requirements, providing a 16.2% energy consumption saving compared to a fixed transmit power. Minimising the base station power consumption is important to reduce the cost, and increase the accessibility of renewable powered base stations such as WindFi discussed in Chapter 3.

The results of the Monte Carlo method matched the probabilistic method. The differences between the results provided by the probabilistic and BBN methods were discussed and it was shown that the BBN method provides a good approximation. Therefore the BBN provides a flexible alternative to the probabilistic model, by allowing additional conditional dependences to be introduced into the network for future analysis, such as shadow fading and the impact of terrain.

## Chapter 7

# Conclusions and Further Work

This work presented the “Hopscotch” wireless network as a solution to the rural broadband problem. Providing broadband internet access to rural locations is challenging for a number of reasons. The long distances between exchanges and households limit the effectiveness of ADSL, the most common broadband access technology. The sparse population density limits return on investment for high speed solutions common at present in urban and suburban environments such as fiber and 3G/4G wireless. The challenging terrain increases fixed infrastructure costs and limits the performance of wireless links in traditional frequency bands. These challenges, and the limitations of existing solutions, as discussed in Chapter 2, have restricted the roll-out of high speed broadband internet access to rural communities, reducing the effectiveness of on-line services and increasing the distance penalty that accompanies living in a rural location.

Hopscotch uses a network of renewable powered base stations, termed “WindFi”, connected by PTP links to deliver internet access to rural communities. A combination of 5 GHz and TVWS bands are used to create PTMP links between base stations and households. The use of dual frequency bands in a heterogeneous network combines the high bandwidth 5 GHz links with the benign propagation characteristics of TVWS links. This allows Hopscotch to reach more users than existing networks and therefore to be a viable solution to the rural broadband problem. Hopscotch trials have been running on two Scottish islands, Bute and Tiree since 2010 and 2011 respectively. The main contributions and findings reported in this thesis are discussed in detail in the following sections.

### 7.1 TV “White Space” for Rural Broadband

Chapter 2 reviewed existing rural broadband access networks and introduced the Hopscotch network. One of the main differences between Hopscotch and existing wireless access net-

works is the use of the TVWS frequency band in addition to the traditional 5 GHz bands.

The availability of TVWS bands for uses other than broadcast services provides an excellent opportunity for rural broadband delivery. Chapter 2 discussed the numerous advantages of the UHF band for fixed wireless access, in which TVWS resides, compared to the traditional 5 GHz band. The FSPL, diffraction loss and attenuation due to foliage are all substantially less in the TVWS band compared to the 5 GHz band. Due to the distance of links required and the challenging terrain, these factors are very significant in rural scenarios.

The reduced path loss between transmitter and receiver in TVWS bands offer a number of benefits when designing a network. More flexibility is provided when determining base station placement due to the increased range. This may allow for fixed infrastructure such as mains power or wireline IP-access to be used. The improved propagation properties may also lead to fewer base stations being required to serve a community as demonstrated in Chapter 2. Reducing the infrastructure required reduces the main barrier to providing internet access to a rural community; the cost. Therefore the use of TVWS is ideal for this scenario, especially in rural locations where much of the band is presently vacant. The reduced path loss also reduces the transmit power required to maintain a connection, compared to the 5 GHz band, thus minimising interference and reducing power consumption.

Despite the advantages of wireless access in the TVWS band, Hopscotch transmits over the 5 GHz band for PTP links and some PTMP links. The 20/40 MHz bandwidth offered by COTS IEEE 802.11 based 5 GHz equipment provides a much higher throughput than the 5-8 MHz currently available in TVWS. Therefore the 5 GHz band is better suited to links which require high capacity such as wireless backhaul between base stations if line of sight exists. The use of both frequency bands within the network allows the disadvantages of each individual band to be overcome. This scenario was simulated in Chapter 6.

## 7.2 WindFi Base Station

The WindFi base station is designed to function as an autonomous unit, powered by a combination of wind and solar energy. A battery bank is used to provide a buffer for the generated energy, allowing for continuous operation on overcast or wind-less days. WindFi differs from existing renewables-powered wireless network infrastructure reviewed in Chapter 2 as PTP and PTMP links are used instead of mesh links, and two frequency bands are simultaneously supported, requiring a larger power generation and storage system.

Chapter 3 provided an analysis of typical Hopscotch use-cases by providing examples from the Hopscotch network on the island of Tiree. These use-cases served to drive requirements for the power system of WindFi. Two radio equipment base loads of 25 W and 50 W were shown to meet the use-cases. The sizing of the battery bank to support these base loads

was described with the design of the renewable power generation system at two locations, Prestwick and Tiree airports, located close to WindFi trial locations. Historical wind and solar irradiation data was used to show how the different options for wind turbines and solar panels can be used to meet the base load requirements requirements at when conditions between locations vary.

The design and retrospective analysis of the “Crow’s Nest” renewables-powered relay on Tiree was presented in Chapter 3. Using recorded data, three scenarios were studied. The analysis of low and high wind-speed days enabled an understanding of how to interpret the recorded data. This understanding was applied to a period when the wind turbine failed leading to a loss of service. The analysis showed that the power system behaved as designed, with the system failing due to a depleted battery bank the same day as the design predicted.

### **7.3 Radio Power Consumption and Data Rate Selection Models**

To explore energy saving techniques, such as the optimisation proposed in Chapter 6, the power consumption of the radio equipment, the largest consumer of energy in the base station, must be understood. A lab based characterisation of the power consumption of Ubiquiti XR7 and SR71 radios used within Hopscotch for connectivity in the UHF and 5 GHz bands was carried out to gain this understanding. Chapter 4 described the characterisation of power consumption given a configured transmit power and presented a model for each radio. The power consumption of both radios increase exponentially with the configured transmit power, therefore a power curve models the relationship.

The data rate selection of the radios was characterised for a given receive power to serve as a model for estimating network throughput when modelling path losses. Both the XR7 and SR71 radios exhibited unexpected behaviours. The throughput using the XR7 dropped considerably for a narrow path loss range for all data rates. The SR71 struggled to maintain the 12 Mbps data rate for all path losses and therefore was never automatically selected. Despite these unexpected observations the characterisation provided consistent results, and showed the increased power spectral density when receiving a signal in the smaller 5 MHz bandwidth than the 20 MHz, increased the sensitivity of the receiver.

The models of power consumption and data rate selection were subsequently used in Chapter 6 to determine the optimum assignment of stations between a multi-RAN network through simulation.

## 7.4 Models for Rural Fixed Wireless Scenarios

To enable the accurate simulation of rural wireless networks, such as the energy saving scheme proposed in Chapter 6, three models relevant to the study of wireless networks in rural environments were presented in Chapter 5; household distribution, large-scale path loss, and downstream and upstream bandwidth utilisation. These models were created using data recorded between November 2013 and February 2014 from a trial Hopscotch network on the Scottish island of Tiree, serving over 100 subscribers.

The location of network subscribers relative to the base stations was used to create a model of the distribution of households from a base station at the center of a community. A circularly symmetric normal distribution was shown to be a good fit. This model provides an alternative to the uniform distribution of users often used for analysis in urban environments.

The radio equipment used within the Tiree network allowed the received signal strength to be recorded. This, along with knowledge of the transmit power and antenna gains allowed a large-scale path loss model, based on the simplified path loss formula to be fitted to the radio environment on Tiree. A path loss coefficient was determined by a least square linear regression to best fit the data.

The instantaneous throughputs of all radios within the networks were recorded every 20 minutes and analysed to create a model of the time-varying downstream and upstream data usage within the network. The analysed data showed a clear diurnal pattern where usage peaked at 21:00 before dropping 80% to a minimum at 05:00. The proposed model was tested against an available model for urban data and with a diurnal usage pattern.

## 7.5 Optimised Multi-Radio Network for Energy Efficiency

The main cost component of a WindFi base station is the renewable power generation system, therefore techniques to minimise the energy consumption are important to the viability of Hopscotch. The simultaneous use of two RANs within Hopscotch; a 5 GHz RAN to offer capacity, and a UHF RAN to provide extended coverage, creates an opportunity for energy saving optimisations. Chapter 6 presented an optimisation to minimise the energy consumption by altering the assignment of stations between the two RANs by scaling the GHz RAN transmit power, whilst maximising the individual station data rates.

Through simulation the assignment of stations between the two RANs was obtained which maximises the individual station throughput for a scenario of 20 stations served by a base station when using the rural network and radio performance models created in Chapters 4

and 5. This optimum assignment differed from the intuitive assumption that due to the GHz RAN theoretically offering four times the capacity of the UHF RAN, the assignment of stations should match this balance. This is because stations on the UHF RAN are served at a higher data rate than the GHz RAN at the same distance. It is therefore preferable to add an “easy” station to the UHF RAN than add a station served at a low data rate to the GHz RAN, which will slow the entire RAN.

Chapter 6 additionally proposed a scheme whereby dynamically changing the station assignment according to the required network utilisation reduced the energy consumption of the network by 16.2% compared to using a fixed transmission power. The network bandwidth utilisation model created in Chapter 5 provided the driver for the optimisation, and the radio power consumption model creating in Chapter 4 allowed the power consumption to be estimated.

Three methods were used to perform the optimisations. A probabilistic method using the PDFs of station receive powers to estimate network throughput served as the baseline for the optimisation results. A Monte Carlo method was used to validate the probabilistic method by creating an ensemble of sets of stations drawn from the model of household distribution and averaging the calculated throughputs over the whole ensemble. A BBN was also used as an alternative method, and provided a good approximation for the probabilistic method. The BBN method provides scope for additional conditional dependences to be added to the model in future analysis which is more difficult with the probabilistic method.

## 7.6 Further Work

The work covered in this thesis gives rise to a number of suggestions for future research work and development:

Trials of Hopscotch have been carried out on the Scottish islands of Bute and Tiree. Currently the Tiree trial uses only a 5 GHz network, but an overlay UHF network is planned and would offer an excellent opportunity to study the interaction of the two RAN on a larger scale. The inherent low-cost and scalability of Hopscotch has generated interest in other countries. Initial work has been undertaken to design a “SunFi” base station for a network in Kenya or Sudan which would operate using only solar energy. A Hopscotch trial in these locations would provide an excellent opportunity to study the characteristics of a network in a different climate and culture, including the usage patterns and the distribution of households.

The study of the optimum assignment of users between the UHF and GHz RAN presented in Chapter 6 could be further extended. A study of the implications of adding additional RANs, such as additional TVWS channels would be interesting and could lead to further energy reduction opportunities. Extending the simulation to include neighbouring base stations would

allow the interference created by scaling the RAN to be considered which is relevant in a practical system. It would be of value to study the impact of the distribution of households served by the base station on the expected throughput and energy consumption. The standard deviation of the model presented in Chapter 5 describes the distribution of the community. A study of the impact of this parameter would be valuable in addition to a study of the results using a uniform distribution. The BBN presented in Chapter 6 provides an opportunity to include additional parameters within the model, as nodes can be added easily. An example of additional variables to study are shadow fading and a random variable representing the affect of weather on link performance.

An extension to the Ttree or Bute networks would allow the proposed dual RAN energy saving scheme of scaling the GHz RAN transmit power to be tested in the field. This would allow the energy saving capabilities to be validated and would uncover implementation issues such as the behaviour of radios which are “on the edge” and could associate with either network depending on small changes to the receive signal quality. An additional interesting future study would be methods to make the most of excess energy generated by the renewable energy system if an abundance of energy and bandwidth is available and cannot be used, i.e. the battery bank is fully charged and users do not require bandwidth. One possible use of this energy and bandwidth would be to locally cache video at the base station during times of plenty, such as proposed for cells in [?], to reduce the bandwidth required when the video must be delivered and resources may not be available. Conversely another important area of study is how to optimally handle a power system failure. This scenario could be formulated as a constrained optimisation to best serve users with a finite energy supply.

Finally a number of the contributions in this thesis could be combined to create an enhanced planning tool for Hopscotch networks. The planning tool would calculate the optimum base station assignment to serve a community based on a number of factors. The location of households along with GIS data would provide the information required for modelling radio propagation, e.g. elevation and clutter. The tool would also be aware of TVWS ability and therefore be able to design the links and number of sectors required given the bandwidth available. The tool would be able to calculate the optimum assignment between the TVWS and 5 GHz RANs to maximise individual throughput and minimise power consumption. Lastly the wind and solar irradiation would be available to size the power system which would depend on the local conditions and number of radios required. The tool could trade off between expected individual user receive power strength and the cost of the base station power system and could potentially be used to locate areas where Hopscotch would be most suitable.